Queen Mary
University of London

Joint Spatial and Spectrum Cooperation in Wireless Network.

Deng, Yansha

The copyright of this thesis rests with the author and no quotation from it or information derived from it may be published without the prior written consent of the author

For additional information about this publication click this link.
http://qmro.qmul.ac.uk/jspui/handle/123456789/8926

Information about this research object was correct at the time of download; we occasionally make corrections to records, please therefore check the published record when citing. For more information contact scholarlycommunications@qmul.ac.uk

Joint Spatial and Spectrum Cooperation in Wireless Network

by

Yansha Deng

Doctor of Philosophy

Department of Electronic Engineering and Computer Science
Queen Mary University of London
United Kingdom

March 2015

TO MY FAMILY

Abstract

The sky-rocketing growth of multimedia infotainment applications and broadband-hungry mobile devices exacerbate the stringent demand for ultra high data rate and more spectrum resources. Along with it, the unbalanced temporal and geographical variations of spectrum usage further inspires those spectral-efficient networks, namely, cognitive radio and heterogeneous cellular networks (HCNs). This thesis focuses on the system design and performance enhancement of cognitive radio (CR) and HCNs. Three different aspects of performance improvement are considered, including link reliability of cognitive radio networks (CNs), security enhancement of CNs, and energy efficiency improvement of CNs and HCNs.

First, generalized selection combining (GSC) is proposed as an effective receiver design for interference reduction and reliability improvement of CNs with outdated CSI. A unified way for deriving the distribution of received signal-to-noise ratio (SNR) is developed in underlay spectrum sharing networks subject to interference from the primary transmitter (PU-Tx) to the secondary receiver (SU-Rx), maximum transmit power constraint at the secondary transmitter (SU-Tx), and peak interference power constraint at the PU receiver (PU-Rx), is developed. Second, transmit antenna selection with receive generalized selection combining (TAS/GSC) in multi-antenna relay-aided communication is introduced in CNs under Rayleigh fading and Nakagami-m fading. Based on newly derived complex statistical properties of channel power gain of TAS/GSC, exact ergodic capacity and high SNR ergodic capacity are derived over Nakagami-m fading. Third, beamforming and artificial noise generation (BF&AN) is introduced as a robust scheme to enhance the secure transmission of large-scale spectrum sharing networks with multiple randomly located eavesdroppers (Eves) modeled as homogeneous Poisson Point Process (PPP). Stochastic geometry is applied to model and analyze the impact of

BF&AN on this complex network. Optimal power allocation factor for BF&AN which maximizes the average secrecy rate is further studied under the outage probability constraint of primary network. Fourth, a new wireless energy harvesting protocol is proposed for underlay cognitive relay networks with the energy-constrained SU-Txs. Exact and asymptotic outage probability, delay-sensitive throughput, and delay-tolerant throughput are derived to explore the tradeoff between the energy harvested from the PU-Txs and the interference caused by the PU-Txs. Fifth, a harvest-then-transmit protocol is proposed in K-tier HCNs with randomly located multiple-antenna base stations (BSs) and single antenna mobile terminals (MTs) modeled as homogeneous PPP. The average received power at MT, the uplink (UL) outage probability, and the UL average ergodic rate are derived to demonstrate the intrinsic relationship between the energy harvested from BSs in the downlink (DL) and the MT performance in the UL. Throughout the thesis, it is shown that link reliability, secrecy performance, and energy efficiency of CNs and HCNs can be significantly leveraged by taking advantage of multiple antennas, relays, and wireless energy harvesting.

Acknowledgments

First of all, I would like to express my sincere gratitude to my supervisors, Dr Maged Elkashlan and Dr Akram Alomainy, for offering me a chance to pursue my PhD at Queen Mary University of London, and for their continuous and valuable technical guidance and unconditional support throughout my PhD. Special thanks to my primary supervisor, Maged Elkashlan, who introduced me to the area of cognitive radio and heterogeneous networks, and opened up new opportunities for my following academic career. His nice personality, strong research enthusiasm, and hard-working attitude have influenced and inspired me all along my PhD. Every discussions with him helped me to connect with the state of art in academia, and shaped my vision for my future research. Every time confusion emerged in my mind, his prompt reply and feedback gave me strength and power to carry on. His generosity and kindness in arranging visiting study in University of New South Wales (UNSW) and University of British Columbia (UBC) for me and facilitating my collaborations with excellent researchers, built my research experiences and promoted my research ability. I am extremely lucky to work under his supervision, and this thesis would not exist without his generous help and support.

Second, I would like to thank Dr. Felix Cuadrado for serving as my progression panel lead and for his constructive advice. I would also like to thank Prof. Steve Uhlig for his invaluable comments and suggestions. My special thanks to my collaborators: Dr. Nan Yang, Dr. Phil Yeoh, Dr. Quang Trung Duong, Dr. Malcolm Egan, Dr. Kyeong Jin Kim, Prof. Ranjan K. Mallik, Prof. George K. Karagiannidis, and Prof. Arumugam Nallanathan, for introducing new methods and collaborating with me on various ideas. Working with them are excellent experiences for me. I would like to express my appreciation and thanks for Prof. Jinhong Yuan for hosting me in UNSW, which led to our joint work on security of CNs. I would also like to thank Prof. Robert Schober,

Dr. Karen C. Cheung, and Adam Noel for hosting me in UBC, and the invaluable discussions with me.

Third, I would like to express my gratitude to my dear lab mates in Network group, Ammar Lilamwala, Lexi Xu, Hongyi Xiong, Ling Xu, Fei Peng, Bo Zhong, Nan Wang, Xin Chen, Yue Liu, Xiuxian Lao, Dan Zhao, Yun Li, Amna Abdul Wahid, Sabri E Zaman, Gareth Tyson, Marjan Falahrastegar, Zhijin Qin, Dantong Liu, Yuanwei Liu, Jingjing Zhao for their various ways of support and help. My special thanks to Lifeng Wang for the everyday discussions and constant support both in academia and life. I also would like to express my thanks to my best friends, Mingfeng Wang, Xu Zhen, Jieyu Lv, Tian Cheng, for caring me in daily life. Thanks for the companionship and acompanying during my PhD.

Last but not least, my deepest gratitude goes to my family for the relentless support and encouragement and for sharing the happiness or sadness, success or failure with me as always. They are my internal motivation driving me to work hard and pursue better life through all these years.

Table of Contents

List of Figures

List of Abbreviations

AF	Amplify-and-Forward
AN	Artificial Noise
ADC	Analog-to-Digital Converter
AWGN	Additive White Gaussian Noise
BS	Base Station
BF	Beamforming
BPSK	binary phase shift keying
CR	Cognitive Radio
CNs	Cognitive Radio Networks
CSI	Channel State Information
CDF	Cumulative Distribution Function
CCDF	complementary cumulative distribution function
DL	Downlink
DC	direct current
D2D	Device-to-Device
DF	Decode-and-Forward
EH-IT	Energy Harvesting-Information Transfer
FCC	Federal Communications Commission
GSC	Generalized Selection Combining

HDTV	High Definition Television
H-AP	Hybrid Access Point
HCNs	Heterogeneous Cellular Networks
HetNets	Heterogeneous Networks
iid	independent and identically distributed
LOS	Line-of-Sight
LTE	Long Term Evolution
LPF	low-pass filter
MT	Mobile Terminal
MRC	Maximal Ratio Combining
M-PAM	M-ary Pulse Amplitude Modulation
MGF	moment generating function
MIMO	Multiple Input Multiple Output
OFDM	Orthogonal Frequency Division Multiplexing
PPP	Poisson Point Process
PU	Primary User
PDF	Probability Density Function
QoS	Quality of Service
QPSK	quadrature phase shift keying
RF	Radio Frequency
Rx	Receiver
SU	Secondary User
SC	Selection Combining
SIMO	Single Input Multiple Output
SISO	Single Input Single Output
SNR	signal-to-noise ratio
SINR	Signal-to-Interference-Plus-Noise Ratio
SIR	Signal-to-Interference Ratio

SER	Symbol Error Rate
SWIPT	Simultaneous Wireless Information and Power Transfer
SDMA	Space-Division-Multiple-Access
TAS	Transmit Antenna Selection
Tx	Transmitter
TDMA	Time Division Multiple Access
UL	Uplink
WiMAX	Worldwide Interoperability for Microwave Access
WLAN	Wireless Local Area Network
WPCN	Wireless Powered Communication Network
3D	Three-Dimensional
3G	Third Generation
3GPP	Third Generation Partnership Project
4G	Fourth-Generation
5G	Fifth-Generation

Chapter 1

Introduction

1.1 Background

Driven by the fast proliferation of data-hungry applications, such as symmetric video call, multimedia download, and High Definition Television (HDTV), there exists an urgent requirement for high data rate and ubiquitous mobile broadband [10]. According to the target of Qualcomm's "1000x data challenge", it is estimated that the requirement over a decade are approximately 1000x increase in capacity, and 10x in spectral efficiency and energy efficiency [11, 12]. This trend will further accelerate in the future. It is expected that the number of devices will increase exponentially and reach the tens or even hundreds of billions when the fifth-generation (5G) comes to reality [13, 14]. "How to achieve 1000x increase in capacity, and 10x increase in spectral efficiency and energy efficiency?" is the big challenge faced by both academia and industry.

Situation: Spectrum shortage due to inefficient utilization and demand

Conventional spectrum allocation policy regulates that the frequency spectrum is allocated for a specific service usage (cellular, TV broadcast, etc.) in advance. For example, cellular providers are only allowed to access to the carrier frequency spectrum between 700 MHz and 2.6 GHz for video and multimedia service delivering [15]. This allocation policy is simple, easy to manage, and can avoid possible interference from

other transmitters. However, according to the Federal Communications Commission (FCC) report [16], only certain portions of licensed frequency bands are heavily used, and other unlicensed spectrums remain unoccupied for 90% of the time. On one hand, the average utilization of licensed band is reported as low as 5%, according to Ofcom in United Kingdom [17]. On the other hand, the spectrum resources are becoming extremely precious and scarce. The US frequency allocation reported that the most frequently used bands (< 3 GHz) in wireless communication are crowded with little spectrum resource available for emerging wireless products and services [18].

Millimeter wave* & *WiFi's unlicensed spectrum

Except for the frequently used spectrum between 700 MHz and 2.6 GHz, the abundant non-congested millimeter wave spectrum in 3-300 GHz and the WiFi's unlicensed spectrum in the 5 GHz band open up new possibilities for cellular users [19]. However, the propagation characteristic of millimeter wave spectrum is different from conventional cellular spectrum, and the channel modeling and hardware design suitable for millimeter wave are still in its infant age [15]. Time and continuous efforts are needed to make it work for cellular transmission.

Cognitive radio

The unbalanced temporal and geographical variations in spectrum usage and scarce spectrum resources have inspired FCC to "remove regulatory barriers and facilitate the development of secondary markets in spectrum usage rights among Wireless Radio Services" [20]. Herein, cognitive radio, first coined by Mitola [21], is proposed as a promising technology to solve the inefficient spectrum usage and alleviate the pressure due to scarce spectrum resources [22]. Cognitive radio, built on a software-defined radio, is defined as an intelligent wireless communication system that is aware of its environment and uses the methodology of understanding-by-building to learn from the environment and adapt to statistical variations in the input stimuli, with two primary objectives in mind: 1) highly reliable communication whenever and wherever needed; and 2) efficient utilization

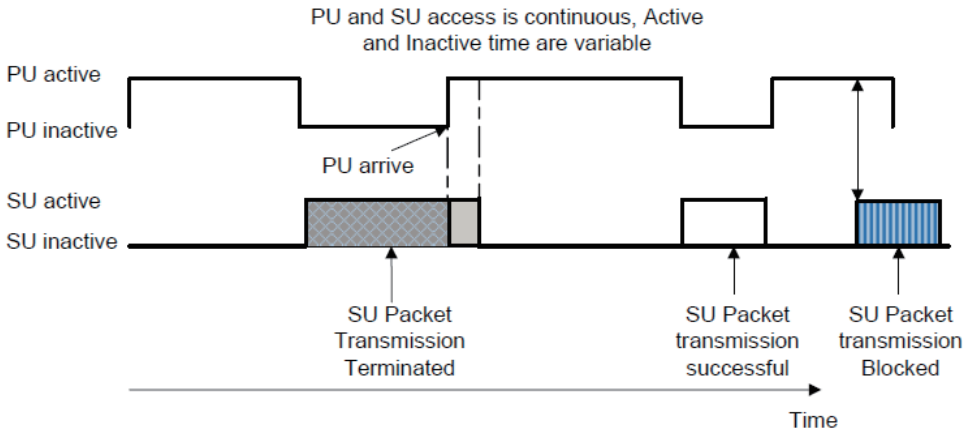

Figure 1.1: The interweave paradigm [1].

of the radio spectrum [23].

The basic idea of cognitive radio networks (CNs) is to allow the unlicensed user to access to the licensed spectrum intelligently at a certain time or geographic region. In this case, the unlicensed user, which is also called secondary user (SU), can share the same spectrum resources with the licensed user, namely primary user (PU). The PU has the privilege to access the licensed spectrum with priority, and the Quality of Service (QoS) constraint of primary network needs to be satisfied anytime. The SU has "cognitive" ability to sense and adjust its parameters to ensure the interference at the PU below a certain level. Cognitive radio (CR) can be categorized into three main paradigms in terms of the ways the SU accessing the PU's spectrum, namely interweave, overlay, and underlay CR [24].

Interweave paradigm (Interference avoiding)

The original motivation of CR is the interweave paradigm, where the SU is capable of sensing and accessing the PU's temporary space-time-frequency voids, which are not in constant occupation. The space-time-frequency voids are also called spectrum holes. The spectrum holes change over time and space, the SU needs to adaptively change its parameters corresponding to the available spectral resources of licensed band. Note that no concurrent transmission of the PU and the SU is allowed in this paradigm,

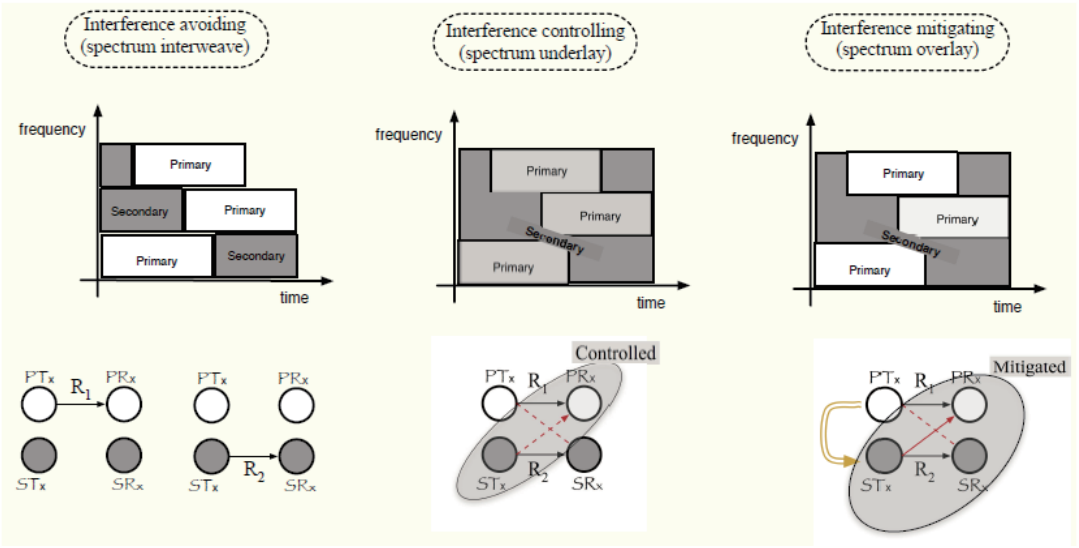

Figure 1.2: The classification of CR [2].

thus, in some cases, the SU's transmission may be cut off due to the appearance of PU transmission, as shown in Fig. 1.1. Therefore, the throughput of SU is dependent on the forced termination probability and the blocking probability.

Overlay paradigm (Interference mitigating)

In the overlay paradigm, the SU is allowed to transmit on the same spectrum allocated to the PU, and the knowledge of PU's message and codebooks are known by the SU initially, as shown in Fig. 1.2. With these key knowledge from the PU, the SU can cancel the interference from the PU using some techniques, such as dirty paper coding. Meanwhile, the SU can help as a relay to transmit the PU's message to the PU-Rx using part of its transmit power, and the rest of the power can be used to transmit the SU's message. By doing so, the detrimental effect on the PU-Rx due to the interference from the SU can be compensated by the assistant relay transmission via the SU-Tx. This "cooperative" behavior of the SU can improve both the PU and the SU transmissions, whereas the implementation is sophisticated.

Underlay paradigm (Interference controlling)

The underlay paradigm has received increasing interests due to its simplicity compared with the overlay and interweave paradigms, and its capability of operating in the dense-user area with small amount of spectrum holes. In underlay paradigm [25, 26], the unlicensed SU is permitted to concurrently access to the same spectrum as the licensed PU under the premise that the interference inflicted by the SU on the PU does not violate the QoS of primary network. The QoS requirement of primary network can be guaranteed by either the peak interference power constraint at the PU or the outage probability requirement of primary network [26, 27]. For the quasi-static channel, such as TV unit, the peak interference power constraint is effective, while for the random channel, the outage probability requirement of primary network might be a better choice to protect the PU's QoS. These constraints can be fulfilled by steering the SU's signal away from the PU-Rx using multiple antennas, or spread the SU's signal over wide bandwidth to reduce its resulted interference below noise. Alternatively, the SU needs to obtain the knowledge of the PU's location and the interference channel gain between the SU-Tx and the PU-Rx or the channel between the PU-Tx and the PU-Rx, in order to strictly control its transmit power that can satisfy the QoS requirement of primary network.

Heterogeneous Cellular Networks

To achieve the 10x increase in spectral efficiency and the approximately 1000x increase in capacity requirement of 5G, several other approaches have been taken into consideration, such as using Massive multiple-input multiple-output (MIMO) to improve the spectral efficiency of transmission link or adding more spectrum. However, the point-to-point link capacity has been largely improved till the theoretic limit. Massive MIMO, where the BS with hundreds or thousands of antennas provides service for tens of users concurrently is an alternative to provide huge spatial multiplexing gains. Besides, adding more spectrum is expensive and is not a promising solution for the problem of long-term spectrum shortage [28]. One practical and promising approach is the so called heterogeneous cellular networks (HCNs) where the traditional macrocells are overlaid with low-power small cells, such as picocells, femtocells, and relays as shown in Fig. 1.3.

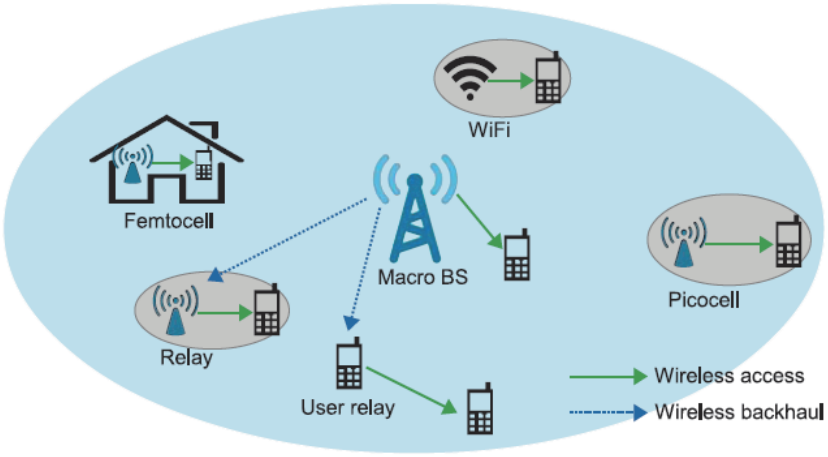

Figure 1.3: An example of HCNs architecture [3].

The small cells with relatively low network overhead and energy consumption, are deployed to offload the macrocells, compensate the user performance in deadzones or cell-edge, and increase the spectral efficiency per unit area via spatial reuse [29]. In HCNs, the transmit power of BSs, the density of BSs, the signal-to-interference-plus-noise ratio (SINR) targets, and the path loss exponent vary among different types of cells. As such, HCNs offer a fast, flexible and cost-efficient extension for traditional macro cellular networks, that can coordinate the areas with uneven traffic distribution. However, the users in HCNs suffer from increased interference due to the universal spectrum use of different cells.

Due to coverage footprints largely changed by the deployment of small cells, the modeling of multi-tier HCNs does not follow the traditional hexagonal grid model as in the single-tier cellular network [30]. The difference between the topology of the hexagonal grid model, the actual 4G deployment, and the two-tier HCNs is shown in Fig. 1.4.

A new modeling approach using random spatial models in stochastic geometry has now been widely applied to capture the topological randomness of HCNs, and it leads to tractable analytical evaluations [31]. Here, random spatial model means the locations of BSs in each tier follow a specific probability distribution. In [32], the locations of BSs are modeled as homogeneous Poisson Point Process (PPP) with density λ, and the users are

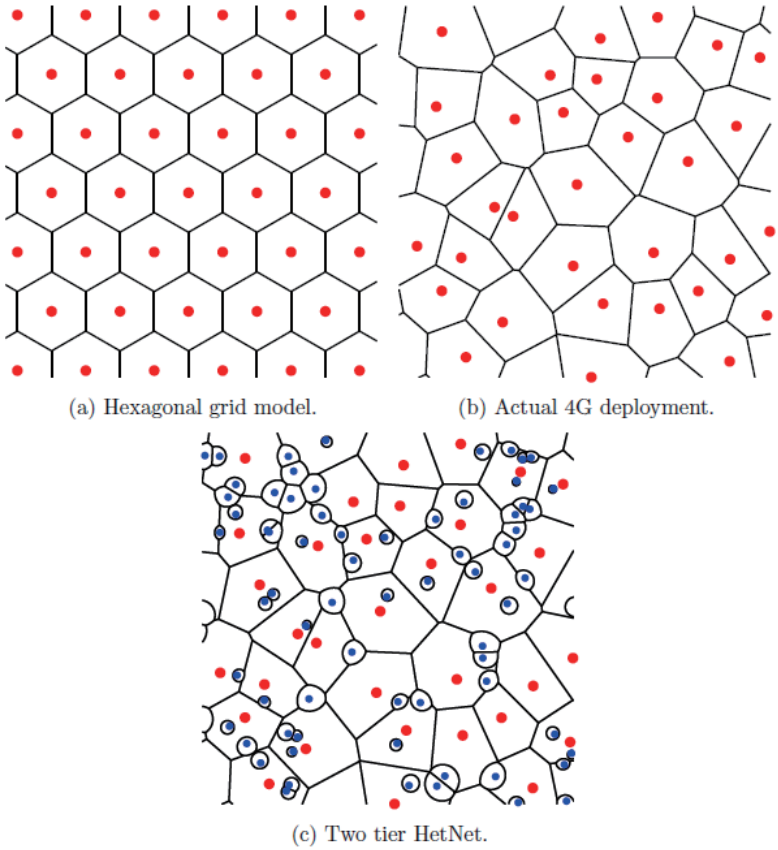

(a) Hexagonal grid model. (b) Actual 4G deployment.

(c) Two tier HetNet.

Figure 1.4: Cellular Network Topology [4].

modeled as homogeneous PPP. Here, homogeneous PPP implies that the density of the points is constant. The results in [32] showed that the coverage probability using PPP model provides a lower bound for that with actual 4G deployment, while the coverage probability using the conventional grid model provides an upper bound for that with actual 4G deployment. This result along with others in [30, 32–34] prove the accuracy and feasibility of the PPP model in evaluating HCNs.

1.2 Research Motivation

In this section, research motivations for link reliability and security enhancement of CNs, and energy efficiency improvement of CNs and HCNs are described.

1.2.1 Link reliability of CNs

The challenge of underlay spectrum sharing network is to effectively coordinate the transmit power at the secondary network and the interference power constraint at the primary network. Enhancing the link reliability of the secondary network, and fulfilling the interference requirements of the primary network are often contradictory [35]. The constrained transmit power at the SU typically results in unstable transmission and restricted coverage. This drives the demand for robust transmission techniques suitable for networks with transmit power and interference power constraints.

The first promising technique is MIMO [36, 37], where both the transmitter and receiver are equipped with multiple antennas. At the transmitter, the same signal is sent on each antenna, and propagates through different fading channels. The receiver collects the different copies of the signal, and thus achieves diversity gain. By equipping the SU-Tx and the SU-Rx with multiple antennas, the same performance of secondary network as the CNs equipped with single antenna, can be realized with less transmit power at the SU, thus imposes less interference on the PU-Rx.

To meet the goal of low cost radio deployment, the concept of cooperative CR is an exciting emerging technology that has the potential of dealing with the stringent requirement and scarcity of the radio resources. Cooperative CR has been recognized as one of the key technologies to solve the spectrum scarcity issue in next generation multi-tier large-scale networks. Specifically, emerging wireless applications such as wireless sensor and mesh networks have an increasing demand for small and low cost devices that are densely deployed over large areas. These small size devices may be hard to be installed with multiple antennas, whereas the cooperative relaying can act as an alternative technique to achieve spatial diversity. The main idea behind the cooperative diversity is to exploit independent paths between transmitter and receiver via relays, which forms a virtual antenna array. As such, this allows nodes with diverse radio resources (power, bandwidth, and channel qualities) to cooperate and relay each other's

messages to the destination.

Herein, MIMO transmission and cooperative diversity are well suited for coverage extension, performance enhancement, and interference reduction of underlay spectrum sharing networks. While single-antenna relays are able to boost the coverage and enhance the performance of the secondary network, MIMO enables multi-fold capacity and diversity enhancement without additional spectrum resources [38–40].

Transmit antenna selection with receive generalized selection combining (TAS/GSC) is regarded as a promising candidate for the performance enhancement of cognitive relay networks. At the transmitter, TAS substantially reduces implementation complexity and feedback overhead due to the reduced number of RF chains requirement and simple feedback requirement–the index of the selected transmit antenna. As such, the transmitter does not require channel state information (CSI) of all the antennas compared with alternative MIMO techniques such as precoding and BF [41]. Indeed, the advantages of antenna selection have been recognized in many IEEE standards including IEEE 802.11n for WLAN [42], IEEE 802.16 for WiMAX [43], and LTE-Advanced [44]. At the receiver, GSC offers a performance/implementation trade-off between maximal ratio combining (MRC) and selection combining (SC)[45, 46]. Compared to other diversity combining techniques, GSC is also capable to combat channel estimation errors by eliminating those weak signal-to-interference ratios (SIRs) [47]. In light of these motivations, part of my research is based on the network design and performance evaluation of cognitive MIMO relay network, which is given in Chapters 3, 4, and 5.

1.2.2 Security Enhancement of CNs

Due to the open and dynamic characteristics of cognitive wireless channels (opportunistic utilization of licensed channels), new classes of security threats and challenges are introduced into CNs [48]. Amongst the six major types of attacks on CR from the physical layer aspect, commonly known as primary user emulation, objective function attack,

learning attack, spectrum sensing data falsification, jamming attack, and eavesdropping [49, 50], this thesis focuses on the eavesdropping attacks targeted at the SUs. In this case, the Eves attempt to intercept the transmissions of the secondary transceivers [50]. Note that the Eves always keep silent without transmitting any signals, and can hardly be detected by the SUs.

Traditional security, which is achieved through higher layer cryptographic authentication and identification, becomes expensive and vulnerable to attacks [51]. Especially for sensor and ad hoc networks where the terminals are power-limited and centralized hardware for security does not exist, the implementation and management of higher-layer key distribution face challenges in practice [52]. More importantly, for the large-scale decentralized spectrum sharing networks, the security becomes more expensive and difficult to achieve with the cryptographic authentication and identification using secret keys.

To cope with these, physical layer security has been proposed as an alternative security method to protect the confidential information from eavesdropping [53]. Compared with conventional networks, there exists several major specialties in the security of CR: 1) the QoS requirement of the primary network needs to be satisfied while taking into account the co-channel interference from the SU-Tx; 2) the SU-Rx is subject to the aggregate interference from the PU-Txs; and 3) the secondary network is more susceptible to security threats since CNs has the ability to sense a high dynamic range of frequency. Motivated by these, the security enhancement and performance evaluation of large-scale spectrum sharing networks are studied in Chapter 6 in terms of secrecy outage probability and average secrecy rate.

1.2.3 Energy Efficiency of CNs and HCNs

The goal of green telecommunications is to design new architectures that tackle the energy efficiency and carbon footprint of wireless networks. Spurred by the exponential

growth of data traffic, network operators are increasingly aware of the need to mitigate the associated rise in energy consumption and CO2 emissions. It is estimated that energy costs alone account for as much as half of the annual operating expenditure. This has prompted concerted efforts by major operators such as Orange and Vodafone to drastically reduce CO2 emissions by up to 50 % over the next 10 years [54].

The high depletion of energy evokes the arising of various energy harvesting technologies, which is capable of improving the energy efficiency of wireless networks and reducing the detrimental effects on the environment at the same time. Traditional energy harvesting sources, such as solar, wind, hydroelectric, thermoelectric may not always be accessible in some location or environments. Alternatively, radio frequency (RF) wireless power transfer can be a cost-effective energy harvesting technique to harvest energy from ambient RF signals radiated by the energy transmitters in such environments [55]. Additionally, in wireless energy constrained networks, the battery powered mobile devices easily suffer from battery power shortage, and the replacement of battery can be difficult in some cases [56]. The RF wireless power transfer can be a good solution to prolong the lifetime of mobile devices and provide continuous and stable microwave energy for wireless energy constrained networks.

CNs

In the spectrum sharing networks, the SU-Rx inevitably suffers from the interference from the PU-Tx, the interference can be strong when the PU-Tx is located near the SU-Rx, or the number of PU-Txs are large. In this case, this ambient interference due to the RF signals radiated by the PU-Tx can be utilized for powering the SU. Another reason, which makes the RF wireless power transfer well suited for underlay spectrum sharing networks, is that the transmit power at the SU-Txs are typically quite low, even small amount of energy harvested from the PU-Tx can satisfy the low transmit power requirement of the SU. Motivated by this, a new RF wireless power transfer protocol is proposed in Chapter 7 to enhance the energy efficiency of underlay spectrum sharing networks.

HCNs

The advent of HCNs marks a new era for the viability of RF wireless power transfer in multi-tier cellular networks. In downlink (DL) HCNs, each MT is associated with the BS which provides the maximum received power. As such, the associated typical BS acts as the dedicated RF energy source, similar as the function of "power beacons" in [57], which provides reliable and sustainable energy for energy-constrained typical MT. Meanwhile, due to the universal frequency reuse, the typical MT also endure high level of interferences from other densely deployed interfering BSs, which are usually located close to the typical MT [58]. Those ambient interference from the interfering BSs are collected and transferred to DC power. By doing so, the interfering BS becomes another energy source for energy-constrained typical MT. Therefore, RF wireless power transfer is a low-cost solution for sustainable operations of HCNs without modifying the hardware at the BS side.

1.3 Related Works

In this section, the related works of my thesis surrounding cognitive relay networks, MIMO in cognitive relay networks, security in cognitive relay networks, and RF wireless power transfer are discussed, respectively.

1.3.1 Cognitive Relay Networks

Relaying is regarded as a cost-effective approach for supporting high speed and long distance networks [59, 60]. Due to its dramatic enhancement in transmission reliability and coverage expansion, cognitive relay networks have attracted increasing research interests. Majority of existing studies on cognitive relay networks have focused on single-antenna protocols.

In [61] and [62], a two-phase protocol based on cooperative relaying was considered,

where the SU-Tx is acted as the decode-and-forward (DF) relay to decode the primary signal in the first phase, and the SU-Tx forwards the primary signal and the secondary signal simultaneously in the second phase. In [63], the conventional cooperative relaying technique was proposed in spectrum sharing network, where the average symbol error rates of secondary network with single DF relay case and multiple DF relays case were both examined. In [64], the outage probability of the secondary network with the best DF relay selection under the maximum transmit power constraint at the SU and the peak interference power constraint at the PU was examined. In [65], the outage probability of DF cognitive dual-hop systems under peak interference power constraint over Nakagami-m fading channels was evaluated.

In [66], the outage probability and the ergodic capacity of DF relay aided secondary network were studied under the peak interference constraints at the multiple PU-Rxs. In [67], the outage probability of a cyclic prefixed single-carrier relay network under the peak interference power constraint at the PU-Rx and the interference from the PU-Tx was analyzed. In [68], the exact and asymptotic outage probability, average symbol error rate, and ergodic capacity of cognitive relay network with best relay selection over non-identical Rayleigh fading were derived. In [69], the average bit error rate of secondary network with amplify-and-forward (AF) partial relay selection was addressed subject to peak and average interference power constraint at the PU-Rx, while in [70], the outage probability of secondary network with AF best relay selection under co-channel interference from the PU-Tx was addressed subject to average interference power constraint at the PU-Rx. In [71], the relay which maximizes the minimum signal-to-noise ratio (SNR) between the source-to-relay link and the relay-to-destination link was selected to assist the secondary transmission, the outage probability of secondary network with the proposed relay selection scheme was derived. The outage probability of secondary network with best relay based on different relay selection criterion was examined in [72–75]. In [76], the outage probability of a dual-hop cognitive relay network with multiple PU-Rxs and multiple secondary destinations (SDs) was derived. In [77], the impact of multiple

primary transceivers on the outage probability of dual hop single relay aided secondary network was examined.

1.3.2 MIMO in CNs

MIMO techniques, well-known for their benefits including enhanced reliability [78], spectral efficiency [79], and co-channel interference suppression [80], open up new dimensions for CR. For example, as shown in [81], with convex optimization techniques, spatial multiplexing and substantial capacity gains can be achieved by employing MIMO techniques.

To maximize the link reliability of the secondary network and minimize the interference at the primary network, receive diversity at the SU has been applied in interference-limited spectrum sharing networks. In [82, 83], MRC was applied at the SU. In [83], the impact of peak interference power constraint and maximum transmit power constraint on the ergodic capacity and the average symbol error rate of secondary network were characterized. In [82], it was shown that the estimation error due to imperfect channel information between the SU-Tx and the PU-Rx could be compensated by deploying MRC at the SU-Rx. In [84], without perfect channel state information, the effective capacity of spectrum sharing networks with GSC at the SU was examined over Rayleigh fading.

Different from [82–84], multiple antennas at the SU and the PU was considered in [85, 86]. In [85], the ergodic and outage capacity of secondary network with transmit antenna selection and receive MRC were analyzed. In [86], the ergodic capacity of secondary network with MRC at both PU and SU was examined under peak or average interference power constraints. Apart from capacity, the outage probability is another important metric to comprehend the fundamental limits of CR [87, 88]. In [89], the DF relay is able to help both the primary transmission and secondary transmission, it was shown that the outage probability at the PU-Rxs and the SU-Rxs with multiple

antennas and cognitive relaying outperform that without cognitive relaying. However, works in [82–84, 87–89] all assumed that the SU has full CSI between the SU-Tx and the PU-Rxs, and the impact of GSC in the presence of multiple primary transceivers under imperfect CSI in spectrum sharing network is less well understood.

The transmit diversity technique was studied in [90, 91]. In [90], the effect of TAS/MRC on the the ergodic capacity of secondary network under peak interference power constraint was analyzed. In [91], the exact and asymptotic outage probability of relay aided secondary network with TAS/MRC and TAS/SC were examined over Nakagami-m fading channel. However, the impact of TAS/GSC on spectrum sharing networks has not been well studied over Rayleigh fading channel and Nakagami-m fading channel.

1.3.3 Security in CNs

Recently, the research on enhancing the security at the physical layer of CNs has attracted continuously growing attention. In [92], multiple Eves try to intercept the secondary transmission under QoS constraint of primary network, multiuser scheduling was proposed to improve the security level of secondary transmission.

In [93], it was proved that beamforming (BF) is the optimal transmission strategy to secure multiple input single output (MISO) secondary network with perfect CSI of all channels. The authors then extended their work to the networks with imperfect CSI of the secondary channel, the interfering channel between the SU-Tx and the PU-Rx, and the eavesdropping channel in [94]. Note that [92–94] only considered stationary nodes. Nowadays, physical layer security has been introduced into large-scale wireless networks, such as cellular networks, ad hoc and sensor networks, where stochastic geometry and random geometric graphs are used for the modeling of these networks [95, 96]. This modeling approach captures the topological randomness of these networks, and provides a simple and tractable model to characterize the performance [30]. In [50], the secrecy

capacity of the primary network was discussed in CNs with the PUs, the SUs, and the Eves following the mutually independent homogeneous PPP, however, detailed analytical results and expressions have not been derived.

Various advanced techniques have been developed to steer up the security by enhancing the quality of the main link, whereas degrading the eavesdropper's link, such as the BF and AN-based technique [97–99]. In the AN-based method, the power allocation between the information-bearing signal and the AN at the transmitter is especially important, which reflects the tradeoff between enhancing the main channel by increasing the power allocated to information-bearing signal and degrading the eavesdropper's channel by allocating more power to the AN. In [100] and [101], an optimal power allocation strategy to enhance the security was investigated in the conventional wireless networks with fixed nodes, and wireless ad hoc network with mobile nodes, respectively. However, all these works [97–101] only considered physical layer security in non-spectrum sharing networks.

1.3.4 RF wireless power transfer

Simultaneous wireless information and power transfer (SWIPT) technique is proposed to realize the dual purpose of transporting the energy and information in the same waveform [102–104]. An upsurge of interest has piqued on applying SWIPT in orthogonal frequency division multiplexing (OFDM) systems [105], interference channels [106], two way channels [107], and relay channels [108].

Recently, RF wireless power transfer has been introduced into CNs in [109–116]. In [109], the energy harvesting was introduced in hybrid underlay-overlay CNs, in which the SU was chosen to sense the primary channel or harvest energy from primary channel when the primary channel is busy, and the SU only transmits the signal when primary channel is free. It was shown that the proposed hybrid underlay-overlay CNs can achieve higher throughput by harvesting energy from both ambient sources and primary chan-

nel than harvesting energy only from ambient sources. In [111], the SU-Tx harvested energy from the ambient signals, and opportunistically access the PU's spectrum. An optimal spectrum sensing policy which aims to maximize the throughput subject to an energy constraint and a collision constraint was investigated. In [110], an optimal mode selection policy that the SU switches between energy harvesting mode and access mode was proposed to maximize the total throughput of CR sensor networks. In [112], the throughput of overlay spectrum sharing network with SWIPT at AF secondary relay (SR) was maximized via joint optimization of power splitter factor and relay energy allocation. In [116], the transmission probability of the SU-Txs and the throughput of secondary network were examined in a CNs with harvesting zone around the PU-Tx, and guard zone around the PU-Rx. The SU-Tx is permitted to harvest energy from ambient RF signal when it is inside the harvesting zone, and is allowed to transmit signal when it is outside the guard zone. In [114], the outage probability was analyzed for the primary network and the secondary network where the SU can harvest energy from the PU-Tx while assisting the primary transmission. Note that the aforementioned studies have not considered underlay CNs.

In [113, 115], the RF wireless power transfer was studied in underlay CNs. In [113], the sum of harvested power at the multiple SU-Rxs in a MIMO underlay CNs with SWIPT was maximized subject to two constraints (i.e., a target minimum-square-error at multiple CR information receivers and the peak interference power constraint at the PU-Rxs). In [115], multiuser scheduling SWIPT for the DL secondary network was studied in underlay spectrum sharing network, where the SU-Rx can choose either information decoding mode or energy harvesting mode.

One practical application of RF wirelss power transfer is the wireless powered communication network (WPCN), in which the mobile users perform UL information transmission using the energy harvested from the DL wireless power transmission [117]. In [117], the harvest-then-transmit protocol was proposed where the distributed users with no other energy sources harvest energy from the hybrid access point (H-AP) with constant

energy supply via the DL, and then utilize the stored energy to power the operating circuits and transmit information to the H-AP through time division multiple access (TDMA) in the UL. The work in [117] has been extended to WPCNs in [118] where all users transmit to multi-antenna H-AP via space-division-multiple-access (SDMA) using the energy harvested from the DL energy beamfoming. It was shown that the double-near-far problem that the geographically remote users harvest less energy but with high energy demand for UL information transmission, can be alleviated by controlling user transmit power in the UL and designing the energy BF. Various techniques such as the user cooperation [119], full-duplex transmission [120], and massive MIMO [121] were proposed to enhance the performance of WPCNs.

Different from the above single-cell WPCNs [117–121], multi-cell WPCNs were studied in [57, 122]. In [57], the energy sources, namely, power beacons, were implemented in the existing cellular network to power the UL information transmission of mobile devices. Using the stochastic geometry modeling, the tradeoff between the network parameters was studied for isotropic and directed microwave power transfer cellular networks with small/large energy storage mobile devices. In [122], a cognitive underlay device-to-device (D2D) communication in multi-channel cellular networks was considered, where the D2D transmitters harvest energy from the DL and the UL information transmission of macro base stations (BSs) and cellular users. It was shown that RF wireless power transfer is an efficient way to provide sufficient energy without jeopardizing the performance of the cognitive D2D communication. Note that the RF wireless power transfer has never been explored in HCNs.

1.4 Research Contents and Contributions

Spectrum Sharing Networks with GSC: In Chapter 3, GSC is proposed for underlay spectrum sharing networks in the presence of multiple primary transceivers with outdated channel information. The main motivation is to determine the impact of GSC and

outdated channel information on the outage probability of CNs subject to two practical power constraints: 1) the maximum transmit power constraint at the SU-Tx, and 2) the peak interference power constraint at the PU-Rx. The new closed-form expressions for the exact and asymptotic outage probability are derived in Rayleigh fading. Those expressions provide concise representations of the diversity order and the array gain. It is revealed that the diversity order of GSC is entirely dependent on the secondary network and is equal to the available number of receive antennas at the SU. This result is consistent with those of MRC and SC. More importantly, it is shown that the outage probability decreases with increasing the correlation coefficient of the outdated channel.

Spectrum Sharing Networks with TAS/GSC: In Chapters 4 and 5, TAS/GSC is proposed in dual-hop cognitive DF relay networks for reliability enhancement and interference relaxation. In this setting, a single antenna which maximizes the receive SNR is selected at the SU-Tx and a subset of receive antennas with the highest SNRs are combined at the SU-Rx.

To demonstrate the advantages of the proposed framework over Rayleigh fading, the new exact closed-form expressions for the outage probability and the symbol error rate of the secondary network are derived. Easy-to-evaluate asymptotic expressions are also derived in the high SNR regime to gain practical insights. Several important design insights are reached. Under the proportional interference power constraint, the full diversity gain is achieved and is entirely determined by the total number of antennas available in the secondary network. The positive impact of the number of receive antennas combined and the negative impact of the number of primary users on the secondary network are showcased by the SNR gain. Under the fixed interference power constraint, the error floors are displayed and the diversity gain is lost.

In an effort to assess the performance improvement brought by TAS/GSC over Nakagami-m fading channels, the new exact closed-form expressions for the outage probability, the symbol error rate, and the ergodic capacity are derived. More importantly, by deriving the asymptotic expressions for the outage probability and the symbol error rate,

as well as the high SNR approximations of the ergodic capacity, new design insights are established under the two distinct constraint scenarios: 1) the proportional interference power constraint, and 2) the fixed interference power constraint. For the first scenario, the high SNR slope of the ergodic capacity is 1/2. For the second scenario, the high SNR slope of the ergodic capacity is zero with capacity ceiling.

Physical Layer Security in Large-Scale Spectrum Sharing Networks: Chapter 6 introduces BF&AN at the SU-Txs to establish secure transmission in large-scale spectrum sharing networks, where multiple non-colluding Eves attempt to intercept the secondary transmission. A comprehensive analytical framework to accurately assess the secrecy performance under the QoS constraint of primary network is developed. The aim is to characterize the impact of BF&AN on this complex large-scale network. The exact expressions for the average secrecy rate and the secrecy outage probability are first derived. Then, easy-to-evaluate asymptotic average secrecy rate and asymptotic secrecy outage probability when the number of antennas at the SU-Tx goes to infinity are derived. The results show that there exists an average secrecy rate wall beyond which the QoS of primary network is violated. Interestingly, it is revealed that different from the conventional network with fixed nodes, where equal power allocation achieves near optimal average secrecy rate, the equal power allocation may not bring optimal average secrecy rate for large-scale spectrum sharing networks.

RF Wireless Power Transfer in Cognitive Relay Networks: In Chapter 7, a new energy harvesting protocol is proposed for an underlay cognitive relay network with the PU transceivers. In this protocol, the secondary nodes can harvest energy from the primary network while sharing the licensed spectrum belongs to the PU. In order to assess the impact of different system parameters on the proposed network, the exact expressions for the outage probability, the throughput for both the delay-sensitive and the delay-tolerant transmission modes are derived. To obtain practical design insights, the asymptotic closed-form expressions for the outage probability and the delay-sensitive throughput and the delay-tolerant throughput as the number of PU transceivers goes to

infinity are also derived. The results show that the outage probability improves when PU-Txs are located near secondary source (SS) and sufficiently far from SR and SD. The results show that when the number of PU-Txs is large, the detrimental effect of interference from the PU-Txs outweighs the benefits of energy harvested from the PU-Txs.

RF Wireless Power Transfer in HCNs: In Chapter 8, the DL wireless power transfer and UL information transmission of K-tier HCNs with randomly located BSs and MTs are modeled and analyzed. In the DL and UL, each energy-constrained MT pairs up with its corresponding BSs, which provides the maximum received power at the MT. Due to the densely located BSs and universal frequency reuse between all tiers in HCNs, the typical MT is allowed to harvest energy from typical BS by direct BF and from other interfering BSs via interference signals. Equipped with a large storage battery, the typical MT utilizes the harvested energy to provide constant transmit power for the UL transmission. Stochastic geometry is used to model the proposed networks and evaluate the intrinsic relationship between the energy harvested from BS in the DL and the UL transmission performance. The expressions for the average received power at MT, the UL outage probability, and the UL average ergodic rate are first derived. The asymptotic expressions for the average received power, the UL outage probability, and the UL average ergodic rate, as the number of BS antennas goes to infinity, are then derived. The results show that, on one hand, the overall outage probability and overall average ergodic rate are not significantly improved by increasing the time allocation factor and improving the energy conversion efficiency, but on the other hand the UL performance can be largely enhanced by using massive antenna arrays at the BSs.

1.5 Author's Publication

Submitted Journal Papers

1. **Y. Deng**, K. J. Kim, T. Q. Duong, M. Elkashlan, George K. Karagiannidis, and A. Nallanathan, "Full-Duplex Spectrum Sharing in Cooperative Single Carrier Systems with Amplify-and-Forward Relays," *IEEE Trans. on Commun.*, under review.

2. **Y. Deng**, L. Wang, S. A. R. Zaidi, J. Yuan, and M. Elkashlan, "Enhancing security in large-scale spectrum sharing networks," *IEEE Trans. on Wireless Commun.*, under review.

3. **Y. Deng**, L. Wang, M. Elkashlan, M. Di Renzo, and J. Yuan, "K-tier Heterogeneous Cellular Networks with Wireless Power Transfer," *IEEE Trans. Wireless Commun.*, under review.

4. **Y. Deng**, L. Wang, M. Elkashlan, A. Nallanathan, and R. Mallik, "Physical Layer Security in Three-Tier Wireless Sensor Networks: A Stochastic Geometry Approach," *IEEE Trans. on Commun.*, under review.

5. S. A. Mousavifar, Y. Liu, **Y. Deng**, C. Leung, and M. Elkashlan, "Wireless Energy Harvesting in a Cognitive Relay Networ", *IEEE Trans. Wireless Commun.*, under review.

Author's Publication/Accepted Journal Papers

1. **Y. Deng**, M. Elkashlan, N. Yang, P. L. Yeoh, and R. Mallik, "Impact of primary network on secondary network with generalized selection combining," *IEEE Trans. Veh. Technol.*, vol.16, no.11, pp.1792-1795, Nov. 2014.

2. **Y. Deng**, M. Elkashlan, P. L. Yeoh, N. Yang, and R. Mallik, "Cognitive MIMO

relay networks with generalized selection combining," *IEEE Trans. Wireless Commun.*, vol.13, no.9, pp.4911-4922, Sept. 2014

3. **Y. Deng**, L. Wang, M. Elkashlan, K. J. Kim, T. Q. Duong, "Generalized selection combining for cognitive relay networks over Nakagami-m fading," *IEEE Trans. on Signal Process.*, accepted to appear.

Conference papers

1. **Y. Deng**, M. Elkashlan, P. L. Yeoh, T. Q. Duong, and R. K. Mallik, "Generalized selection combining in cognitive MIMO relay networks," *Proc. IEEE Int. Communications Conf. (ICC'14)*, Sydney, Australia, Jun. 2014, pp.1472-1477.

2. **Y. Deng**, L. Wang, M. Elkashlan, K. J. Kim, and T. Q. Duong, "Ergodic capacity of cognitive TAS/GSC relaying in Nakagami-m fading channels," *Proc. IEEE Int. Communications Conf. (ICC'14)*, Sydney, Australia, Jun. 2014, pp.5348-5353.

3. M. Egan, **Y. Deng**, M. Elkashlan, and T. Q. Duong, "Variance-constrained capacity of the molecular timing channel with synchronization error," *Proc. IEEE Global Telecommunications Conference (Globecom 14')*, Austin, USA, Dec. 2014.

4. **Y. Deng**, K. J. Kim, T. Q. Duong, M. Elkashlan, George K. Karagiannidis, and A. Nallanathan, "Full-Duplex Spectrum Sharing in Cooperative Single Carrier Systems with Amplify-and-Forward Relays," in Proc. IEEE Wireless Commun. Netw. Conf. (WCNC 15'), New Orleans, USA, March. 2015.

5. **Y. Deng**, L. Wang, S. A. R. Zaidi, J. Yuan, and M. Elkashlan, "On the Security of Large-Scale Spectrum Sharing Networks," in Proc. IEEE Int. Communications Conf. (ICC'15), London, UK, Jun. 2015.

1.6 Thesis Organization

The reminder of this thesis is organized as follows. Chapter 2 introduces the background knowledge of this thesis. The technical contributions of this thesis are covered from Chapters 3 through 8. Chapter 3 proposes GSC as a low-power design in interference-limited spectrum sharing networks under outdated CSI between the SU-Tx and the PU-Rxs. Chapters 4 and 5 propose TAS/GSC in dual-hop cognitive relay networks for reliability enhancement and interference relaxation over Rayleigh fading and Nakagami-m fading, respectively. Chapter 6 proposes the BF&AN as an effective way to enhance the secure transmission of large-scale spectrum sharing networks. Chapter 7 presents a new energy harvesting protocol for dual-hop cognitive relay networks as an energy supply for the energy-constrained secondary network. Chapter 8 studies the UL performance of K-tier HCNs with RF wireless power transfer. Chapter 9 concludes the thesis and discusses the future research directions.

Chapter 2

Fundamental Concepts

This chapter provides the background knowledge for the technical works presented in the rest of the Chapters. The basic fading channel characterization, MIMO techniques, and cooperative relaying are first presented. Stochastic geometry modeling of large-scale wireless networks is then introduced for a complete understanding of the technical works in Chapter 6 and 8. The concept of physical layer security and RF wireless power transfer are described in the last two sections of this Chapter, which lays a solid foundation for the technical works in Chapters 6, 7, and 8.

2.1 Fading Channel Characterization

Fading is an important characteristic for the wireless communication channel, which is a deviation affecting a signal over certain propagation media. It is a complicated phenomenon which results from multipath and shadowing, as shown in Fig. 2.1. Regardless of its complexity, many research works have formulated the statistical model for fading channels. The fading effects can be categorized into large scale and small scale fading.

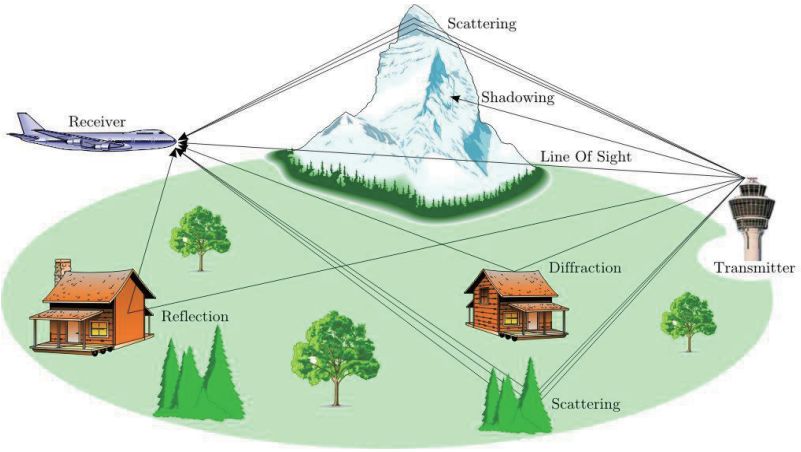

Figure 2.1: The fading effect [5].

2.1.1 Large Scale Fading

The large scale fading are mostly due to the path loss and the shadowing by large obstacles. In this thesis, the effect of shadowing is not considered, since it is highly dependent on the practical environment, such as the surrounded tall buildings and mountains. In the path loss model, the power degrades relative to the distance. In order to capture the main characteristics of ray tracing, the following simplified model is used

$$P_r = P_t K \left[\frac{d_0}{d}\right]^{\alpha}, \tag{2.1}$$

where K is a constant factor, d_0 is a reference distance, and α is the path loss exponent. The simplified path loss model is used in Chapters 6, 7, and 8.

2.1.2 Small Scale Fading

The small scale fading is due to the multipath effect that the transmitted signals experience rapid fluctuation over short period of time. According to the relationship between the signal parameters (bandwidth, symbol period) and the channel parameters (coherence time, coherence bandwidth), different types of transmitted signals experience dif-

ferent types of fading. Based on the multipath time delay spread, the small scale fading can be classified into slow fading and fast fading [123]. If the symbol time duration is smaller than the the coherence time, then we regard it as the slow fading. Conversely, we regard it as the fast fading. Throughout my thesis, the slow fading is considered where the amplitude and phase change through the propagation channel can be viewed as constant.

Another type of classification is flat fading and frequency-selective fading based on doppler spread, which depends on the frequency selectivity characteristic of fading channels [123]. In flat fading, the bandwidth of transmitted signal is much smaller than the coherence bandwidth, and the magnitude of fading will be the same for different frequency. While the bandwidth of transmitted signal is bigger than the coherence bandwidth in frequency-selective fading, and different frequency experience different degree of fading. We will further explore the flat fading in Chapters 3 - 8.

In the following, several typical channel models describing the statistical behavior of multipath effect used in this thesis are presented.

2.1.2.1 Rayleigh Fading

Rayleigh fading is a widely used multipath model, which assumes that the magnitude of a signal changes randomly through the propagation according to the Rayleigh distribution [124]. This model is highly applicable to model the effect of urban area with heavily loaded buildings when there is no direct line-of-sight (LOS) path. The probability density function (PDF) of the channel power gain $|h|^2$ is given by

$$f_{|h|^2}(\gamma) = \frac{1}{\bar{\gamma}} \exp\left(-\frac{\gamma}{\bar{\gamma}}\right), \tag{2.2}$$

where $\bar{\gamma} = \mathbb{E}\left[|h|^2\right]$.

2.1.2.2 Nakagami-m Fading

Nakagami-m fading is a more general fading model which includes Rayleigh fading and Rician fading as special cases. More importantly, the Nakagami-m fading environment has the versatility in providing a good match to various empirically obtained measurement data [125]. The channel power gain are Gamma distributed with fading severity parameters m. The PDF of the channel power gains $|h|^2$ is given by

$$f_{|h|^2}(\gamma) = \frac{m^m \gamma^{m-1}}{\Gamma(m)\,\bar{\gamma}^m} e^{-\frac{m\gamma}{\bar{\gamma}}}, \tag{2.3}$$

where $\bar{\gamma} = \mathbb{E}\left[|h|^2\right]$ and $\Gamma()$ is the Gamma function.

2.2 Multiple Antennas systems

Multiple antennas equipped at the transmitter/receiver can exploit the space dimension to improve wireless systems capacity, range, and reliability, by taking advantage of the multipath effect. Introducing multiple antennas into the wireless communication system, the diversity and SNR gains are achieved compared with single antenna system [126, 127]. Diversity gain is the enhancement of reliability obtained by combining multiple received copies of transmitted signal. It measures how fast the probability level of outage can be reduced by increasing SNR. The SNR gain quantifies the increase in average received SNR obtained by coherently combining the incoming/outgoing signals. In the following, several multiple antenna techniques used in this thesis are listed.

2.2.1 TAS

TAS technology has been acknowledged as a core component for UL 4G long term evolution (LTE) and LTE Advanced systems due to its low feedback requirement compared with closed-loop transmit diversity [128]. In TAS, the signal is multiplied by a

branch weight associated with a specific antenna before transmission. Then, the transmit antenna which achieves the largest receive SNR at the receiver is selected for data transmission. Note that only the index of the selected transmit antenna needs to be fed back to the transmitter. This technique is used in Chapters 4 and 5.

2.2.2 GSC

With the merits of low power requirement and RF cost, GSC offers a performance/implementation tradeoff between MRC and SC for the secondary network [45, 46], and it is well applied to commercial wireless networks where the receiver is subject to resource constraints, such as limited RF chains due to size and complexity limitations [26]. In Fig. 2.2 , the GSC receiver estimates the SNR of each receive antenna, and then ranks those SNRs in decreasing order. Among all the SNRs of receive antenna, the first L_c branches with larger SNRs are selected as receiving antennas, and the SNRs of those selected L_c antennas are combined to be the total SNR. We also see that, by excluding the antenna chains with weak channel powers, GSC can be more robust to channel estimation errors than MRC [129]. This technique is used in Chapters 3, 4, and 5.

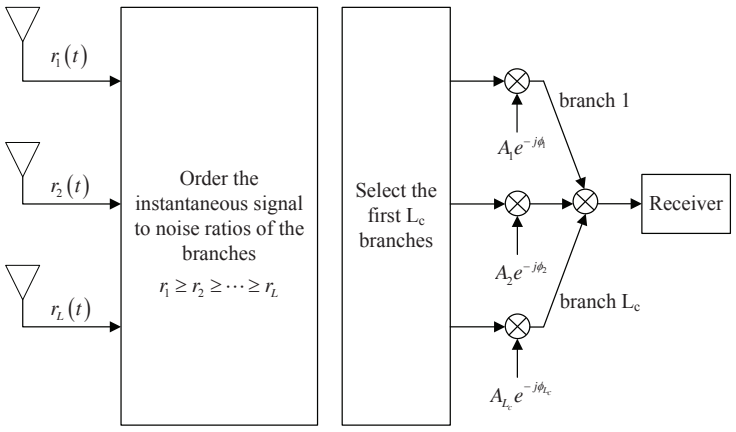

Figure 2.2: The GSC receiver [6].

2.2.3 BF

BF has become a promising candidate for the DL transmission between access point and user in the 802.11ac standard [130, 131]. Instead of omnidirectional antennas where energy is sent in all directions, BF technique can focus energy toward a receiver by controlling the amplitude and phase of each antenna. For a MISO channel with N transmit antenna and single receive antenna, the signal before transmission will be multiplied by a BF vector as

$$\mathbf{x} = \frac{\mathbf{h}^H}{\|\mathbf{h}\|}\tilde{x}. \tag{2.4}$$

Then the transmitted signal propagates through the channel can be expressed as

$$y = \mathbf{h}\mathbf{x} + n = \|\mathbf{h}\|\tilde{x} + n, \tag{2.5}$$

where $\mathbf{h} = [h_1, \ldots, h_N]$, and $n \sim \mathcal{CN}(0, \sigma^2)$ is the additive Gaussian noise. The resulting SNR is given by $\gamma = \frac{P\|\mathbf{h}\|^2}{\sigma^2}$. Here, P is the power constraint. Chapter 8 is based on this technique.

2.2.4 MRC

As in Fig. 2.3, with MRC, the output received signal is a weighted sum of all antennas [132]. For a SIMO channel with single transmit antenna and N receive antenna, the transmitted signal propagates through the channel can be expressed as

$$y = \mathbf{h}x + \mathbf{n}, \tag{2.6}$$

where $\mathbf{h} = [h_1, \ldots, h_N]$, and $\boldsymbol{n} \sim \mathcal{CN}(\mathbf{0}, \sigma^2 \mathbf{I}_N)$ is the additive Gaussian noise. The detected received signal after MRC is

$$\tilde{y} = \frac{\mathbf{h}^H}{\|\mathbf{h}\|} y = \|\mathbf{h}\| x + \frac{\mathbf{h}^H}{\|\mathbf{h}\|} \mathbf{n}. \tag{2.7}$$

The resulted SNR is given by $\gamma = \frac{P\|\mathbf{h}\|^2}{\sigma^2}$, which is the largest achievable received SNR. It will be further discussed in Chapter 8.

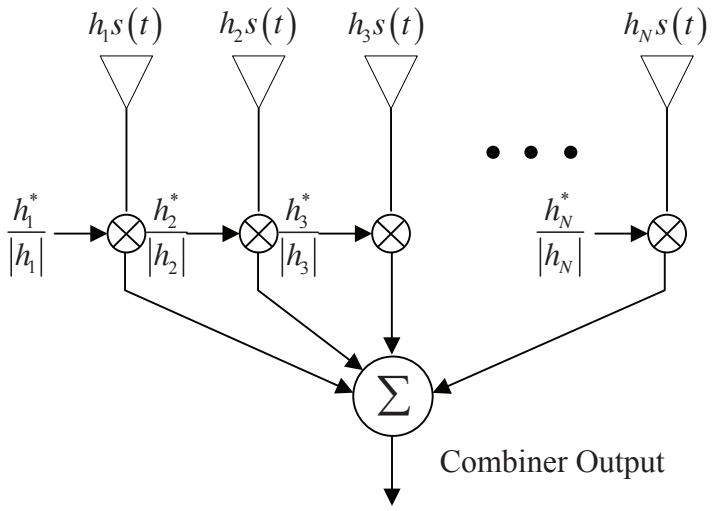

Figure 2.3: The MRC receiver .

2.3 Cooperative Communication

The benefits brought by MIMO systems are well known, however, for some scenarios, such as nodes in wireless sensor networks or handsets, size, hardware, and cost have limitations that render the multiple antennas deployment. Herein, the cooperative communication arises as a technology which makes the benefits of MIMO systems becomes accessible for single antenna nodes. In detail, cooperative communication allows single-antenna nodes in a multi-node scenario to share their antennas to create a virtual MIMO network. As such, this allows nodes with diverse radio resources (power, bandwidth, and channel

qualities) to cooperate and relay each other's messages to the destination. It is further known that cooperative communications has been included in 3GPP LTE-Advanced (LTE-A) [133].

Relay can operate in full-duplex mode and half-duplex mode. In full-duplex mode, the reception and transmission of signal at the relay can be operated simultaneously, which means that the source-to-relay link and relay-to-destination share a common time-frequency signal-space. In half-duplex mode, the orthogonality exists between transmitted and received signals at the relay in time or frequency domain. From the theoretical point of view, the full-duplex relaying outperforms the half-duplex relaying in terms of spectral efficiency. From the implementation point of view, the full-duplex relaying loses its superiority due to the self-interference between the transmit antenna and receive antenna. More details and investigations of half-duplex relaying are presented in Chapters 4, 5, and 7.

Depending on how the information processed at the relay, the relaying protocol can be categorized into AF relaying protocol and DF relaying protocol [132].

2.3.1 AF Relaying Protocol

As shown in Fig. 2.4, once the relay receives the noisy version of signal from source, it amplifies and retransmits the received signal to the destination. As can be seen that the noise is also amplified during this AF process, however, the destination can receive and combine two copies of signal with MRC, one from source, and the other one from relay. Thus, this protocol achieves the diversity order of two. In this protocol, the instantaneous mutual information is given by

$$I_{AF} = \frac{1}{2}\log\left(1 + \gamma_{sd} + \frac{\gamma_{sr}\gamma_{rd}}{\gamma_{sr} + \gamma_{rd} + 1}\right), \tag{2.8}$$

where $\gamma_{s,d}, \gamma_{s,r}, \gamma_{r,d}$ are the instantaneous SNR of source-to-destination link, source-to-relay link, and relay-to-destination link.

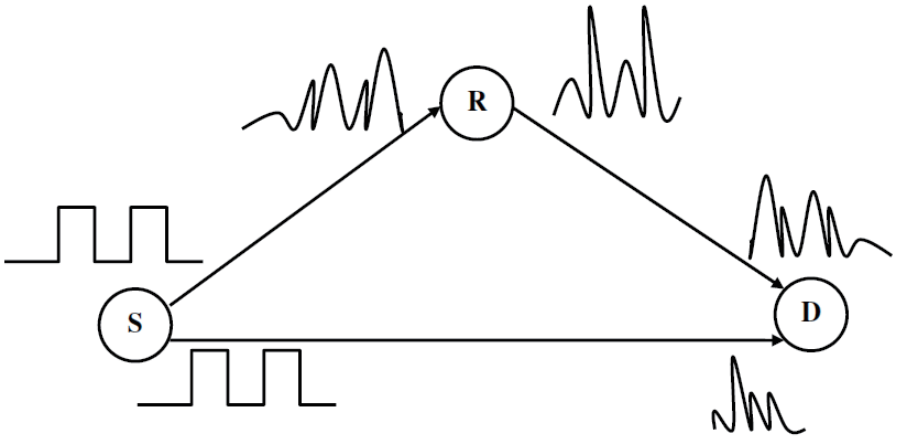

Figure 2.4: The AF relaying [7].

2.3.2 DF Relaying Protocol

As shown in Fig. 2.5, the relay decodes the received signal from source, and re-encodes it to transmit to the destination. In this case, the decoding process for the received signal at the relay may exists error, which degrades the end-to-end performance. Thus, the mutual information between the source and destination is determined by the mutual information of the weaker link between the source-to-relay link and the combined source-to-destination link and relay-to-destination link. The mutual information between the source and destination can be expressed as

$$I_{DF} = \frac{1}{2} \min \left\{ \log\left(1+\gamma_{sd}\right), \log\left(1+\gamma_{sd}+\gamma_{rd}\right) \right\}. \tag{2.9}$$

The DF relay is investigated in Chapters 4, 5, and 7.

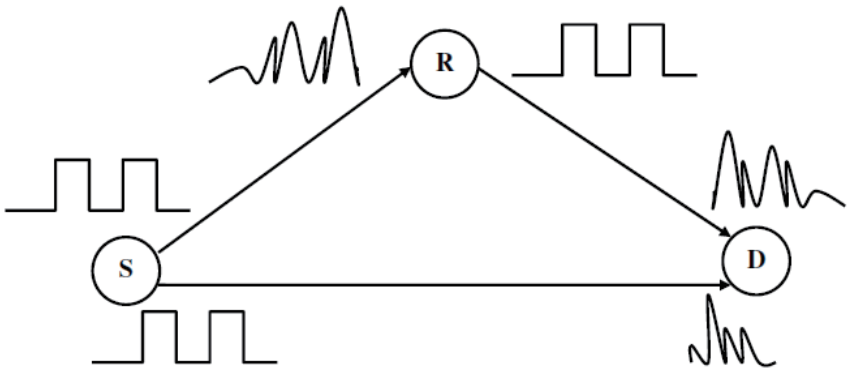

Figure 2.5: The DF relaying [7].

2.4 Stochastic Geometry Methods for Large-Scale Wireless Network

Recently, large-scale networks, where a large number of nodes randomly deployed in a vast spatial area, is becoming popular in modeling the emerging wireless networks, such as ad hoc, sensor networks and single-tier/multi-tier cellular networks. In large-scale networks, there exists high uncertainty on the locations and channels of wireless terminals. In this case, the stochastic geometry is proposed as a simple and tractable approach to study the average behavior over many spatial realizations of network with its location following a specific probability distribution [134].

2.4.1 Point Process

To analyze the large-scale wireless networks, point process is the basic spatial model, which can represent a random accumulation of points that are located in a large geographical area. The point process is defined as a measurable mapping Φ from some probability space to the space of point measures on area A, which is given by a discrete

sum of Dirac measures on A as [135]

$$\Phi = \sum_i \delta_{X_i}, \tag{2.10}$$

where $\{X_i\}$ are the points of Φ.

The intensity measure Λ is given as

$$\Lambda(B) = \mathbb{E}\Phi(B), \tag{2.11}$$

where $\Phi(B)$ denotes the number of points in $\Phi \cap B$.

2.4.2 Poisson Point Process

The general point process becomes PPP only when 1) All the disjoint subsets satisfy $S_1, \cdots, S_n \subset A$; 2) Any random variable $\Phi(S_i)$, $i \in [1, \cdots, n]$ is Poisson [134]. Depending on the relationship between the density and the node's location, the PPP can be categorized as homogeneous PPP and inhomogeneous PPP. The density of homogeneous PPP is independent of location, while the density of inhomogeneous PPP is a function of location. In Chapters 6 and 8, the homogeneous PPP is considered.

In order to model the aggregate interference from the interfering transmitters, which are distributed following homogeneous PPP, our focus is on the decaying power law shot noise process. Let us first define a shot noise process $I(t) = \sum_j f(h_j, t - t_j)$, where the arrival time $\{t_j\}$ are Poisson with arrival rate μ, and $\{h_j\}$ are i.i.d random variables following some distribution. By taking h_j from a discrete set $H_1, H_2, \cdots$ with probability $p_1, p_2, \cdots$, the shot noise process can be represented as $I(t) = \sum_i F_i(t)$, where $F_i(t) = \sum_j f(H_i, t - t_j)$ is the sum of deterministic impulse response with Poisson arrival and

constant H_i [136]. The moment generating function of $F(t)$ can be expressed as

$$\Phi(s) = \mathbb{E}\left[e^{-s\sum_i F_i(t)}\right] = \prod_i \Phi_i(s). \tag{2.12}$$

According to the deterministic impulse response in [137], $\Phi(s)$ is derived as

$$\Phi(s) = \exp\left\{-\mu \int_{-\infty}^{\infty} \mathbb{E}_h\left(1 - \exp\left\{-sf(h,t)\right\}\right) dt\right\}. \tag{2.13}$$

For decaying power law shot noise process, it is known that $f(h,t) = ht^{-\alpha},\ t \in (0,\infty)$, thus

$$\Phi(s) = \exp\left\{-\mu \mathbb{E}_h\left[h^{1/\alpha}\right] \Gamma(1 - 1/\alpha)\, s^{1/\alpha}\right\}. \tag{2.14}$$

To calculate the mean of a sum over a point process, the Campbell's theorem is presented in the following theorem.

Theorem 1. *Let Φ be a point process on $\mathbb{R}^d$ and f, the random sum $S = \sum_{x\in\Phi} f(x)$, the mean of the random sum is [31]*

$$\mathbb{E}S = \int_{\mathbb{R}^d} f(x)\, \lambda dx, \tag{2.15}$$

where λ is the intensity of Φ.

2.5 Physical Layer Security

One inherent characteristic of wireless communication is broadcasting, which allows the transmitted signal received by other unintended receivers, and makes the intended transmission vulnerable to security threats, such as eavesdropping, jamming, and network injection. The burst growth of wide range of wireless networks and applications, such as

D2D and HCNs, coexists with each other, further imposes challenges for secure transmission. The security and privacy has been of long-standing importance for wireless networks, especially for military networks.

Traditional security is always addressed above the physical layer. For example, the widely applied key-based cryptographic technique is operated at the higher layer, while the error-free link is assumed to be established in the physical layer. Two main cryptographic protocols to combat eavesdropping are public-key and private-key protocol. In public-key protocol, it is assumed that the Eves are unable to decrypt the secure information, due to its limited computational power and lack of capability to decrypt the encryption keys [138, 139]. In private-key protocol, the random encryption keys are only shared between the legitimate transmitter and receiver, thus brings difficulty for the Eves to capture the knowledge of the encryption keys [140]. These protocols both assume that it is computationally infeasible for the Eves to decipher the key, but this is still mathematically questionable. With the improvement of Eves' capability in computing and deciphering, the security measure implementation in physical layer may be a cost-effective complement for the key-based cryptographic techniques [141].

The physical layer security is based on Wyner's wire-tap channel theory, in which the secret bits transmission can be achieved using the superiority of main channel over eavesdropping channel. By exploiting the randomness of fading channel with noise, the secret information can be securely transmitted through the main channel, and be kept confidential from the Eves. In [142], it is shown that the positive maximum transmission rate can be achieved when the eavesdropping channel is more"noisier" than the main channel. With proper channel coding (wiretap code), the secret message can be safely received by the legitimate receiver without information leakage to the Eves.

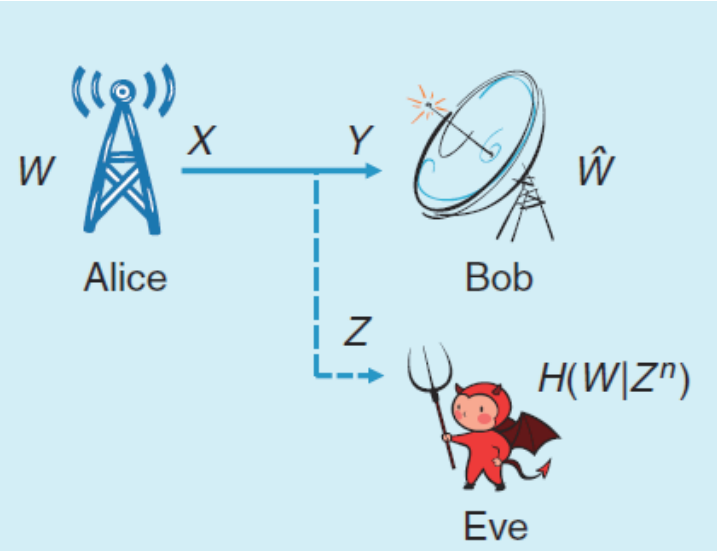

Figure 2.6: The physical layer security model [8].

Fig. 2.6 plots the Wyner's wiretap channel model with noisy channel, where Alice transmits confidential information to Bob, while Eve overhears their transmission. In this general wiretap channel, the secrecy capacity is defined as

$$C_s = \max_X I(X;Y) - I(X;Z), \tag{2.16}$$

where $I(X;Z)$ is the confusion rate. Based on the information theory, it is known that as long as the code rate is no larger than C_s, Bob can successfully decode the confidential message and the confusion message. However, those messages are viewed very similar for Eve, due to its channel decoding ability limited by $I(X;Z)$. In this case, the difference between the main channel and eavesdropper channel gives possibility for the confidential message transmission [8]. Physical layer security is further discussed in Chapter 6.

2.6 RF Wireless Power Transfer

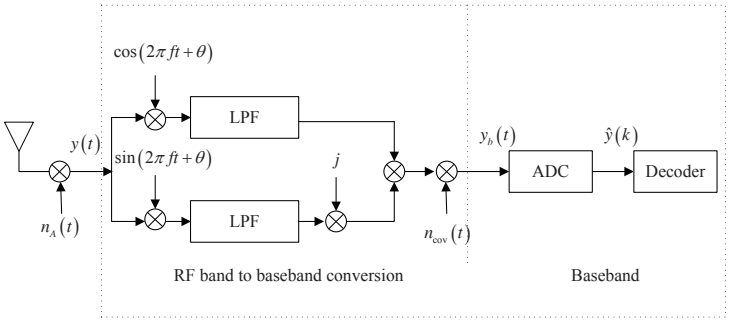

Figure 2.7: Information receiver [9].

With the recent advances in hardware and antenna design, RF wireless power transfer has become a promising technique to improve the energy efficiency of wireless networks, especially for those energy-constrained wireless networks with limited device battery life. Traditional energy harvesting sources, such as solar, wind, hydroelectric, thermoelectric may not always be accessible in some locations or environments. Alternatively, RF wireless power transfer can be a cost-effective energy harvesting technique that enables energy harvested from ambient RF signals, that are radiated by the RF signal transmitters [143]. This technique is usually operated on the electromagnetic wave signals with frequency from 3 kHz to 300 GHz. The applications of RF wireless power transfer include wireless sensor networks [144], wireless charging system [55], wireless body sensor networks [145], as well as cellular networks [57].

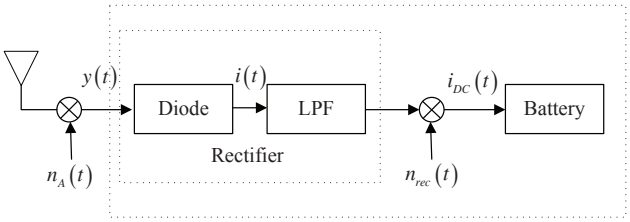

Figure 2.8: Energy receiver [9].

SWIPT was first advocated in [104], where the RF signals are utilized as energy and information carrier at the same time. As such, the energy-constrained wireless network becomes self-sustainable without the need to update the hardware at the transmitter. The authors in [104] propose two receiver designs for co-located receiver, namely time switching and power splitting. Here, co-located receiver is a bifunctional receiver which enable information decoding and energy harvesting at the same antennas. In the time switching receiver, the receive antenna switches between the energy harvesting block and the information decoding block periodically. In the power splitting receiver, the received signal is divided into two stream, one for energy harvesting, and the other one for information decoding.

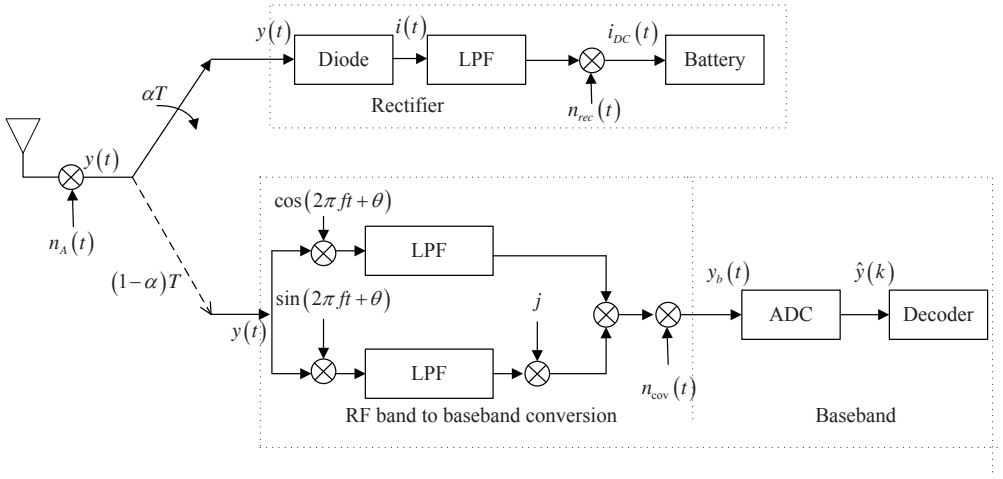

Figure 2.9: Time switching receiver [9].

In [9], a practical receiver design was studied for the information and energy receivers. Fig. 2.7 shows the information receiver design that the RF band signal is first converted to the baseband signal with coherent demodulation, then the analog-to-digital converter (ADC) is used to sample and digitalize the complex baseband signal, after that the decoding process is operated. The energy receiver design is considered in Fig. 2.8 using the rectenna architecture. The RF band received signal first goes through the rectifier with a Schottky diode and a passive low-pass filter (LPF) to be converted to direct

current (DC) signal. The DC signal is then stored by charging the battery. More details concerning the signal processing is found in [9]. With information and energy receiver design, the time switching receiver and power splitting receiver are presented in Fig. 2.9 and Fig. 2.10, respectively, where T is the block transmission time, α is the fraction of the block time for energy harvesting, and ρ is the the fraction of power allocated for energy harvesting.

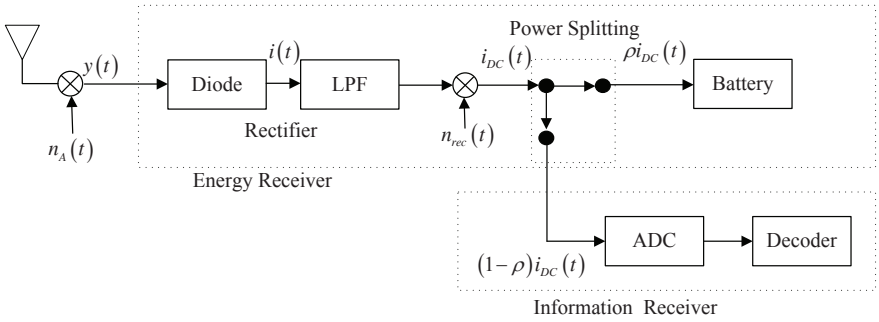

Figure 2.10: Power splitting receiver [9].

Chapter 3

Impact of primary network on secondary network with generalized selection combining over Rayleigh Fading

3.1 Introduction

In this chapter, CR is viewed from the viewpoint of GSC as a low power design in interference-limited spectrum sharing networks under outdated CSI between the SU-Tx and the PU-Rxs. A general scenario where the SU transmits in the presence of M PU-Txs and M PU-Rxs is considered. The main objective is to lower the interference power at the PU while guaranteeing transmission reliability at the SU, which can be achieved by determining varied numbers of combining antennas at the SU-Rx using GSC. Note that GSC compromises the merits of robust performance of maximal ratio combining and simplicity of selection combining. Different from previous works, the SU are allowed to select a subset of their receive antennas so as to balance the SU transmit power and the PU interference power. By doing so, less transmit power at the SU-Tx is required to achieve the same outage performance, which in turn reduces the interference at the PU-Rxs.

To answer some of the pressing questions that face spectrum sharing networks, the

maximum transmit power at the SU is related with the peak interference power at the PU. Outcomes are presented in the form of new expressions for the exact and the asymptotic outage probability of secondary network. The results bridge the gap between MRC and SC by allowing the SU to combine the L_c strongest out of its L available receive antennas. It is shown that the full diversity order is achieved, and is entirely determined by the secondary network and equal to L. The performance gaps between GSC, MRC, and SC are presented as a simple ratio of their respective SNR gains. An interesting conclusion is reached that M imposes a negative impact on the outage probability, while L_c has a positive impact on the outage probability. Furthermore, the outage probability decreases with increasing correlation coefficient of the outdated CSI channel.

3.2 Network and Channel Description

A realistic underlay spectrum sharing network with one pair of SU transceiver and M pairs of PU transceivers is considered. In the secondary network, the receiver diversity is assumed where the SU-Rx is equipped with L receive antennas. The L_c receive antennas are selected based on the channel from the SU-Tx to the SU-Rx. All other terminals are equipped with only one antenna. Only partial channel knowledge of the interference channel from the SU-Tx to the PU-Rxs is available at the SU-Tx. The CSI of h_{1m} provided to the SU-Tx is outdated due to the time-varying nature of the wireless link [146]. The outdated CSI of the SU-Tx to the mth PU-Rx channel is described using the correlation model [147, 148] as

$$h_{1m} = \rho \hat{h}_{1m} + \sqrt{1-\rho^2}\varepsilon, \tag{3.1}$$

where $m \in \{1, ..., M\}$, $\hat{h}_{1m}$ is the outdated channel information available at the SU-Tx, ε is a complex Gaussian random variable with zero mean and unit variance, and uncorrelated with h_{1m}. The correlation coefficient ρ is a constant, which is used to evaluate the impact of channel estimation error, mobility, and feedback delay on the CSI

[148]. Note that it is assumed that both the outdated channel information $\hat{h}_{1m}$ and the correlation coefficient ρ are available at the SU-Tx.

It is assumed that both the secondary channel and the primary channel are subject to quasi-static fading where the channel coefficients are constant for each transmission block but vary independently between different blocks. The primary and secondary networks are subject to independent and identically distributed (i.i.d.) Rayleigh fading. The estimated channel power gain from the SU-Tx to the mth PU-Rx channel is an exponentially distributed RV with parameter $\frac{1}{\hat{\alpha}_1}$. The instantaneous channel power gains from the SU-Tx to the mth PU-Rx channel, from the mth PU-Tx to the lth transmit antenna at SU-Rx, and from the SU-Tx to the lth receive antenna at the SU-Rx are exponentially distributed RVs with parameters$\frac{1}{\alpha_1}$, $\frac{1}{\alpha_2}$, and $\frac{1}{\alpha_3}$, respectively, where $l \in \{1, ..., L\}$ and $\alpha_1 = \rho^2\hat{\alpha}_1 + \left(1 - \rho^2\right)$. Note that here the main focus is the outdated channel effect and the impact of GSC, thus, the different path-loss and shadowing effect between the SU-Tx and the PU-Rxs links resulting from the geometry are not taken into consideration in this work. This assumption is also applicable to the scenario where the PU-Rxs are located in a compact and small area.

3.2.1 Interference Outage Probability

According to underlay spectrum sharing, the interference from the secondary network impinged on the primary network should remain below a pre-defined peak interference temperature Q [149]. When only the outdated interference channel information is available at the SU-Tx, this strict interference requirement can not be satisfied at all times. Therefore, the PU-Rxs should tolerate outages occuring for a certain percentage of time, which is named as the interference outage. In [148], it has been proved that the interference outage probability is always 0.5 as long as the maximum transmission power is ignored. Therefore, instead of the strict peak interference constraint, a more flexible constraint known as the power margin, which is based on the interference outage probability is considered to prevent the primary transmission from degradation. The transmit

power and the interference outage probability are denoted as

$$P\Big(\rho, \big|\hat{h}_{1m^*}\big|^2\Big) = \min\big(P_T, k_I \frac{Q}{\big|\hat{h}_{1m^*}\big|^2}\big), \tag{3.2}$$

and

$$P_o = 1 - \Pr\left\{\min\big(P_T, k_I \frac{Q}{\big|\hat{h}_{1m^*}\big|^2}\big)\big|h_{1m^*}\big|^2 \leq Q\right\}, \tag{3.3}$$

respectively, where P_{T} is the maximum available transmit power at the SU-Tx, and $\big|\hat{h}_{1m^*}\big|^2$ is the largest estimated channel power gain from the SU-Tx to the M PU-Rxs available at the SU-Tx. The power margin factor is assumed to be $k_I = 1$ for the perfect CSI between the SU-Tx and the PU-Rx link. Since the closed-form expression for the power margin factor k_I is intractable [147], therein, k_I is numerically evaluated based on (3.3).

3.3 Signal-to-Interference Ratio

In the secondary network, GSC is applied to combine the L_c $(1 \leq L_c \leq L)$ antennas with the strongest received signals from L available receive antennas at the SU-Rx. The channel coefficients from the SU-Tx to the lth receive antenna at the SU-Rx are denoted as g_l $(1 \leq l \leq L)$. Let $|g_1|^2 \geq |g_2|^2 \geq \cdots |g_L|^2 \geq 0$ be the order statistics obtained by sorting $\{g_l\}_{l=1}^{L}$ in decreasing order of magnitude [84]. After performing GSC [150], the received signal at the SU-Rx is given by

$$y = \frac{\boldsymbol{G}^H}{\|\boldsymbol{G}\|}\boldsymbol{G}x_T + \underbrace{\sum_{m=1}^{M} \frac{\boldsymbol{G}^H}{\|\boldsymbol{G}\|}\boldsymbol{H}_{2m}x_m}_{\text{Interferences from PU - Txs}} + \frac{\boldsymbol{G}^H}{\|\boldsymbol{G}\|}\boldsymbol{n} \tag{3.4}$$

where x_T is the transmit signal at the SU-Tx, $\boldsymbol{G} = [g_1, g_2, \ldots, g_{L_c}]^T$ is the selected channel vector at the SU-Rx, x_m is the transmit signal at the mth PU-Tx, $\boldsymbol{H}_{2m}$ is the $L_c \times 1$ channel vector from the mth PU-Tx to L_c antennas with strongest receive signals

at the SU-Rx, and $\boldsymbol{n} \sim \mathcal{CN}(\mathbf{0}, \sigma^2 \mathbf{I}_{L_c})$ is the $L_c \times 1$ AWGN vector. Similar to some practical applications such as cellular CDMA networks and dense ad hoc networks [151], the interference-limited scenario of cognitive networks with multiple primary transceivers is considered where the noise is typically negligible compared to the sum of interferences from the multiple PU-Txs. As such, the SIR can be used interchangeably with SINR without much appreciable loss of accuracy [152–154]. Based on (3.4), the instantaneous received SIR is given by

$$\tilde{\gamma} = \min\left(P_{\mathrm{T}}, \frac{k_I Q}{Y}\right) \frac{X}{V}, \tag{3.5}$$

where $X = \|\boldsymbol{G}\|^2$, $Y = \left|\hat{h}_{1m^*}\right|^2$, $V = \sum_{m=1}^{M} P_{\mathrm{I}} \left|\frac{\boldsymbol{G}^H \boldsymbol{H}_{2m}}{\|\boldsymbol{G}\|}\right|^2$ is the interference power from the PU-Txs to the SU-Rx, and P_I is the transmit power of PU-Txs.

3.4 Outage Probability

3.4.1 Exact Analysis

Outage probability is an important metric to characterize the performance of cognitive radio networks in practice. In cognitive radio networks, an outage occurs if the instantaneous received SIR at the SU drops below a given threshold γ_{th}. Based on this, the outage probability is formulated as

$$P_{\mathrm{out}} = \Pr\left\{\tilde{\gamma} \leq \gamma_{\mathrm{th}}\right\} = F_{\tilde{\gamma}}\left(\gamma_{\mathrm{th}}\right), \tag{3.6}$$

where $\Pr\{\cdot\}$ denotes the probability and $F_{\tilde{\gamma}}(\gamma_{\mathrm{th}})$ denotes the CDF of $\tilde{\gamma}$. To derive $F_{\tilde{\gamma}}(\gamma_{\mathrm{th}})$, the statistics of the channel power gain $\|\boldsymbol{G}\|^2$ are presented as follows.

The CDF of $\|\boldsymbol{G}\|^2$ is obtained using [150, eq. (4)] and the multinomial expansion

[155] which results in

$$F_{\|\boldsymbol{G}\|^2}(x) = \sum_{S_k \in S_K} \alpha_k x^{\beta_k} e^{-\delta_k \frac{x}{\alpha_3}}, \tag{3.7}$$

where $S_K = \left\{ S_k | \sum_{l=0}^{L} m_{k,l} = 1 \right\}$ with $\{m_{k,l}\} \in Z^+$. It is noted that S_K refers to all possible combinations of $\{m_{k,l}, l = 0, 1, \ldots, L\}$, which satisfy $\sum_{l=0}^{L} m_{k,l} = 1$. The parameters in (3.7) are defined as

$$\alpha_k = (\varepsilon_0)^{m_{h,0}} \prod_{l=1}^{L_c} \left(\frac{\varepsilon_l}{\Gamma(l)} \right)^{m_{h,l}} \prod_{l=L_c+1}^{L} {\varepsilon_l}^{m_{h,l}}, \tag{3.8}$$

$$\beta_k = \sum_{l=1}^{L_c} (l-1) m_{k,l}, \tag{3.9}$$

and

$$\delta_k = \sum_{l=1}^{L_c} m_{k,l} + \sum_{l=L_c+1}^{L} \frac{l}{L_c} m_{k,l}, \tag{3.10}$$

where ε_l is given by

$$\varepsilon_l = \begin{cases} 1 & l = 0 \\ \alpha_3^{1-l} \left[-1 + \sum\limits_{k=L_c+1}^{L} (-1)^{k-l} \frac{\binom{L}{L-k}\binom{k-1}{k-L_c-1}}{\left(\frac{k}{L_c}-1\right)^{L_c-l+1}} \right] & 1 \le l < L_c \\ -\alpha_3^{1-L_c} \binom{L}{L-L_c} & l = L_c \\ \frac{(-1)^l \binom{L}{L-l}\binom{l-1}{l-L_c-1}}{\left(\frac{l}{L_c}-1\right)^{L_c}} & L_c < l \le L. \end{cases} \tag{3.11}$$

The CDF of $\left|\hat{h}_{1m^*}\right|^2$ is given by

$$F_{\left|\hat{h}_{1m^*}\right|^2}(x) = \left(1 - e^{-\frac{x}{\hat{\alpha}_1}}\right)^M. \tag{3.12}$$

Recall that $V = \sum_{m=1}^{M} P_{\mathrm{I}} \left| \frac{\mathbf{G}^H \mathbf{H}_{2m}}{\|\mathbf{G}\|} \right|^2$ is defined. According to [156], $\frac{\mathbf{G}^H \mathbf{H}_{2m}}{\|\mathbf{G}\|}$ is a zero-mean complex Gaussian vector, which is independent of $\mathbf{G}^H$ and $\|\mathbf{G}\|$, and $\left| \frac{\mathbf{G}^H \mathbf{H}_{2m}}{\|\mathbf{G}\|} \right|^2$ follows the chi-square distribution with 2 degrees of freedom. As such, the probability distribution function (PDF) of V is given by

$$f_V(x) = \left(\frac{1}{P_I \alpha_2}\right)^M \frac{x^{M-1} e^{-\frac{x}{P_I \alpha_2}}}{\Gamma(M)}. \tag{3.13}$$

Based on the CDF and PDF of X, Y, and V, the closed-form expression for the outage probability is presented in the following theorem.

Theorem 1. *The closed-form expression for the outage probability of spectrum sharing networks with GSC and outdated CSI between the SU-Tx and the PU-Rxs is derived as*

$$P_{out}(\gamma_{th}) = \frac{\Gamma(\beta_k + M)}{\Gamma(M)} \sum_{S_k \in S_K} \alpha_k {\gamma_{th}}^{\beta_k} \Xi(\gamma_{th}), \tag{3.14}$$

where

$$\begin{aligned}
\Xi(\gamma_{th}) = & \left(1 - e^{-\frac{k_I Q}{\hat{\alpha}_1 P_T}}\right)^M \left(\frac{1}{P_I \alpha_2}\right)^M \left(\frac{1}{P_T}\right)^{\beta_k} \\
& \frac{1}{\left(\frac{\delta_k \gamma_{th}}{P_T \alpha_3} + \frac{1}{P_I \alpha_2}\right)^{\beta_k + M}} + \sum_{m=1}^{M} \binom{M}{m} (-1)^{m+1} \left(\frac{\alpha_3}{\hat{\alpha}_1 \delta_k \gamma_{th}}\right)^{\beta_k + M} \\
& \left(\frac{k_I Q}{P_I \alpha_2}\right)^M \beta_k! e^{-\frac{m k_I Q}{\hat{\alpha}_1 P_T}} \sum_{i=0}^{\beta_k} \frac{\left(\frac{k_I Q}{P_T}\right)^i}{i!} \left(\frac{m}{\hat{\alpha}_1}\right)^{i+M} \\
& \Phi\left(\beta_k + M, M + i; \left(\frac{1}{P_I \alpha_2} + \frac{\delta_k \gamma_{th}}{\alpha_3 P_T}\right) \frac{\alpha_3 m k_I Q}{\hat{\alpha}_1 \delta_k \gamma_{th}}\right),
\end{aligned} \tag{3.15}$$

where $\Gamma(\cdot)$ is the gamma function [157, Eq. (8.310.1)], and $\Phi(\cdot, \cdot; \cdot)$ is the confluent hypergeometric function [157, Eq. (9.211.4)].

Proof. See Appendix A.1. □

Lemma 1. *The outage probability of spectrum sharing networks with perfect CSI, and only one pair of primary transceiver and secondary transceiver with single antenna is*

derived as

$$P_{out}\left(\gamma_{th}\right) = 1 - \frac{\left(1 - e^{-\frac{Q}{\hat{\alpha}_1 P_T}}\right)}{\left(\frac{P_I \alpha_2 \gamma_{th}}{P_T \alpha_3} + 1\right)} - \frac{\alpha_3 Q}{P_I \alpha_2 \hat{\alpha}_1 \gamma_{th}} e^{\frac{\alpha_3 Q}{P_I \alpha_2 \hat{\alpha}_1 \gamma_{th}}} \Gamma\left(0, \left(\frac{1}{P_I \alpha_2} + \frac{\gamma_{th}}{\alpha_3 P_T}\right) \frac{\alpha_3 Q}{\hat{\alpha}_1 \gamma_{th}}\right), \tag{3.16}$$

which is equivalent to [158, Eq. (15)] with $\sigma = 0$, and this also demonstrates the generality of our result.

Note that the closed-form expression for the outage probability with perfect CSI can be obtained by substituting $k_I = 1$ into (3.14).

3.4.2 Asymptotic Analysis

In this subsection, the asymptotic behavior of the outage probability in the operating region of high transmit power constraint P_{T} is characterized. Throughout this subsection, the SU-Tx power is considered to be proportional to the PU-Rx interference. This indicates that the diversity order exists when the PU-Rx is able to tolerate a high amount of interference from the SU-Tx. This will benefit the secondary network without violating the transmission at the primary network. With this in mind, A deeper understanding of the effect of power scaling on the outage probability is gathered. Similar to [87], $Q = \mu P_{\mathrm{T}}$ is considered, where μ is positive constant.

In the high-SIR regime with $P_{\mathrm{T}} \to \infty$, [157, Eq. (3.354.1)] and [157, Eq. (1.211.1)] are applied to derive the first order expansion of $F_{\|\boldsymbol{G}\|^2}\left(x\right)$ as

$$F^{\infty}_{\|\boldsymbol{G}\|^2}\left(x\right) \approx \frac{1}{{L_c}^{L-L_c} L_c!} x^L. \tag{3.17}$$

Substituting (3.17) into (A.1.1), the asymptotic outage probability with proportional interference power constraint is presented in the following theorem.

Theorem 2. *When $Q = \mu P_T$, the asymptotic outage probability of spectrum sharing*

networks with GSC and multiple PU transceivers as $P_T \to \infty$ is derived as

$$P_{\text{out}}^{\infty} \approx (G_c P_T)^{-G_d}, \tag{3.18}$$

where the diversity order is $G_d = L$ and the array gain is

$$G_c = \Big[\frac{\Theta}{{L_c}^{L-L_c} L_c!} \frac{\Gamma\big(M+L\big)}{\Gamma\big(M\big)}\Big]^{-\frac{1}{L}} \frac{1}{\alpha_2 P_I \gamma_{th}}, \tag{3.19}$$

with $\Theta = \big(1 - e^{-\frac{k_I \mu}{\hat{\alpha}_1}}\big)^M + \sum_{m=1}^{M} \binom{M}{m} (-1)^{m+1} \frac{\Gamma\Big(L+1, \frac{k_I \mu m}{\hat{\alpha}_1}\Big)}{(\alpha_3 k_I \mu m/\hat{\alpha}_1)^L}$.

Similarly, the asymptotic outage probability with perfect CSI can be obtained by substituting $k_I = 1$ into (3.18). Based on (3.18), it is confirmed that the diversity order is entirely determined by the available number of receive antennas at the SU-Rx L, but independent of the number of combined antennas at the SU-Rx L_c and the correlation coefficient ρ.

The outage tradeoff between GSC, MRC, and SC is then examined. Given that GSC, MRC, and SC maintain the same diversity order, the tradeoff between them is entirely determined by their respective array gains. Based on our results in (3.19), the following remarks are presented.

Remark 1: It is assumed that $L_c = L$ in (3.19) to obtain the array gain of MRC as

$$G_c^{\text{MRC}} = \left[\frac{\Theta \Gamma\left(M+L\right)}{L! \Gamma\left(M\right)}\right]^{-\frac{1}{L}} \frac{1}{\alpha_2 P_I \gamma_{th}}. \tag{3.20}$$

Using (3.19) and (3.20), the SNR gap between GSC and MRC is expressed as

$$\Delta_1 = 10 \log\left(\frac{G_c}{G_c^{\text{MRC}}}\right) = \left(\frac{10}{L}\right) \log\left(\frac{{L_c}^{L-L_c} L_c!}{L!}\right) \text{ dB}. \tag{3.21}$$

Remark 2: Setting $L_c = 1$ in (3.19), the array gain of SC is obtained as

$$G_c^{\mathrm{SC}} = \left[\frac{\Theta\Gamma\left(M+L\right)}{\Gamma\left(M\right)}\right]^{-\frac{1}{L}} \frac{1}{\alpha_2 P_{\mathrm{I}}\gamma_{th}}. \tag{3.22}$$

Using (3.19) and (3.22), the SIR gap between GSC and SC is expressed as

$$\Delta_2 = 10\log\left(\frac{G_c}{G_c^{\mathrm{SC}}}\right) = \left(\frac{10}{L}\right)\log\left(L_c^{L-L_c}L_c!\right) \text{ dB}. \tag{3.23}$$

Remark 3: Using (3.20) and (3.22), the SIR gap between MRC and SC is expressed as

$$\Delta_3 = 10\log\left(\frac{G_c^{\mathrm{MRC}}}{G_c^{\mathrm{SC}}}\right) = \left(\frac{10}{L}\right)\log\left(L!\right) \text{ dB}. \tag{3.24}$$

Based on *Remarks 1, 2*, and *3*, it is confirmed that the SIR gaps Δ_1, Δ_2, and Δ_3 are fully described by two parameters: the number of available receive antennas at the SU-Rx L and the number of combined antennas at the SU-Rx L_c.

3.5 Numerical Results

Numerical examples are provided to highlight the impact of GSC on the performance of underlay spectrum sharing networks with imperfect CSI. In all figures, it is assumed that the threshold SIR is $\gamma_{\mathrm{th}} = 1$ dB and the interference power from the PU-Tx is $P_{\mathrm{I}} = 3$ dB, $\hat{\alpha}_1 = 2$, $\alpha_2 = 3$, and $\alpha_3 = 1$. A perfect match between the simulations and the exact analytical curves (plotted from (3.14)) can be seen. It is also seen that the asymptotic analytical lines (plotted from (3.18)) are in precise agreement with the exact analytical curves in the medium-to-high regime of P_{T}.

Fig. 3.1 plots the outage probability versus P_{T} for various M. Here, it is assumed $L = 3$, $L_c = 2$, $P_0 = 10\%$, and $\rho = 0.9$. It is observed that the diversity order is

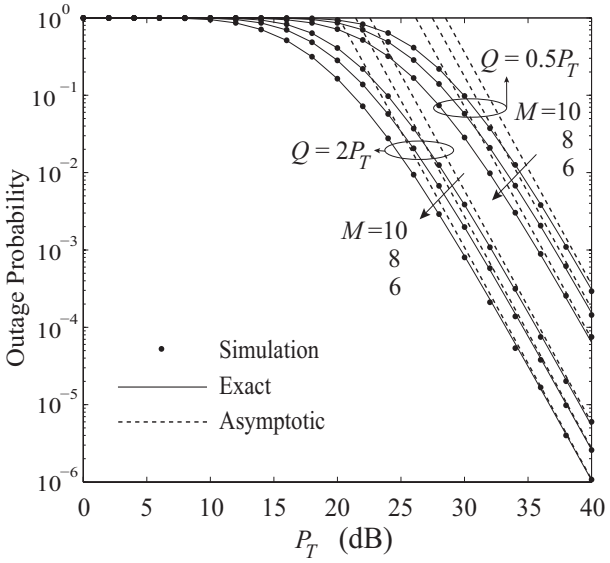

Figure 3.1: Outage probability with $L_c = 2$, $L = 3$, $P_0 = 10\%$, and $\rho = 0.9$.

independent of M as indicated by the parallel slopes of the asymptotes. The diversity order is entirely determined by the number of antennas at the SU-Rx as $G_d = L$. As expected, the outage probability decreases with decreasing M. This is due to the fact that the array gain in (3.19) increases with decreasing M. This result is not surprising, since the interference from the PU-Tx to the SU-Rx increases with increasing M, as shown in (3.5), which negatively impacts the secondary network. It also observed that setting $Q = 2P_{\mathrm{T}}$ achieves a lower outage probability compared to $Q = 0.5P_{\mathrm{T}}$. This is due to the fact that the array gain in (3.19) increases with increasing μ. In other words, the higher peak interference power constraint at the PUs enables more reliable transmission of the secondary network.

Fig. 3.2 plots the outage probability versus P_{T} as we vary L_c. Here, it is assumed $M = 6$, $Q = 2P_{\mathrm{T}}$, $P_0 = 10\%$, and $\rho = 0.9$. It is observed that the diversity order is $G_d = L$ regardless of L_c. Setting $L_c = L$ and $L_c = 1$, it is easy to obtain the special cases of MRC and SC, respectively. It is also observed that the SIR gap between MRC and SC are accurately predicted according to (3.24). As expected, it is observed that the outage probability decreases with increasing L_c. This is due to the fact that the array

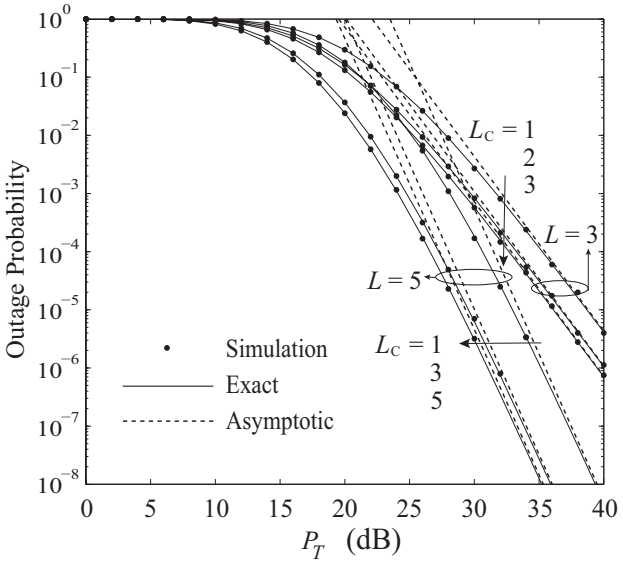

Figure 3.2: Outage probability with $M = 6$, $Q = 2P_{\mathrm{T}}$, $P_0 = 10\%$, and $\rho = 0.9$.

gain increases with increasing L_c, as shown in (3.19). Moreover, it is noticed that the lower outage probability can be achieved by employing more antennas L, which can be explained by the fact that the array gain increases with increasing L.

Fig. 3.3 plots the outage probability versus P_{T} for various ρ and P_0. Here, it is assumed $M = 5$, $L = 5$, $L_c = 3$, and $Q = 1.5P_{\mathrm{T}}$. The same parallel slopes for different coefficients ρ indicates that the diversity order is independent of ρ and P_0. Interestingly, for the case of $P_0 = 0.1$, the outage probability decreases as ρ increases; for the case of $\rho = 0.9$, the outage probability decreases with increasing P_0. This can be explained by the fact that increasing ρ and P_0 ensure the higher transmit power of the SU-Tx, and thus brings about better outage performance. As expected, for $\rho = 1$, which refers to perfect CSI, the lowest outage probability is achieved.

Fig. 3.4 plots the outage probability versus Q for various L_c. Here, it is assumed $M = 5$, $P_{\mathrm{T}} = 25$ dB, $P_0 = 10\%$, and $\rho = 0.9$. As expected, the outage probability decreases with increasing Q when P_T is not a linear function of Q. Furthermore, the outage probability decreases with increasing L_c.

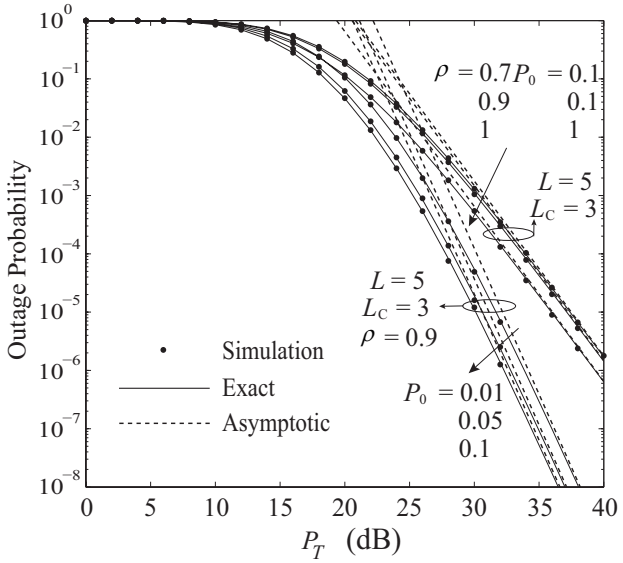

Figure 3.3: Outage probability with $L_c = 3$, $L = 5$, and $M = 5$.

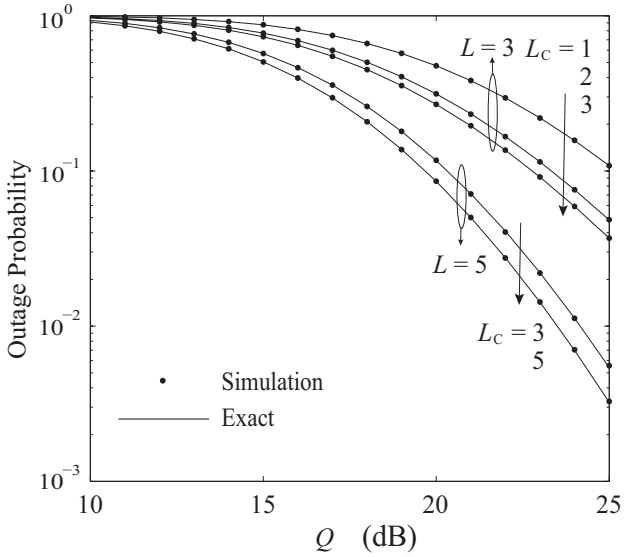

Figure 3.4: Outage probability with $M = 5$, $P_T = 25$ dB, $P_0 = 10\%$, and $\rho = 0.9$.

3.6 Summary

GSC is proposed in interference-limited spectrum sharing networks with outdated CSI and multiple PU transceivers. The aim is to examine the impact of GSC and outdated

channel on the outage probability. To facilitate this, the new closed-form expressions for the exact and the asymptotic outage probability are derived. The SU-Rx is allowed to combine the L_c strongest antennas out of L antennas. With this in mind, fundamental question of how L_c, M, and ρ affect the transmit power at the SU-Tx, the interference from the SU-Tx to the PU-Rx, and the interference from the PU-Tx to the SU-Rx is answered. The valuable insights are reached that the interference power at the SU-Rx increases as M increases, and the outage probability is improved with more accurate CSI.

Chapter 4

Cognitive MIMO Relay Networks with Generalized Selection Combining over Rayleigh Fading

4.1 Introduction

In Chapter 4 and 5, TAS/GSC is introduced in cognitive relay networks. In this setting, a dual-hop secondary network is considered where TAS/GSC is applied in the source-to-relay link and relay-to-destination link. A DF relay is utilized to assist the transmission and compensate the restricted coverage resulting from the peak interference power constraint [159]. In detail, a single transmit antenna that maximizes the SNR at secondary source (SS) and secondary relay (SR) is selected, while a subset of receiver antennas with the highest SNRs are combined at SR and secondary destination (SD).

Note that selecting the strongest transmit antenna for the SU corresponds to a random transmit antenna for the PU, which reduces the interference at the PU. In addition, GSC is a promising compromise between the more complex MRC and the less complex SC in terms of complexity and performance. Therefore, the competing demands on the transmit power to maximize the performance in the secondary network and to minimize the interference in the primary network can be well balanced at no extra cost of spectrum resources. Note that in Chapter 4 and 5, the outdated CSI is not taken into account to

focus on the impact of TAS/GSC on CNs.

In this chapter, the cognitive relay networks with TAS/GSC is considered in Rayleigh fading channels. The goal is to examine the impact of TAS/GSC under two key constraints: i) peak interference power at the PUs, Q , and ii) maximum transmit power at the SUs, P. The major contributions of this chapter are summarized as follows.

- New exact closed-form expressions for the CDF of the instantaneous received end-to-end SNR are derived. The relationship between the peak interference power and the maximum transmit power constraints is quantified.

- New exact closed-form expressions for the outage probability and the symbol error rate (SER) are derived based on our newly derived CDF. It is accurately examined how the number of PUs, the total number of antennas available, and the number of receive antennas combined contribute to those two important performance metrics.

- New first-order expansions for the CDF of the end-to-end SNR is derived to facilitate the asymptotic analysis of the outage probability and the SER with binary phase shift keying (BPSK) and quadrature phase shift keying (QPSK) in the high SNR regime. Based on those asymptotic expressions, two important design measures, the diversity gain and the SNR gain, are characterized.

It is shown that the outage probability and the SER decrease as the number of receive antennas combined at SR and SD increases. It is also shown that the outage probability and the SER increase as the number of PUs increases. The positive impact of the number of receive antennas combined and the negative impact of the number of PUs on the secondary network are reflected on the SNR gain. Furthermore, under a proportional interference power constraint where Q is directly proportional to P, the full diversity gain is achieved in the high SNR regime. This diversity gain is entirely determined by the total number of antennas available in the secondary network. Under a fixed interference power constraint where Q is fixed and independent of P, the error floors are displayed in the high maximum transmit power to noise ratio regime and the

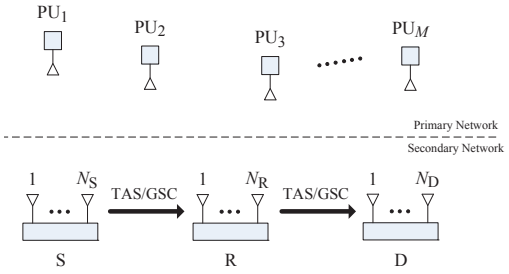

Figure 4.1: Cognitive spectrum sharing with TAS/GSC and DF relaying.

diversity gain is lost.

4.2 Network and Channel Description

A cognitive spectrum sharing network with dual-hop relaying is considered where the secondary network is allowed to utilize the same spectrum licensed to the primary network. As shown in Fig. 4.1, the primary network consists of M PUs, each with a single antenna. The secondary network consists of a SS with N_S antennas, a SR with N_R antennas, and a SD with N_D antennas. The secondary network and the primary network are subject to independent identically distributed (i.i.d.) Rayleigh fading. The channel coefficients of the links SS $\rightarrow$ SR, SR $\rightarrow$ SD, SS $\rightarrow$ PUs, and SR $\rightarrow$ PUs, are denoted as g_{1ij}, g_{2jk}, h_{1im}, and h_{2jm}, respectively, where $i \in \{1, \ldots, N_S\}$, $j \in \{1, \ldots, N_R\}$, $k \in \{1, \ldots, N_D\}$, and $m \in \{1, \ldots, M\}$. In the following, $\| \cdot \|$ is the Euclidean norm, $| \cdot |$ is the absolute value, and $\mathbb{E}[\cdot]$ is the expectation.

In the proposed underlay spectrum sharing network, the interference power at the PUs originating from the SUs must not exceed a predetermined threshold level. According to this paradigm, the transmit powers at SS and SR are constrained according to

$$P_S = \min\left(P, \frac{Q}{|h_{1i^*}|^2}\right) \tag{4.1}$$

and

$$P_R = \min\left(P, \frac{Q}{|h_{2j^*}|^2}\right), \tag{4.2}$$

respectively, where P is the maximum transmission power and Q is the maximum permissible interference power. $|h_{1i^*}| = \max_m\{|h_{1i^*m}|\}$ is denoted as the largest channel coefficient from the transmit antenna at SS to the M PUs, and $|h_{2j^*}| = \max_m\{|h_{2j^*m}|\}$ as the largest channel coefficient from the transmit antenna at R to the M PUs.

In the SS $\rightarrow$ SR link, a single transmit antenna is selected at SS and the receive antennas at SR are combined using GSC. Based on GSC, $\{\|g_{1ij}\|\}_{j=1}^{N_R}$ is sorted in descending order to obtain $\|g_{1i(1)}\| \geq \|g_{1i(2)}\| \geq \cdots \geq \|g_{1i(N_R)}\| \geq 0$. The first L_R $(1 \leq L_R \leq N_R)$ variable(s) are combined to obtain $\theta_i = \sum_{j=1}^{L_R} \|g_{1i(j)}\|$ at SR. The index of the selected transmit antenna at SS is determined as $i^* = \arg\max_{1\leq i\leq N_S}\{\theta_i\}$ and the largest channel vector is denoted as $\|\mathbf{g}_{1i^*\theta_{i^*}}\|$.

In the SR $\rightarrow$ SD link, a single transmit antenna is selected at SR and the receive antennas at SD are combined using GSC. By arranging $\{\|g_{2jk}\|\}_{k=1}^{N_D}$ in descending order and combining the L_D $(1 \leq L_D \leq N_D)$ strongest antenna(s), $\theta_j = \sum_{k=1}^{L_D} \|g_{2j(k)}\|$ is obtained at SD. As such, the index of the selected transmit antenna at SR is $j^* = \arg\max_{1\leq j\leq N_R}\{\theta_j\}$ and the largest channel vector is $\left\|\mathbf{g}_{2j^*\theta_{j^*}}\right\|$.

Applying (4.1) and (4.2), the instantaneous end-to-end SNR of the cognitive relay network with TAS/GSC and DF relaying is defined as

$$\gamma = \min(\gamma_1, \gamma_2), \tag{4.3}$$

where the instantaneous SNR in the SS $\rightarrow$ SR link is

$$\gamma_1 = \min\left(\left\|\mathbf{g}_{1i^*\theta_{i^*}}\right\|^2 \bar{\gamma}_P, \frac{\left\|\mathbf{g}_{1i^*\theta_{i^*}}\right\|^2 \bar{\gamma}_Q}{|h_{1i^*}|^2}\right) \tag{4.4}$$

and the instantaneous SNR in the SR $\rightarrow$ SD link is

$$\gamma_2 = \min\left(\left\|\mathbf{g}_{2j^*\theta_{j^*}}\right\|^2 \bar{\gamma}_P, \frac{\left\|\mathbf{g}_{2j^*\theta_{j^*}}\right\|^2 \bar{\gamma}_Q}{|h_{2j^*}|^2}\right). \tag{4.5}$$

In (4.4) and (4.5), we define $\overline{\gamma}_P = \frac{P}{N_0}$ and $\overline{\gamma}_Q = \frac{Q}{N_0}$, where N_0 is the noise power of the AWGN.

4.3 Statistical Properties of the End-To-End SNR

In this section, a new exact expression for the CDF of the end-to-end SNR of the secondary network is derived. The CDF will lay the foundation for deriving the exact and asymptotic outage probability. In [46], the statistics of GSC in non-spectrum sharing networks without relays was derived under Rayleigh fading. Based on [46], the CDF of the end-to-end SNR in cognitive relay networks with TAS/GSC is derived. Then the CDFs of $\left\|\mathbf{g}_{1i^*\theta_{i^*}}\right\|^2$ and $|h_{1i^*}|^2$ are derived as follows.

The CDF of $\left\|\mathbf{g}_{1i^*\theta_{i^*}}\right\|^2$ in the SS $\rightarrow$ SR link is derived by applying [46, eq. (4)] and the multinomial expansion[155, p.166], which results in

$$F_{\left\|\mathbf{g}_{1i^*\theta_{i^*}}\right\|^2}(x) = \sum_{S_k \in S_K} \alpha_k x^{\beta_k} e^{-\delta_k x}, \tag{4.6}$$

where $S_K = \left\{(m_{k,0}, \ldots, m_{k,N_R}) | \sum_{l_R=0}^{N_R} m_{k,l_R} = N_S\right\}$ with $\{m_{k,l_R}\} \in Z^+$. The parameters in (4.6) are defined as

$$\alpha_k \triangleq \frac{N_S!}{\prod_{l_R=0}^{N_R} m_{k,l_R}!} \prod_{l_R=1}^{L_R} \left(\frac{\varepsilon_{l_R}}{\Gamma(l_R)}\right)^{m_{k,l_R}} \prod_{l_R=L_R+1}^{N_R} {\varepsilon_{l_R}}^{m_{k,l_R}}, \tag{4.7}$$

$$\beta_k \triangleq \sum_{l_R=1}^{L_R} (l_R - 1) m_{k,l_R}, \tag{4.8}$$

and

$$\delta_k \triangleq \sum_{l_R=1}^{L_R} m_{k,l_R} + \sum_{l_R=L_R+1}^{N_R} \frac{l_R}{L_R} m_{k,l_R}, \tag{4.9}$$

where $\varepsilon_{l_\mathrm{R}}$ in (4.7) is given by

$$\varepsilon_{l_\mathrm{R}} = \begin{cases} 1 & l_\mathrm{R} = 0 \\ -1 + \sum\limits_{k_\mathrm{R}=L_\mathrm{R}+1}^{N_\mathrm{R}} \frac{\Upsilon(N_\mathrm{R}, L_\mathrm{R}, k_\mathrm{R})}{(-1)^{l_\mathrm{R}} \left(\frac{k_\mathrm{R}}{L_\mathrm{R}} - 1\right)^{1-l_\mathrm{R}}} & 1 \le l_\mathrm{R} < L_\mathrm{R} \\ -\binom{N_\mathrm{R}}{N_\mathrm{R}-L_\mathrm{R}} & l_\mathrm{R} = L_\mathrm{R} \\ \Upsilon\left(N_\mathrm{R}, L_\mathrm{R}, l_\mathrm{R}\right) & L_\mathrm{R} < l_\mathrm{R} \le N_\mathrm{R}, \end{cases} \tag{4.10}$$

and $\Upsilon\left(N, L, \zeta\right) = (-1)^{\zeta} \binom{N}{N-\zeta} \binom{\zeta-1}{\zeta-L-1} \Big/ \left(\frac{\zeta}{L} - 1\right)^{L}$.

The CDF of $|h_{1i^*}|^2$ in the SS $\rightarrow$ PU link is written as

$$F_{|h_{1i^*}|^2}(x) = \left(1 - e^{-x}\right)^{M}. \tag{4.11}$$

Based on the CDFs of $\left\|\mathbf{g}_{1i^*\theta_{i^*}}\right\|^2$ and $|h_{1i^*}|^2$, the exact CDF of γ_1 is presented in the following theorem.

Theorem 3. *A closed-form expression for the CDF of γ_1 is given by*

$$F_{\gamma_1}(x) = \sum_{S_K} \alpha_k x^{\beta_k} \left[e^{-\frac{\delta_k}{\overline{\gamma}_P} x} \left(\frac{1}{\overline{\gamma}_P}\right)^{\beta_k} \left(1 - e^{-\frac{Q}{P}}\right)^{M} + \sum_{m=1}^{M} \binom{M}{m} (-1)^{m+1} \frac{\overline{\gamma}_Q m}{\left(\overline{\gamma}_Q + \delta_k x\right)^{\beta_k+1}} \right.$$
$$\left. \times \Gamma\left(\beta_k + 1, \left(m + \frac{\delta_k x}{\overline{\gamma}_Q}\right) \frac{Q}{P}\right) \right]. \tag{4.12}$$

It is highlighted that (4.12) consists of simple finite summations of power functions, exponential functions, and the incomplete gamma function. Importantly, the derived CDF expression is valid for general operating scenarios with arbitrary M, N_R, and L_R.

Moreover, this expression is applicable in the point-to-point transmission with TAS/GSC.

Proof. See Appendix B.1. □

The CDF of γ_2 follows from (4.12) by interchanging the parameters $\alpha_k \to \alpha_t$, $\beta_k \to \beta_t$, $\delta_k \to \delta_t$, and $S_K \to S_T$, where $S_T = \left\{ (m_{t,0}, \ldots, m_{t,N_D}) | \sum_{l_D=0}^{N_D} m_{t,l_D} = N_R \right\}$ with $\{m_{t,l_D}\} \in Z^+$. Here, it is defined that

$$\alpha_t \triangleq \frac{N_R!}{\prod_{l_D=0}^{N_D} m_{t,l_D}!} \prod_{l_D=1}^{L_D} \left(\frac{\varepsilon_{l_D}}{\Gamma(l_D)} \right)^{m_{t,l_D}} \prod_{l_D=L_D+1}^{N_D} {\varepsilon_{l_D}}^{m_{t,l_D}}, \tag{4.13}$$

$$\beta_t \triangleq \sum_{l_D=1}^{L_D} (l_D - 1) m_{t,l_D}, \tag{4.14}$$

and

$$\delta_t \triangleq \sum_{l_D=1}^{L_D} m_{t,l_D} + \sum_{l_D=L_D+1}^{N_D} \frac{l_D}{L_D} m_{t,l_D}, \tag{4.15}$$

where $\varepsilon_{l_\mathrm{D}}$ in (4.13) is given by

$$\varepsilon_{l_\mathrm{D}} = \begin{cases} 1 & l_\mathrm{D} = 0 \\ -1 + \sum\limits_{k_\mathrm{D}=L_\mathrm{D}+1}^{N_\mathrm{D}} \frac{\Upsilon(N_\mathrm{D}, L_\mathrm{D}, k_\mathrm{D})}{(-1)^{l_\mathrm{D}} \left(\frac{k_\mathrm{D}}{L_\mathrm{D}} - 1 \right)^{1 - l_\mathrm{D}}} & 1 \le l_\mathrm{D} < L_\mathrm{D} \\ -\binom{N_\mathrm{D}}{N_\mathrm{D} - L_\mathrm{D}} & l_\mathrm{D} = L_\mathrm{D} \\ \Upsilon(N_\mathrm{D}, L_\mathrm{D}, l_\mathrm{D}) & L_\mathrm{D} < l_\mathrm{D} \le N_\mathrm{D}. \end{cases} \tag{4.16}$$

4.4 Outage Probability

In this section, the joint impact of the maximum transmit power P and the peak interference power Q on the exact and asymptotic outage probability is addressed.

4.4.1 Exact Analysis

In DF relaying, the end-to-end outage probability is determined by the worst link between the SS $\rightarrow$ SR and SR $\rightarrow$ SD links. Due to the independence between the SS $\rightarrow$ SR and SR $\rightarrow$ SD links, the end-to-end outage probability is given by [160]

$$P_{out}\left(\gamma_{th}\right) = \Pr\left(\min(\gamma_1, \gamma_2) \leq \gamma_{th}\right) = F_{\gamma_1}\left(\gamma_{th}\right) + F_{\gamma_2}\left(\gamma_{th}\right) - F_{\gamma_1}\left(\gamma_{th}\right) F_{\gamma_2}\left(\gamma_{th}\right), \quad (4.17)$$

where $\Pr\{\cdot\}$ denotes the probability. Based on the CDFs of γ_1 and γ_2, a new closed-form expression for the exact outage probability of cognitive spectrum sharing with TAS/GSC and DF relaying is presented as

$$P_{out}\left(\gamma_{th}\right) = 1 - \big(1 - \sum_{S_k \in S_K} \alpha_k {\gamma_{th}}^{\beta_k} \Xi\left(\beta_k, \delta_k\right)\big)\big(1 - \sum_{S_t \in S_T} \alpha_t {\gamma_{th}}^{\beta_t} \Xi\left(\beta_t, \delta_t\right)\big), \quad (4.18)$$

where

$$\begin{aligned}\Xi\left(\beta, \delta\right) =& e^{-\frac{\delta}{\overline{\gamma}_P}\gamma_{th}} \left(\frac{1}{\overline{\gamma}_P}\right)^{\beta} \left(1 - e^{-\frac{Q}{P}}\right)^M + \\ & \sum_{m=1}^{M} \binom{M}{m} \frac{(-1)^{m+1} \overline{\gamma}_Q m}{\left(\overline{\gamma}_Q + \delta\gamma_{th}\right)^{\beta+1}} \Gamma\left(\beta + 1, \left(m + \frac{\delta\gamma_{th}}{\overline{\gamma}_Q}\right)\frac{Q}{P}\right). \end{aligned} \quad (4.19)$$

Note that the result in (4.18) is in exact closed-form, which involves easy-to-evaluate finite summations and the standard incomplete gamma function [161, eq. (8.350.2)].

Corollary 1. The exact closed-form expression for the outage probability of cognitive spectrum sharing with TAS/SC and DF relaying is given as

$$P_{out}\left(\gamma_{th}\right) = 1 - \big(1 - \sum_{S_K} \alpha_k \mathrm{X}\left(\delta_k\right)\big)\big(1 - \sum_{S_T} \alpha_t \mathrm{X}\left(\delta_t\right)\big), \quad (4.20)$$

where

$$\mathrm{X}\left(\delta\right) = e^{-\frac{\delta}{\overline{\gamma}_P}\gamma_{th}} \big(1 - e^{-\frac{Q}{P}}\big)^M + \sum_{m=1}^{M} \binom{M}{m} \frac{(-1)^{m+1} \overline{\gamma}_Q m}{\left(\overline{\gamma}_Q m + \delta\gamma_{th}\right)} e^{-\left(m + \frac{\delta\gamma_{th}}{\overline{\gamma}_Q}\right)\frac{Q}{P}}. \quad (4.21)$$

Corollary 2. The exact closed-form expression for the outage probability of cognitive spectrum sharing with TAS/MRC and DF relaying follows from (4.18) and (4.19), where

$$\alpha_k \triangleq \frac{N_S!}{\prod_{l_R=0}^{N_R} m_{k,l_R}!} \prod_{l_R=1}^{N_R} \left(\frac{\varepsilon_{l_R}}{\Gamma\left(l_R\right)} \right)^{m_{k,l_R}}, \tag{4.22}$$

$$\beta_k \triangleq \sum_{l_R=1}^{N_R} (l_R - 1) m_{k,l_R}, \tag{4.23}$$

and

$$\delta_k \triangleq \sum_{l_R=1}^{N_R} m_{k,l_R}. \tag{4.24}$$

4.4.2 Asymptotic Analysis

Next, the asymptotic outage probability is examined in the high SNR regime. The main purpose behind the asymptotic analysis is to extract two important design parameters: 1) diversity gain, and 2) SNR gain. In doing so, two practical scenarios are considered: 1) proportional interference power constraint where the peak interference power Q is proportional to the maximum transmit power P (i.e., $\overline{\gamma}_Q = \mu \overline{\gamma}_P$), and 2) fixed interference power constraint where the peak interference power Q is fixed and independent of the maximum transmit power P (i.e., $\overline{\gamma}_Q = \rho$). Here, μ and ρ are positive constants. Note that there is no operational difference between the fixed and the proportional interference constraints in managing interference at the PU [162].

4.4.2.1 Proportional Interference Power Constraint

Similar to [71, 77], the proportional interference power constraint is considered where Q at the PUs is scaled according to P at SS and SR. As such, it is assumed that both P and Q grow large in the high maximum transmit power to noise ratio regime. This applies

to the scenario where the PU is able to tolerate a high amount of interference from SS and SR. This assumption with proportional interference power constraint benefits the secondary network without violating the transmission at the primary network. With this in mind, the effect of the so-called *power scaling* on the outage probability is taken into account and studied. In the following theorem, the asymptotic outage probability under the proportional interference power constraint is studied.

The first non-zero order expansion of the CDF of $\left\|\mathbf{g}_{1i^*\theta_{i^*}}\right\|^2$ is derived by applying [161, eq. (1.211.1)] and [161, eq. (3.354.1)]

$$F^{\infty}_{\left\|\mathbf{g}_{1i^*\theta_{i^*}}\right\|^2}(x) = \left(\frac{x^{N_R}}{{L_R}^{N_R-L_R}L_R!}\right)^{N_S}. \tag{4.25}$$

Substituting (4.25) into (A.2.1), the first non-zero order expansion of the CDF of γ_1 and γ_2 is attained and substituted into (4.17) to yield the asymptotic outage probability as (4.26) in the following theorem.

Theorem 4. *When Q scales with P, the asymptotic outage probability of cognitive spectrum sharing with TAS/GSC and DF relaying as $\overline{\gamma}_P \to \infty$ is given by*

$$P^{\infty}_{out}(\gamma_{th}) = \left(G_c\overline{\gamma}_P\right)^{-G_d} + o\left({\overline{\gamma}_P}^{-G_d}\right), \tag{4.26}$$

where the diversity gain is

$$G_d = N_R \min\left\{N_S, N_D\right\} \tag{4.27}$$

and the SNR gain is

$$G_c = \begin{cases} \Delta_1 & N_{\mathrm{S}} < N_{\mathrm{D}} \\ \Delta_2 & N_{\mathrm{S}} > N_{\mathrm{D}} \\ \Delta_1 + \Delta_2 & N_{\mathrm{S}} = N_{\mathrm{D}}\,, \end{cases} \tag{4.28}$$

with

$$\Delta_1 = \frac{\left(L_R{}^{N_R-L_R} L_R!\right)^{\frac{1}{N_R}}}{\gamma_{th}} \Bigg[\left(1-e^{-\mu}\right)^M + \sum_{m=1}^{M} \binom{M}{m} (-1)^{m+1} \left(\frac{1}{\mu m}\right)^{N_R N_S} \Gamma\left(N_S N_R + 1, \mu m\right)\Bigg]^{-\frac{1}{N_R N_S}}, \tag{4.29}$$

and

$$\Delta_2 = \frac{\left(L_D{}^{N_D-L_D} L_D!\right)^{\frac{1}{N_D}}}{\gamma_{th}} \Bigg[\left(1-e^{-\mu}\right)^M + \sum_{m=1}^{M} \binom{M}{m} (-1)^{m+1} \left(\frac{1}{\mu m}\right)^{N_R N_D} \Gamma\left(N_R N_D + 1, \mu m\right)\Bigg]^{-\frac{1}{N_R N_D}}. \tag{4.30}$$

The result in *Theorem 4* is valid for the practical cognitive scenario where the SU transmit power is designed according to the PU interference temperature. It is noted that the diversity gain is independent of the primary network. In fact, it is shown in (4.27) that the diversity gain is entirely determined by the total number of antennas N_S, N_R, and N_D, rather than the number of selected antennas L_R and L_D. Furthermore, it is evident from (4.28) that the SNR gain increases as the number of PUs decreases.

Corollary 3. By substituting $L_R = 1$ and $L_R = N_R$ into (4.29) and (4.30), the SNR gains of cognitive spectrum sharing with TAS/SC and TAS/MRC are derived, respectively. As such, the SNR gap between GSC and SC is obtained as

$$G_c^{SC} = \begin{cases} \frac{10}{N_R} \log\left(L_R{}^{N_R-L_R} L_R!\right) & N_{\mathrm{S}} < N_{\mathrm{D}} \\ \frac{10}{N_D} \log\left(L_D{}^{N_D-L_D} L_D!\right) & N_{\mathrm{S}} > N_{\mathrm{D}} \\ 10 \log\left[\frac{1}{2}\left(\left(L_R{}^{N_R-L_R} L_R!\right)^{\frac{1}{N_R}} + \left(L_D{}^{N_D-L_D} L_D!\right)^{\frac{1}{N_D}}\right)\right] & N_{\mathrm{S}} = N_{\mathrm{D}}\,, \end{cases} \tag{4.31}$$

and the SNR gap between GSC and MRC as

$$G_c^{MRC} = \begin{cases} \frac{10}{N_R}\log\left(\frac{{L_R}^{N_R-L_R}L_R!}{N_R!}\right) & N_{\mathrm{S}} < N_{\mathrm{D}} \\ \frac{10}{N_D}\log\left(\frac{{L_D}^{N_D-L_D}L_D!}{N_D!}\right) & N_{\mathrm{S}} > N_{\mathrm{D}} \\ 10\log\left[\frac{\left({L_R}^{N_R-L_R}L_R!\right)^{\frac{1}{N_R}}}{(N_R!)^{\frac{1}{N_R}}+(N_D!)^{\frac{1}{N_D}}}\right. & \\ \left. +\frac{\left({L_D}^{N_D-L_D}L_D!\right)^{\frac{1}{N_D}}}{(N_R!)^{\frac{1}{N_R}}+(N_D!)^{\frac{1}{N_D}}}\right] & N_{\mathrm{S}} = N_{\mathrm{D}}\ . \end{cases} \tag{4.32}$$

It is shown that the SNR gaps are independent of the primary network. Notably, they are only determined by N_R, L_R, N_D, and L_D.

4.4.2.2 Fixed Interference Power Constraint

Different from the proportional interference power constraint, in this subsection, the focus is the fixed interference power constraint where Q is fixed and only P grows large in the high maximum transmit power to noise ratio regime [163, 164]. This applies to the scenario where the PU can only tolerate a limited amount of interference from SS and SR. As such, when P exceeds Q, the actual transmit power at SS and SR is effectively constrained by Q as defined in (4.1) and (4.2). The asymptotic outage probability with the fixed interference power constraint is derived in the following theorem.

Theorem 5. *When $\overline{\gamma}_Q$ is fixed, the asymptotic outage probability of cognitive spectrum sharing with TAS/GSC and DF relaying as $\overline{\gamma}_P \to \infty$ is given by*

$$P_{out}^{\infty}(\gamma_{th}) = \begin{cases} \Phi_1\left(\frac{\gamma_{th}}{\overline{\gamma}_P}\right)^{N_R N_S} + \Xi_1\left(\frac{\gamma_{th}}{\overline{\gamma}_Q}\right)^{N_R N_S} & N_{\mathrm{S}} < N_{\mathrm{D}} \\ \Phi_2\left(\frac{\gamma_{th}}{\overline{\gamma}_P}\right)^{N_R N_D} + \Xi_2\left(\frac{\gamma_{th}}{\overline{\gamma}_Q}\right)^{N_R N_D} & N_{\mathrm{S}} > N_{\mathrm{D}} \\ (\Phi_1+\Phi_2)\left(\frac{\gamma_{th}}{\overline{\gamma}_P}\right)^{N_R N_S} + & \\ \qquad (\Xi_1+\Xi_2)\left(\frac{\gamma_{th}}{\overline{\gamma}_Q}\right)^{N_R N_S} & N_{\mathrm{S}} = N_{\mathrm{D}}\ , \end{cases} \tag{4.33}$$

where

$$\Phi_1 = \left(\frac{1}{{L_R}^{N_R-L_R}L_R!}\right)^{N_S}\left(1-e^{-\frac{Q}{P}}\right)^M, \tag{4.34}$$

$$\Phi_2 = \left(\frac{1}{{L_D}^{N_D-L_D}L_D!}\right)^{N_R}\left(1-e^{-\frac{Q}{P}}\right)^M, \tag{4.35}$$

$$\Xi_1 = \left(\frac{1}{{L_R}^{N_R-L_R}L_R!}\right)^{N_S}\sum_{m=1}^{M}\binom{M}{m}(-1)^{m+1}\frac{\Gamma\left(N_SN_R+1,\frac{Q}{P}m\right)}{m^{N_RN_S}}, \tag{4.36}$$

and

$$\Xi_2 = \left(\frac{1}{{L_D}^{N_D-L_D}L_D!}\right)^{N_R}\sum_{m=1}^{M}\binom{M}{m}(-1)^{m+1}\frac{\Gamma\left(N_RN_D+1,\frac{Q}{P}m\right)}{m^{N_RN_D}}. \tag{4.37}$$

The result in *Theorem 5* is valid for practical cognitive scenarios where the maximum SU transmit power is independent of the PU interference temperature when $\overline{\gamma}_Q$ is fixed. It is seen from (4.33) that an error floor exists with a zero diversity gain when $\overline{\gamma}_P \to \infty$.

4.5 Symbol Error rate

In this section, the focus is another important metric for quantifying the proposed framework, namely, SER. For well-known modulation schemes, the SER of cognitive spectrum sharing with TAS/GSC and DF relaying can be expressed as

$$P_s = 1-(1-P_{s1})(1-P_{s2}), \tag{4.38}$$

where P_{s1} and P_{s2} can be expressed as [165]

$$P_{s1} = \frac{a}{2}\sqrt{\frac{b}{\pi}}\int_0^\infty \frac{e^{-b\gamma}}{\sqrt{\gamma}}F_{\gamma_1}(\gamma)d\gamma, \tag{4.39}$$

and

$$P_{s2} = \frac{a}{2}\sqrt{\frac{b}{\pi}}\int_0^\infty \frac{e^{-b\gamma}}{\sqrt{\gamma}} F_{\gamma_2}(\gamma)d\gamma. \tag{4.40}$$

In (4.39) and (4.40), a and b are modulation specific constants. For example, $a = 1$, $b = 1$ for BPSK, $a = 2(M-1)/M$, $b = 3/(M^2-1)$ for M-PAM, and $a = 2$, $b = \sin^2(\pi/M)$ for M-PSK.

4.5.1 Exact Analysis

Substituting (4.12) into (4.39), and after some algebra, the SER of the first hop can be expressed as

$$P_{s1} = \frac{a}{2}\sqrt{\frac{b}{\pi}}\sum_{S_K}\alpha_k\Big[\left(\frac{1}{\bar{\gamma}_P}\right)^{\beta_k}\left(1-e^{-\frac{Q}{P}}\right)^M \underbrace{\int_0^\infty \frac{e^{-b\gamma}}{\sqrt{\gamma}}\gamma^{\beta_k}e^{-\frac{\delta_k}{\bar{\gamma}_P}\gamma}d\gamma}_{\eta_1} + \sum_{m=1}^{M}\binom{M}{m}(-1)^{m+1}m\left(\frac{1}{\bar{\gamma}_Q}\right)^{\beta_k}$$
$$\underbrace{\int_0^\infty e^{-b\gamma}\gamma^{\beta_k-\frac{1}{2}}\frac{\Gamma\left(\beta_k+1,\left(m+\frac{\delta_k\gamma}{\bar{\gamma}_Q}\right)\frac{Q}{P}\right)}{\left(1+\frac{\delta_k\gamma}{\bar{\gamma}_Q}\right)^{\beta_k+1}}d\gamma}_{\eta_2}\Big]. \tag{4.41}$$

η_1 is derived as

$$\eta_1 = \frac{\Gamma\left(\beta_k+\frac{1}{2}\right)}{\left(\frac{\delta_k}{\bar{\gamma}_P}+b\right)^{\beta_k+\frac{1}{2}}}. \tag{4.42}$$

With the help of [161, eq.8.352.4], η_2 is then derived as

$$\eta_2 = \beta_k!\sum_{n=0}^{\beta_k}\frac{1}{n!}\left(\frac{Q}{P}\right)^n e^{-m\frac{Q}{P}}m^{n-\beta_k-1}\underbrace{\int_0^\infty \gamma^{\beta_k-\frac{1}{2}}e^{-\left(b+\frac{\delta_k}{\bar{\gamma}_P}\right)\gamma}\left(1+\frac{\delta_k\gamma}{m\bar{\gamma}_Q}\right)^{n-\beta_k-1}d\gamma}_{\omega}, \tag{4.43}$$

By applying [161, eq.9.211.4.8], the integral ω can be solved as

$$\omega = \big(\frac{m\bar{\gamma}_Q}{\delta_k}\big)^{\beta_k+\frac{1}{2}}\Gamma\big(\beta_k+\frac{1}{2}\big)\Psi\big(\beta_k+\frac{1}{2},n+\frac{1}{2};\big(b+\frac{\delta_k}{\bar{\gamma}_P}\big)\frac{\bar{\gamma}_Q m}{\delta_k}\big). \tag{4.44}$$

Integrating (4.44), (4.42) and (4.43) into (4.41), a new exact expression for the SER of the first hop is derived as

$$P_{s1} = \frac{a}{2}\sqrt{\frac{b}{\pi}}\sum_{S_K}\alpha_k\Lambda\left(\beta_k,\delta_k\right). \tag{4.45}$$

The exact SER of the second hop follows from (4.45). Therefore, the exact expression of the end-to-end SER is derived in the following theorem.

Theorem 6. *A new closed-form expression for the SER of DF relaying is given by*

$$P_s = 1-\left(1-\frac{a}{2}\sqrt{\frac{b}{\pi}}\sum_{S_k\in S_K}\alpha_k\Lambda\left(\beta_k,\delta_k\right)\right)\times\left(1-\frac{a}{2}\sqrt{\frac{b}{\pi}}\sum_{S_t\in S_T}\alpha_t\Lambda\left(\beta_t,\delta_t\right)\right), \tag{4.46}$$

where

$$\begin{aligned}\Lambda\left(\beta,\delta\right) = \Bigg[&\left(\frac{1}{\overline{\gamma}_P}\right)^{\beta}\left(1-e^{-\frac{Q}{P}}\right)^{M}\frac{\Gamma\left(\beta+\frac{1}{2}\right)}{\left(\frac{\delta}{\overline{\gamma}_P}+b\right)^{\beta+\frac{1}{2}}}+\beta!\left(\frac{1}{\delta}\right)^{\beta+\frac{1}{2}}\overline{\gamma}_Q{}^{\frac{1}{2}}\sum_{m=1}^{M}\binom{M}{m}(-1)^{m+1}e^{-m\frac{Q}{P}}\\&\times\sum_{n=0}^{\beta}\frac{m^{n+\frac{1}{2}}}{n!}\left(\frac{Q}{P}\right)^{n}\Gamma\left(\beta+\frac{1}{2}\right)\times\Psi\left(\beta+\frac{1}{2},n+\frac{1}{2};\left(b+\frac{\delta}{\overline{\gamma}_P}\right)\frac{\overline{\gamma}_Q m}{\delta}\right)\Bigg].\end{aligned} \tag{4.47}$$

Note that (4.46) is comprised of simple finite summations of the confluent hypergeometric function $\Psi\left(\alpha,\gamma;z\right)$ [161, eq.9.211.4.8], and the incomplete gamma function $\Gamma\left(\cdot,\cdot\right)$ [161, eq.8.350.2].

4.5.2 Asymptotic Analysis

In this subsection, the asymptotic performance of the SER in the high SNR regime is examined to gain deeper insights into the impact of L_R, L_D, and M on the SER. The asymptotic SER is presented in the following theorem.

4.5.2.1 Proportional Interference Power Constraint

Theorem 7. *When Q is proportional to P, the asymptotic SER of cognitive spectrum sharing with TAS/GSC and DF relaying as $\overline{\gamma}_P \to \infty$ is given by*

$$P_s^{\infty} = \left(G_c \overline{\gamma}_P\right)^{-G_d} + o\left(\overline{\gamma}_P{}^{-G_d}\right), \tag{4.48}$$

where the diversity gain is

$$G_d = N_R \min\left\{N_S, N_D\right\} \tag{4.49}$$

and the SNR gain is

$$G_c = \begin{cases} \Theta_1 & N_{\mathrm{S}} < N_{\mathrm{D}} \\ \Theta_2 & N_{\mathrm{S}} > N_{\mathrm{D}} \\ \Theta_1 + \Theta_2 & N_{\mathrm{S}} = N_{\mathrm{D}}\ , \end{cases} \tag{4.50}$$

with

$$\begin{aligned} \Theta_1 = &\left(L_R{}^{N_R - L_R} L_R!\right)^{\frac{1}{N_R}} \Bigg[\frac{a}{2}\sqrt{\frac{b}{\pi}}\frac{\Gamma\left(N_R N_S + \frac{1}{2}\right)}{b^{N_R N_S + \frac{1}{2}}} \times \Bigg(\left(1 - e^{-\mu}\right)^L + \sum_{l=1}^{L} \binom{M}{m} \frac{(-1)^{m+1}}{(\mu l)^{N_R N_S}} \\ &\times \Gamma\left(N_S N_R + 1, \mu m\right)\Bigg)\Bigg]^{-\frac{1}{N_R N_S}}, \end{aligned} \tag{4.51}$$

and

$$\Theta_2 = \left({L_D}^{N_D-L_D} L_D!\right)^{\frac{1}{N_D}} \Big[\frac{a}{2}\sqrt{\frac{b}{\pi}}\frac{\Gamma\left(N_R N_D+\frac{1}{2}\right)}{b^{N_R N_D+\frac{1}{2}}} \times \ Big(\left(1-e^{-\mu}\right)^L + \sum_{l=1}^{L}\binom{M}{m}\frac{(-1)^{m+1}}{(\mu l)^{N_R N_D}} \times \Gamma\left(N_R N_D+1, \mu m\right)\Big)\Big]^{-\frac{1}{N_R N_D}}. \tag{4.52}$$

The result in *Theorem 7* is valid for the practical cognitive scenario where $\overline{\gamma}_Q = \mu\overline{\gamma}_P$. From (4.49), it is obvious that the diversity gain is independent of the modulation scheme, and only determined by N_S, N_R, and N_D in the secondary network. The impact of modulation is entirely reflected on the SNR gain. It is observed from (4.50) that the SNR gain is inversely proportional to the modulation specific constants a and the number of PUs M, and is directly proportional to b.

4.5.2.2 Fixed Interference Power Constraint

Theorem 8. *When $\overline{\gamma}_Q$ is fixed, the asymptotic outage probability of cognitive spectrum sharing with TAS/GSC and DF relaying as $\overline{\gamma}_P \to \infty$ is given by*

$$P_s^{\infty} = \begin{cases} \Omega_1\left(\frac{1}{\overline{\gamma}_P}\right)^{N_R N_S} + \Upsilon_1\left(\frac{1}{\overline{\gamma}_Q}\right)^{N_R N_S} & N_{\mathrm{S}} < N_{\mathrm{D}} \\ \Omega_2\left(\frac{1}{\overline{\gamma}_P}\right)^{N_R N_D} + \Upsilon_2\left(\frac{1}{\overline{\gamma}_Q}\right)^{N_R N_D} & N_{\mathrm{S}} > N_{\mathrm{D}} \\ \left(\Omega_1+\Omega_2\right)\left(\frac{1}{\overline{\gamma}_P}\right)^{N_R N_S} & \\ \qquad + \left(\Upsilon_1+\Upsilon_2\right)\left(\frac{1}{\overline{\gamma}_Q}\right)^{N_R N_S} & N_{\mathrm{S}} = N_{\mathrm{D}}\ , \end{cases} \tag{4.53}$$

where

$$\Omega_1 = \frac{a}{2}\sqrt{\frac{b}{\pi}}\frac{\left(1-e^{-\frac{Q}{P}}\right)^M}{\left({L_R}^{N_R-L_R} L_R!\right)^{N_S}}\frac{\Gamma\left(N_R N_S+\frac{1}{2}\right)}{b^{N_R N_S+\frac{1}{2}}}, \tag{4.54}$$

$$\Omega_2 = \frac{a}{2}\sqrt{\frac{b}{\pi}}\frac{\left(1-e^{-\frac{Q}{P}}\right)^M}{\left({L_D}^{N_D-L_D}L_D!\right)^{N_R}}\frac{\Gamma\left(N_R N_D+\frac{1}{2}\right)}{b^{N_R N_D+\frac{1}{2}}}, \tag{4.55}$$

$$\Upsilon_1 = \frac{a}{2}\sqrt{\frac{b}{\pi}}\left(\frac{1}{{L_R}^{N_R-L_R}L_R!}\right)^{N_S}\frac{\Gamma\left(N_R N_S+\frac{1}{2}\right)}{b^{N_R N_S+\frac{1}{2}}}\times\sum_{m=1}^{M}\binom{M}{m}(-1)^{m+1}\frac{\Gamma\left(N_S N_R+1,\frac{Q}{P}m\right)}{m^{N_R N_S}}, \tag{4.56}$$

and

$$\Upsilon_2 = \frac{a}{2}\sqrt{\frac{b}{\pi}}\left(\frac{1}{{L_D}^{N_D-L_D}L_D!}\right)^{N_R}\frac{\Gamma\left(N_R N_D+\frac{1}{2}\right)}{b^{N_R N_D+\frac{1}{2}}}\times\sum_{m=1}^{M}\binom{M}{m}(-1)^{m+1}\frac{\Gamma\left(N_R N_D+1,\frac{Q}{P}m\right)}{m^{N_R N_D}}. \tag{4.57}$$

The result in *Theorem 8* is valid for the practical cognitive scenario when $\overline{\gamma}_Q$ is fixed . It is seen from (4.53) that an error floor exists with a zero diversity gain when $\overline{\gamma}_P \to \infty$.

4.6 Numerical Results

Numerical results are presented to examine the impact of TAS/GSC on the outage probability and SER of cognitive relay networks. The following two scenarios are considered: 1) proportional interference power constraint with $\mu = 2$, and 2) fixed interference power constraint with $\rho = 25$ dB. The threshold SNR is assumed as $\gamma_{th} = 1$ dB.

Fig. 4.2 plots the exact and asymptotic outage probability of the secondary network under proportional interference power constraint from (4.18) and (4.26), respectively, for varying M. It is easy to note that the exact curves precisely agree with the simulation points, and the asymptotic curves accurately predict the diversity gain and SNR gain of the network. As expected, the outage probability decreases with decreasing M. This can be explained by the fact that the SNR gain, as indicated in (4.28), increases with decreasing number of PUs, M. It is also observed that the diversity gain remains the

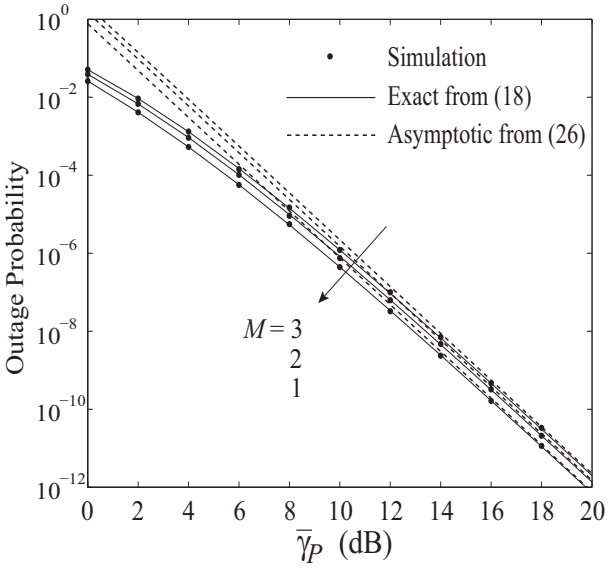

Figure 4.2: Cognitive spectrum sharing with TAS/GSC and DF relaying: $N_{\mathrm{S}} = 2$, $L_{\mathrm{R}} = L_{\mathrm{D}} = 2$, and $\overline{\gamma}_Q = 2\overline{\gamma}_P$.

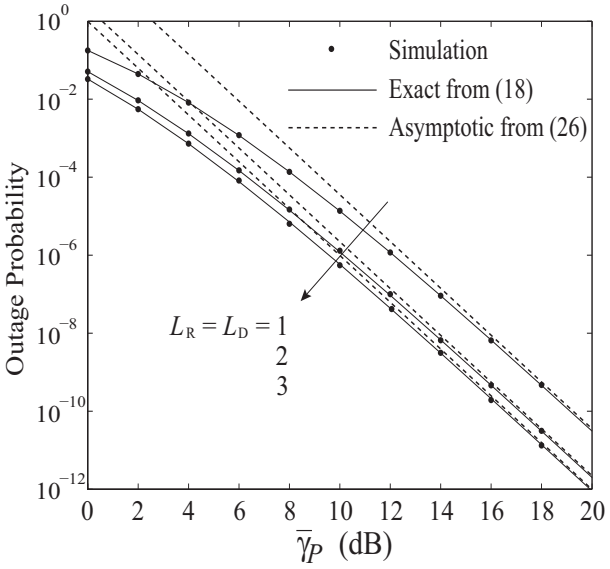

Figure 4.3: Cognitive spectrum sharing with TAS/GSC and DF relaying: $N_{\mathrm{S}} = 2$, $M = 3$, and $\overline{\gamma}_Q = 2\overline{\gamma}_P$.

same under different M which is reflected by the parallel slopes of the asymptotes, which confirms the derived result in (4.27).

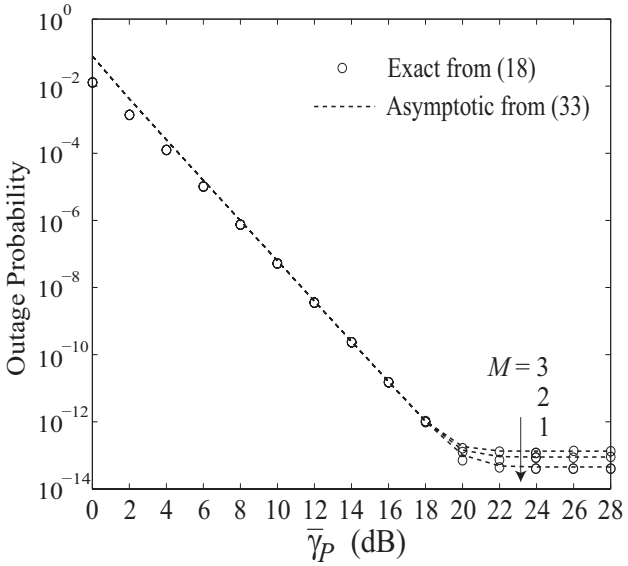

Figure 4.4: Cognitive spectrum sharing with TAS/GSC and DF relaying: $N_{\mathrm{S}} = 2$, $L_{\mathrm{R}} = L_{\mathrm{D}} = 2$, and $\overline{\gamma}_Q = 25$ dB.

Fig. 4.3 plots the exact and asymptotic outage probability of the secondary network under proportional interference power constraint from (4.18) and (4.26), respectively, for varying L_R and L_D. By doing so, the influence of TAS/GSC in each hop on the outage probability is examined. It is seen that the diversity gain is independent of L_R and L_D, as shown by the parallel slopes of the asymptotes. The special cases of TAS/MRC and TAS/SC are characterized by setting $L_R = L_D = 3$ and $L_R = L_D = 1$, respectively. As expected, TAS/GSC outperforms TAS/SC whereas TAS/MRC outperforms TAS/GSC. This is due to the fact that the SNR gain increases with increasing L_R and L_D, as indicated by (4.28).

Fig. 4.4 and Fig. 4.5 plot the exact and asymptotic outage probability of the secondary network under fixed interference power constraint from (4.18) and (4.33), respectively, for varying M and varying L_R, L_D. In the figures, the asymptotic results correctly predict the behavior of the outage probability in the high maximum transmit power to noise ratio regime. As expected, the outage probability decreases with decreasing M, and with increasing L_R and L_D, as indicated in (4.33). It is noticed that the outage probability saturates beyond 22 dB, and displays error floors in the high maximum

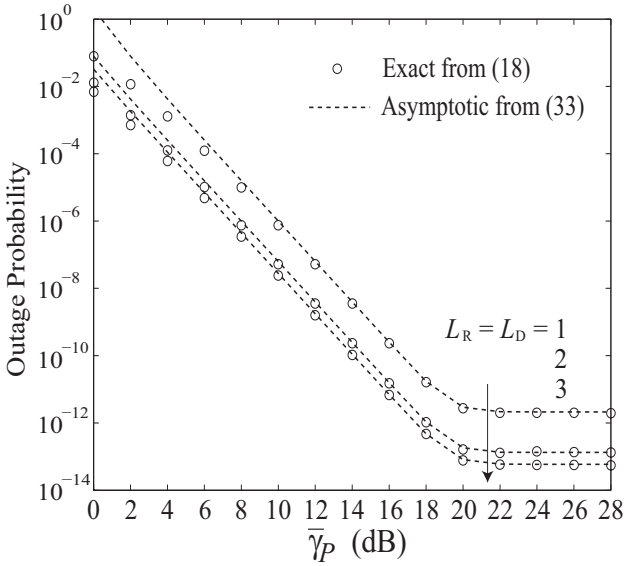

Figure 4.5: Cognitive spectrum sharing with TAS/GSC and DF relaying: $N_S = 2$, $M = 3$, and $\overline{\gamma}_Q = 25$ dB.

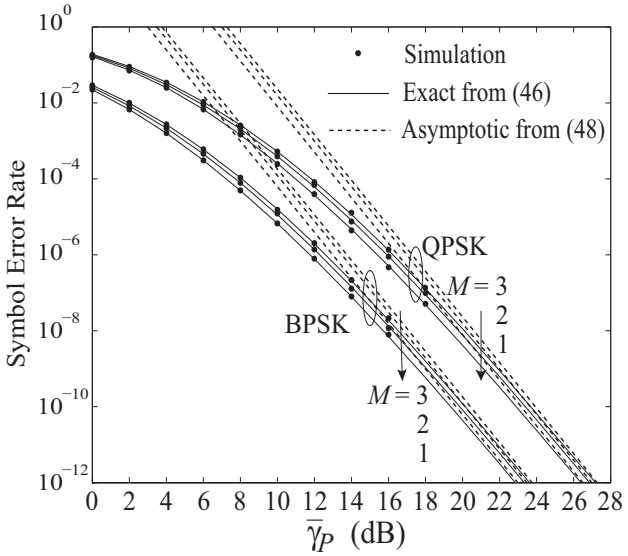

Figure 4.6: Cognitive spectrum sharing with TAS/GSC and DF relaying: $N_S = 2$, $L_R = L_D = 2$, and $\overline{\gamma}_Q = 2\overline{\gamma}_P$.

transmit power to noise ratio regime. This is due to the fact that the fixed interference power constraint limits the transmit power of S and R, which in turn limits the outage probability.

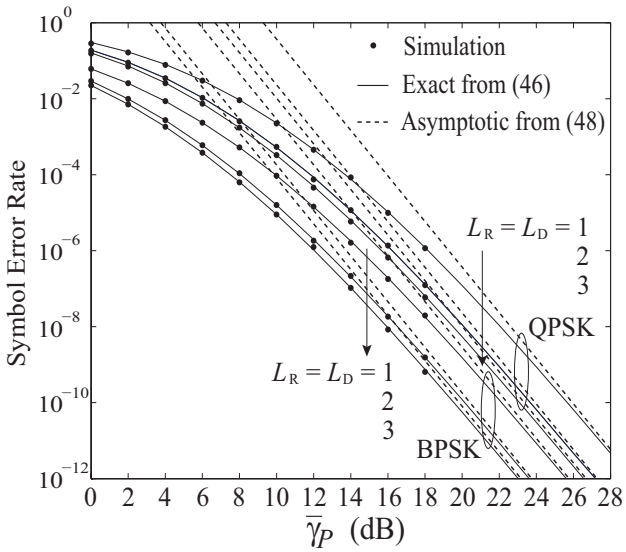

Figure 4.7: Cognitive spectrum sharing with TAS/GSC and DF relaying: $N_S = 2$, $M = 3$, and $\overline{\gamma}_Q = 2\overline{\gamma}_P$

Fig. 4.6 plots the exact and asymptotic SER of the secondary network under proportional interference power constraint from (4.46) and (4.48), respectively, for varying M. It is obvious that the exact curves matches well with the simulation points. It is seen that the SER of the proposed network with BPSK outperforms QPSK. It is also seen that the SER decreases as the number of PU M decreases. It is confirmed that BPSK and QPSK achieve the same diversity gain, and are independent of the primary network, as shown in (4.49). Furthermore, the negative impact of the primary network on the SER is displayed in the SNR gain, as indicated in (4.50).

Fig. 4.7 plots the exact and asymptotic SER of the secondary network under proportional interference power constraint from (4.46) and (4.48), respectively, for varying L_R and L_D. Similar to Fig. 4.6, this network with BPSK outperforms QPSK. It is noticed that the SER decreases with increasing the L_R and L_D. It is also observed that the diversity gain of BPSK and QPSK are the same, and are independent of L_R and L_D, which is indicated in (4.49). The positive impact of L_R and L_D on the SER is shown in the SNR gain in (4.50). By setting $L_R = L_D = 3$ and $L_R = L_D = 1$, it is noticed that TAS/MRC outperforms TAS/GSC whereas TAS/GSC outperforms TAS/SC.

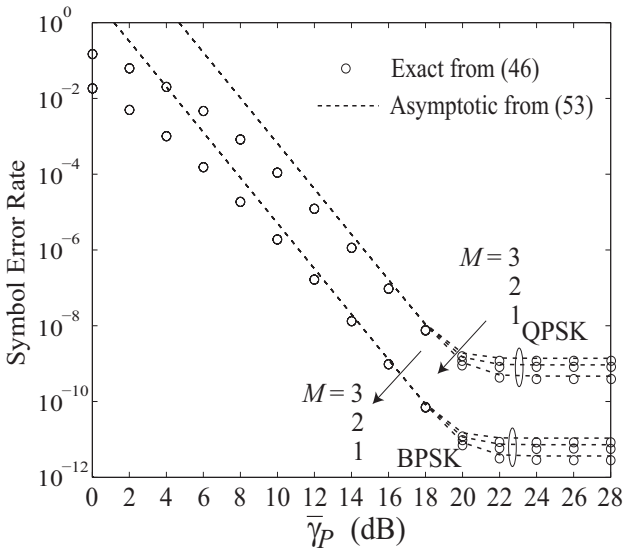

Figure 4.8: Cognitive spectrum sharing with TAS/GSC and DF relaying: $N_{\mathrm{S}} = 2$, $L_{\mathrm{R}} = L_{\mathrm{D}} = 2$, and $\overline{\gamma}_Q = 25$ dB.

Fig. 4.8 and Fig. 4.9 plot the exact and asymptotic SER of the secondary network under fixed interference power constraint from (4.46) and (4.53), respectively, for varying M and varying L_R, L_D. In the low-to-medium maximum transmit power to noise ratio regime, the SER decreases with decreasing M, and with increasing L_R and L_D, as indicated in (4.53). In the high maximum transmit power to noise ratio regime, the SER saturates and exhibits error floors. In these cases, the diversity gain is lost.

4.7 Summary

Cognitive spectrum sharing with TAS/GSC and DF relaying in the presence of multiple primary users is proposed. This setup is well suited to extend the coverage of the secondary network and reduce the interference in the primary network. With this in mind, new closed-form expressions for the exact and asymptotic outage probability and SER of the secondary network with proportional and fixed interference power constraints are derived. The results are valid for arbitrary M primary users, N_S antennas at SS, N_R antennas at SR, and N_D antennas at SD. For the proportional interference power

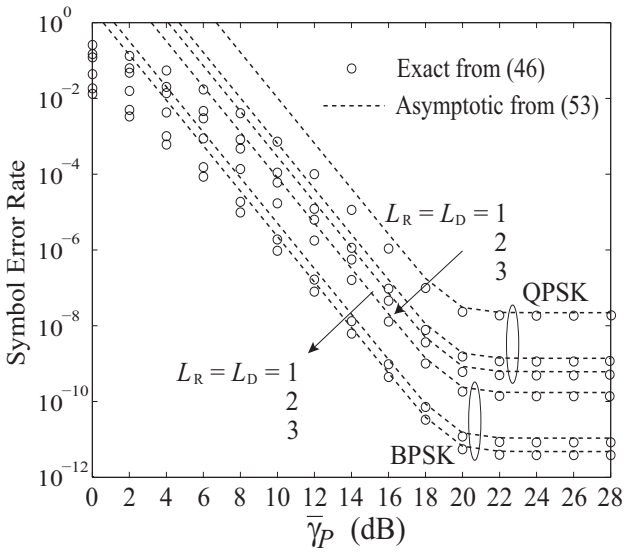

Figure 4.9: Cognitive spectrum sharing with TAS/GSC and DF relaying: $N_S = 2$, $M = 3$, and $\overline{\gamma}_Q = 25$ dB.

constraint, the new closed-form expressions indicate that the diversity gain is entirely determined by the total number of antennas in the secondary network and independent of the primary network. In fact, it is shown that the diversity gain is equal to $N_R \times \min\{N_S, N_D\}$. For the fixed interference power constraint, it is shown that an error floor exists and the diversity gain is lost.

Chapter 5

Cognitive MIMO Relay Networks with Generalized Selection Combining over Nakagami-m Fading

5.1 Introduction

The objective of this chapter is to further examine the impact of TAS/GSC in underlay cognitive relay networks with single primary receiver over Nakagami-m fading. The Nakagami-m fading environment is considered due to its versatility in providing a good match to various empirically obtained measurement data [125]. Note that the transmit powers at SS and SR are limited by two constraints: 1) the peak interference constraint at the primary receiver, and 2) the peak transmit power constraint at SS and SR. It is also important to note that the performance of underlay spectrum sharing is typically restricted due to these two strict power constraints. With the help of TAS/GSC relaying, less transmit power is required at SS and SR, which in turn reduces the interference at the PU, allowing for high speed data services over wide area coverage. The main contributions of this chapter are summarized as follows.

- New exact closed-form expressions for the CDF of the SNR with TAS/GSC are derived. Although the CDF expressions were presented in [45, 166] with the aid of

the trapezoidal rule, they are not in closed-form and cannot be used to derive the CDF of the SNR with TAS/GSC.

- New exact closed-form expressions for the outage probability and the SER are derived to accurately assess the joint impact of antenna configuration and channel fading. The asymptotic expressions for the outage probability and the SER are further derived under the two cases: 1) proportional interference power constraint, and 2) fixed interference power constraint. It is confirmed that the full diversity order is achieved for the proportional interference power constraint. For the fixed interference power constraint, the diversity order is zero with error floors in the high maximum transmit power to noise ratio regime.

- An exact closed-form expression for the ergodic capacity is derived. Notably, this is the first closed-form expression for the ergodic capacity in cognitive relay networks with TAS/GSC in Nakagami-m fading channels. More importantly, a tight high SNR approximation of the ergodic capacity is derived for the two cases: 1) proportional interference power constraint, and 2) fixed interference power constraint. Interesting conclusions are reached. On the one hand, the high SNR slope is independent of the antenna configuration and the fading parameters, but on the other hand, the high SNR power offset is fully described by the antenna configuration and the fading parameters in the primary and secondary networks. The high SNR slope is 1/2 for the proportional interference power constraint, and is equal to zero for the fixed interference power constraint.

5.2 Network and Channel Description

A dual-hop cognitive DF relay network consisting of SS with N_S antennas, SR with N_R antennas, SD with N_D antennas, and PU with a single antenna is considered. It is assumed that the PU-Tx is located far away from the secondary network. This assumption is typical in large-scale networks where the interference from the PU-Tx is negligible

[163, 167, 168]. It is also assumed there is no direct link between SS and SD due to long distance and deep fades [169]. Both the primary channel and the secondary channel are assumed to undergo quasi-static fading with independent and identically distributed (i.i.d.) Nakagami-m distribution. It is assumed perfect CSI between the secondary transmitter and the PU can be obtained through direct feedback from the PU [149], indirect feedback from a third party, and periodic sensing of pilot signal from the PU [170]. In the secondary network, a single transmit antenna among N_S antennas which maximizes the GSC output SNR at SR is selected at SS, while the L_R ($1 \leq L_R \leq N_R$) strongest receive antennas are combined at SR. The signal transmitted by SR is decoded and forwarded using a single transmit antenna among N_R antennas which maximizes the GSC output SNR at SD, and then combined at SD with the L_D ($1 \leq L_D \leq N_D$) strongest receive antennas. Let $\{g_{1ij}\}$ denote the channel coefficients of the $N_S \times N_R$ channels from SS to SR with $i \in \{1, \ldots, N_S\}$, $j \in \{1, \ldots, N_R\}$, and $\{g_{2jk}\}$ denote the channel coefficients of the $N_R \times N_D$ channels from SR to SD with $k \in \{1, \ldots, N_D\}$. Also, $\{h_{1i}\}$ denote the channel coefficients of the $N_S \times 1$ channels from SS to PU, and $\{h_{2j}\}$ denote the channel coefficients of the $N_R \times 1$ channels from SR to PU. The channel coefficients follow the Nakagami-m distribution with fading parameters m_{g1}, m_{g2}, m_{h1}, and m_{h2}, and average channel power gains Ω_{g1}, Ω_{g2}, Ω_{h1}, and Ω_{h2}. In the following, $\| \cdot \|$ is the Euclidean norm, $| \cdot |$ is the absolute value, and $\mathbb{E}[\cdot]$ is the expectation.

The pilot symbol block P_i, ($1 \leq i \leq N_S$), are transmitted from each transmit antenna at different time slots. Based on these pilot symbols, SR perfectly estimates CSI, then arranges $\left\{\left|g_{1ij}\right|^2\right\}_{j=1}^{N_R}$ in descending order as $\left|g_{1i(1)}\right|^2 \geq \left|g_{1i(2)}\right|^2 \geq \cdots \geq \left|g_{1i(N_R)}\right|^2 \geq 0$ for the each transmit antenna i at SS. Note that before the transmission process, the selected number of antenna chains L_R and L_D at the receivers are determined by the limited number of RF chains due to size and complexity limitations. According to the rule of GSC, the first L_R ($1 \leq \mathrm{L}_R \leq N_R$) received signal power(s) are combined at the SR to obtain $\theta_i = \sum_{j=1}^{L_R} \left|g_{1i(j)}\right|^2$. The selected transmit antenna i^* is determined at the SR

by

$$i^* = \underset{1\leq i\leq N_S}{\arg\max} \left\{ \theta_i = \sum_{j=1}^{L_R} |g_{1i(j)}|^2 \right\}, \tag{5.1}$$

which maximizes the total received signal power. To this end, the index of the selected transmit antenna is sent back to SS through the feedback channel, so that only $\lceil \log_2 (N_S) \rceil$ bits needs to be sent to SS. As such, the selected channel vector is denoted as $\mathbf{g}_{1i^*\theta_{i^*}} = \left[g_{1i^*(1)}, \cdots, g_{1i^*(L_R)} \right]$. Similarly, in the second hop, the index of the selected transmit antenna at SR is determined by

$$j^* = \underset{1\leq j\leq N_R}{\arg\max} \left\{ \theta_j = \sum_{k=1}^{L_D} \left| g_{2j(k)} \right|^2 \right\}. \tag{5.2}$$

As such, the selected channel vector is denoted as $\mathbf{g}_{2j^*\theta_{j^*}} = \left[g_{2j^*(1)}, \cdots, g_{2j^*(L_D)} \right]$.

According to underlay cognitive relay networks, the transmit powers at SS and SR are constrained as

$$P_S = \min \left(P, \frac{Q}{|h_{1i^*}|^2} \right) \quad \text{and} \quad P_R = \min \left(P, \frac{Q}{|h_{2j^*}|^2} \right), \tag{5.3}$$

respectively, where P is the maximum transmit power constraint at SS and SR, and Q is the peak interference power constraint at the PU.

The instantaneous end-to-end SNR of the spectrum sharing network with TAS/GSC and DF relaying is defined as $\gamma = \min \{\gamma_1, \gamma_2\}$, where the instantaneous SNR of SS $\rightarrow$ SR link is

$$\gamma_1 = \min \left(\left\| \mathbf{g}_{1i^*\theta_{i^*}} \right\|^2 \bar{\gamma}_P, \frac{\left\| \mathbf{g}_{1i^*\theta_{i^*}} \right\|^2 \bar{\gamma}_Q}{|h_{1i^*}|^2} \right) \tag{5.4}$$

and the instantaneous SNR of SR $\rightarrow$ SD link is

$$\gamma_2 = \min\Big(\Big\|\mathbf{g}_{2j^*\theta_{j^*}}\Big\|^2 \bar{\gamma}_P, \frac{\Big\|\mathbf{g}_{2j^*\theta_{j^*}}\Big\|^2 \bar{\gamma}_Q}{|h_{2j^*}|^2}\Big). \tag{5.5}$$

In (5.4) and (5.5), it is defined that $\overline{\gamma}_P = \frac{P}{N_0}$ and $\overline{\gamma}_Q = \frac{Q}{N_0}$, where N_0 is the noise power of AWGN.

5.3 New Statistical Properties

In this section, new statistical properties of the end-to-end SNR is derived, which is a challenging problem due to the complex nature of TAS/GSC in Nakagami-m fading. Based on these statistical characteristics, the exact and asymptotic outage probability, SER, and ergodic capacity are presented. Without loss of generality, these new statistics can be easily applied to other wireless networks with TAS/GSC.

Based on the expressions of γ_1 and γ_2 in (5.4) and (5.5), respectively, the CDF of $\left\|\mathbf{g}_{1i^*\theta_{i^*}}\right\|^2$ is first derived in the following lemmas.

5.3.1 Expressions for CDF of $\|\mathbf{g}_{1i^*\theta_{i^*}}\|^2$ in the Secondary Channel

Lemma 2. *The expression for the CDF of* $\left\|\mathbf{g}_{1i^*\theta_{i^*}}\right\|^2$ *is derived as*

$$F_{\left\|\mathbf{g}_{1i^*\theta_{i^*}}\right\|^2}(x) = \Big(\frac{L_R}{(m_{g1}-1)!}\binom{N_R}{L_R}\Big)^{N_S} N_S! \widetilde{\sum_{\mathcal{S}_R^{|\mathcal{S}_K|}}} \hbar_k x^{\theta_k} e^{-\eta_k x}, \tag{5.6}$$

where $\widetilde{\sum_{\mathcal{S}_R^{|\mathcal{S}_K|}}} \triangleq \sum_{\mathcal{S}_R}\sum_{\mathcal{S}_R^1}\cdots\sum_{\mathcal{S}_R^k}\cdots\sum_{\mathcal{S}_R^{|\mathcal{S}_K|}}$, $\mathcal{S}_R = \Big\{\big(n_{\tau,1},\ldots,n_{\tau,|\mathcal{S}_K|}\big)\Big|\sum_{k=1}^{|\mathcal{S}_K|} n_{\tau,k} = N_S\Big\}$ *with* $\{n_{\tau,k}\} \in \mathbb{Z}^+$, $|\mathcal{S}_K|$ *is the cardinality of the set* $\mathcal{S}_K$, *and* $\mathcal{S}_K$ *denotes a set of* $(2m_{g1}+1)$*-tuples sat-*

isfying the following condition

$$\mathcal{S}_K = \big\{ \big(n^{\Phi}_{k,0}, \ldots, n^{\Phi}_{k,m_{g1}-1}, n^{F}_{k,0}, \ldots, n^{F}_{k,m_{g1}}\big) \big| \sum_{i=0}^{m_{g1}-1} n^{\Phi}_{k,i} = L_R - 1; \sum_{j=0}^{m_{g1}} n^{F}_{k,j} = N_R - L_R \big\},$$

thereby $|\mathcal{S}_K| = \binom{m_{g1}+L_R-2}{m_{g1}-1}\binom{m_{g1}+N_R-L_R}{m_{g1}}$, *and* $\mathcal{S}^k_R = \big\{ \big(n_{\rho_k,0}, \ldots, n_{\rho_k,m_{g1}L_R+b^F_k}\big) \big| \sum_{n=0}^{m_{g1}L_R+b^F_k} n_{\rho_k,n} = n_{\tau,k} \big\}$, $k = 1, \cdots, |\mathcal{S}_K|$, *with* $\{n^{\Phi}_{k,i}\}$, $\{n^{\Phi}_{k,i}\}$, $\{\, n^{F}_{k,j}\}$, *and* $\{n_{\rho_k,n}\} \in \mathbb{Z}^+$. *In* (5.6), $\hbar_k$, θ_k, *and* η_k *are respectively given by*

$$\hbar_k = \prod_{k=1}^{|\mathcal{S}_K|} \Big(a^{\Phi}_k a^{F}_k \frac{(n_2-1)!}{{L_R}^{n_2}} \Big)^{n_{\tau,k}} \Big(\frac{\prod_{n=0}^{m_{g1}L_R+b^F_k} \ell_k(n)^{n_{\rho_k,n}}}{\prod_{n=0}^{m_{g1}L_R+b^F_k} n_{\rho_k,n}!} \Big), \tag{5.7}$$

$$\theta_k = \sum_{k=1}^{|\mathcal{S}_K|} \sum_{n=0}^{m_{g1}L_R+b^F_k} \mu_k(n) n_{\rho_k,n}, \tag{5.8}$$

and

$$\eta_k = \sum_{k=1}^{|\mathcal{S}_K|} \sum_{n=0}^{m_{g1}L_R+b^F_k} \nu_k(n) n_{\rho_k,n}, \tag{5.9}$$

where n_2, $\mu_k(n)$, $\nu_k(n)$, $\ell_k(n)$ a^{Φ}_k, a^{F}_k, b^{Φ}_k, b^{F}_k, Υ_{k1}, Υ_{k2}, Υ_{k3}, *and* Υ_{k4} *are defined in the following proof.*

Proof. See Appendix C.1. □

5.3.2 Expressions for the CDF of $\left\|\mathbf{g}_{2j^*\theta_{j^*}}\right\|^2$ in the Secondary Channel

The CDF of $\left\|\mathbf{g}_{2j^*\theta_{j^*}}\right\|^2$ follows from (5.6) by interchanging the parameters $m_{g1} \to m_{g2}$, $m_{h1} \to m_{h2}$, $L_R \to L_D$, $N_R \to N_D$, $N_S \to N_R$, $\mathcal{S}_R \to \mathcal{S}_D$, $|\mathcal{S}_K| \to |\mathcal{S}_T|$, $\mathcal{S}^{|\mathcal{S}_K|}_R \to \mathcal{S}^{|\mathcal{S}_T|}_D$, $\hbar_k \to \hbar_t$, $\theta_k \to \theta_t$, and $\eta_k \to \eta_t$, where $\widetilde{\sum_{\mathcal{S}^{|\mathcal{S}_T|}_D}} \triangleq \sum_{\mathcal{S}_D} \sum_{\mathcal{S}^1_D} \cdots \sum_{\mathcal{S}^t_D} \cdots \sum_{\mathcal{S}^{|\mathcal{S}_T|}_D}$, $\mathcal{S}_D = \big\{ \big(n_{\tau,1}, \ldots, n_{\tau,|\mathcal{S}_T|}\big) \big| \sum_{t=1}^{|\mathcal{S}_T|} n_{\tau,t} = N_R \big\}$ with $\{n_{\tau,t}\} \in \mathbb{Z}^+$, $|\mathcal{S}_T|$ is the cardinality of the

set $\mathcal{S}_T$, and $\mathcal{S}_T$ denotes a set of $(2m_{g2}+1)$-tuples satisfying the following condition

$$\mathcal{S}_T = \big\{\big(n^{\Phi}_{t,0},\ldots,n^{\Phi}_{t,m_{g2}-1},n^{F}_{t,0},\ldots,n^{F}_{t,m_{g2}}\big)\big|\sum_{i=0}^{m_{g2}-1} n^{\Phi}_{t,i}=L_D-1;\sum_{j=0}^{m_{g2}} n^{F}_{t,j}=N_D-L_D\big\},$$

thereby $|\mathcal{S}_T|=\binom{m_{g2}+L_D-2}{m_{g2}-1}\binom{m_{g2}+N_D-L_D}{m_{g2}}$, and $\mathcal{S}^t_D = \big\{\big(n_{\rho_t,0},\ldots,n_{\rho_t,m_{g2}L_D+b^F_t}\big)\Big|\sum_{n=0}^{m_{g2}L_D+b^F_t} n_{\rho_t,n}=n_{\tau,t}\big\}$, $t=1,\cdots,|\mathcal{S}_T|$, with $\big\{n^{\Phi}_{t,i}\big\}$, $\big\{n^{\Phi}_{t,i}\big\}$, $\big\{\ n^{F}_{t,j}\big\}$, and $\big\{n_{\rho_t,n}\big\}\in\mathbb{Z}^+$. Note that $\hbar_t$, θ_t, η_t follow from (5.7), (5.8), (5.9) by interchanging the parameters $\mu_k(n)\to\mu_t(n)$, $\nu_k(n)\to\nu_t(n)$, $\ell_k(n)\to\ell_t(n)$ $a^{\Phi}_k\to a^{\Phi}_t$, $b^{\Phi}_k\to b^{\Phi}_t$, $c^{\Phi}_k\to c^{\Phi}_t$, $a^{F}_k\to a^{F}_t$, $b^{F}_k\to b^{F}_t$, $c^{F}_k\to c^{F}_t$, $\Upsilon_{k1}\to\Upsilon_{t1}$, $\Upsilon_{k2}\to\Upsilon_{t2}$, $\Upsilon_{k3}\to\Upsilon_{t3}$, and $\Upsilon_{k4}\to\Upsilon_{t4}$. Here, $\mu_t(n)$, $\nu_t(n)$, $\ell_t(n)$ a^{Φ}_t, b^{Φ}_t, c^{Φ}_t, a^{F}_t, b^{F}_t, c^{F}_t, Υ_{t1}, Υ_{t2}, Υ_{t3}, and Υ_{t4} follow from (C.15), (C.16), (C.14), (C.6), (C.7), (C.9), (C.10), (C.17), (C.18), (C.19), and (C.20) by interchanging the parameters $m_{g1}\to m_{g2}$, $m_{h1}\to m_{h2}$, $\Omega_{h1}\to\Omega_{h2}$, $L_R\to L_D$, $N_R\to N_D$, $N_S\to N_R$, $\mathcal{S}_R\to\mathcal{S}_D$, $|\mathcal{S}_K|\to|\mathcal{S}_T|$, $\mathcal{S}_R^{|\mathcal{S}_K|}\to\mathcal{S}_D^{|\mathcal{S}_T|}$, $n_{\tau,k}\to n_{\tau,t}$, $n^{\Phi}_{k,i}\to n^{\Phi}_{t,i}$, $n^{\Phi}_{k,i}\to n^{\Phi}_{t,i}$, $n^{F}_{k,j}\to n^{F}_{t,j}$, and $n_{\rho_k,n}\to n_{\rho_t,n}$.

5.3.3 Expressions for the CDF of γ_1

With the help of the CDF of $\big\|\mathbf{g}_{1i^*\theta_{i^*}}\big\|^2$ and $|h_{1i^*}|^2$, the closed-form CDF of γ_1 is evaluated in the following lemma.

Lemma 3. *The expression for the CDF of γ_1 is represented as*

$$F_{\gamma_1}(x) = \Big(\frac{L_R}{(m_{g1}-1)!}\binom{N_R}{L_R}\Big)^{N_S} N_S!\widetilde{\sum_{\mathcal{S}_R^{|\mathcal{S}_K|}}}\hbar_k\Xi_k(x), \tag{5.10}$$

where

$$\Xi_k(x) = \Big(1-\frac{\Gamma\big(m_{h1},\frac{m_{h1}Q}{\Omega_{h1}P}\big)}{\Gamma(m_{h1})}\Big)\Big(\frac{x}{\bar{\gamma}_P}\Big)^{\theta_k}e^{-\eta_k\frac{x}{\bar{\gamma}_P}}+ \Big(\frac{m_{h1}}{\Omega_{h1}}\Big)^{m_{h1}}\Big(\frac{x}{\bar{\gamma}_Q}\Big)^{\theta_k}\frac{\Gamma\big(\theta_k+m_{h1},\big(\frac{m_{h1}}{\Omega_{h1}}+\frac{\eta_k x}{\bar{\gamma}_Q}\big)\frac{Q}{P}\big)}{(m_{h1}-1)!\big(\frac{m_{h1}}{\Omega_{h1}}+\frac{\eta_k x}{\bar{\gamma}_Q}\big)^{\theta_k+m_{h1}}}. \tag{5.11}$$

Proof. See Appendix C.2. □

5.3.4 Expressions for the CDF of γ_2

Similarly, the CDF of γ_2 follows from (5.10) and (5.11) by interchanging the parameters $m_{g1} \to m_{g2}$, $m_{h1} \to m_{h2}$, $\Omega_{h1} \to \Omega_{h2}$, $\eta_k \to \eta_t$, and $\theta_k \to \theta_t$. Note that these expressions are valid for arbitrary fading severity parameters in all the links.

5.4 Outage Probability

In this section, the focus is the outage probability. A new closed-form expression for the exact outage probability is derived. In order to assess the performance at high SNRs, the asymptotic outage probabilities with the proportional interference power constraint and the fixed interference power constraint are also derived.

5.4.1 Exact Analysis

In DF relaying, the end-to-end outage probability is determined by the worst link between SS $\to$ SR and SR $\to$ SD links, which is given by [160]

$$\begin{aligned} P_{out}\left(\gamma_{th}\right) &= \Pr\left(\min(\gamma_1, \gamma_2) \leq \gamma_{th}\right) \\ &= F_{\gamma_1}\left(\gamma_{th}\right) + F_{\gamma_2}\left(\gamma_{th}\right) - F_{\gamma_1}\left(\gamma_{th}\right) F_{\gamma_2}\left(\gamma_{th}\right). \end{aligned} \tag{5.12}$$

By substituting (5.10) and the CDF of γ_2 into (5.12), the outage probability is finally derived in the following theorem.

Theorem 9. *The closed-form expression for the outage probability of spectrum sharing*

networks with TAS/GSC and DF relaying over Nakagami-m fading is derived as

$$P_{out}\left(\gamma_{th}\right) = 1 - \left(1 - \left(\frac{L_R}{\left(m_{g1}-1\right)!}\binom{N_R}{L_R}\right)^{N_S} N_S! \widetilde{\sum_{\mathcal{S}_R^{|\mathcal{S}_K|}}} \hbar_k \Xi_k\left(\gamma_{th}\right)\right) \left(1 - \left(\frac{L_D}{\left(m_{g2}-1\right)!}\binom{N_D}{L_D}\right)^{N_R} N_R! \widetilde{\sum_{\mathcal{S}_D^{|\mathcal{S}_T|}}} \hbar_t \Xi_t\left(\gamma_{th}\right)\right). \tag{5.13}$$

This new closed-form expression for the outage probability is valid for an arbitrary number of antennas of the secondary network and arbitrary fading severity parameters in all the links.

5.4.2 Asymptotic Analysis

5.4.2.1 Proportional Interference Power Constraint

The asymptotic behavior with the proportional interference power constraint is first examined. As such, it is assumed that both P and Q grow large in the high SNR regime. This applies to the scenario where the PU is able to tolerate a high amount of interference from SS and SR. With this in mind, the effect of the so-called *power scaling* on the outage probability is studied. Similar to [77, 167], it is assumed $Q = \mu P$, where μ is the power scaling factor and is a positive constant.

Theorem 10. *When Q scales with P, the asymptotic outage probability of cognitive spectrum sharing with TAS/GSC and DF relaying in Nakagami-m fading at high SNRs is derived as*

$$P_{out}^{\infty}\left(\gamma_{th}\right) = \left(G_c \overline{\gamma}_P\right)^{-G_d} + o\left({\overline{\gamma}_P}^{-G_d}\right), \tag{5.14}$$

where the diversity order is

$$G_d = N_R \times \min\left\{m_{g1} N_S, m_{g2} N_D\right\} \tag{5.15}$$

and the SNR gain is

$$G_c = \begin{cases} \frac{\Delta_1(L_R)}{\gamma_{th}} & m_{g1}N_{\rm S} < m_{g2}N_{\rm D} \\ \frac{\Delta_2(L_R)}{\gamma_{th}} & m_{g1}N_{\rm S} > m_{g2}N_{\rm D} \\ \frac{\Delta_1(L_R)}{\gamma_{th}} + \frac{\Delta_2(L_R)}{\gamma_{th}} & m_{g1}N_{\rm S} = m_{g2}N_{\rm D}\ , \end{cases} \tag{5.16}$$

with

$$\Delta_1(L_R) = \frac{\Omega_{g1}}{m_{g1}}\Big[\frac{\mathrm{K}\big(\mathcal{S}_K^{\Phi}, N_R, L_R, m_{g1}, a_k^{\Phi}, b_k^{\Phi}\big)}{(m_{g1}N_R)!}\Big]^{-\frac{1}{m_{g1}N_R}} \Big[\Phi\big(m_{h1}, \Omega_{h1}\big) + \frac{\Xi\big(m_{g1}, m_{h1}, \Omega_{h1}, N_S\big)}{\mu^{m_{g1}N_RN_S}}\Big]^{-\frac{1}{m_{g1}N_RN_S}}, \tag{5.17}$$

and

$$\Delta_2(L_R) = \frac{\Omega_{g2}}{m_{g2}}\Big[\frac{\mathrm{K}\big(\mathcal{S}_T^{\Phi}, N_D, L_D, m_{g2}, a_t^{\Phi}, b_t^{\Phi}\big)}{(m_{g2}N_D)!}\Big]^{-\frac{1}{m_{g2}N_D}} \Big[\Phi\big(m_{h2}, \Omega_{h2}\big) + \frac{\Xi\big(m_{g2}, m_{h2}, \Omega_{h2}, N_D\big)}{\mu^{m_{g2}N_RN_D}}\Big]^{-\frac{1}{m_{g2}N_RN_D}}. \tag{5.18}$$

In (5.17) *and* (5.18),

$$\mathrm{K}\big(\mathcal{S}^{\Phi}, N, L, m_g, a^{\Phi}, b^{\Phi}\big) = \frac{L\binom{N}{L}}{(m_g-1)!(m_g!)^{N-L}} \sum_{\mathcal{S}^{\Phi}} a^{\Phi} \frac{(b^{\Phi} + m_g(N-L+1)-1)!}{(L)^{b^{\Phi}+m_g(N-L+1)}}, \tag{5.19}$$

$$\Phi\big(m_h, \Omega_h\big) = 1 - e^{-\mu\frac{m_h}{\Omega_h}} \sum_{j=0}^{m_h-1} \frac{\big(\mu\frac{m_h}{\Omega_h}\big)^j}{j!}, \quad \Xi\big(m_g, m_h, \Omega_h, N\big) = \frac{\Gamma(m_gN_RN + m_h, \mu\frac{m_h}{\Omega_h})}{(m_h-1)!(\frac{m_h}{\Omega_h})^{m_gN_RN}}. \tag{5.20}$$

Proof. See Appendix C.3. □

Based on (5.15), it can be seen that the diversity order is dominated by the fading severity parameter of the two hops and the total number of antennas at SS, SR, and SD. Interestingly, it is independent of the fading severity parameters of the interference channel, and the selected number of antennas at SR and SD. The negative impact of the peak interference power constraint is reflected in the SNR gain.

Corollary 1. *The SNR gap between GSC and SC is derived as*

$$G_c = \begin{cases} -\frac{10}{m_{g1}N_R}\log\left(\mathrm{T}_1\right) & m_{g1}N_{\mathrm{S}} < m_{g2}N_{\mathrm{D}} \\ -\frac{10}{m_{g2}N_D}\log\left(\mathrm{T}_2\right) & m_{g1}N_{\mathrm{S}} > m_{g2}N_{\mathrm{D}} \\ 10\log\left(\frac{\Delta_1(L_R)+\Delta_2(L_R)}{\Delta_1(1)+\Delta_2(1)}\right) & m_{g1}N_{\mathrm{S}} = m_{g2}N_{\mathrm{D}}\ , \end{cases} \tag{5.21}$$

where

$$\mathrm{T}_1 = \frac{\left(m_{g1}!\right)^{N_R-1}\left(m_{g1}-1\right)!}{N_R\left(m_{g1}N_R-1\right)!}\mathrm{K}(S_K^{\Phi}, N_R, L_R, m_{g1}, a_k^{\Phi}, b_k^{\Phi}) \tag{5.22}$$

and

$$\mathrm{T}_2 = \frac{\left(m_{g2}!\right)^{N_D-1}\left(m_{g2}-1\right)!}{N_D\left(m_{g2}N_D-1\right)!}\mathrm{K}(S_T^{\Phi}, N_D, L_D, m_{g2}, a_t^{\Phi}, b_t^{\Phi}). \tag{5.23}$$

5.4.2.2 Fixed Interference Power Constraint

Different from the proportional interference power constraint which can tolerate an extremely high peak interference power constraint and may potentially violate and harm the PU transmission [163], this subsection considers a stricter constraint where the peak interference power constraint is fixed [164]. The asymptotic outage probability with the fixed interference power constraint is presented in the following theorem.

Theorem 11. *Under the fixed interference power constraint, the asymptotic outage probability of cognitive spectrum sharing with TAS/GSC and DF relaying in Nakagami-m*

fading at high SNRs is derived as

$$P_{out}^{\infty}\left(\gamma_{th}\right)=\begin{cases}\mathrm{H}_1\big(\Phi_1\big(\frac{\gamma_{th}}{\bar{\gamma}_P}\big)^{m_{g1}N_RN_S}+\Xi_1\big(\frac{\gamma_{th}}{\bar{\gamma}_Q}\big)^{m_{g1}N_RN_S}\big) & \\ \qquad\qquad m_{g1}N_{\mathrm{S}}<m_{g2}N_{\mathrm{D}} & \\ \mathrm{H}_2\big(\Phi_2\big(\frac{\gamma_{th}}{\bar{\gamma}_P}\big)^{m_{g2}N_RN_D}+\Xi_2\big(\frac{\gamma_{th}}{\bar{\gamma}_Q}\big)^{m_{g2}N_RN_D}\big) & \\ \qquad\qquad m_{g1}N_{\mathrm{S}}>m_{g2}N_{\mathrm{D}} & \\ \big(\mathrm{H}_1\Phi_1+\mathrm{H}_2\Phi_2\big)\big(\frac{\gamma_{th}}{\bar{\gamma}_P}\big)^{m_{g1}N_RN_S} & \\ \qquad +\big(\mathrm{H}_1\Xi_1+\mathrm{H}_2\Xi_2\big)\big(\frac{\gamma_{th}}{\bar{\gamma}_Q}\big)^{m_{g1}N_RN_S} & \\ \qquad\qquad m_{g1}N_{\mathrm{S}}=m_{g2}N_{\mathrm{D}}\ , & \end{cases} \tag{5.24}$$

where

$$\mathrm{H}_1=\Big[\frac{\big(\frac{m_{g1}}{\Omega_{g1}}\big)^{m_{g1}N_R}\mathrm{K}\big(\mathcal{S}_K^{\Phi},N_R,L_R,m_{g1},a_k^{\Phi},b_k^{\Phi}\big)}{(m_{g1}N_R)!}\Big]^{N_S}, \tag{5.25}$$

$$\mathrm{H}_2=\Big[\frac{\big(\frac{m_{g2}}{\Omega_{g2}}\big)^{m_{g2}N_D}\mathrm{K}\big(\mathcal{S}_T^{\Phi},N_D,L_D,m_{g2},a_t^{\Phi},b_t^{\Phi}\big)}{(m_{g2}N_D)!}\Big]^{N_R}, \tag{5.26}$$

$$\Phi_1=\Phi\left(m_{h1},\Omega_{h1}\right), \tag{5.27}$$

$$\Phi_2=\Phi\left(m_{h2},\Omega_{h2}\right), \tag{5.28}$$

$$\Xi_1=\Xi\left(m_{g1},m_{h1},\Omega_{h1},N_S\right), \tag{5.29}$$

and

$$\Xi_2=\Xi\left(m_{g2},m_{h2},\Omega_{h2},N_D\right). \tag{5.30}$$

Proof. The proof can be done in the same way as the proof of Theorem 2. □

From (5.24), it is shown that the diversity order of the outage probability tends to zero under the fixed interference power constraint.

5.5 Symbol Error Rate

This section focus on the SER as another important performance evaluation metric. For most modulation schemes, the SER of a conventional wireless communication system can be expressed as [171]

$$P_e = \frac{a}{2}\sqrt{\frac{b}{\pi}}\int_0^\infty \frac{e^{-b\gamma}}{\sqrt{\gamma}} F_\gamma(\gamma) d\gamma, \tag{5.31}$$

where a and b are modulation specific constants. For example, $a = 1$, $b = 1$ for BPSK , $a = 2(M-1)/M$, $b = 3/(M^2-1)$ for M-PAM , and $a = 2$, $b = \sin^2(\pi/M)$ for M-PSK.

5.5.1 Exact Analysis

Substituting (5.10) into (5.31), the SER of SS $\rightarrow$ SR link can be derived by utilizing [172, eq.8.310.1], [172, eq.8.352.2], [172, eq.9.211.4.8] and the polynomial expansion. Using the same method, P_{e2}, which is the SER of SR $\rightarrow$ SD link can be easily computed. Substituting the derived expressions of P_{e1} and P_{e2} into

$$P_e = 1 - \big(1 - P_{e1}\big) \times \big(1 - P_{e2}\big), \tag{5.32}$$

yields the SER of cognitive relay networks with TAS/GSC and DF relaying in the following theorem.

Theorem 12. *The closed-form expression for the SER of cognitive spectrum sharing*

with TAS/GSC and DF relaying in Nakagami-m fading is derived as

$$P_e = 1 - \big(1 - \frac{a}{2}\sqrt{\frac{b}{\pi}}\big(\frac{L_R}{(m_{g1}-1)!}\binom{N_R}{L_R}\big)^{N_S} N_S! \widetilde{\sum_{\mathcal{S}_R^{|\mathcal{S}_K|}}} \hbar_k \Pi\left(m_{h1}, \Omega_{h1}, \theta_k, \eta_k\right)\big)$$
$$\big(1 - \frac{a}{2}\sqrt{\frac{b}{\pi}}\big(\frac{L_D}{(m_{g2}-1)!}\binom{N_D}{L_D}\big)^{N_R} N_R! \widetilde{\sum_{\mathcal{S}_D^{|\mathcal{S}_T|}}} \hbar_t \Pi\left(m_{h2}, \Omega_{h2}, \theta_t, \eta_t\right)\big), \tag{5.33}$$

where

$$\Pi\left(m_h, \Omega_h, \theta, \eta\right) = \big[\big(1 - \frac{\Gamma\big(m_h, \frac{m_h Q}{\Omega_h P}\big)}{\Gamma(m_h)}\big)\frac{\Gamma\big(\theta+\frac{1}{2}\big)}{\big(b+\frac{\eta}{\bar{\gamma}_P}\big)^{\theta+\frac{1}{2}}}\big(\frac{1}{\bar{\gamma}_P}\big)^{\theta} + \frac{1}{(m_h-1)!}(\theta+m_h-1)!e^{-\frac{m_h Q}{\Omega_h P}}$$
$$\big(\frac{1}{\eta}\big)^{\theta+\frac{1}{2}}\Gamma\big(\theta+\frac{1}{2}\big)\sum_{m=0}^{\theta+m_h-1}\frac{1}{m!}\big(\frac{Q}{P}\big)^{m}\big(\frac{m_h}{\Omega_h}\big)^{m+\frac{1}{2}}\bar{\gamma}_Q^{\frac{1}{2}}\Psi\big(\theta+\frac{1}{2}, m-m_h+\frac{3}{2}; \big(b+\frac{\eta Q}{\bar{\gamma}_Q P}\big)\frac{\bar{\gamma}_Q m_h}{\eta\Omega_h}\big)\big]. \tag{5.34}$$

5.5.2 Asymptotic Analysis

5.5.2.1 Proportional Interference Power Constraint

Substituting (5.14) into (5.31), together with the help of [172, eq. (3.310)], the asymptotic SER under the proportional interference power constraint is derived in the following theorem.

Theorem 13. *When Q is proportional to P, the asymptotic SER of cognitive spectrum sharing with TAS/GSC and DF relaying in Nakagami-m fading at high $\overline{\gamma}_P$ is derived as*

$$P_e^{\infty} = \left(G_c \overline{\gamma}_P\right)^{-G_d} + o\left(\overline{\gamma}_P{}^{-G_d}\right), \tag{5.35}$$

where the diversity order is

$$G_d = N_R \times \min\left\{m_{g1} N_S, m_{g2} N_D\right\} \tag{5.36}$$

and the SNR gain is

$$G_c = \begin{cases} \Lambda_1 \Delta_1 & m_{g1} N_{\mathrm{S}} < m_{g2} N_{\mathrm{D}} \\ \Lambda_2 \Delta_2 & m_{g1} N_{\mathrm{S}} > m_{g2} N_{\mathrm{D}} \\ \Lambda_1 \Delta_1 + \Lambda_2 \Delta_2 & m_{g1} N_{\mathrm{S}} = m_{g2} N_{\mathrm{D}} \ , \end{cases} \tag{5.37}$$

where

$$\Lambda_1 = \Big[\frac{a}{2}\sqrt{\frac{1}{\pi}}\Gamma\big(m_{g1} N_R N_S + \frac{1}{2}\big)\Big]^{-\frac{1}{m_{g1} N_R N_S}} b, \tag{5.38}$$

$$\Lambda_2 = \Big[\frac{a}{2}\sqrt{\frac{1}{\pi}}\Gamma\big(m_{g2} N_R N_D + \frac{1}{2}\big)\Big]^{-\frac{1}{m_{g2} N_R N_D}} b, \tag{5.39}$$

and Δ_1 *and* Δ_2 *are given in* (5.17) *and* (5.18)*, respectively.*

Based on (5.35), it is noticed that the diversity order is independent of the modulation scheme and the peak interference power constraint Q. The fading severity parameters of each hop and the antenna configuration have a direct impact on the diversity order while the interference power constraint at the PU has a direct impact on the SNR gain.

5.5.2.2 Fixed Interference Power Constraint

Substituting (5.24) into (5.31), the asymptotic SER under the fixed interference power constraint is derived in the following theorem.

Theorem 14. *Under the fixed interference power constraint, the asymptotic SER of cognitive spectrum sharing with TAS/GSC and DF relaying in Nakagami-m fading at*

$\overline{\gamma}_P$ *is derived as*

$$P_e^{\infty} = \begin{cases} \Theta_1\big(\Phi_1\big(\frac{1}{\overline{\gamma}_P}\big)^{m_g N_R N_S} + \Xi_1\big(\frac{1}{\overline{\gamma}_Q}\big)^{m_g N_R N_S}\big) \\ \qquad\qquad\qquad\qquad m_{g1}N_{\mathrm{S}} < m_{g2}N_{\mathrm{D}}, \\ \Theta_2\big(\Phi_2\big(\frac{1}{\overline{\gamma}_P}\big)^{m_{g1} N_R N_D} + \Xi_2\big(\frac{1}{\overline{\gamma}_Q}\big)^{m_{g2} N_R N_D}\big) \\ \qquad\qquad\qquad\qquad m_{g1}N_{\mathrm{S}} > m_{g2}N_{\mathrm{D}}, \\ \big(\Theta_1\Phi_1 + \Theta_2\Phi_2\big)\big(\frac{1}{\overline{\gamma}_P}\big)^{m_g N_R N_S} \\ \qquad + \big(\Theta_1\Xi_1 + \Theta_2\Xi_2\big)\big(\frac{1}{\overline{\gamma}_Q}\big)^{m_g N_R N_S} \\ \qquad\qquad\qquad\qquad m_{g1}N_{\mathrm{S}} = m_{g2}N_{\mathrm{D}}\ , \end{cases} \tag{5.40}$$

where

$$\Theta_1 = \frac{a\Gamma(m_{g1}N_R N_S + \frac{1}{2})}{2\sqrt{\pi}b^{m_{g1}N_R N_S}}\mathrm{H}_1, \tag{5.41}$$

$$\Theta_2 = \frac{a\Gamma(m_{g2}N_R N_D + \frac{1}{2})}{2\sqrt{\pi}b^{m_{g2}N_R N_D}}\mathrm{H}_2, \tag{5.42}$$

and H_1, H_2, Φ_1, Φ_2, Ξ_1, *and* Ξ_2 *are given by* (5.25), (5.26), (5.27), (5.28), (5.29), (5.30), *respectively.*

From (5.40), it is shown that the diversity order of the SER goes to zero under the fixed interference power constraint.

5.6 Ergodic Capacity

The ergodic capacity is an important performance indicator for cognitive underlay spectrum sharing. It is defined as the maximum achievable long-term rate, where no delay limit is taken into account. Under these assumptions, the ergodic capacity is expressed

as

$$C_{erg} = \frac{1}{2}\int_0^\infty \log_2(1+x)\, f_\gamma(x)dx = \frac{1}{2\ln 2}\int_0^\infty \frac{1-F_\gamma(x)}{1+x}dx. \tag{5.43}$$

To simplify (5.43), it is defined that $F_{\gamma_1}(x) = 1 + \tilde{F}_{\gamma_1}(x)$ and $F_{\gamma_2}(x) = 1 + \tilde{F}_{\gamma_2}(x)$, and rewrite (5.43) as

$$C_{erg} = \frac{1}{2\ln 2}\int_0^\infty \frac{\tilde{F}_{\gamma_1}(x)\,\tilde{F}_{\gamma_2}(x)}{1+x}dx, \tag{5.44}$$

where

$$\tilde{F}_{\gamma_1}(x) = \Big(\frac{L_R}{(m_{g1}-1)!}\binom{N_R}{L_R}\Big)^{N_S} N_S! \widetilde{\sum_{\mathcal{S}_R^{|\mathcal{S}_K|}}} \hbar_k \mathrm{sgn}(\eta_k)\,\Xi_k(x) \tag{5.45}$$

and

$$\tilde{F}_{\gamma_2}(x) = \Big(\frac{L_D}{(m_{g2}-1)!}\binom{N_D}{L_D}\Big)^{N_R} N_R! \widetilde{\sum_{\mathcal{S}_D^{|\mathcal{S}_T|}}} \hbar_t \mathrm{sgn}(\eta_t)\,\Xi_t(x). \tag{5.46}$$

In the following, it is assumed that $m_{h1} = m_{h2} = m_h$ and $\Omega_{h1} = \Omega_{h2} = \Omega_h$.

5.6.1 Exact Analysis

Substituting (5.45) and (5.46) into (5.44), and with the help of [172, eq.8.352.2], [172, eq.9.211.4.8], and the partial fraction expression [172, eq.2.102], a general closed-form expression for the ergodic capacity is derived in the following theorem.

Theorem 15. *The new closed-form expression for the ergodic capacity of cognitive TAS/GSC relaying in Nakagami-m fading is given in* (5.47) *at the top of the next page. In* (5.47)*, the following terms are defined*

$$
\begin{aligned}
C_{erg} = {} & \frac{1}{2\ln 2}\Big(\frac{L_R}{(m_{g1}-1)!}\binom{N_R}{L_R}\Big)^{N_S} N_S!\widetilde{\sum_{\mathcal{S}_R^{|\mathcal{S}_K|}}}\hbar_k \mathrm{sgn}\left(\eta_k\right)\Big(\frac{L_D}{(m_{g2}-1)!}\binom{N_D}{L_D}\Big)^{N_R} \\
& N_R!\widetilde{\sum_{\mathcal{S}_D^{|\mathcal{S}_T|}}}\hbar_t \mathrm{sgn}\left(\eta_t\right)\Bigg[\nabla\left(\theta_k\right)\nabla\left(\theta_t\right)\nu\left(\bar{\gamma}_Q m_h/\Omega_h,1,0,0\right)+\Delta\left(\theta_t,\eta_t,j_2,k_2\right)\nabla\left(\theta_k\right) \\
& \frac{\Big(\nu\left(\bar{\gamma}_Q m_h/\Omega_h,1,0,k_2\right)-\sum\limits_{l_2=1}^{\theta_t+m_h}\frac{\nu(\eta_t,l_2,0,k_2)}{(\bar{\gamma}_Q m_h/\eta_t\Omega_h-1)^{1-l_2}}\Big)}{\left(m_h/\Omega_h-\eta_t/\bar{\gamma}_Q\right)^{\theta_t+m_h}} \\
& +\frac{\Big(\nu\left(\bar{\gamma}_Q m_h/\Omega_h,1,k_1,0\right)-\sum\limits_{l_1=1}^{\theta_k+m_h}\frac{\nu(\eta_k,l_1,k_1,0)}{(\bar{\gamma}_Q m_h/\eta_k\Omega_h-1)^{1-l_1}}\Big)}{\left(m_h/\Omega_h-\eta_k/\bar{\gamma}_Q\right)^{\theta_k+m_h}}\nabla\left(\theta_t\right)\Delta\left(\theta_k,\eta_k,j_1,k_1\right) \\
& +\Delta\left(\theta_k,\eta_k,j_1,k_1\right)\Delta\left(\theta_t,\eta_t,j_2,k_2\right)\big(\frac{\bar{\gamma}_Q}{\eta_k}\big)^{\theta_k+m_h}\big(\frac{\bar{\gamma}_Q}{\eta_t}\big)^{\theta_t+m_h}\Bigg[\partial\left(\eta,1\right)\nu\left(\bar{\gamma}_Q m_h/\Omega_h,1,k_1,k_2\right) \\
& +\sum_{l_1=1}^{\theta_k+m_h}\Big(-\partial\left(\eta_k,l_1\right)+\sum_{j=1}^{\theta_t+m_h}\frac{\kappa\big(\theta_k,\eta_k,l_1,j\big)}{\big(\bar{\gamma}_Q m_h/\eta_t\Omega_h-1\big)^{\theta_t+m_h-j+1}}\Big)\nu\left(\eta_k,l_1,k_1,k_2\right) \\
& +\mathrm{sgn}\left(|\eta_k-\eta_t|\right)\nu\left(\eta_t,l_2,k_1,k_2\right)\sum_{l_2=1}^{\theta_t+m_h}\Big(-\partial\left(\eta_t,l_2\right) \\
& +\sum_{i=1}^{\theta_k+m_h}\frac{(-1)^{i+\theta_t+m_h-l_2}}{\left(\bar{\gamma}_Q m_h/\eta_k\Omega_h-1\right)^{\theta_k+m_h-i+1}}\kappa\left(\theta_t,\eta_t,l_2,i\right)\Big) \\
& -\sum_{l_3=\theta_k+m_h+1}^{\theta_k+\theta_t+2m_h}\frac{\left(1-\mathrm{sgn}\left(|\eta_k-\eta_t|\right)\right)\nu\left(\eta_k,l_3,k_1,k_2\right)}{\left(\bar{\gamma}_Q m_h/\eta_k\Omega_h-1\right)^{\theta_k+\theta_t+2m_h-m+1}}\Bigg]\Bigg]. \qquad (5.47)
\end{aligned}
$$

$$
\nabla\left(\theta\right)\triangleq\Big(1-\Gamma\big(m_h,\frac{Q}{P}\frac{m_h}{\Omega_h}\big)\Big/\Gamma\left(m_h\right)\Big)\big(\frac{1}{\bar{\gamma}_P}\big)^{\theta}, \qquad (5.48)
$$

$$
\Delta\left(\theta,\eta,j,k\right)\triangleq\frac{\left(\theta+m_h-1\right)!}{\left(m_h-1\right)!}\big(\frac{1}{\bar{\gamma}_Q}\big)^{\theta}e^{-\frac{m_h Q}{\Omega_h P}}\sum_{j=0}^{\theta+m_h-1}\frac{1}{j!}\big(\frac{Q}{P}\big)^{j}\sum_{k=0}^{j}\binom{j}{k}\big(\frac{m_h}{\Omega_h}\big)^{m_h+j-k}\big(\frac{\eta}{\bar{\gamma}_Q}\big)^{k}, \qquad (5.49)
$$

$$
\nu\left(\eta,l,k_1,k_2\right)\triangleq\Gamma\left(\tau\right)\left(\bar{\gamma}_Q m_h/\eta\Omega_h\right)^{\tau-l}\Psi\left(\tau\,,\tau+1-l;\left(\eta_t+\eta_k\right)\bar{\gamma}_Q m_h/\bar{\gamma}_p\eta\Omega_h\right), \qquad (5.50)
$$

$$\partial\left(\eta,l\right)\triangleq\frac{\left(\bar{\gamma}_{Q}m_{h}/\eta\Omega_{h}-1\right)^{l-1}}{\left(\bar{\gamma}_{Q}m_{h}/\eta_{t}\Omega_{h}-1\right)^{\theta_{t}+m_{h}}\left(\bar{\gamma}_{Q}m_{h}/\eta_{k}\Omega_{h}-1\right)^{\theta_{k}+m_{h}}},\tag{5.51}$$

$$\kappa\left(\theta,\eta,l,j\right)\triangleq\frac{\left(-1\right)^{\theta+m_{h}-l+1}\binom{j+\theta+m_{h}-l-1}{j-1}}{\left(\bar{\gamma}_{Q}m_{h}/\Omega_{h}\right)^{j+\theta+m_{h}-l}\left(1/\eta_{t}-1/\eta_{k}\right)^{j+\theta+m_{h}-l}},\tag{5.52}$$

with $\tau=\theta_{k}+k_{1}+\theta_{t}+k_{2}+1$.

The result can be applied and simplified to the special cases of TAS/MRC and TAS/SC in Nakagami-m fading channel, as well as TAS/GSC in Rayleigh fading channels.

5.6.2 High SNR Capacity analysis

To examine the capacity performance in the high maximum transmit power to noise ratio regime with $\overline{\gamma}_{P}\rightarrow\infty$, the high SNR approximation of the ergodic capacity is derived in closed-form. With the aid of the Jensen's inequality, a tight upper bound on the ergodic capacity is given by [173]

$$C_{erg}=\frac{1}{2}\mathbb{E}\left[\log_{2}\left(1+\gamma\right)\right]\leq\frac{1}{2}\log_{2}\mathbb{E}\left(1+\gamma\right).\tag{5.53}$$

Thus, the tight maximum transmit power to noise ratio approximation of the ergodic capacity is presented as [173, 174]

$$C_{erg}^{\infty}\approx\frac{1}{2}\log_{2}\mathbb{E}\left(1+\gamma\right)\approx\frac{1}{2}\log_{2}\mathbb{E}\left(\gamma\right).\tag{5.54}$$

Therefore, (5.54) is given as

$$C_{erg}^{\infty} \approx \frac{1}{2}\log_2\Big(\int_0^{\infty} x f_{\gamma}(x)\, dx\Big) = \frac{1}{2}\log_2\Big(\int_0^{\infty} (1 - F_{\gamma}(x))\, dx\Big)$$
$$= \frac{1}{2}\log_2 \int_0^{\infty} \tilde{F}_{\gamma_1}(x)\, \tilde{F}_{\gamma_2}(x)\, dx. \tag{5.55}$$

5.6.2.1 Proportional Interference Power Constraint

Based on (5.55), the high SNR approximation for the ergodic capacity with the proportional interference power constraint is written as

$$C_{erg}^{\infty} = \frac{1}{2}\big[\log_2(\bar{\gamma}_P) + \log_2\big(\int_0^{\infty} \tilde{F}_{\gamma_1}(x)\tilde{F}_{\gamma_2}(x) d\big(\frac{x}{\bar{\gamma}_P}\big)\big)\big]. \tag{5.56}$$

Substituting (5.45) and (5.46) into (5.56), and with the help of [172, eq.8.352.2], [172, eq.9.211.4.8] and the binomial expansion, the high SNR approximation for ergodic capacity with the proportional interference power constraint is derived in the following theorem.

Theorem 16. *When Q is proportional to P, the high SNR approximation of the ergodic capacity is derived as*

$$C_{erg}^{\infty} \approx \frac{1}{2}\log_2(\overline{\gamma}_P) + \frac{1}{2}\log_2(\Upsilon), \tag{5.57}$$

where

$$\Upsilon = \Big(\frac{L_R}{(m_{g1}-1)!}\binom{N_R}{L_R}\Big)^{N_S} N_S! \widetilde{\sum_{\mathcal{S}_R^{|\mathcal{S}_K|}}} \hbar_k \mathrm{sgn}(\eta_k) \Big(\frac{L_D}{(m_{g2}-1)!}\binom{N_D}{L_D}\Big)^{N_R} N_R! \widetilde{\sum_{\mathcal{S}_D^{|\mathcal{S}_T|}}} \hbar_t \mathrm{sgn}(\eta_t)$$
$$\Bigg[\lambda^2 \frac{\Gamma(\theta_k+\theta_t+1)}{(\eta_k+\eta_t)^{\theta_k+\theta_t+1}} + \lambda \sum_{j_2=0}^{\theta_t+m_h-1} \sum_{k_2=0}^{j_2} \Delta_s(\theta_t, j_2, k_2) \frac{\nu_s(\eta_t, \theta_t, 0, k_2)}{(1/\mu)^{\theta_k+j_2+1}}$$
$$+ \lambda \sum_{j_1=0}^{\theta_k+m_h-1} \sum_{k_1=0}^{j_1} \frac{\Delta_s(\theta_k, j_1, k_1)}{(1/\mu)^{\theta_t+j_1+1}} \nu_s(\eta_k, \theta_k, k_1, 0) + \sum_{j_1=0}^{\theta_k+m_h-1} \sum_{k_1=0}^{j_1} \sum_{j_2=0}^{\theta_t+m_h-1} \sum_{k_2=0}^{j_2} \Omega$$
$$\frac{\Delta_s(\theta_k, j_1, k_1)\Delta_s(\theta_t, j_2, k_2)}{(m_h/\Omega_h)^{\theta_k+\theta_t+1}(1/\mu)^{j_1+j_2+1}}\Bigg]. \tag{5.58}$$

In (5.58)*, it is defined*

$$\Delta_s(\theta, j, k) \triangleq \frac{(\theta+m_h-1)!}{(m_h-1)!j!} e^{-\mu\frac{m_h}{\Omega_h}} \binom{j}{k} \left(\frac{m_h}{\Omega_h}\right)^{\theta_k+\theta_t+j+1-\theta}, \tag{5.59}$$

$$\kappa_s(\theta, \eta, l) \triangleq \frac{(-1)^{(\theta+m_h-l)}\binom{\theta_k+\theta_t+2m_h-l-1}{\theta+m_h-l}}{(1/\eta_t - 1/\eta_k)^{\theta_k+\theta_t+2m_h-l} \eta^{k_1+k_2-l}}, \tag{5.60}$$

$$\nu_s(\eta, \varepsilon, k_1, k_2) \triangleq \Gamma(\theta_k+k_1+\theta_t+k_2+1)(1/\eta)^{\theta_k+\theta_t+1}$$
$$\Psi\Big(\theta_k+k_1+\theta_t+k_2+1,\ \theta_k+k_1+\theta_t+k_2+2-m_h-\varepsilon; \frac{(\eta_t+\eta_k)m_h\mu}{\Omega_h\eta}\Big), \tag{5.61}$$

and

$$\Omega \triangleq (1-\mathrm{sgn}(|\eta_k-\eta_t|))\nu_s(\eta_k, \theta_k+\theta_t+m_h, k_1, k_2), + \frac{\mathrm{sgn}(|\eta_k-\eta_t|)}{\eta_k^{\theta_k+m_h-k_1}\eta_t^{\theta_t+m_h-k_2}}$$
$$\Bigg[\sum_{l_1=1}^{\theta_k+m_h} \kappa_s(\theta_k, \eta_k, l_1)\nu_s(\eta_k, l_1-m_h, k_1, k_2) + \sum_{l_2=1}^{\theta_t+m_h} (-1)^{\theta_k+\theta_t+2m_h-l_2}$$
$$\kappa_s(\theta_t, \eta_t, l_2)\nu_s(\eta_t, l_2-m_h, k_1, k_2)\Bigg]. \tag{5.62}$$

Note that similar to the asymptotic ergodic capacity, the tight high SNR approxi-

mations can well predict the performance behaviours in the high SNR regime. Thus, the high SNR scaling law can be deduced from the high SNR approximations similar to the approach in [175] and [176]. Based on (5.57), two key parameters determining the affine approximation of the ergodic capacity in the high SNR regime are characterized, namely the high SNR slope and the high SNR power offset [177]. The high SNR slope is also known as the degrees of freedom or the multiplexing gain [178]. The high SNR power offset captures the joint effects of the fading model, the number of antennas at each terminal, and the interference power constraint. The high SNR approximation of the ergodic capacity is obtained as [177]

$$C_{erg}^{\infty} \approx S_{\infty} \left(\log_2 \left(\overline{\gamma}_P \right) - \mathcal{L}_{\infty} \right), \tag{5.63}$$

where S_{∞} is the high SNR slope in bits/s/Hz/(3 dB)

$$S_{\infty} = \lim_{\overline{\gamma}_P \to \infty} \frac{C_{erg}^{\infty}}{\log_2 \left(\overline{\gamma}_P \right)} = \frac{1}{2} \tag{5.64}$$

and $\mathcal{L}_{\infty}$ is the high SNR power offset in 3 dB units

$$\mathcal{L}_{\infty} = \lim_{\overline{\gamma}_P \to \infty} \left(\log_2 \left(\overline{\gamma}_P \right) - \frac{C_{erg}^{\infty}}{S_{\infty}} \right) = -\log_2 \left(\Upsilon \right). \tag{5.65}$$

From (5.64), it is shown that the high SNR slope S_{∞} is independent of the interference power constraint, the selected number of antennas at the receiver, and the primary network. It is also seen that the high SNR power offset $\mathcal{L}_{\infty}$ is independent of $\overline{\gamma}_P$ from (5.65).

5.6.2.2 Fixed Interference Power Constraint

Substituting (5.45) and (5.46) into (5.55), the high maximum transmit power to noise ratio approximation of the ergodic capacity under the fixed interference power constraint is obtained.

$$C_{erg}^{\infty} = \frac{1}{2}\log_2\Bigg[\Big(\frac{L_R}{(m_{g1}-1)!}\binom{N_R}{L_R}\Big)^{N_S} N_S! \widetilde{\sum_{\mathcal{S}_R^{|\mathcal{S}_K|}}} \hbar_k \mathrm{sgn}\left(\eta_k\right)\Big(\frac{L_D}{(m_{g2}-1)!}\binom{N_D}{L_D}\Big)^{N_R}$$
$$N_R! \widetilde{\sum_{\mathcal{S}_D^{|\mathcal{S}_T|}}} \hbar_t \mathrm{sgn}\left(\eta_t\right)\Bigg[\lambda^2\bar{\gamma}_P \frac{\Gamma\left(\theta_k+\theta_t+1\right)}{\left(\eta_k+\eta_t\right)^{\theta_k+\theta_t+1}} + \bar{\gamma}_Q\Bigg[\lambda \sum_{j_2=0}^{\theta_t+m_h-1}\sum_{k_2=0}^{j_2}\Delta_s\left(\theta_t,j_2,k_2\right)$$
$$\nu_s\left(\eta_t,\theta_t,0,k_2\right)\left(\frac{\bar{\gamma}_Q}{\bar{\gamma}_P}\right)^{\theta_k+j_2} + \lambda \sum_{j_1=0}^{\theta_k+m_h-1}\sum_{k_1=0}^{j_1}\left(\frac{\bar{\gamma}_Q}{\bar{\gamma}_P}\right)^{\theta_t+j_1}\Delta_s\left(\theta_k,j_1,k_1\right)\nu_s\left(\eta_k,\theta_k,k_1,0\right)$$
$$+ \sum_{j_1=0}^{\theta_k+m_h-1}\sum_{k_1=0}^{j_1}\sum_{j_2=0}^{\theta_t+m_h-1}\sum_{k_2=0}^{j_2}\frac{\Delta_s\left(\theta_k,j_1,k_1\right)\Delta_s\left(\theta_t,j_2,k_2\right)}{\left(m_h/\Omega_h\right)^{\theta_k+\theta_t+1}(P/Q)^{j_1+j_2}}\Omega\Bigg]\Bigg]\Bigg]. \tag{5.66}$$

Theorem 17. *When Q is fixed, the high maximum transmit power to noise ratio approximation of the ergodic capacity is given in* (5.66) *at the top of the next page.*

From (5.66), it is noticed that for the fixed interference power constraint, the high SNR slope collapses to zero.

5.7 Numerical Results

This section presents numerical results to verify the new analytical derivations for cognitive TAS/GSC relaying over Nakagami-m fading channels. The threshold SNR is set as $\gamma_{th} = 5$ dB. All the figures clearly show that the exact curves are in precise agreement with the Monte Carlo simulations. Importantly, the asymptotic lines accurately predict the exact behavior in the high SNR regime.

Fig. 5.1 plots the outage probability with the proportional interference constraint for various μ, L_R and L_D. The exact and asymptotic curves are plotted by using (5.13) and (5.14), respectively. For the same μ, it is observed that the outage probability decreases with increasing L_R and L_D, due to an increase in the SNR gain (5.37). It is also confirmed that the diversity order is independent of L_R and L_D as reflected by the parallel slope. Another observation is that the outage probability decreases with increasing μ, which is due to the relaxed interference power constraint at the PU.

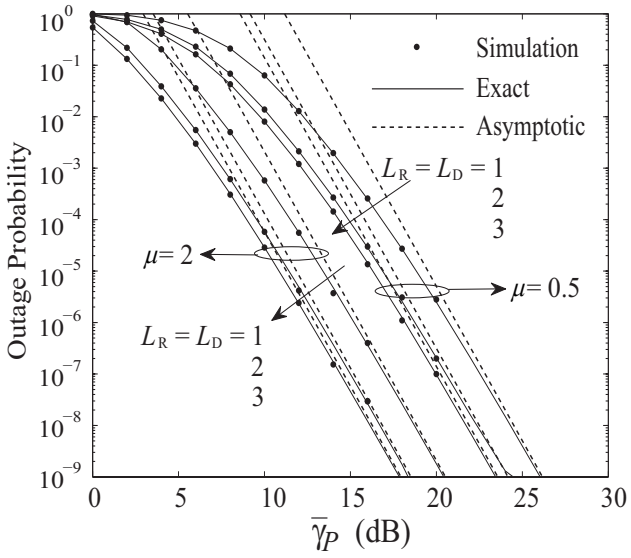

Figure 5.1: Cognitive spectrum sharing with TAS/GSC and DF relaying: $N_S = 2$, $N_R = 3$, $N_D = 3$, $m_{g1} = 1$, $m_{g2} = 2$, $m_{h1} = m_{h2} = 2$, and $\overline{\gamma}_Q = 2\overline{\gamma}_P$.

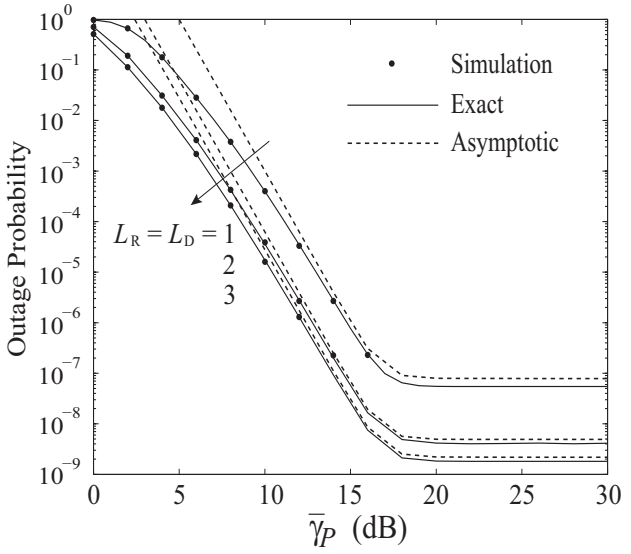

Figure 5.2: Cognitive spectrum sharing with TAS/GSC and DF relaying: $N_S = 2$, $N_R = 3$, $N_D = 3$, $m_{g1} = 1$, $m_{g2} = 2$, $m_{h1} = m_{h2} = 2$, and $\overline{\gamma}_Q = 20$ dB.

Fig. 5.2 examines the impact of the fixed interference power constraint on the outage probability as varying L_R and L_D. The exact and asymptotic curves are plotted using (5.13) and (5.24), respectively. Interestingly, the outage probability becomes saturated

for $\overline{\gamma}_P > 18$ dB. This is due to the fact that when $\overline{\gamma}_P \to \infty$, $\min\left(P, Q\Big/|h_{1i^*}|^2\right) \approx \left(Q\Big/|h_{1i^*}|^2\right)$ and $\min\left(P, Q\Big/|h_{2j^*}|^2\right) \approx \left(Q\Big/|h_{2j^*}|^2\right)$, as such the fixed peak interference power constraint becomes the dominant factor. By setting $L_R = L_D = 1$ and $L_R = L_D = 3$, it is also seen that TAS/MRC outperforms TAS/GSC, and TAS/GSC outperforms TAS/SC.

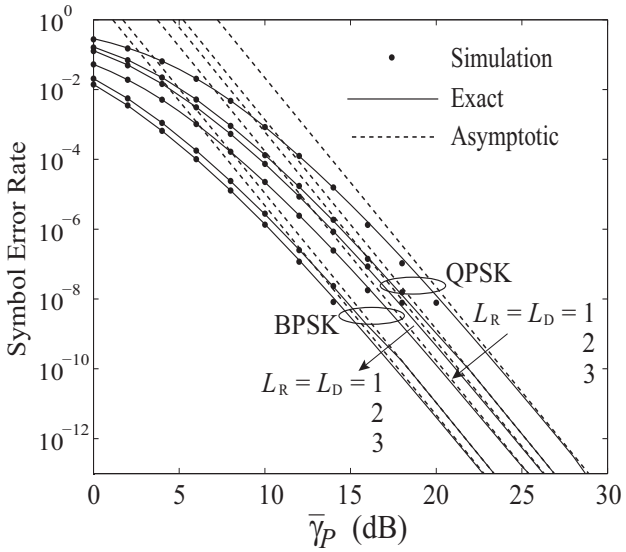

Figure 5.3: Cognitive spectrum sharing with TAS/GSC and DF relaying: $N_S = 2$, $N_R = 3$, $N_D = 3$, $m_{g1} = 1$, $m_{g2} = 2$, and $\overline{\gamma}_Q = 2\overline{\gamma}_P$.

Fig. 5.3 plots the exact and asymptotic SER with the proportional interference power constraint from (5.33) and (5.35), respectively. The plot confirms that the diversity order is independent of the modulation scheme, L_R, and L_D. It is observed that the SER decreases as L_R and L_D increase. It is also observed that BPSK outperforms QPSK, which is predicted from the SNR gain (5.37).

Fig. 5.4 plots the exact and asymptotic SER with the fixed interference power constraint from (5.33) and (5.40), respectively. It is also seen that the SER decreases as L_R and L_D increase, and BPSK outperforms QPSK. Similar to Fig. 5.2, the SER becomes saturated for $\overline{\gamma}_P > 22$ dB, which confirms that the diversity order goes to zero.

Fig. 5.5 plots the exact ergodic capacity and its high SNR approximation with the proportional interference power constraint from (5.47) and (5.57), respectively. It is also

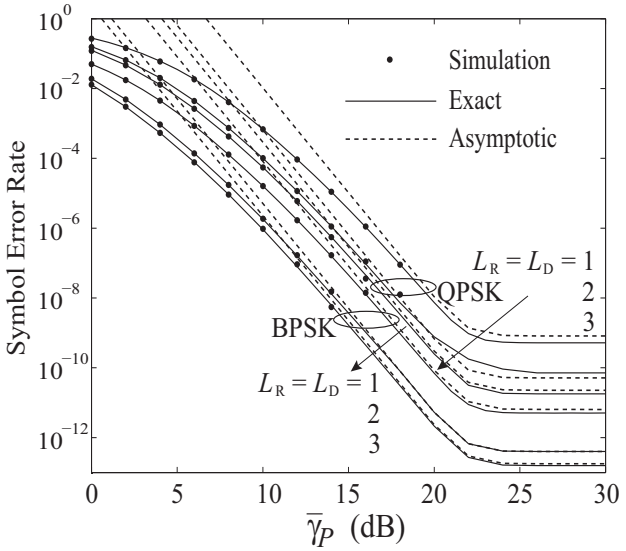

Figure 5.4: Cognitive spectrum sharing with TAS/GSC and DF relaying: $N_S = 2$, $N_R = 3$, $N_D = 3$, $m_{g1} = 1$, $m_{g2} = 2$, and $\overline{\gamma}_Q = 25$ dB.

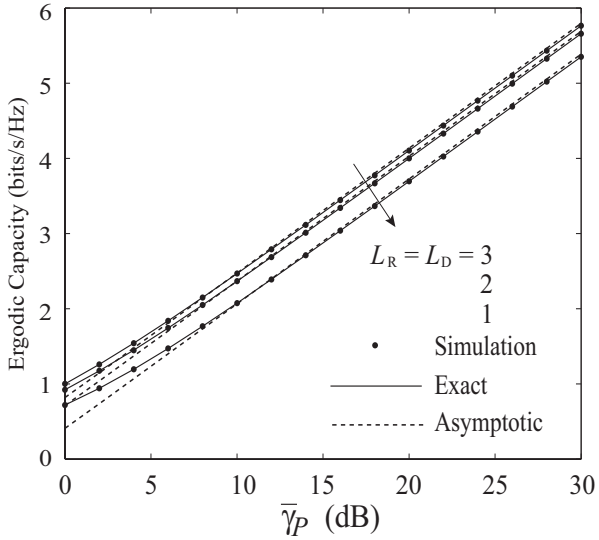

Figure 5.5: Cognitive spectrum sharing with TAS/GSC and DF relaying: $N_S = 2$, $N_R = 3$, $N_D = 3$, $m_{g1} = 1$, $m_{g2} = 2$, $m_{h1} = m_{h2} = 2$, and $\overline{\gamma}_Q = 2\overline{\gamma}_P$.

seen that the high SNR approximations of the ergodic capacity are tight and well predict the behavior of the ergodic capacity at high SNRs. It is obvious that the ergodic capacity can be improved by increasing L_R and L_D. The parallel curves confirm that the high SNR slope is independent of L_R and L_D.

Fig. 5.6 examines the impact of the fixed interference power constraint on the ergodic capacity. The exact ergodic capacity and its high maximum transmit power to noise ratio approximation are from (5.47) and (5.66), respectively. Interestingly, it is noticed that the capacity ceiling occurs for $\overline{\gamma}_P > 30$ dB. This is due to the fact that when $\gamma_P \to \infty$, $\min\left(P, {}^{Q}\!/\!_{\left|h_{1i^*}\right|^2}\right) \approx \left({}^{Q}\!/\!_{\left|h_{1i^*}\right|^2}\right)$ and $\min\left(P, {}^{Q}\!/\!_{\left|h_{2j^*}\right|^2}\right) \approx \left({}^{Q}\!/\!_{\left|h_{2j^*}\right|^2}\right)$. Once again, the fixed interference power constraint becomes the dominant factor. By setting $L_R = L_D = 1$ and $L_R = L_D = 3$, it is shown that TAS/MRC outperforms TAS/GSC and TAS/GSC outperforms TAS/SC.

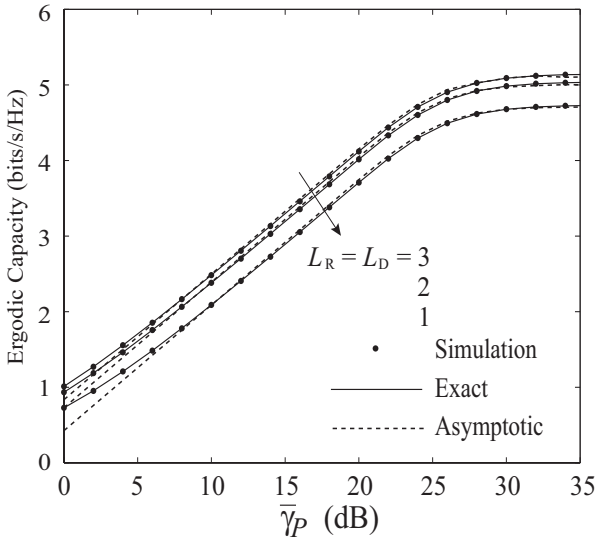

Figure 5.6: Cognitive spectrum sharing with TAS/GSC and DF relaying: $N_S = 2$, $N_R = 3$, $N_D = 3$, $m_{g1} = 1$, $m_{g2} = 2$, $m_{h1} = m_{h2} = 2$, and $\overline{\gamma}_Q = 25$ dB.

5.8 Summary

The cognitive DF relay network with TAS/GSC is considered over Nakagami-m fading. This framework is well suited for the reliability enhancement of the secondary network and interference alleviation of the primary network. New statistical properties of the end-to-end SNR are derived. Based on these, the closed-form expressions for the exact and asymptotic outage probability, symbol error rate, and ergodic capacity with the

proportional and the fixed interference power constraints are derived. These results are valid for Nakagami-m fading and arbitrary number of antennas in the secondary network. Based on the relationship of the maximum transmit power constraint and peak interference power constraint, it is concluded that: 1) under the proportional interference power constraint, the diversity order is determined by the fading parameter and the antenna configuration of the secondary network, and the high SNR slope is 1/2; and 2) under the fixed interference power constraint, the diversity order is zero with error floor, and the high SNR slope is zero with capacity ceiling.

Chapter 6

Secure Transmission with Artificial Noise in Large-Scale Spectrum Sharing Networks

6.1 Introduction

This chapter studies the secrecy performance of large-scale spectrum sharing networks with BF&AN at the SU-Txs. In underlay spectrum sharing networks, the prerequisite is to guarantee the primary network's QoS, which can be fulfilled by constraining the outage probability at the PU-Rx below a predetermined threshold, namely the peak allowable outage probability. Equipping the SU-Tx with multiple antennas capable of transmitting information signal and AN simultaneously brings array gains at the legitimate receiver and disrupts the reception at the Eve. Although BF&AN at the legitimate transmitter in the conventional physical layer security network has been well treated in [100], no work has considered BF&AN in large-scale spectrum sharing networks. Therefore, the question of *how BF&AN impacts the security design of such a complex network* remains unknown. The contributions of this chapter are summarized as follows:

- The exact closed-form expressions for the CDF of SIR at the typical SU-Rx and the CDF of SIR at the most detrimental Eve are derived. Based on these statistics, the exact expressions for the average secrecy rate and the secrecy outage probability of

the secondary network with BF&AN at the SU-Txs are presented in **Theorems 3** and **4**. The aim is to quantify the impacts of the power allocation factor, the number of antennas at the SU-Tx, and the path loss exponent on the average secrecy rate and the secrecy outage probability under various densities.

- It is shown that there exists an average secrecy rate wall beyond which the PU-Rx's QoS is violated. The peak of the wall also showcases the optimal achievable average secrecy rate (as indicated by Figs. 6.2(a) and 6.2(b)). It is revealed that the optimal power allocation factor that achieves the maximum average secrecy rate varies for different system parameters.

- For comparison, the exact expressions for the maximum permissive transmit power, the average secrecy rate, and the secrecy outage probability of the secondary network with BF at the SU-Txs are derived in **Theorems 5, 6,** and **7**. It is shown that there exists the same average secrecy rate wall for BF&AN and BF. The advantage of BF&AN over BF on the average secrecy rate is lost for some specific values of the density and the transmit power at the PUs and the SUs.

- The asymptotic average secrecy rate and the asymptotic secrecy outage probability of the secondary network with BF&AN at the SU-Txs when the number of SU transmit antennas N_s goes to infinity are derived in **Propositions 2 and 3**. These asymptotic results can well predict the exact performance in the medium and large N_s regime. For the same average secrecy rate, it showcases the antenna gap between the curves with different densities.

6.2 Network and Channel Description

This chapter considers the secure communication in an underlay spectrum sharing network where the SU-Txs communicate with the corresponding SU-Rxs under the potential malicious attempt of multiple Eves as shown in Fig. 6.1. Each SU-Tx has N_s antennas,

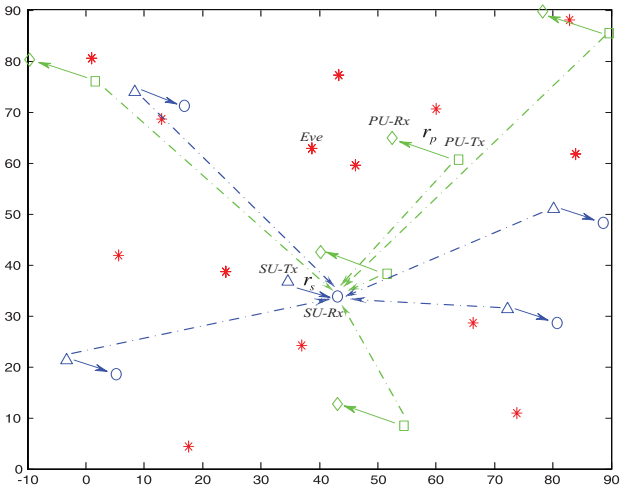

Figure 6.1: A realization of a large-scale spectrum sharing network model describing the received signal at a SU-Rx. In this network, the green square represents the PU-Tx, the diamond represents the PU-Rx, the triangle represents the SU-Tx, the circle represents the SU-Rx, and the red star represents the Eve. The blue solid line represents the secondary transmission, the green solid line represents the primary transmission, the blue dashed line represents the interference from the SU-Tx, and the green dashed line presents the interference from the PU-Tx.

and others in this model are all single-antenna nodes. Sets of PU-Txs, SU-Txs, and Eves locations, denoted by Φ_p, Φ_s and Φ_e are considered, in which Φ_p, Φ_s and Φ_e follow independent homogeneous PPPs with densities λ_p, λ_s and λ_e, respectively. This model is practical and representative for the decentralized networks where each node has substantial mobility or networks deployed randomly [179]. Following the bipolar network model [135], it is assumed that each PU/SU-Tx communicates with its unique associated intended PU/SU-Rx at distances r_p and r_s, respectively.

The wireless channels are modeled as independent quasi-static Rayleigh fading. The Eves interpret the SU-Tx's signal without trying to modify it. In this complex CNs, the interference-limited case is considered where the thermal noise is negligible compared with the aggregate interference from other transmitters. Similar to [100, 101, 180], the SIR is utilized to characterize the performance.

The beamformed broadcast information is masked with the AN at the SU-Txs to

confuse the Eves. Each SU-Tx broadcasts the information-bearing signals and AN simultaneously. The AN is transmitted in the null space of the intended SU-Rx's channel, thus imposing no effect on the secondary channel, but degrading the Eve's channel. The intended channel vector between the ith SU-Tx ($i \in \Phi_s$) and the corresponding SU-Rx is denoted as $\mathbf{h}_{i,s_i} \in \mathcal{C}^{1\times N_s}$, the CSI of which is known at the ith SU-Tx. An orthonormal basis of $\mathcal{C}^{N_s\times N_s}$ is generated at the ith SU-Tx as $\left[\mathbf{h}_{i,s_i}^{\dagger}/\|\mathbf{h}_{i,s_i}\|,\, \mathbf{G}_{i,s_i}\right]_{N_s\times N_s}$ [1], where $\mathbf{G}_{i,s_i}$ is a $N_s \times (N_s-1)$ matrix. Note that each column of $\mathbf{G}_{i,s_i}$ and $\mathbf{h}_{i,s_i}^{\dagger}/\|\mathbf{h}_{i,s_i}\|$ are mutually orthogonal. Let us define b_i as the information-bearing signal, and $\mathbf{n}_A$ as the AN. The transmitted BF&AN symbol vector is modeled as

$$\mathbf{x}_{s_i} = \frac{\mathbf{h}_{i,s_i}^{\dagger}}{\|\mathbf{h}_{i,s_i}\|} b_i + \mathbf{G}_{i,s_i}\mathbf{n}_A, \tag{6.1}$$

where $\mathbb{E}\left\{b_i b_i^{\dagger}\right\} = \delta_s^2$, and $N_s - 1$ elements of $\mathbf{n}_A$ are independent and identically distributed (i.i.d) complex Gaussian random variables with zero mean and variance σ_n^2. Thus, the total transmit power per transmission P_s is given by $P_s = P_I + P_A$, where the power allocated to the information signal is $P_I = \sigma_s^2$ and the power allocated to the AN is $P_A = (N_s - 1)\,\sigma_n^2$. μ is also defined as the fraction of power assigned to the information signal, thus, $P_I = \mu P_s$.

In the primary network, it is assumed that the typical PU-Rx is located at the origin of the coordinate system, and the distance between the typical PU-Tx and its associated PU-Rx is r_p. According to the Slivnyak's theorem [134], adding a probe point to the homogeneous PPP at an arbitrary location does not affect the law of the point process. The received SIR at the typical PU-Rx is given by

$$\gamma_{\mathtt{SIR}}^{p,AN} = \frac{|h_{p_0}|^2 {r_p}^{-\alpha}}{I_{p,p_0} + P_p^{-1} I_{s,p_0}}, \tag{6.2}$$

where $I_{p,p_0} = \sum_{j\in\Phi_p\setminus\{0\}} |h_{j,p_0}|^2 |X_{j,p_0}|^{-\alpha}$, $I_{s,p_0} = \sum_{i\in\Phi_s} [\sigma_s^2 |\mathbf{h}_{i,p_0} \frac{\mathbf{h}_{i,s_i}^{\dagger}}{\left\|\mathbf{h}_{i,s_i}^{\dagger}\right\|}|^2 + \sigma_n^2 \|\mathbf{h}_{i,p_0}\mathbf{G}_{i,s_i}\|^2]$ $|X_{i,p_0}|^{-\alpha}$. In (6.2), α is the path-loss exponent, h_{p_0} is the channel fading gain between

[1] † is the conjugate transpose operator.

the typical PU-Tx and the typical PU-Rx, h_{j,p_0} and $|X_{j,p_0}|$ are the interfering channel fading gain and distance between the jth PU-Tx and the typical PU-Rx, respectively, $\mathbf{h}_{i,p_0} \in \mathcal{C}^{1\times N_s}$ and $|X_{i,p_0}|$ are the interfering channel vector and distance between the ith SU-Tx and the typical PU-Rx, respectively, and P_p is the transmit power at the PU-Tx.

In the secondary network, $\mathbf{h}_{0,s_0} \in \mathcal{C}^{1\times N_s}$ and r_s are assumed to be the channel vector and distance between the typical SU-Tx and corresponding typical SU-Rx. Note that each SU-Tx transmits the signal vector expressed as (6.1), the effective signal at the typical SU receiver is obtained as $\mathbf{h}_{0,s_0}\mathbf{x}_{s_0} = \mathbf{h}_{0,s_0}\frac{\mathbf{h}_{0,s_0}^{\dagger}}{\|\mathbf{h}_{0,s_0}\|}b_0 + \mathbf{h}_{0,s_0}\mathbf{G}_{0,s_0}\mathbf{n}_A = \|\mathbf{h}_{0,s_0}\|b_0$. The received SIR at the typical SU-Rx is given by

$$\gamma_{\mathtt{SIR}}^{s,AN} = \frac{\sigma_s^2\|\mathbf{h}_{0,s_0}\|^2 {r_s}^{-\alpha}}{I_{s,s_0} + P_p I_{p,s_0}}, \tag{6.3}$$

where $I_{p,s_0} = \sum_{j\in\Phi_p}|h_{j,s_0}|^2|X_{j,s_0}|^{-\alpha}$, $I_{s,s_0} = \sum_{i\in\Phi_s\setminus\{0\}}[\sigma_s^2|\mathbf{h}_{i,s_0}\frac{\mathbf{h}_{i,s_i}^{\dagger}}{\|\mathbf{h}_{i,s_i}^{\dagger}\|}|^2 + \sigma_n^2\|\mathbf{h}_{i,s_0}\mathbf{G}_{i,s_i}\|^2]$ $|X_{i,s_0}|^{-\alpha}$ and $|X_{j,s_0}|$ are the channel fading gain and distance between the jth PU-Tx and the typical SU-Rx, respectively, $\mathbf{h}_{i,s_0} \in \mathcal{C}^{1\times N_s}$ and $|X_{i,s_0}|$ are the interfering channel vector and distance between the ith SU-Tx and the typical SU-Rx, respectively.

In the eavesdropping channel, the most detrimental Eve that has the highest SIR for a typical SU-Tx is considered [181]. Note that Eves are only interested in the secondary transmissions, and interpret the primary transmissions as interference[2]. Let us assume $\mathbf{h}_{0,e_k} \in \mathcal{C}^{1\times N_s}$ to be the channel vector between the typical SU-Tx and an arbitrary Eve $e_k \in \Phi_e$. With BF&AN at the SU-Tx, the received signal from the typical SU-Tx at the kth Eve is given by $\mathbf{h}_{0,e_k}\mathbf{x}_{s_0} = \mathbf{h}_{0,e_k}\frac{\mathbf{h}_{0,s_0}^{\dagger}}{\|\mathbf{h}_{0,s_0}\|}b_0 + \mathbf{h}_{0,e_k}\mathbf{G}_{0,s_0}\mathbf{n}_A$, where the first part is the useful received information signal, and the second part is the received AN. As such, the

[2]This assumption is practical since the primary networks operate in the Digital Video Broadcasting (DVB) spectrum and broadcast the public service to households, which do not have any confidential messages.

SIR at the most detrimental Eve is expressed as

$$\gamma_{\mathtt{SIR}}^{e,AN} = \max_{e_k \in \Phi_e} \left\{ \frac{\sigma_s^2 \left| \mathbf{h}_{0,e_k} \frac{\mathbf{h}_{0,s_0}^{\dagger}}{\left\| \mathbf{h}_{0,s_0}^{\dagger} \right\|} \right|^2 |X_{e_k}|^{-\alpha}}{I_{s,e_k} + P_p I_{p,e_k} + \sigma_n^2 I_{s_0,e_k,an}} \right\}, \tag{6.4}$$

In (6.4), $I_{p,e_k} = \sum_{j \in \Phi_p} |h_{j,e_k}|^2 |X_{j,e_k}|^{-\alpha}$, $I_{s,e_k} = \sum_{i \in \Phi_s \setminus \{0\}} [\sigma_s^2 |\mathbf{h}_{i,e_k} \frac{\mathbf{h}_{i,s_i}^{\dagger}}{\left\| \mathbf{h}_{i,s_i}^{\dagger} \right\|}|^2 + \sigma_n^2 \|\mathbf{h}_{i,e_k} \mathbf{G}_{i,s_i}\|^2] |X_{i,e_k}|^{-\alpha}$, $I_{s_0,e_k,an} = \|\mathbf{h}_{0,e_k} \mathbf{G}_{0,s_0}\|^2 |X_{e_k}|^{-\alpha}$. Note that h_{j,e_k} and $|X_{j,e_k}|$ are the channel fading gain and distance between the jth PU-Tx and the kth Eve, respectively, $\mathbf{h}_{i,e_k} \in \mathcal{C}^{1 \times N_s}$ and $|X_{i,e_k}|$ are the channel vector and distance between the ith SU-Tx and the kth Eve, respectively, $|X_{e_k}|$ is the distance between the typical SU-Tx and the kth Eve.

To facilitate the performance analysis, the Laplace transform of the aggregate interference from SU-Txs $I_{s,z} = \sum_{i \in \Phi_s} W_{s_i,z} |X_{i,z}|^{-\alpha}$ in (6.2), (6.3), and (6.4) are derived in the following lemma, where $z \in \{p_0, d_0, e_k\}$. Here, it is defined that $W_{s_i,z} = \sigma_s^2 \left| \mathbf{h}_{i,z} \frac{\mathbf{h}_{i,s_i}^{\dagger}}{\left\| \mathbf{h}_{i,s_i}^{\dagger} \right\|} \right|^2 + \sigma_n^2 \left\| \mathbf{h}_{i,z} \mathbf{G}_{i,s_i} \right\|^2$, where $\mathbf{h}_{i,s_i}$ is the intended channel, and the BF&AN signal $\mathbf{x}_{s_i}$ in (6.1) transmitted by the ith SU-Tx is received by the non-intended receiver z, rather than the ith SU-Rx.

Lemma 4. *The Laplace transform of the interference from the SU-Txs with BF&AN to the non-intended receiver $I_{s,z}$ is derived as*

$$\mathcal{L}_{I_{s,z}}(s) = \begin{cases} \exp\left(-\lambda_s \pi P_s^{\frac{2}{\alpha}} \Upsilon_1 \Gamma\left(1 - \frac{2}{\alpha}\right) s^{\frac{2}{\alpha}} \right) & \mu \neq \frac{1}{N_s} \\ \exp\left(-\lambda_s \pi (\mu P_s)^{\frac{2}{\alpha}} \Gamma\left(N_s + \frac{2}{\alpha}\right) \frac{\Gamma\left(1 - \frac{2}{\alpha}\right)}{\Gamma(N_s)} s^{\frac{2}{\alpha}} \right) & \mu = \frac{1}{N_s}, \end{cases} \tag{6.5}$$

where

$$\begin{aligned} \Upsilon_1 = & \left(1 - \frac{(1-\mu)}{(N_s - 1)\,\mu}\right)^{1-N_s} \Big[\mu^{\frac{2}{\alpha}} \Gamma\left(1 + \frac{2}{\alpha}\right) - \frac{1}{\mu} \left(\frac{(1-\mu)}{N_s - 1}\right)^{1+\frac{2}{\alpha}} \\ & \sum_{k=0}^{N_s - 2} \left(1 - \frac{(1-\mu)}{(N_s - 1)\,\mu}\right)^k \frac{\Gamma\left(k + 1 + \frac{2}{\alpha}\right)}{\Gamma(k+1)} \Big]. \end{aligned} \tag{6.6}$$

Proof. See Appendix D.1. □

6.3 Exact Secrecy Perfromance

In this section, the SU's permissive transmit power region is first presented, and then the exact expressions for the average secrecy rate and the secrecy outage probability in large scale spectrum sharing network with BF&AN at the SU-Txs is presented. In order to obtain deep insights through comparing BF&AN with BF, the exact expressions for the average secrecy rate and the secrecy outage probability in large-scale spectrum sharing network with BF at the SU-Txs are also derived.

6.3.1 BF&AN

6.3.1.1 PUs' QoS Requirement

According to the rule of underlay spectrum sharing networks, the concurrent transmission of PUs and SUs occurs under the prerequisite that the QoS requirement of the primary network is satisfied. As such, the transmit power operating region at the SU-Txs is first examined under the PU's QoS constraint. The QoS of primary network is characterized that the outage probability should be no larger than the peak allowable value $\rho^{p}_{\mathtt{out}}$, which is expressed as

$$P^{\{p\}}_{out} = Pr\{\gamma^{p,AN}_{\mathtt{SIR}} < \gamma^{\{p\}}_{th}\} < \rho^{\{p\}}_{out}, \tag{6.7}$$

where $\gamma^{\{p\}}_{th}$ is the desired SIR threshold at the PU-Rx.

In the following theorem, the SU's permissive transmit power region is presented.

Theorem 2. *With BF&AN at the SU-Txs, the permissive transmit power region at the*

SU-Tx is given as $P_s \in (0,\, P_s^{\max}]$*, where*

$$P_s^{\max} = \begin{cases} \left(-\frac{\Theta}{\Upsilon_1 \lambda_s}\right)^{\frac{\alpha}{2}} P_p & \mu \neq \frac{1}{N_s} \\ \left(-\frac{\Theta \Gamma(N_s)}{\lambda_s \Gamma\left(N_s + \frac{2}{\alpha}\right)}\right)^{\frac{\alpha}{2}} \frac{P_p}{\mu} & \mu = \frac{1}{N_s}, \end{cases} \tag{6.8}$$

where Υ_1 *is given by* (6.6)*, and*

$$\Theta = \frac{\ln\left(1 - \rho_{out}^{\{p\}}\right)}{\pi \Gamma\left(1 - \frac{2}{\alpha}\right) \left(\gamma_{th}^{\{p\}}\right)^{\frac{2}{\alpha}} {r_p}^2} + \lambda_p \Gamma\left(1 + \frac{2}{\alpha}\right). \tag{6.9}$$

Proof. See Appendix D.2. □

Remark 1. Here are some observations from (6.8):

- For the fixed QoS constraint of primary network, the maximum permissive transmit power at the SU-Tx can be relaxed by reducing the distance of the typical PU transceivers r_p, due to the fact that the PU can tolerate more interference from the SU-Txs in such case.
- With the number of SU nodes and PU nodes per unit area increases, the transmit power constraint imposed on the SU-Tx will be more severe, which results from the increased aggregate interference from the SU-Txs and the other PU-Txs.
- The higher transmit power the PU-Tx can have, the larger transmit power the SU-Tx can be permitted and the more dense the network can be.

6.3.1.2 New Statistics

In order to examine the secrecy performance, the CDFs of SIRs at the typical SU-Rx and the most detrimental Eve are derived in the following **Lemma 5** and **Lemma 6**, respectively.

Lemma 5. *With BF&AN at the SU-Txs, the CDF of SIR at the typical SU-Rx is derived*

as

$$F^{\{s\}}_{\gamma^{s,AN}_{\mathtt{SIR}}}\big(\gamma^{\{s\}}_{th}\big) = 1 - \exp\big(-\Lambda_l\big(\gamma^{\{s\}}_{th}\big)^{\frac{2}{\alpha}} r_s^2\big) - \sum_{m=1}^{N_s-1} \frac{(r_s^{\alpha})^m}{m!(-1)^m} \sum \frac{m!}{\prod_{i=1}^{m} m_i! i!^{m_i}} \exp\big(-\Lambda_l\big(\gamma^{\{s\}}_{th}\big)^{\frac{2}{\alpha}} r_s^2\big) \prod_{j=1}^{m} \Big(\big(-\Lambda_l\big(\gamma^{\{s\}}_{th}\big)^{\frac{2}{\alpha}}\big)(r_s)^{2-j\alpha} \prod_{k=0}^{j-1} \big(\frac{2}{\alpha} - k\big)\Big)^{m_j}, \quad (6.10)$$

where

$$\Lambda_l = \begin{cases} \Lambda_2 & \mu = \frac{1}{N_s} \\ \Lambda_3 & \mu \neq \frac{1}{N_s}. \end{cases} \quad (6.11)$$

In (6.11)*,* Λ_2 *and* Λ_3 *are given by*

$$\Lambda_2 = \pi\Big(\lambda_s \frac{\Gamma\big(N_s + \frac{2}{\alpha}\big)}{\Gamma\big(N_s\big)} + \lambda_p \Gamma\big(1 + \frac{2}{\alpha}\big)\big(\mu \frac{P_s}{P_p}\big)^{-\frac{2}{\alpha}}\Big)\Gamma\big(1 - \frac{2}{\alpha}\big), \quad (6.12)$$

$$\Lambda_3 = \pi\Big(\lambda_p \Gamma\big(1 + \frac{2}{\alpha}\big)\big(\frac{P_s}{P_p}\big)^{-\frac{2}{\alpha}} + \lambda_s \Upsilon_1\Big)\Gamma\big(1 - \frac{2}{\alpha}\big)(\mu)^{-\frac{2}{\alpha}}, \quad (6.13)$$

respectively. Here, $\sum_{i=1}^{m} i \cdot m_i = m$*, and* Υ_1 *is given by* (6.6)*, and* P_s *is the maximum permissive transmit power, which is given in* (6.8)*.*

Proof. See Appendix D.3. □

Based on the SIR at the most detrimental Eve in (6.4), the CDF for $\gamma^{e,AN}_{\mathtt{SIR}}$ is derived in the following lemma.

Lemma 6. *With BF&AN at the SU-Txs, the CDF of SIR at the most detrimental Eve is derived as*

$$F^{\{e\}}_{\gamma^{e,AN}_{\mathtt{SIR}}}\big(\gamma^{\{e\}}_{th}\big) = \exp\Big(-\frac{\pi\lambda_e}{\Lambda_l}\big(\gamma^{\{e\}}_{th}\big)^{-\frac{2}{\alpha}}\big(\frac{1-\mu}{\big(N_s-1\big)\mu}\gamma^{\{e\}}_{th} + 1\big)^{1-N_s}\Big), \quad (6.14)$$

where Λ_l *is given in* (6.11)*. Note that* P_s *is the maximum permissive transmit power,*

which is given in (6.8).

Proof. See Appendix D.4. □

Different from [101] and [182] where only the approximation or bound on CDF of SIR at the Eve was derived, this result is derived in a simple exact closed-form expression. It is observed from (6.14) that the CDF of $\gamma_{\mathtt{SIR}}^{e,AN}$ is an increasing function of λ_s and λ_p, and a decreasing function of λ_e.

Based on these new statistics in **Lemma 5** and **Lemma 6**, the impact of BF&AN on the secrecy performance of this large-scale spectrum sharing network is studied by considering two important metrics: the average secrecy rate and the secrecy outage probability.

6.3.1.3 Average Secrecy Rate

The instantaneous secrecy rate is defined as [181]

$$C_{\mathtt{se}} = [C_{\mathtt{su}} - C_{\mathtt{E}}]^+. \tag{6.15}$$

where $[x]^+ = \max\{x, 0\}$, $C_{\mathtt{su}} = \log_2\left(1 + \gamma_{\mathtt{SIR}}^{s,AN}\right)$ is the capacity of a typical secondary link, and $C_{\mathtt{E}} = \log_2\left(1+\gamma_{\mathtt{SIR}}^{e,AN}\right)$ is the capacity of the eavesdropping channel between the typical SU-Tx and the most detrimental Eve. Here, $\gamma_{\mathtt{SIR}}^{e,AN} = \max\limits_{e_k \in \Phi_e} \left\{\gamma_{\mathtt{SIR}}^{e_k,AN}\right\}$ corresponds to the non-colluding eavesdropping case [183].

The average secrecy rate is the average of the instantaneous secrecy rate $C_{\mathtt{se}}$ over $\gamma_{\mathtt{SIR}}^{s,AN}$ and $\gamma_{\mathtt{SIR}}^{e,AN}$. As such, the average secrecy rate is given by [51]

$$\begin{aligned}\bar{C}_{\mathtt{se}} &= \int_0^\infty \int_0^\infty C_{\mathtt{se}} f_{\gamma_{\mathtt{SIR}}^{s,AN}}(x_1)\, f_{\gamma_{\mathtt{SIR}}^{e,AN}}(x_2) dx_1 dx_2 \\ &= \frac{1}{\ln 2} \int_0^\infty \frac{F_{\gamma_{\mathtt{SIR}}^{e,AN}}(x_2)}{1+x_2} \left(1 - F_{\gamma_{\mathtt{SIR}}^{s,AN}}\left(x_2\right)\right) dx_2. \end{aligned} \tag{6.16}$$

By substituting the CDF of $\gamma_{\mathtt{SIR}}^{s,AN}$ in (6.10) and the CDF of $\gamma_{\mathtt{SIR}}^{e,AN}$ in (6.14) into (6.16), the average secrecy rate is derived in the following theorem.

Theorem 3. *With BF&AN at the SU-Txs, the average secrecy rate is derived as*

$$\bar{C}_{se,AN} = \frac{1}{\ln 2}\int_0^{\infty} \frac{\exp(-\frac{\pi\lambda_e}{\Lambda_l} x_2{}^{-\frac{2}{\alpha}}(\frac{1-\mu}{(N_s-1)\mu}x_2+1)^{1-N_s})}{1+x_2} \exp\left(-\Lambda_l x_2{}^{\frac{2}{\alpha}} r_s^2\right) \Big[1+\sum_{m=1}^{N_s-1} \frac{(r_s^{\alpha})^m}{m!(-1)^m} \sum m! \prod_{j=1}^{m} \frac{((-\Lambda_l x_2{}^{\frac{2}{\alpha}})(r_s)^{2-j\alpha}\prod_{k=0}^{j-1}(\frac{2}{\alpha}-k))^{m_j}}{m_j! j!^{m_j}}\Big] dx_2, \quad (6.17)$$

where Λ_l is given in (6.11)*. Here, P_s is the maximum permissive transmit power, which is given in* (6.8)*.*

Note that the average secrecy rate given in (6.17) is applicable to arbitrary N_s, μ and α.

6.3.1.4 Secrecy Outage Probability

The secrecy outage is declared when the secrecy capacity C_{se} is less than the expected secrecy rate R_s. As such, the secrecy outage probability is defined as [51]

$$P_{out}(R_s) = \Pr(C_{\mathtt{se}} < R_s) = \int_0^{\infty} f_{\gamma_{\mathtt{SIR}}^{e,AN}}(x_2)\, F_{\gamma_{\mathtt{SIR}}^{s,AN}}\left(2^{R_s}(1+x_2)-1\right) dx_2. \quad (6.18)$$

By substituting the PDF of $\gamma_{\mathtt{SIR}}^{e,AN}$ and CDF of $\gamma_{\mathtt{SIR}}^{s,AN}$ into (6.18), the secrecy outage probability is derived in the following theorem.

Theorem 4. *With BF&AN at the SU-Txs, the secrecy outage probability is derived as*

$$P_{out,AN}\left(R_s\right)=\int_0^{\infty}\frac{\pi\lambda_e {x_2}^{-\frac{2}{\alpha}}\left(\frac{2}{\alpha}{x_2}^{-1}\left(\frac{1-\mu}{(N_s-1)\mu}x_2+1\right)+1\right)}{\Lambda_l\left(\frac{1-\mu}{(N_s-1)\mu}x_2+1\right)^{N_s}}$$
$$\exp\left(-\frac{\pi\lambda_e}{\Lambda_l}{x_2}^{-\frac{2}{\alpha}}\left(\frac{1-\mu}{(N_s-1)\,\mu}x_2+1\right)^{1-N_s}\right)\Big[1-\exp\left(-\Lambda_3\left(2^{R_s}\left(1+x_2\right)-1\right)^{\frac{2}{\alpha}}r_s^2\right)$$
$$\Big(1+\sum_{m=1}^{N_s-1}\frac{\left(r_s^{\alpha}\right)^m}{m!\left(-1\right)^m}\sum m!\prod_{j=1}^{m}\frac{((-\Lambda_l(2^{R_s}(1+x_2)-1)^{\frac{2}{\alpha}})(r_s)^{2-j\alpha}\prod_{k=0}^{j-1}(\frac{2}{\alpha}-k))^{m_j}}{m_j!j!^{m_j}}\Big)\Big]dx_2, \tag{6.19}$$

where Λ_l is given in (6.11)*. Here, P_s is the maximum permissive transmit power, which is given in* (6.8)*.*

6.3.2 Numerical Examples for BF & AN

1. *Average secrecy rate wall*

   Fig. 6.2(a) and Fig. 6.2(b) plot the average secrecy rate of large-scale underlay spectrum sharing network under the primary network's QoS constraint $\rho_{out}^{\{p\}}=0.1$ with the transmit power adaptation scheme. From these figures, it is observed that the exact analytical curves are well validated by Monte Carlo simulations. The solid lines represent the operational achievable average secrecy rate where the QoS constraint of primary network is always satisfied, i.e. $P_{out}^{pri,AN}\left(\gamma_{th}^{\{p\}}\right)\leq 0.1$. The dashed lines represent the unachievable average secrecy rate where the QoS constraint of primary network is violated, i.e. $P_{out}^{pri,AN}\left(\gamma_{th}^{\{p\}}\right)>0.1$. The solid line is named as the "average secrecy rate wall". The vertical line of this "average secrecy rate wall" is determined by the maximum permissive transmit power at the SU P_s^{max}, which is quantified and evaluated by using (6.8). Different from the conventional physical layer security network, the average secrecy rate of the large-scale spectrum sharing network with transmit power adaptation is strictly constrained by the QoS constraint of primary network. Of course, the dashed average secrecy

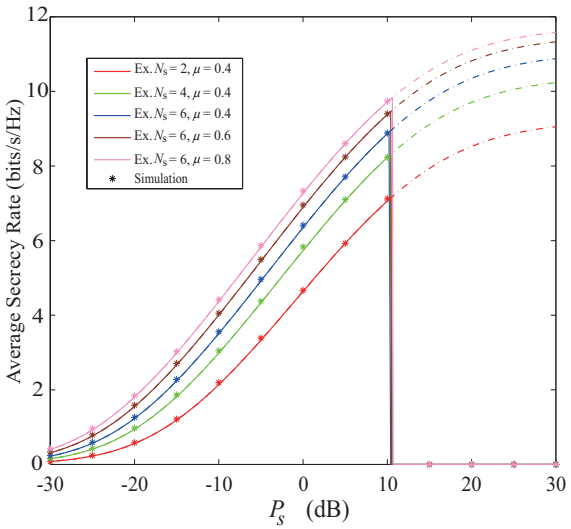

(a) Parameters: $\lambda_e = \lambda_p = \lambda_s = 10^{-4}$, $\alpha = 3$, $r_p = 6$, $r_s = 3$, $P_p = 15$ dB, and $\gamma_{th}^{\{p\}} = 6$ dB.

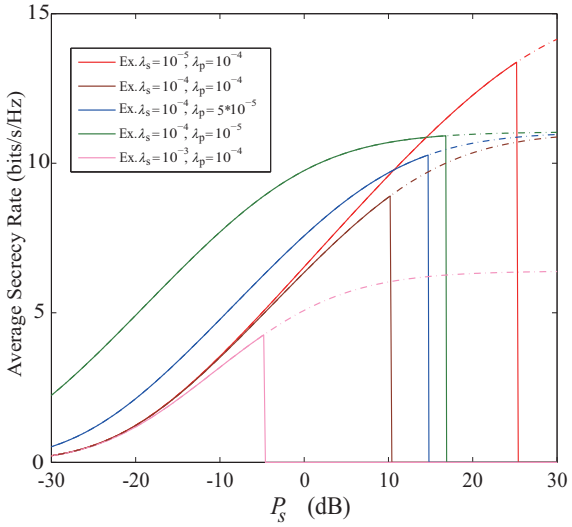

(b) Parameters: $\lambda_e = 10^{-4}$, $N_s = 6$, $\alpha = 3$, $r_p = 6$, $r_s = 3$, $\mu = 0.4$, $P_p = 15$ dB, and $\gamma_{th}^{\{p\}} = 6$ dB.

Figure 6.2: Average secrecy rate of a large-scale spectrum sharing network with the transmit power adaptation scheme.

rate lines become achievable by relaxing the QoS constraint of primary network $\rho_{out}^{\{p\}}$, increasing the transmit power at the PU-Tx P_p, or deactivating the existing PUs and SUs per unit area.

2. *Impact of N_s and μ on the average secrecy rate*

Fig. 6.2(a) plots the average secrecy rate versus the SU's transmit power with various numbers of transmit antennas N_s at the SU and power allocation factor μ, and the same density for PUs, SUs, and Eves is considered. The exact analytical curves are obtained from (6.17). Several observations can be concluded as follows: 1) The width of the "average secrecy rate wall" is weakly dependent on the number of transmit antennas at the SU and the power allocation factor, which can be explained by (6.8); 2) For the fixed power allocation factor $\mu = 0.4$, the average secrecy rate increases with increasing N_s; 3) For the same N_s, the average secrecy rate improves with increasing μ, which shows more power should be allocated to the information signal in this scenario.

3. *Impact of λ_s and λ_p on the average secrecy rate*

   Fig. 6.2(b) plots the average secrecy rate versus P_s for various densities of PUs and SUs. It is observed that 1) the "average secrecy rate wall" will be pushed to the left as the PUs and SUs become more dense. This can be predicted from (6.8) that $P_s^{\max}$ is a decreasing function of λ_p and λ_s; 2) With the identical density of PUs, it is seen that the average secrecy rate decreases with increasing the density of SUs. This is because the aggregate interference from other SUs increases with increasing λ_s, which restricts the secrecy performance of the typical SU; 3) Given the fixed density of SUs, the average secrecy rate decreases with increasing λ_p due to the increased aggregate interference from the PUs.

4. *Optimal μ for the average secrecy rate*

   Fig. 6.3(a) plots the average secrecy rate versus the power allocation factor μ for various densities of Eve λ_e. Here, the maximum permissive transmit power is used to transmit the signal at the SU, which is given by (6.17), and it is assumed that $P_s = P_s^{max}$ and $\rho_{out}^{\{p\}} = 0.1$. The triangles represent the maximum achievable average secrecy rate. For the scenarios where the density of Eve is higher than the density of PU and SU, the average secrecy rate first increase and then decrease with increasing μ, there exists μ^* that achieves the maximum average secrecy rate. For

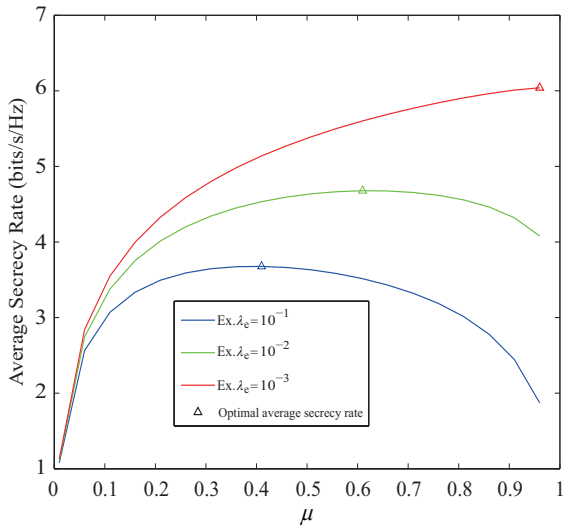

(a) Parameters: $\lambda_p = 10^{-4}$, $\lambda_s = 10^{-3}$, $\alpha = 3$, $r_p = 6$, $r_s = 3$, $N_s = 6$, $P_p = 15$ dB, and $\gamma_{th}^{\{p\}} = 0$ dB.

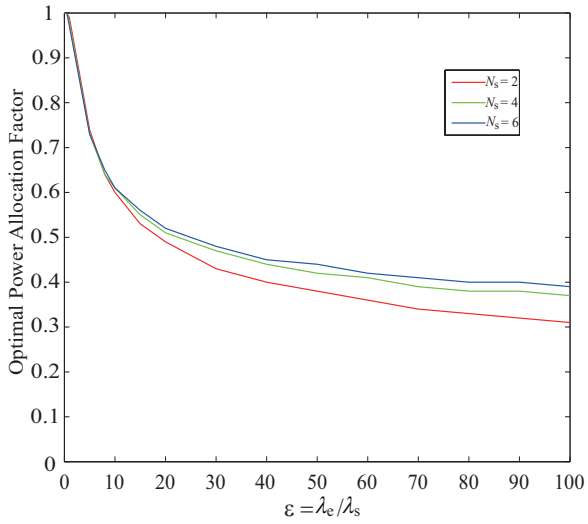

(b) Parameters: $\lambda_s = 10^{-3}$, $\lambda_p = \lambda_s/10$, $\rho_{out}^{\{p\}} = 0.1$, $\alpha = 3$, $r_p = 6$, $r_s = 3$, $P_p = 15$ dB, and $\gamma_{th}^{\{p\}} = 0$ dB.

Figure 6.3: Optimum μ that acheives the maximum average secrecy rate in a large-scale spectrum sharing network.

the region $\mu < \mu^*$, it is seen that increasing the power allocated to the useful signal ensures the message delivering and plays a dominant role in improving average secrecy rate; for the region $\mu > \mu^*$, considering that the density of Eves is high compared with the densities of SUs and PUs, thus increasing the power allocated

to AN can confuse the Eves and improve the secrecy performance. In other words, less power allocated to the AN degrades the average secrecy rate in this scenario. It is concluded that there exists a tradeoff between enhancing the SU information transmission and deteriorating the eavesdropping.

Interestingly, it is noticed that in Fig. 6.3(a) the optimal power allocation factor μ^* varies for different λ_e. It is revealed that less power should be allocated to the AN for the network with less dense Eves. More importantly, when $\lambda_e = 10^{-3}$, the optimal μ for achieving the maximum average secrecy rate is close to 1. It is concluded that the equal power allocation can not achieve the maximum average secrecy rate.

5. *Impact of density ratio on the optimal μ*

   To better illustrate the relationship between the optimal power allocation factor and the density of SUs and Eves. The ratio between λ_e and λ_s is defined as $\varepsilon = \lambda_e/\lambda_s$. In Fig. 6.3(b), the optimal power allocation factor μ^* versus the density ratio ε for various N_s is plotted numerically. It is assumed that $P_s = P_s^{max}$, $\lambda_s = 10^{-3}$, and $\lambda_p = 10^{-4}$. It is noticed that 1) For $\lambda_e \leq \lambda_s$, most of the power at the SU-Tx should be allocated to the information signal to achieve the maximum average secrecy rate (more than 95%). This reveals that improving the information delivery is more important than combating the eavesdropping in this scenario; 2) For $\lambda_e = 20\lambda_s$, nearly half of the power should be allocated to the AN from the aspect of average secrecy rate, in order to confuse the severe eavesdropping; 3) When $\lambda_e > 10\lambda_s$, the optimal power allocation factor increases with increasing N_s. It also indicates that more power can still be allowed to be allocated to the information signal with adding number of antennas at SU-Tx, in order to achieve the maximum average secrecy rate.

6. *Impact of N_s and α on the secrecy outage probability*

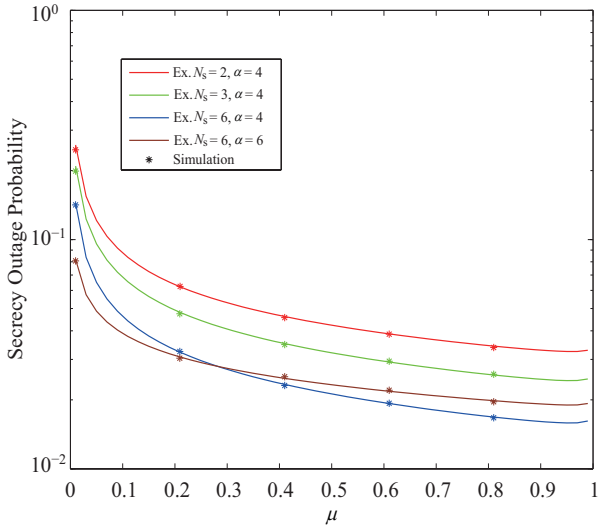

Figure 6.4: Secrecy outage probability versus μ for various N_s and α. Parameters: $\rho_{out}^{\{p\}} = 0.1$, $\lambda_e = 10^{-4}$, $\lambda_p = 10^{-4}$, $\lambda_s = 10^{-3}$, $r_p = 6$, $r_s = 3$, $Rs = 1$, $P_p = 15$ dB, and $\gamma_{th}^{\{p\}} = 0$ dB.

Fig. 6.4 plots the secrecy outage probability versus the power allocation factor μ for various numbers of antennas at the SU-Tx N_s. The exact analytical curves are obtained from (6.19), which are well validated by Monte Carlo simulations. It is assumed that $P_s = P_s^{max}$. It is seen that the secrecy outage probability decreases with increasing μ. When μ approaches 1, the lowest secrecy outage probability can be achieved. This is because when the density of Eves is set to be small compared with the density of SU, the effect of delivering information overtakes the effect of combating the eavesdropping on the secrecy outage probability. As expected, the secrecy outage probability decreases with increasing N_s, which is due to the array gains brought by additional antennas.

6.3.3 Beamforming

This subsection provides the analysis for the large-scale spectrum sharing networks with BF, where no transmit power is allocated to the AN. By doing so, the secrecy performance between the BF with and without AN is compared , and the potential benefits for the

secrecy performance due to the AN is examined. Note that the BF case can be viewed as a special case for BF&AN, i.e. $\mu = 1$.

In the following theorem, the SU's permissive transmit power region is presented by substituting $\mu = 1$ into (6.8).

Theorem 5. *With BF at the SU-Txs, the permissive transmit power region at the SU-Tx is given as* $P_s \in (0,\, P_s^{\max}]$*, where*

$$P_s^{\max} = \Big[-\Big(\frac{\ln\big(1-\rho_{out}^{\{p\}}\big)}{\pi\Gamma\big(1+\frac{2}{\alpha}\big)\Gamma\big(1-\frac{2}{\alpha}\big)\big(\gamma_{th}^{\{p\}}\big)^{\frac{2}{\alpha}} {r_p}^2} + \lambda_p\Big)\frac{1}{\lambda_s}\Big]^{\frac{\alpha}{2}} P_p. \tag{6.20}$$

6.3.3.1 Average Secrecy Rate

The average secrecy rate is presented in the following theorem by substituting $\mu = 1$ into (6.17).

Theorem 6. *With BF at the SU-Txs, the average secrecy rate is derived as*

$$\begin{aligned}\bar{C}_{se} =& \frac{1}{\ln 2}\int_0^{\infty} \frac{1}{1+x_2}\exp\left(-\Upsilon_2 {x_2}^{-\frac{2}{\alpha}}\right)\exp\left(-\Lambda_1 {r_s}^2 {x_2}^{\frac{2}{\alpha}}\right)\Big[1+\sum_{m=1}^{N_s-1}\frac{\big(r_s^{\alpha}\big)^m}{m!\big(-1\big)^m} \\ & \sum m!\prod_{j=1}^{m}\frac{\big((-\Lambda_1 {x_2}^{\frac{2}{\alpha}})(r_s)^{2-j\alpha}\prod_{k=0}^{j-1}\big(\frac{2}{\alpha}-k\big)\big)^{m_j}}{m_j!\, j!^{m_j}}\Big]dx_2,\end{aligned} \tag{6.21}$$

where

$$\Lambda_1 = \pi\left(\big(\frac{P_s}{P_p}\big)^{-\frac{2}{\alpha}}\lambda_p + \lambda_s\right)\Gamma\left(1+\delta\right)\Gamma\left(1-\delta\right), \tag{6.22}$$

and

$$\Upsilon_2 = \frac{\lambda_e}{\big(\lambda_p + \big(\frac{P_s}{P_p}\big)^{-\frac{2}{\alpha}}\lambda_s\big)\Gamma\big(1+\frac{2}{\alpha}\big)\Gamma\big(1-\frac{2}{\alpha}\big)}, \tag{6.23}$$

respectively.

6.3.3.2 Secrecy Outage Probability

The secrecy outage probability is presented in the following theorem by substituting $\mu = 1$ into (6.19).

Theorem 7. *With BF at the SU-Txs, the secrecy outage probability is derived as*

$$P_{out}(R_s) = \int_0^{\infty} \frac{2\Upsilon_2}{\alpha} x_2^{-\frac{2}{\alpha}-1} \exp\left(-\Upsilon_2 x_2^{-\frac{2}{\alpha}}\right) \Big[1 - \exp\left(-\Lambda_1 {r_s}^2 \left(2^{R_s}\left(1+x_2\right)-1\right)^{\frac{2}{\alpha}}\right) (1 + \sum_{m=1}^{N_s-1} \frac{(r_s^{\alpha})^m}{m!(-1)^m} \sum m! \prod_{j=1}^{m} \frac{1}{m_j! j!^{m_j}} (-\Lambda_1 (2^{R_s}(1+x_2)-1)^{\frac{2}{\alpha}})(r_s)^{2-j\alpha} \prod_{k=0}^{j-1} (\frac{2}{\alpha} - k))^{m_j})\Big] dx_2, \quad (6.24)$$

where Λ_1 *and* Υ_2 *are given in* (6.22) *and* (6.23)*, respectively.*

6.3.4 Numerical examples for the comparison between BF&AN and BF

In this subsection, the average secrecy rate between the proposed network with BF&AN and with BF only is compared.

In Fig. 6.5(a) and Fig. 6.5(b), the operational achievable average secrecy rate region for the large-scale spectrum sharing network with BF&AN and with BF is compared. It is shown that the same permissive transmit power region for BF&AN scheme and BF scheme in each figure. This is because, from the typical PU-Rx's aspect, both the AN and the information signal transmitted from the SU are viewed as the interference, which is equivalent to the case of BF. In both figures, it is noticed that the same unachievable average secrecy rate region located in $P_s \in (10, 30)$ dB with $P_p \in (-10, -30)$ dB. This can be explained by the fact that the QoS constraint is severely violated in this setting when the aggregate interference is much higher compared to the useful signal received at the PU.

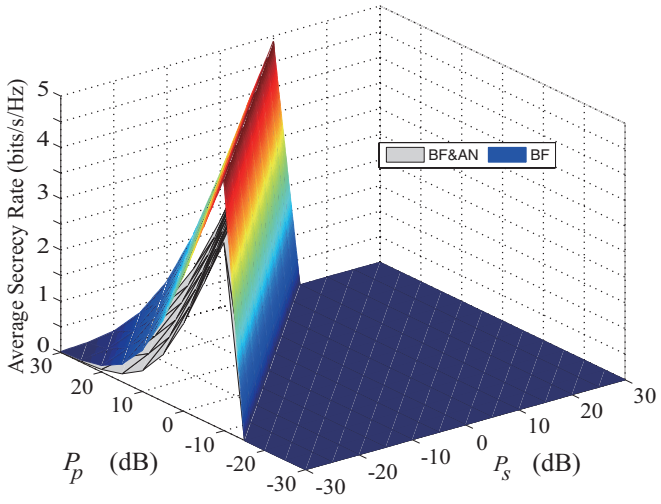

(a) Parameters: $\lambda_p = \lambda_e = 10^{-4}$, $\lambda_s = 10^{-3}$, $\rho_{out}^{\{p\}} = 0.1$, $\mu = 0.4$, $r_p = 6$, $r_s = 3$, and $\alpha = 3$.

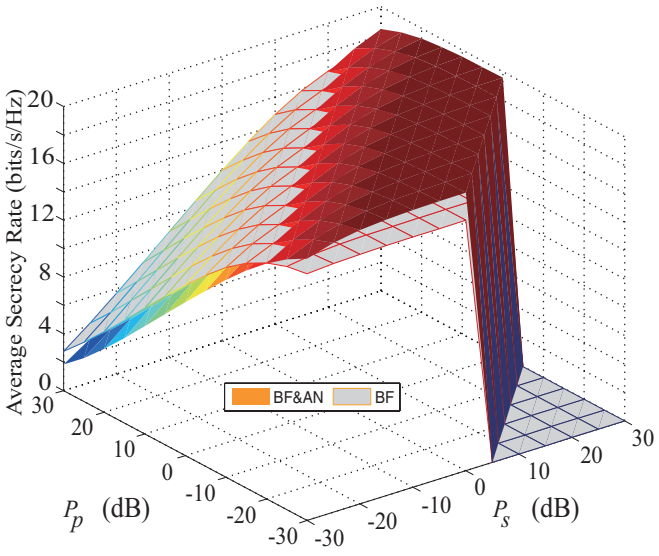

(b) Parameters: $\lambda_p = \lambda_s = 10^{-6}$, $\lambda_e = 10^{-5}$, $\rho_{out}^{\{p\}} = 0.1$, $\mu = 0.4$, $r_p = 6$, $r_s = 3$, and $\alpha = 3$.

Figure 6.5: Comparison of average secrecy rate versus P_s and P_p between BF&AN and BF.

In contrast to the fact that it is often beneficial to emit AN on top of the information-bearing signal in the physical layer security model with fixed nodes [184]. In Fig. 6.5(a), it is shown that BF scheme outperforms the BF&AN scheme in the operational region where $P_s \in (-30, 10)$ dB with $P_p \in (-15, 30)$ dB. This is because the strong aggregate interference from the PUs overtakes the effect of the AN generated by the SU. In this

case, more power needs to be allocated to transmit information at the SUs to contend with the interference from the PUs. Interestingly, Fig. 6.5(b) shows that the BF&AN scheme outperforms the BF scheme where $P_s \in (-30, 5)$ dB with $P_p \in (-30, -20)$ dB, owing to the fact that the effect of the AN generated by the SU overtakes the relatively low aggregate interference from the PUs. In this case, more power needs to be allocated to transmit AN to disrupt eavesdropping.

6.4 Large Antenna Arrays Analysis

This section studies the asymptotic secrecy performance of the large-scale spectrum sharing networks where the SU-Txs are equipped with large antenna arrays. The asymptotic behavior of the average secrecy rate and the secrecy outage probability are examined, when the number of antennas at the SU-Txs goes to infinity.

Lemma 7 is first presented based on the law of large numbers as follows:

Lemma 7. $\lim_{N_s\to\infty} \|\mathbf{h}_z\|^2 = N_s$, *and* $\lim_{N_s\to\infty} \|\mathbf{h}_{i,z}\mathbf{G}_{i,s_i}\|^2 = N_s - 1$.

Proof. This is due to the fact that $\|\mathbf{h}_z\|^2 \sim Gamma\,(N_s, 1)$ and $\|\mathbf{h}_{i,z}\mathbf{G}_{i,s_i}\|^2$ $\sim Gamma\,(N_s - 1, 1)$. □

By using **Lemma 7**, the SIR at the typical PU in (6.2) is rewrote as

$$\gamma_{\mathtt{SIR}}^{p,\infty} \overset{d}{\sim} \frac{|h_{p_0}|^2 {r_p}^{-\alpha}}{I_{p,p_0} + \eta I_{s,p_0,\infty}}, \tag{6.25}$$

where $I_{p,p_0} = \sum_{j\in\Phi_p\setminus\{0\}} |h_{j,p_0}|^2 |X_{j,p_0}|^{-\alpha}$ and $I_{s,p_0,\infty} = \sum_{i\in\Phi_s} [\mu |\mathbf{h}_{i,p_0} \frac{\mathbf{h}_{i,s_i}^\dagger}{\mathbf{h}_{i,s_i}^\dagger}|^2$ $+(1-\mu)]|X_{i,p_0}|^{-\alpha}$.

For large N_s, the SIR at the typical SU is given as

$$\gamma_{\mathtt{SIR}}^{s,\infty} \overset{d}{\sim} \frac{\mu N_s {r_s}^{-\alpha}}{I_{s,s_0,\infty} + \eta^{-1} I_{p,s_0}}, \tag{6.26}$$

where $I_{p,s_0} = \sum_{j\in\Phi_p}|h_{j,s_0}|^2|X_{j,s_0}|^{-\alpha}$ and $I_{s,s_0,\infty} = \sum_{i\in\Phi_s\setminus\{0\}}[\mu|\mathbf{h}_{i,s_0}\frac{\mathbf{h}_{i,s_i}^\dagger}{\left\|\mathbf{h}_{i,s_i}^\dagger\right\|}|^2 + (1-\mu)]|X_{i,s_i}|^{-\alpha}$, from (6.26), it is noticed that the received SIR at the typical SU scale by N_s.

For large N_s, the SIR at the most detrimental Eve is given as

$$\gamma_{\mathtt{SIR}}^{e,\infty} \overset{d}{\sim} \max_{e_k\in\Phi_e}\left\{\frac{\mu\left|\mathbf{h}_{0,e_k}\frac{\mathbf{h}_{i,s_i}^\dagger}{\left\|\mathbf{h}_{i,s_i}^\dagger\right\|}\right|^2|X_{e_k}|^{-\alpha}}{I_{s_0,e_k,\infty}+\eta^{-1}I_{p,e_k}+(1-\mu)\,|X_{e_k}|^{-\alpha}}\right\}, \tag{6.27}$$

where $I_{p,e_k} = \sum_{j\in\Phi_p}|h_{j,e_k}|^2|X_{j,e_k}|^{-\alpha}$ and $I_{s_0,e_k,\infty} = \sum_{i\in\Phi_s\setminus\{0\}}[\mu\left|\mathbf{h}_{i,e_k}\frac{\mathbf{h}_{i,s_i}^\dagger}{\left\|\mathbf{h}_{i,s_i}^\dagger\right\|}\right|^2 + (1-\mu)]|X_{i,e_k}|^{-\alpha}$.

Based on the SIR at the typical PU in (6.25), with the help of the Laplace transform in [135, eq. (8)], and similar method provided in the proof for the **Theorem 1**, the permissive transmit power region at the SU-Tx at large N_s is presented in the following proposition.

Proposition 1. With BF&AN at the SU-Txs, the permissive transmit power region for the SU-Tx at large N_s is given as $P_s \in (0,\ P_s^{\max}]$, where

$$P_s^{max} = \Big[-\Theta\Big(\int_0^\infty \big(\mu t + \big(1-\mu\big)\big)^{\frac{2}{\alpha}}e^{-t}dt\Big)^{-1}\lambda_s{}^{-1}\Big]^{\frac{\alpha}{2}}P_p, \tag{6.28}$$

and Θ is given by (6.9).

Remark 2. When $N_s \to \infty$, the maximum transmit power constraint is irrelevant to the N_s.

To facilitate the analysis of the average secrecy rate and the secrecy outage probability, the asymptotic CDFs of $\gamma_{\mathtt{SIR}}^{e,\infty}$ and $\gamma_{\mathtt{SIR}}^{s,\infty}$ need to be derived first. Using the method presented in proof of **Theorem 2**, the asymptotic CDF of $\gamma_{\mathtt{SIR}}^{e,\infty}$ given in (6.27) is derived

as

$$F_{\gamma_{\mathtt{SIR}}^{e,\infty}}\big(\gamma_{th}^{\{e\}}\big)=\exp\Big(-\frac{\pi\lambda_e e^{\left(1-\mu^{-1}\right)\gamma_{th}^{\{e\}}}}{\Xi\Gamma\big(1-\frac{2}{\alpha}\big)}\big(\frac{\mu P_s}{\gamma_{th}^{\{e\}}P_p}\big)^{\frac{2}{\alpha}}\Big), \tag{6.29}$$

where

$$\Xi=\lambda_p\Gamma\big(1+\frac{2}{\alpha}\big)+\lambda_s\big(\frac{P_s}{P_p}\big)^{\frac{2}{\alpha}}\int_0^{\infty}\big(\mu t+\big(1-\mu\big)\big)^{\frac{2}{\alpha}}e^{-t}dt. \tag{6.30}$$

To derive the asymptotic CDF of $\gamma_{\mathtt{SIR}}^{s,\infty}$, it is presented that

$$F_{\gamma_{\mathtt{SIR}}^{s,\infty}}\left(\gamma_{th}^{s}\right)=\int_{\frac{\mu N_s}{\gamma_{th}^{s}{r_{s_0}}^{\alpha}}}^{\infty}f_{I_{\mathrm{sec},\infty}}\left(x\right)dx, \tag{6.31}$$

where $I_{\mathrm{sec},\infty}=\mu\sum_{i\in\Phi_s\setminus\{0\}}\big|\mathbf{h}_{i,s_0}\frac{\mathbf{h}_{i,s_i}^{\dagger}}{\left\|\mathbf{h}_{i,s_i}^{\dagger}\right\|}\big|^2\big|X_{i,s_i}\big|^{-\alpha}+\big(1-\mu\big)\sum_{i\in\Phi_s\setminus\{0\}}|X_{i,s_i}|^{-\alpha}+\big(\frac{P_s}{P_p}\big)^{-1}$ $\sum_{j\in\Phi_p}|h_{j,s_0}|^2|X_{j,s_0}|^{-\alpha}$. In (6.31), $f_{I_{\mathrm{sec},\infty}}\left(x\right)$ is the inverse Laplace transform of $\mathcal{L}_{I_{\mathrm{sec},\infty}}\left(s\right)$, which can be expressed as $f_{I_{\mathrm{sec},\infty}}\left(x\right)=\mathcal{L}_{I_{\mathrm{sec},\infty}}^{-1}\left(s\right)$. Due to the intractability of this inverse Laplace transform, some alternative ways have been proposed, such as using numerical inversion to evaluate $\mathcal{L}_{I_{\mathrm{sec},\infty}}^{-1}\left(s\right)$ [185], or the log-normal approximations to approximate $f_{I_{\mathrm{sec},\infty}}\left(x\right)$. However, in this case, there exists singularity at $|X_{i,s_i}|=|X_{j,s_0}|=0$, thus the mean and variance of $I_{\mathrm{sec},\infty}$ derived from the moment generating function diverge [96, 136], which renders the derivation of the PDF of $I_{\mathrm{sec},\infty}$. Alternatively, the Gil-Pelaez theorem [186] is utilized to facilitate the derivation of the asymptotic CDF of SIR at the typical SU in the following lemma.

Lemma 8. *With BF&AN at the SU-Txs, the asymptotic CDF of SIR at the typical SU at large N_s is given as*

$$F_{\gamma_{\mathtt{SIR}}^{s,\infty}}\big(\gamma_{th}^{s}\big)=1-F_{I_{\mathrm{sec},\infty}}\big(\frac{\mu N_s}{\gamma_{th}^{s}{r_{s_0}}^{\alpha}}\big)=\frac{1}{2}+\frac{1}{\pi}\int_0^{\infty}\frac{\mathrm{Im}\big[e^{-\frac{jw\mu N_s}{\gamma_{th}^{s}{r_{s_0}}^{\alpha}}}\varphi^{*}\left(w\right)\big]}{w}dw, \tag{6.32}$$

where $F_{I_{\mathrm{sec},\infty}}\left(x\right)$ is the CDF of $I_{\mathrm{sec},\infty}$, $j=\sqrt{(-1)}$, and $\varphi\left(w\right)$ is the conjugate of the characteristic function, which is given by $\varphi\big(w\big)=\exp\left(-\pi\Xi\Gamma(1-\frac{2}{\alpha})\ \eta^{-\frac{2}{\alpha}}(jw)^{\frac{2}{\alpha}}\right)$.

Since the closed form expression for the general form for the PDF of $I_{\text{sec},\infty}$ can not be derived, the special case for the path loss component $\alpha = 4$ is presented. In the following corollary, the asymptotic CDF of SIR for the typical SU with $\alpha = 4$ is derived.

Corollary 4. With BF&AN at the SU-Txs and $\alpha = 4$, the asymptotic CDF of SIR at the typical SU is derived as

$$F^{\infty}_{\gamma^{s,AN}_{\text{SIR}}}\big(\gamma^{s}_{th}\big) = \Phi\big(\frac{\pi\Xi}{2}\sqrt{\frac{\pi\gamma^{s}_{th}{r_{s_0}}^{\alpha}}{\mu N_s}}\big), \tag{6.33}$$

where $\Phi\left(x\right) = \frac{1}{\sqrt{\pi}}\int_0^{x^2}\frac{e^{-t}}{\sqrt{t}}dt$. Note that this derived asymptotic CDF of SIR at the typical SU for $\alpha = 4$ is in exact closed-form.

6.4.1 Average Secrecy Rate

Based on the CDF of SIR at the most detrimental Eves in (6.29) and the CDF of SIR at the typical SU in (6.32), the general case of the asymptotic average secrecy rate is derived using (6.16) in the following proposition.

Proposition 2. With BF&AN at the SU-Txs, the asymptotic average secrecy rate at large N_s is derived as

$$\begin{aligned}\bar{C}^{\infty}_{se} =& \frac{1}{\ln 2}\int_0^{\infty}\frac{1}{1+x_2}\exp\big(-\frac{\pi\lambda_e e^{\left(1-\mu^{-1}\right)x_2}}{\Xi\Gamma\left(1-\frac{2}{\alpha}\right)}\big(\frac{\mu P_s}{x_2 P_p}\big)^{\frac{2}{\alpha}}\big)\Big[\frac{1}{2}-\frac{1}{\pi}\\ &\int_0^{\infty}\text{Im}[\frac{(\exp(-\pi\Xi\Gamma(1-\frac{2}{\alpha})(\frac{P_s}{P_p})^{-\frac{2}{\alpha}}(jw)^{\frac{2}{\alpha}}))^{*}}{e^{\frac{jw\mu N_s}{x_2{r_{s_0}}^{\alpha}}}}]\frac{1}{w}dw\Big]dx_2.\end{aligned} \tag{6.34}$$

Having (6.29) and (6.33), the asymptotic average secrecy rate for the special case of $\alpha = 4$ is derived in the following corollary.

Corollary 5. With BF&AN at the SU-Txs and $\alpha = 4$, the asymptotic average secrecy

rate at large N_s is derived as

$$\bar{C}_{se}^{\infty} = \frac{1}{\ln 2}\int_0^{\infty} \frac{1}{1+x_2} \exp\big(-\frac{\pi\lambda_e e^{\left(1-\mu^{-1}\right)x_2}}{\Xi\Gamma\left(1-\frac{2}{\alpha}\right)}\big(\frac{\mu}{x_2}\big)^{\frac{2}{\alpha}}\big)\big(1-\Phi\big(\frac{\pi\Xi}{2}\sqrt{\frac{\pi x_2}{\mu N_s {r_{s_0}}^{-\alpha}}}\big)\big)dx_2. \tag{6.35}$$

6.4.2 Secrecy Outage Probability

The attention is then turned to the asymptotic secrecy outage probability. By taking the derivative of the asymptotic CDF of SIR at the most detrimental Eves in (6.29), and substituting it with the asymptotic CDF of SIR at the typical SU in (6.32) into (6.18), the general case of the asymptotic secrecy outage probability is yielded in the following proposition.

Proposition 3. With BF&AN at the SU-Txs, the asymptotic secrecy outage probability at large N_s is derived as

$$\begin{aligned} P_{out,AN}^{\infty}\big(R_s\big) = \int_0^{\infty} & \frac{\pi\lambda_e(\mu P_s/P_p)^{\frac{2}{\alpha}}}{\Xi\Gamma(1-\frac{2}{\alpha}){x_2}^{\frac{2}{\alpha}}} \exp(-\frac{\pi\lambda_e e^{(1-\mu^{-1})x_2}}{\Xi\Gamma(1-\frac{2}{\alpha})}(\frac{\mu P_s}{x_2 P_p})^{\frac{2}{\alpha}}) \\ & e^{\left(1-\mu^{-1}\right)x_2}\Big(\big(1-\mu^{-1}\big)-\big(-\frac{2}{\alpha}\big){x_2}^{-1}\Big) \\ & \Big[\frac{1}{2}+\frac{1}{\pi}\int_0^{\infty}\mathrm{Im}[\frac{(\exp(-\pi\Xi\Gamma(1-\frac{2}{\alpha})(P_s/P_p)^{-\frac{2}{\alpha}}(jw)^{\frac{2}{\alpha}}))^*}{e^{\frac{jw\mu N_s}{(2^{R_s}(1+x_2)-1){r_{s_0}}^{\alpha}}}}]\,\frac{1}{w}dw\Big]\,dx_2. \end{aligned} \tag{6.36}$$

Based on (6.33), the secrecy outage probability for $\alpha = 4$ as a special case is derived in the following corollary.

Corollary 6. With BF&AN at the SU-Txs and $\alpha = 4$, the asymptotic secrecy outage probability at large N_s is derived as

$$\begin{aligned} P_{out,AN}^{\infty}\big(R_s\big) = \int_0^{\infty} & \frac{\pi\lambda_e\mu^{\frac{2}{\alpha}}}{\Xi\Gamma\left(1-\frac{2}{\alpha}\right)} \exp\big(-\frac{\pi\lambda_e e^{\left(1-\mu^{-1}\right)x_2}}{\Xi\Gamma\left(1-\frac{2}{\alpha}\right)}\big(\frac{\mu}{x_2}\big)^{\frac{2}{\alpha}}\big){x_2}^{-\frac{2}{\alpha}}e^{\left(1-\mu^{-1}\right)x_2} \\ & \Big(\big(1-\mu^{-1}\big)-\big(-\frac{2}{\alpha}\big){x_2}^{-1}\Big)\Phi\big(\frac{\pi\Xi}{2}\sqrt{\frac{\pi\left(2^{R_s}\left(1+x_2\right)-1\right)}{\mu N_s {r_{s_0}}^{-\alpha}}}\big)dx_2. \end{aligned} \tag{6.37}$$

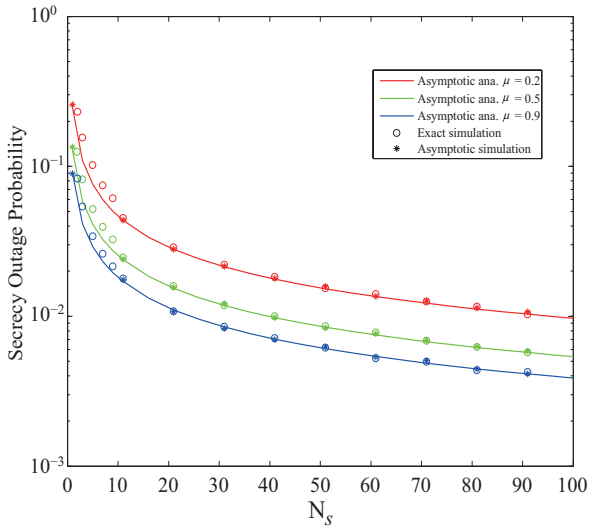

Figure 6.6: Secrecy outage probability for large N_s. Parameters: $\rho_{out}^{\{p\}} = 0.1$, $\lambda_p = 10^{-4}$, $\lambda_s = 10^{-3}$, $\lambda_e = 10^{-4}$, $r_p = 6$, $\alpha = 3$, $r_s = 3$, $R_s = 1$, $P_p = 15$ dB, and $\gamma_{th}^{\{p\}} = 6$ dB.

6.4.3 Numerical examples for the asymptotic secrecy performance of BF&AN

Fig. 6.7 plots the asymptotic average secrecy rate of large-scale spectrum sharing networks with BF&AN for various power allocation factor μ and λ_s. It is assumed that $P_s = P_s^{max}$. The analytical results of asymptotic secrecy rate plotted using (6.34) are in precise agreement with the simulation points of asymptotic secrecy rate. It is also shown that the asymptotic average secrecy rate converges to the exact average secrecy rate at large N_s.

It is observed that the average secrecy rate increases with increasing N_s. This can be indicated by (6.26) that the received SIR at the typical SU proportionally increases with μN_s. For the same μ, to achieve the same average secrecy rate, there exists antenna gaps between the curves with different density of SU. This antenna gap quantifies how many additional antennas needed to be employed at the SU-Tx to achieve the same average secrecy rate when the network double its density of SU.

Fig. 6.6 plots the asymptotic secrecy outage probability versus N_s. The analytical

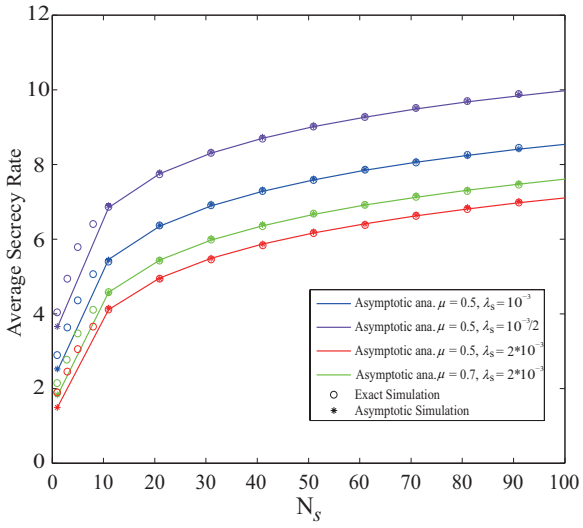

Figure 6.7: Asymptotic average secrecy rate versus N_s. Parameters: $\rho_{out}^{\{p\}} = 0.1$, $\lambda_p = 10^{-4}$, $\lambda_e = 10^{-4}$, $r_p = 6$, $\alpha = 3$, $r_s = 3$, $P_p = 15$ dB, and $\gamma_{th}^{\{p\}} = 6$ dB.

results of asymptotic outage probability plotted using (6.36) are in precise agreement with the simulation points of asymptotic outage probability. Furthermore, the asymptotic secrecy outage probability converges to the exact secrecy outage probability at large N_s. It is observed that the secrecy outage probability decreases with increasing N_s, due to the increase of the array gains at the SU-Rx. It is also seen that the secrecy outage probability decreases with increasing μ, which reflects that for the scenario with relatively less dense Eves, more power should be allocated to transmit useful information to the SU-Rx for the information delivery enhancement.

6.5 Summary

This chapter studied the secure communication in large-scale spectrum sharing network in the presence of multiple non-colluding Eves. The BF&AN is employed at the SU-Txs to achieve the secure transmission against those malicious Eves. The exact expression for the average secrecy rate is obtained, through which the average secrecy rate wall is

observed. The exact expression for the secrecy outage probability is also derived. The impact of different system parameters on the average secrecy rate and secrecy outage probability was demonstrated. It is shown that the optimal power allocation factor that maximizes the average secrecy rate needs not to be the equal power allocation. To better understand the impact of the number of antennas at the secondary transmitter, the asymptotic average secrecy rate and the asymptotic secrecy outage probability when the SU-Txs have large antenna arrays are also derived. Numerical results corroborated our analysis and showed that the asymptotic average secrecy rate can be greatly improved by increasing number of antennas at the SU-Txs. The results in this chapter provide valuable insights for the design of large-scale spectrum sharing networks.

uan

Chapter 7

Wireless Power Transfer in Cognitive Relay Networks

7.1 Introduction

In the underlay spectrum sharing networks, the transmit power of the SU-Tx is typically low, due to the interference power constraint imposed by the PU-Rx. Besides, the SU always subject to the interference from the PU Tx. Under this circumstances, wireless power transfer is well suited for this power-constrained underlay spectrum sharing networks, where the interference from the PU transmitter is utilized as an energy source for the SU-Tx with relatively low energy requirement [114, 115]. It seems even more promising that the required energy at the SU-Tx can be obtained via wireless power transfer from a large number of active PU-Txs. However, as the number of PU-Txs increases, the interference from the PU-Txs on the secondary network also increases. Therefore, the tradeoff between the benefits of energy harvesting from multiple PU-Txs and the harmful effect caused by the interference generated by multiple PU-Txs deserves to be further studied.

In this chapter, a wireless energy harvesting protocol is proposed for a DF relay aided spectrum sharing networks with multiple PU transceivers. In this protocol, both the energy-constrained SS and SR can harvest energy from the RF signals of multiple PU-

Txs to support its own information transmission. The joint impact of harvested energy and PU interference on the outage probability and the throughput of the secondary network are studied. The main contributions of this chapter are summarized as follows:

- An exact expression for the outage probability is derived in cognitive relay networks that subject to three power constraints: 1) the maximum transmit power at SS and SR based on the harvested energy; 2) the peak interference power at each PU-Rx; and 3) the interference power from multiple PU-Txs at SR and SD.The analytical expressions for the throughput in both delay-sensitive and delay-tolerant transmission modes are derived. It is shown that there exists an optimal value that achieves the minimum outage probability and the maximum throughput for the secondary network.

- The asymptotic closed-form expressions for the outage probability and delay-sensitive throughput and an asymptotic expression for the delay-tolerant throughput are derived as the number of PU-Txs and receivers goes to infinity. It is shown that when the number of PU-Txs is large, the negative impact caused by the interference from the PU-Txs outweighs the positive impact brought by the energy harvesting from the PU-Txs on the secondary performance.

7.2 Network Model

As shown in Fig. 7.1, this chapter considers an underlay cognitive relay network where an energy-constrained SS transmits to an energy sufficient SD through an energy-constrained SR using the licensed PU spectrum. The primary network consists of M PU transceivers [187]. It is assumed that there is no direct link between SS and SD [188]. Both SS and SR has no internal energy source, and use the energy harvested from RF signals of the PU-Txs. A battery-free communication system is considered [188–190], where the harvested energy can only be used for information transmission in the current time slot. The primary network consists of two clusters of PUs where the PU-Tx are closely

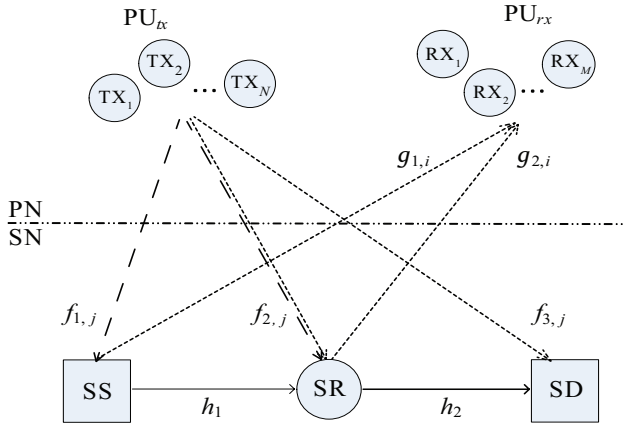

Figure 7.1: System model of the energy harvesting CR. The energy harvesting links, interference links, and information links are illustrated with the dashed, dotted, and solid lines, respectively.

located in one cluster and the PU-Rx are closely located in another cluster [187, 191] [1]. Note that the secondary network shares the spectrum with the primary network in an underlay paradigm, i.e., the interference power from SS and SR to PU should not exceed the peak permissible interference power, denoted by $P_{\mathcal{I}}$. The interference-limited case is considered where the interference power caused by PU-Txs at SR and SD is dominant relative to the noise power [187]. All channel gains are assumed to be independently distributed with flat Rayleigh fading and the fading is considered as a constant over the energy harvesting and the information transmission periods. The exponential decaying path loss model is used, where the channel mean power is proportional to d^{-m} with d denoting the distance between a transmitter and a receiver and m denoting the path loss factor [187]. It is assumed that the energy required to receive/process information is negligible as compared to energy required for the information transmission. This assumption is valid for traditional communication systems [188, 193, 194].

As shown in Fig. 7.1, the channel gain coefficients from SS and SR to the ith $PU-Rx$ are denoted by $g_{1,i}$ and $g_{2,i}$ for $i = 1, 2, \ldots, M$, respectively. The channel gain coefficients from SS to SR and from SR to SD are denoted by h_1 and h_2, respectively. And the channel gain coefficients from the jth PU-Tx to SS, SR, and SD, are denoted by $f_{1,j}$,

[1] In addition, we assume that PU-Rxs apply multi-user detectors to cancel interference from different PU-Txs [192].

$f_{2,j}$, and $f_{3,j}$ for $j = 1, 2, , \ldots, N$, respectively.

The link gain realizations $|h_1|^2$, $|h_2|^2$, $|g_{1,i}|^2$, $|g_{2,i}|^2$, $|f_{1,j}|^2$, $|f_{2,j}|^2$, and $|f_{3,j}|^2$ are exponentially distributed with expectations λ_1, λ_2, $\omega_{1,i}$, $\omega_{2,i}$, $\nu_{1,j}$, $\nu_{2,j}$, and $\nu_{3,j}$, respectively, e.g., $\lambda_1 = d_6^{-m}$. The link gains from PU-Tx to SS are assumed to be identically distributed as wells as those to SR and SD [187], i.e., $\nu_{1,j} = \nu_1$, $\nu_{2,j} = \nu_2$, and $\nu_{3,j} = \nu_3$ for $j = 1, 2, \ldots, N$. Similarly, the link gains from SS to PU-Rx are assumed to be identically distributed as wells as those from SR to PU-Rx, i.e., $\omega_{1,i} = \omega_1$, $\omega_{2,i} = \omega_2$ for $i = 1, 2, \ldots, M$. The distances between the jth PU-Tx and SS, SR, and SD are denoted by $d_{1,j}$, $d_{2,j}$, and $d_{3,j}$, respectively. The distances between SS and SR and the ith PU-Rx are denoted by $d_{4,i}$ and $d_{5,i}$, respectively. And the distances between SS and SR and between SR to SD are denoted by d_6 and d_7, respectively.

As shown in Fig. 7.2, SS and SR harvest energy from RF signals of PU-Tx for a duration of αT at the beginning of each energy harvesting-information transfer (EH-IT) time slot, where T is the duration of one EH-IT time slot and $0 < \alpha < 1$. Subsequent to the harvesting period, SS transmits information to SR for a duration $\beta(1-\alpha)T$, where $0 < \beta < 1$. Then, SR forwards the information to SD for a duration of $(1-\beta)(1-\alpha)T$. For simplicity, it is assumed that $\beta = \frac{1}{2}$ in this network.

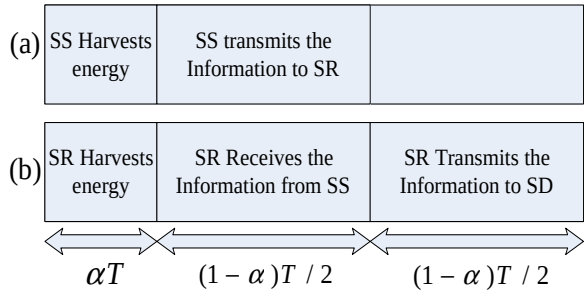

Figure 7.2: (a) illustrates the protocol at SS in one EH-IT time slot and (b) illustrates the protocol at SR in EH-IT time slot

It can be seen from Fig. 7.2 that SS can also harvest energy when SR transmits information to SD. But SS is battery-free and it is unable to store the unused portion of the harvested energy in future EH-IT time slots, if the EH-IT time slots are dis-

tributed sparsely. The energy harvested at SS and SR using the time switching receiver architecture are given by [194]

$$E_{h_s} = \eta P_{PU_{tx}} \sum_{j=1}^{N} |F_{1,j}|^2 \alpha T \tag{7.1}$$

and

$$E_{h_r} = \eta P_{PU_{tx}} \sum_{j=1}^{N} |F_{2,j}|^2 \alpha T, \tag{7.2}$$

respectively, where $0 < \eta \leq 1$ is the energy conversion efficiency [194]. In the case that SS should transmit information in consecutive EH-IT time slots, it can also harvest energy during $(1-\alpha)T/2$ and hence, (7.1) can be written as $E_{h_s} = \eta P_{PU_{tx}} \sum_{j=1}^{N} |F_{1,j}|^2 [\alpha T + (1-\alpha)T/2]$. The maximum power that SS and SR can transmit based on the harvested energy are $\frac{E_{h_s}}{(1-\alpha)T/2}$ and $\frac{E_{h_r}}{(1-\alpha)T/2}$, respectively. Therefore, the transmit power at SS and SR are given by

$$P_s = \min\left(\frac{E_{h_s}}{(1-\alpha)T/2}, \frac{P_{\mathcal{I}}}{\max |G_{1,i}|^2}\right) \tag{7.3}$$

and

$$P_r = \min\left(\frac{E_{h_r}}{(1-\alpha)T/2}, \frac{P_{\mathcal{I}}}{\max |G_{2,i}|^2}\right), \tag{7.4}$$

respectively.

As SS and SR share the same spectrum with PUs, the transmitted signals from SS and SR cause interference to each PU_{rx}. Constraints on the transmit power of SS and SR are imposed in order that the interference power to the PU does not exceed $P_{\mathcal{I}}$.

The SIR at SR and SD are obtained as

$$\Gamma_R = \min\left(\rho Z_1, \frac{P_{\mathcal{I}}}{Y_1}\right) \frac{X_1}{Z_2} \tag{7.5}$$

and

$$\Gamma_D = \min\left(\rho Z_2, \frac{P_{\mathcal{I}}}{Y_2}\right) \frac{X_2}{Z_3}, \tag{7.6}$$

respectively, where $\rho = \frac{2\eta\alpha}{(1-\alpha)}$, $X_1 = |H_1|^2$, $X_2 = |H_2|^2$, $Z_1 = \sum_{j=1}^{N} P_{PU_{tx}}|F_{1,j}|^2$, $Z_2 = \sum_{j=1}^{N} P_{PU_{tx}}|F_{2,j}|^2$, $Z_3 = \sum_{j=1}^{N} P_{PU_{tx}}|F_{3,j}|^2$, $Y_1 = \max_{i=1,\ldots,M} |G_{1,k}|^2$, and $Y_2 = \max_{i=1,\ldots,M} |G_{2,k}|^2$. Note that Γ_R and Γ_D are dependent random variables because they both are functions of Z_2.

7.3 Exact Performance Analysis

In this section, the expressions for outage probability and throughput of secondary network with the proposed energy harvesting protocol are derived. These expressions provide practical design insights into the impact of various parameters on the secondary performance.

7.3.1 Outage Probability

The outage probability P_{out}, is defined as the probability that the equivalent SIR at each hop is below a threshold value, γ_{th}. In this framework, the DF relay assisted spectrum sharing network is considered to be in outage if only one of the links suffer from an outage, i.e.,

$$P_{out}(\gamma_{th}) = 1 - \Pr\{\Gamma_R \geq \gamma_{th}, \Gamma_D \geq \gamma_{th}\}, \tag{7.7}$$

where Γ_R and Γ_D denote the SIR RVs at SR and SD, and are given in (7.5) and (7.6), respectively. To facilitate the analysis, the CDF and the PDF of Z_1, Z_2, Z_3, Y_1, and Y_2 are first derived. Note that each Z_1, Z_2, Z_3 is the sum of N exponential RVs and their distributions are known as chi-square distribution. The PDF and CDF of Z_1, Z_2, and Z_3 can be given by [187]

$$f_Z(z) = \frac{z^{N-1} e^{-\frac{z}{P_{PU_{tx}}\nu}}}{\Gamma(N)(P_{PU_{tx}}\nu)^N} \tag{7.8}$$

and

$$F_Z(z) = \frac{\Gamma(N, \frac{z}{P_{PU_{tx}}\nu})}{\Gamma(N)}, \tag{7.9}$$

respectively, where $\Gamma(.)$ and $\Gamma(.,.)$ denote gamma and incomplete gamma functions, respectively. The PDF and CDF of Y_1 and Y_2 can be given by

$$f_Y(y) = \frac{M}{\omega}\sum_{k}^{M-1}\binom{M-1}{k}(-1)^k e^{-(\frac{k+1}{\omega})y} \tag{7.10}$$

and

$$F_Y(y) = (1-e^{-\frac{y}{\omega}})^M, \tag{7.11}$$

respectively. It is assumed that the distances between PU-Txs in the cluster are relatively smaller than the distances between PU-Tx and SS, SR, and SD. The same assumption is used for the PU-Rx with respect to SS, SR, and SD.

The exact expression for the outage probability is given in the following theorem.

Theorem 18. *The outage probability of secondary network with the proposed energy harvesting protocol is given by*

$$P_{out}(\gamma_{th}) = 1 - \int_0^\infty (\mathcal{J}_{R,I}+\mathcal{J}_{R,II})(\mathcal{J}_{D,I}+\mathcal{J}_{D,II})\frac{z_2^{N-1}e^{-\frac{z_2}{P_{PU_{tx}}\nu_2}}}{\Gamma(N)(P_{PU_{tx}}\nu_2)^N}dz_2, \tag{7.12}$$

where $\mathcal{J}_{R,I}$, $\mathcal{J}_{R,II}$, $\mathcal{J}_{D,I}$, and $\mathcal{J}_{D,II}$ are defined in the following proof.

Proof. See Appendix E.1. □

7.3.2 Throughput

This subsection evaluates the throughput in two transmission modes: delay-sensitive mode and delay-tolerant mode. The evaluation of throughput provides insight into prac-

tical implementations and challenges of energy harvesting cognitive relay network.

7.3.2.1 Delay-sensitive Transmission

In the delay-sensitive transmission mode, SS transmits information to SR at a fixed rate, denoted by R_{ds}, where $R_{ds} \triangleq \log_2(1+\gamma_{th})$. The throughput in delay-sensitive mode is expressed as [188]

$$\tau_{ds} = \frac{\frac{(1-\alpha)T}{2}}{T} R_{ds}(1-P_{out}(\gamma_{th})) = \frac{(1-\alpha)}{2} R_{ds}(1-P_{out}(\gamma_{th})), \tag{7.13}$$

where τ_{ds} is equal to the rate of the successful transmissions during the transmission time, $\frac{(1-\alpha)T}{2}$, when SIR requirement (γ_{th}) is satisfied at SR and SD. Note, the system outage probability is obtained from (7.12).

7.3.2.2 Delay-Tolerant Transmission

In the delay-tolerant transmission mode, users can transmit messages reliably while the transmission rate is less than or equal to the ergodic capacity C_{erg}, which is defined as [195]

$$C_{erg} = \mathbb{E}\{\log_2(1+\Gamma_{th})\},$$

where $\mathbb{E}\{.\}$ denotes the expected value of an argument and Γ_{th} is a random variable defined as $\gamma_{th} = \min(\gamma_R, \gamma_D)$. The delay-tolerant throughput, which is denoted by τ_{dt}, can be derived as

$$\tau_{dt} = \frac{\frac{(1-\alpha)T}{2}}{T} C_{erg} = \frac{(1-\alpha)}{2\ln 2} \int_0^\infty \frac{1-F_{\Gamma_{th}}(x)}{(1+x)} dx, \tag{7.14}$$

where $F_{\Gamma_{th}}(\gamma_{th})$ denotes the CDF of γ_{th}, which can be evaluated by (7.12), i.e., $F_{\Gamma_{th}}(\gamma_{th}) = P_{out}(\gamma_{th})$. In contrast to delay-sensitive mode, where SS is expected to transmit at a fixed rate to satisfy a certain outage probability, in delay-tolerant transmission mode,

SS can transmit at any rate equal or less than the evaluated ergodic capacity.

7.4 Large System Analysis

This section analyzes the asymptotic outage probability, delay-sensitive throughput, and delay-tolerant throughput when the number of PU transceivers grows to infinity. As N increases, more interference imposed on SR and SD may cause outages. On the other hand, as N increases, SS and SR can potentially harvest more energy from multiple PU-Txs. The tradeoff between the positive impact brought by the energy harvesting from multiple PU-Txs and the negative influence brought by the interference of the multiple PU-Txs on SR and SD is then examined.

To do so, the distribution of Z_1, Z_2, and Z_3 as $N \to \infty$ need to be first solved. Since Z_1 is i.i.d. exponential RVs, the distribution of Z_1 is asymptotically normal as $Z_1 \to \infty$. Using the law of large numbers, it is obtained that

$$Z_1 \xrightarrow{d} NP_{PU_{tx}}\nu_1, \tag{7.15}$$

where $A \xrightarrow{d} B$ denotes convergence in distribution of a RV A to a RV B. Similarly, it is obtained that

$$Z_2 \xrightarrow{d} NP_{PU_{tx}}\nu_2 \tag{7.16}$$

and

$$Z_3 \xrightarrow{d} NP_{PU_{tx}}\nu_3. \tag{7.17}$$

In the same manner, the distribution of Y_1 and Y_2 as $M \to \infty$ is then obtained. Since Y_1 is the maximum of M i.i.d. exponential RVs, the distribution of Y_1 is asymptotically

normal, as $Y_1 \to \infty$. From [196, Proposition 1], it is known that

$$Y_1 \xrightarrow{d} \omega_1 + \omega_1 \ln M + \overline{Y}_1, \tag{7.18}$$

where $\overline{Y}_1$ is the normal distribution with $\mathcal{N}(0, 2{\omega_1}^2)$. Similarly, it is known that

$$Y_2 \xrightarrow{d} \omega_2 + \omega_2 \ln M + \overline{Y}_2, \tag{7.19}$$

where $\overline{Y}_2$ is the normal distribution with $\mathcal{N}(0, 2{\omega_2}^2)$. Having the distribution of Y_1, Y_2, Z_1, Z_2, and Z_3 for large number of PU transceivers, the SIRs in (7.5) and (7.6) is rewritten as

$$\Gamma_R^{\infty} \overset{d}{\sim} \min(\rho N P_{PU_{tx}} \nu_1, \frac{P_I}{\omega_1 + \omega_1 \ln M + \overline{Y}_1}) \frac{X_1}{P_{PU_{tx}} N \nu_2} \tag{7.20}$$

and

$$\Gamma_D^{\infty} \overset{d}{\sim} \min(\rho P_{PU_{tx}} N \nu_2, \frac{P_I}{\omega_2 + \omega_2 \ln M + \overline{Y}_2}) \frac{X_2}{P_{PU_{tx}} N \nu_3}, \tag{7.21}$$

respectively. The SIRs in (7.20) and (7.21) are then used to obtain the asymptotic outage probability for large number of PU tranceivers in the next subsection.

7.4.1 Outage probability

The asymptotic outage probability of the secondary network is given by

$$P_{out}^{\infty}(\gamma_{th}) = 1 - \Pr\{\Gamma_R^{\infty} \geq \gamma_{th}, \Gamma_D^{\infty} \geq \gamma_{th}\}. \tag{7.22}$$

In contrast to (7.7), Γ_R^{∞} and Γ_D^{∞} in (7.22) are independent and therefore, the second term in (7.22) is rewritten as the product of two terms.

Theorem 19. *As the number of PU transceivers goes to infinity, the outage probability*

of the proposed cognitive relay network is given in closed form as

$$P_{out}^{\infty}(\gamma_{th}) = 1 - \Theta_R \Theta_D, \tag{7.23}$$

where $\Theta_R = \Pr\{\Gamma_R^{\infty} \geq \gamma_{th}\}$ *and* $\Theta_D = \Pr\{\Gamma_D^{\infty} \geq \gamma_{th}\}$*, respectively.*

Proof. See Appendix E.2. □

7.4.2 Throughput

The delay-sensitive throughput and delay-tolerant throughput are derived in this section. The expression derived in (7.23) is utilized to evaluate τ_{ds}^{∞} and τ_{dt}^{∞}, respectively, as

$$\tau_{ds}^{\infty} = \frac{(1-\alpha)}{2} R_{ds}(1 - P_{out}^{\infty}(\gamma_{th})), \tag{7.24}$$

and

$$\tau_{dt}^{\infty} = \frac{(1-\alpha)}{2\ln 2} \int_0^{\infty} \frac{1 - F_{\Gamma_{th}}(x)}{(1+x)} dx, \tag{7.25}$$

where $F_{\Gamma_{th}}(\gamma_{th})$ can be evaluated using (7.23), i.e., $F_{\Gamma_{th}}(\gamma_{th}) = P_{out}^{\infty}(\gamma_{th})$.

7.5 Numerical Results

This section presents the numerical results to examine the outage probability and the throughput for the proposed cognitive relay networks with energy harvesting protocol. The outage probability and the throughput is shown as functions of $P_{\mathcal{I}}$, $P_{PU_{tx}}$, and the position of PU-Tx. To gain more insights, The asymptotic behaviors of the outage probability and the throughput are examined when the number of PU transceivers goes to infinity. Without the loss of generality, it is assumed that SS, SR, and SD are located at (0,0), (0.5,0), and (1,0) on the X-Y plane, respectively and the cluster of PU-Rx

is located at (1, 0.5). It is specified that the location of the cluster of PU-Txs in the description of each figure. It is assumed that $\alpha = 0.5$ (Figs. 7.3-7.9), $\eta = 1$, and $M = N$ for all the figures.

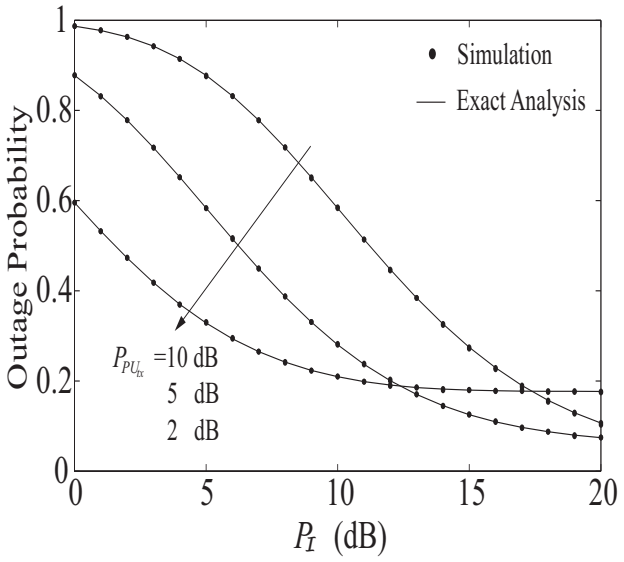

Figure 7.3: The outage probability as a function of $P_{\mathcal{I}}$ for $M = N = 3$ and $P_{PU_{tx}} = 2$, 5 and 10 dB.

Fig. 7.3 shows the outage probability as a function of $P_{\mathcal{I}}$ for various transmit power at PU. It is assumed that the cluster of PU-Tx is located at $(0.5, 1)$. The exact outage probability curves are plotted from (7.12). For a given value of $P_{PU_{tx}}$, the results show that the outage probability decreases as the interference power constraint $P_{\mathcal{I}}$ increases. This is due to the fact that SS and SR can transmit with higher power to offset the interference imposed by the PU-Txs at SR and SD, respectively, as $P_{\mathcal{I}}$ increases. It is also observed that for large value of $P_{\mathcal{I}}$ ($\sim$ 20dB), the outage probability increases as $P_{PU_{tx}}$ decreases. This is contradictory to the conclusion in underlay spectrum sharing network without energy harvesting that the outage probability decreases as $P_{PU_{tx}}$ decreases. The reason is that when the value of $P_{PU_{tx}}$ is low (e. g. $P_{PU_{tx}} = 2$ dB), the energy harvested from the PU-Txs is small, which can not support high transmit power. Thus, the outage probability with low PU transmit power (e.g., $P_{PU_{tx}} = 2$ dB) can not compete with that with high PU transmit power (e. g. $P_{PU_{tx}} = 5$ or 10 dB). However, when the allowed

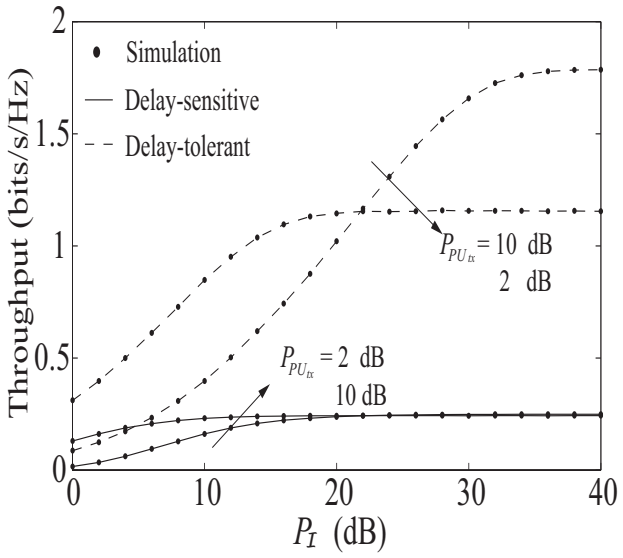

Figure 7.4: The throughput as a function of $P_{\mathcal{I}}$ for $M = N = 3$ and $P_{PU_{tx}} = 2$, and 10 dB.

interference power ($P_{\mathcal{I}}$) is small, the energy harvested from PU-Tx is enough for low power transmission, e.g., the outage probability for $P_{PU_{tx}} = 2$ dB is lower than that for $P_{PU_{tx}} = 5$ and 10 dB, when $P_{\mathcal{I}} = 0 \sim 12$ dB. More investigations show that the outage probability reaches some error floors due to the fact that there is a limit on the maximum transmit power at which SS and SR can transmit given the limitation on the harvested energy in that time slot.

Fig. 7.4 plots the throughput in delay-sensitive and delay-tolerant modes as a function of $P_{\mathcal{I}}$ for various transmit power from the PU-Txs. The cluster of PU-Txs is located at $(0.5, 1)$. The results show that the throughput increases as $P_{\mathcal{I}}$ increases. This is because SS and SR can transmit at higher transmission power without causing interference beyond $P_{\mathcal{I}}$ as it increases. It is expected that the throughput to reach an asymptotic value as $P_{\mathcal{I}}$ goes to infinity because SS and SR can use all the harvested energy to transmit information without causing interference beyond $P_{\mathcal{I}}$. The curve representing the delay-sensitive throughput for $P_{PU_{tx}} = 10$ dB seems to approach that for $P_{PU_{tx}} = 2$ dB. However, further investigation shows that the delay-sensitive throughput does not converge to the same value necessarily. It is also observed that delay-tolerant throughput

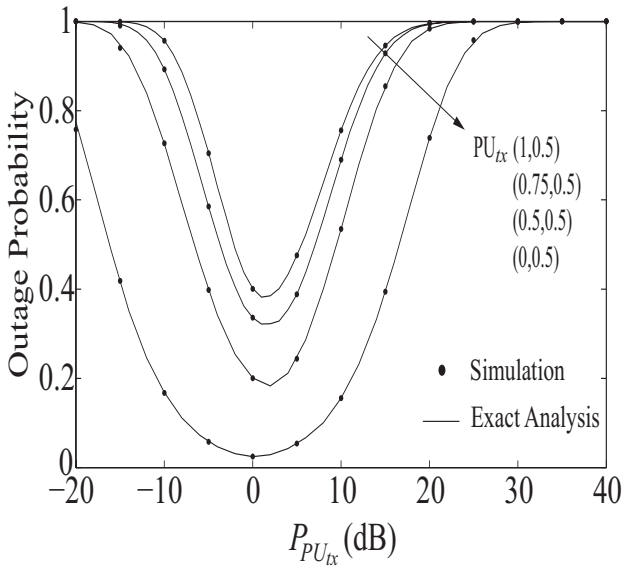

Figure 7.5: The outage probability as a function of $P_{PU_{tx}}$ for $M = N = 3$.

for $P_{PU_{tx}} = 10$ dB reaches an asymptotic value larger than that for $P_{PU_{tx}} = 2$ dB. This is due to the fact that SS and SR can harvest more energy with $P_{PU_{tx}} = 10$ dB and transmit information at higher transmit power as $P_{\mathcal{I}}$ increases. The throughput results for delay-sensitive mode is lower than those in delay-tolerant as expected. In delay-sensitive, the data is time sensitive and therefore, the information is transmitted at a fixed rate. If the rate is above the channel rate, the outage occurs and the throughput suffers. In delay-tolerant transmission mode, the transmission rate is flexible due to the fact that the data at SS can tolerate delays. Therefore, the throughput of delay-tolerant mode is larger than that of delay-sensitive.

Fig. 7.5 plots the outage probability as a function of $P_{PU_{tx}}$ for various locations of PU-Tx cluster. It is assumed that $P_{\mathcal{I}} = 0$ dB. The exact outage probability curves are plotted using (7.12). Note "PU$_{tx}$@" in the legend of 7.5 denotes "PU-Tx cluster is located at". The outage probability is large at low PU transmit power (e.g., $P_{PU_{tx}} = -20$ dB), because SS and SR harvest insufficient energy for reliable information transmission at low $P_{PU_{tx}}$ values. The results also show that the outage probability first decreases and then increases as a function of $P_{PU_{tx}}$. The decrease trend in the outage probability is

due to the fact that SS and SR can harvest more energy from the primary network as $P_{PU_{tx}}$ increases and therefore, can transmit information successfully at higher transmit power levels. However, the harmful effects brought by the interference from the PU-Txs at SR and SD offset the benefits gained from the energy harvesting at SS and SR. As a result the outage probability increases. Note that this first decreasing and then increasing behavior of the outage probability is different from the conventional spectrum sharing network with sufficient energy supply that the outage probability only increases monotonically as $P_{PU_{tx}}$ increases. The outage probability for the secondary network increases as the interference power at SR and SD increases. However, when the energy constraints imposed by the energy harvesting is considered, the outage probability is very large when low amount of energy is harvested and it decreases as more energy becomes available. Therefore, it is observed the outage probability decrease and then increase as as $P_{PU_{tx}}$ increases.

Interestingly, the outage probability decreases as the cluster of PU-Tx moves towards SS and away from SR and SD. This is because less interference is imposed on SR and SD while more energy is harvested at SS (and SR), as the PU-Tx is moving towards SS and away from SR and SD. As a result, SS and SR can transmit information successfully at high power levels, and hence the outage probability for a given $P_{PU_{tx}}$ improves.

Fig. 7.6 plots the outage probability as a function of $P_{PU_{tx}}$ for various $P_{\mathcal{I}}$ values. It is assumed that the PU-Tx is located at $(0, 1)$. The analytical results for the outage probability is plotted using (7.12). The first decreasing and then increasing behavior of the outage probability is observed as $P_{PU_{tx}}$ increases similar to that observed in Fig. 7.5. In addition, it is observed that the outage probability improves as $P_{\mathcal{I}}$ increases. This is predictable since higher interference power constraint $P_{\mathcal{I}}$ allows higher transmit power at SS and SR, which results in lower outage probability. The minimum outage probability shifts to right as $P_{\mathcal{I}}$ increases from 0 dB to 20 dB. This behavior can be explained as follows: 1) as $P_{PU_{tx}}$ increases, SS and SR can use higher transmit power to offset the interference from the PU-Txs at SR and SD, respectively, and 2) as $P_{\mathcal{I}}$

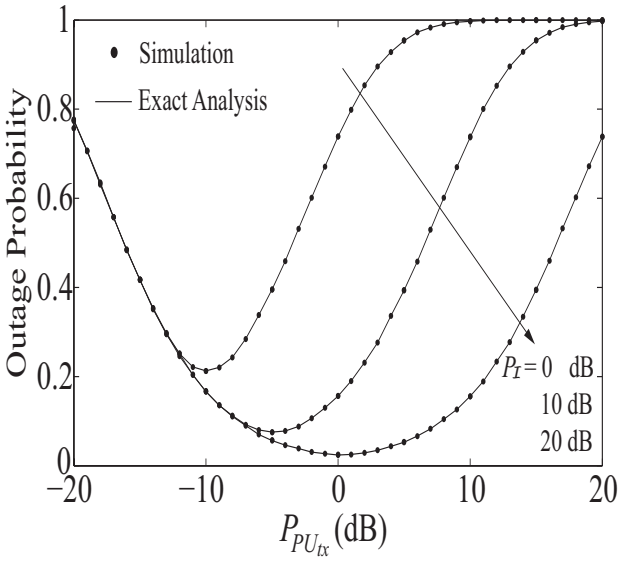

Figure 7.6: The outage probability as a function of $P_{PU_{tx}}$ for $N = M = 3$ and $P_{\mathcal{I}} = 0$, 10, and 20 dB.

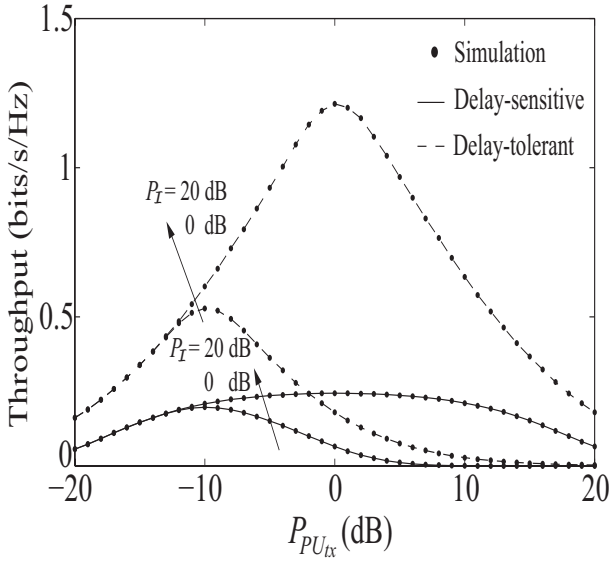

Figure 7.7: The throughput as a function of $P_{PU_{tx}}$ for $N = M = 3$ and $P_{\mathcal{I}} = 0$ and 20 dB.

increases, the transmit power constraints at SS and SR relaxes, therefore, allowing SS and SR to transmit at higher power levels without imposing interference beyond $P_{\mathcal{I}}$. As a result, the minimum outage probability is achieved at higher $P_{PU_{tx}}$ values (i.e., shift to the right).

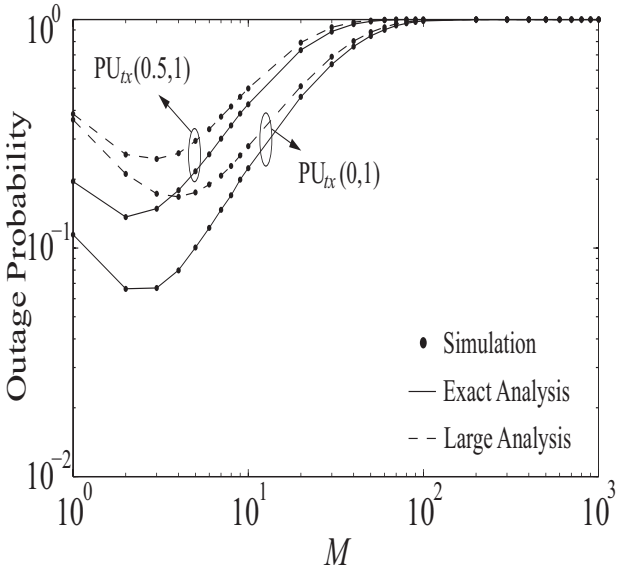

Figure 7.8: The outage probability as a function of M for $N = M$, $P_{\mathcal{I}} = 10$ dB, and $P_{PU_{tx}} = 0$ dB.

Fig. 7.7 plots the throughput for delay-sensitive and delay-tolerant transmission modes as a function of $P_{PU_{tx}}$, where PU-Tx is assumed to be located at $(0, 1)$. It is shown that the throughput increases and then decreases as a function of $P_{PU_{tx}}$. In the extremely low $P_{PU_{tx}}$ region (i.e., $-20 \sim -10$ dB), the positive effect of increased energy harvested from primary network dominates the throughput performance such that the throughput increases with increasing $P_{PU_{tx}}$. In the high $P_{PU_{tx}}$ region (i.e., $10 \sim 20$ dB), the detrimental effect of the interference from the PU-Tx dominates the throughput performance, such that the throughput decreases as $P_{PU_{tx}}$ increases. It is also observed that the maximum throughput increases and moves to the right as $P_{\mathcal{I}}$ increases. This is due to the fact that when $P_{\mathcal{I}}$ is relaxed (i.e., increased), SS and SR can transmit at higher power levels to offset the interference from PU-Txs at SR and SD, respectively, as $P_{PU_{tx}}$ increases. Note that similar to the discussion in Fig. 7.4, the throughput in delay-tolerant mode is higher than that in delay-sensitive mode.

Fig. 7.8 plots the exact outage probability and asymptotic outage probability as a function of M for various PU-Tx positions. It is assumed that $P_{\mathcal{I}} = 10$ dB and $P_{PU_{tx}} = 0$ dB. The exact outage probability and asymptotic outage probability curves are

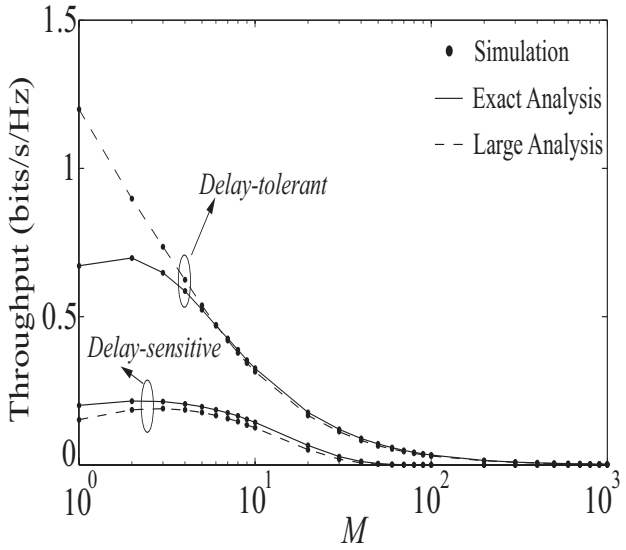

Figure 7.9: The throughput as a function of M for $N = M$, $P_{\mathcal{I}} = 10$ dB, and $P_{PU_{tx}} = 0$ dB.

plotted using (7.12) and (7.23), respectively. The results from the large analysis converge to those from the exact analysis as the number of PU transceivers approaches infinity. There exists an optimal M which achieves the minimum outage probability. It is shown that the outage probability decreases and then increases as the number of PU transceivers grows large. Since SS and SR can harvest energy from all PU-Txs, it is natural to assume that the opportunity to harvest energy from the primary network increases as the number of PU-Txs increases. In order to improve the system outage probability given by (7.12), SS and SR can forward information at higher transmit power as the harvested energy improve. However, the harmful impact of the interference imposed on the secondary network from the primary network counterbalances the benefits gained from the energy harvesting as the number of PU-Txs increases. Similar to the observation in Fig. 7.5, a lower outage probability can be achieved when the PU-Tx is far from SD and SR , and close to SS for the each M value. Given the system parameters in this figure, the minimum outage probabilities for the PU-Tx located at $(0, 1)$ and $(0.5, 1)$ are when $M = 2$ and $M = 3$, respectively. This also shows that increasing the number of PUs can not guarantee lower outage probability.

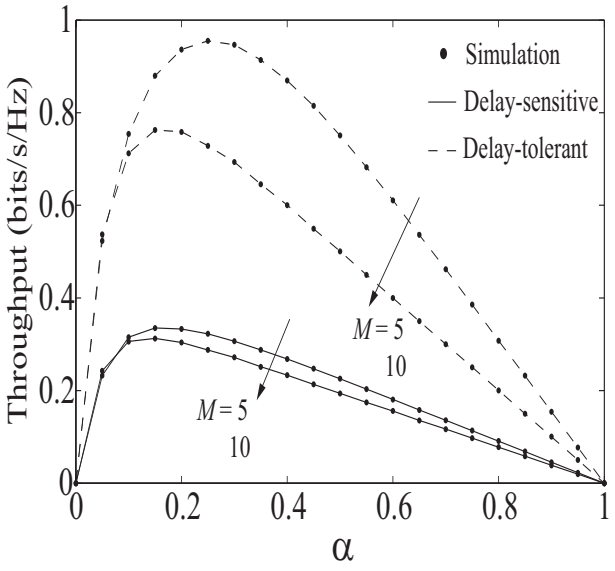

Figure 7.10: The throughput as a function of α for $P_{PU_{tx}} = 0$ and $P_{\mathcal{I}} = 10$ dB.

Fig. 7.9 plots the throughput for delay-sensitive and delay-tolerant transmission modes as a function of M. It is assumed that $P_{\mathcal{I}} = 10$ dB, $P_{PU_{tx}} = 0$ dB, and the PU-Tx is located at $(0, 1)$. It is shown that the throughput increases and then decreases as a function of M. It is observed that the throughput approaches to zero as M grows large ($M \sim 100$) due to excessive interference power from PU-Txs at SR and SD. The large interference power disables SS and SR from communicating the information to SD. The throughput results from the large analysis converges to those from the exact analysis as M increases.

Fig. 7.10 plots the throughput for delay-sensitive and delay-tolerant transmission modes versus α for various values of M. It is assumed that $P_{PU_{tx}} = 0$, $P_{\mathcal{I}} = 10$ dB, and the position of PU-Txs is at $(0, 1)$. The results show that the throughout increases and then decreases as a function of α. For small values of α (~ 0), SS and SR harvest insufficient energy for a reliable information transmission due to short energy harvesting periods and therefore, the throughput is low. For large values of α (~ 1), SS and SR are unable to transmit reliably due to short information transmitting periods. As α increases from small values to large values, the throughput is influenced by the tradeoff

between the energy harvesting and information transmission periods. It is observed that the delay-sensitive and delay-tolerant throughput improve when the number of PU transceivers increase from 5 to 10. This is due to the fact that the negative effects brought by the interference from PU-Txs on SR and SD offsets the positive effects brought by harvesting energy from PU-Txs on SS and SR. The results also show that the optimal α value is not necessarily the same for the delay-sensitive and delay-tolerant transmission modes.

Remark 1: The value chosen for α greatly impacts the outage probability and the throughput of the secondary network. As the value of α increases from 0 to 1, more energy may be available at SS and SR but less time is available to transmit the information. It is desired to find a value for α which maximize the throughput. The optimal value of α can be evaluated numerically (and off-line) using search methods for (7.13) and (7.14). Note that the closed form expression for the optimal α is not tractable due to the complexity of the throughput expressions.

Remark 2: It is desired to deploy SS, SR, and SD at the locations (with respect to the primary network) where the outage probability is minimized and the throughput is maximized. For example, the secondary network can be deployed so that the PU-Txs are located near SS and SR for energy harvesting and away from SR and SD to reduce interference power at SR and SD. In order to reduce the interference from SS and SR at the primary network, it is desired that SS and SR are far from the PU-Rx. This can be observed in Fig. 7.5, at the location where the outage probabilities as a function of $P_{PU_{tx}}$ for four PU-Tx locations are illustrated. If the system engineer can deploy the secondary network network at a desired location and the PU-Tx and the PU-Rx are immobile, the optimal location of SS, SR, and SD with respect to the PU-Tx and the PU-Rx can be obtained. Although a closed-form solution for the optimal location of SS, SR, and SD from (7.12) is intractable, the solution can be obtained offline by numerical searching methods.

7.6 Summary

A wireless energy harvesting protocol was proposed for an underlay cognitive relay network with multiple primary transceivers. The exact analysis as well as asymptotic analysis of the outage probability and throughput as the number of PU transceivers goes to infinity were performed. Expressions for the exact outage probability and the exact throughput for two transmission modes, namely delay-sensitive and delay-tolerant, were derived. For a sufficiently large number of PUs transceivers, the closed-form expressions for the asymptotic outage probability and delay-sensitive throughput and an analytical expression for the asymptotic delay-tolerant throughput were derived. The results shown that the detrimental effect caused by the interference from the multiple PU-Txs at the secondary network offsets the benefits brought by harvesting energy when the number of PU transceivers is large. The results also shown that as PU-Txs move closer to SS and farther away from SR and SD, more energy is harvested at SS and less interference is imposed on SR and SD, such that the outage probability of secondary network improves.

Chapter 8

K-tier Heterogeneous Cellular Networks with Wireless Power Transfer

8.1 Introduction

In this chapter, inspired by the joint design of DL power transfer and UL information transmission in WPCNs in [117, 118], a new breed of multi-cell wireless powered HCNs is proposed in which all the multiple antennas BSs with constant power supply provide RF energy to the single antenna MTs without internal energy sources in the DL, then the MTs utilize the harvested energy to deliver the information to the BSs in the UL. Stochastic geometry is used to model and analyze the proposed HCNs. This work pioneers the modeling of RF wireless power transfer in multi-tier HCNs. The goal is to address the fundamental questions surrounding the effect of DL power transfer on the UL information transmission. The main contributions of this paper are summarized as follows:

- A tractable model for both DL wireless power transfer and UL information transmission in HCNs with biased-received-power cell association policy is defined. Assuming large storage battery at each MT, the expression for the exact average received power of typical MT associated with kth tier via the DL power is

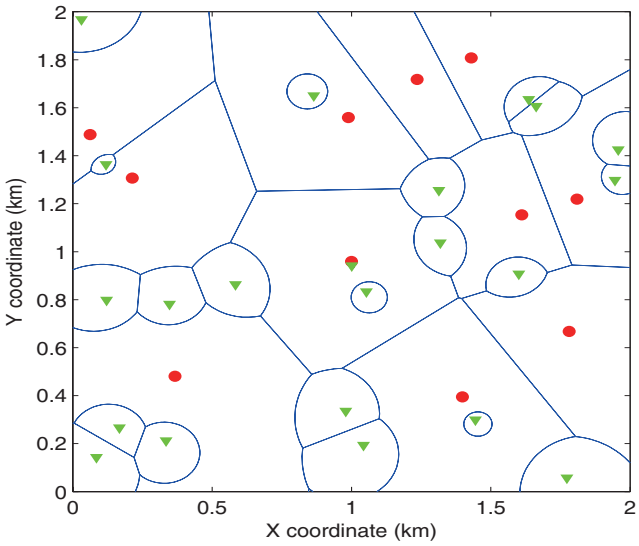

Figure 8.1: Two-Tier HCNs.

derived. Importantly, the results show that the dedicated signal from the typical BS with MRT BF contributes far more energy than the interference signals from other BSs in different tiers to the average received power of typical MT. It is also revealed that the average received power of typical MT associated with kth tier will not change by increasing the number of antennas at the interfering tier BS.

- Based on the average received power, the exact expression for the UL outage probability and UL average ergodic rate are derived to characterize the link reliability and the spectral efficiency. The results show that the overall outage probability and overall average ergodic rate may not necessarily be improved by increasing the density of picocell BS, the transmit power of BS in a specific tier, and the bias factor of picocell. It is surprising that the UL performance is not significantly improved by increasing the time allocation factor and improving the energy conversion efficiency.

- To examine the impact of massive antenna arrays at all BSs, the expression for the asymptotic averaged received power, asymptotic outage probability, and asymptotic average ergodic rate, as the number of antennas at BSs goes to infinity, are

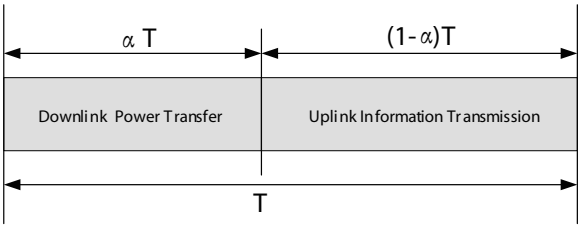

Figure 8.2: Frame Structure

derived. These asymptotic expressions are more easy to compute than the exact expressions. It is confirmed that the asymptotic and the exact results converge as the number of antennas grows large. An important observation is that the UL performance is significantly improved with the help of massive antenna arrays.

8.2 System Description

This Chapter considers the K-tier HCNs in which the BSs of each tier are spatially distributed in $\mathbb{R}^2$ according to K independent homogeneous PPPs, Φ_k, with density λ_k. Fig. 8.1 gives an example for the Two-tier HCNs topology. Each tier is assumed to have a different transmit power, $P_{t,k}$, a different path-loss exponent, η_k, and a different bias factor, B_k, for $k \in \{1, \cdots, K\}$ [33, 197, 198]. In addition, the MTs are assumed to be spatially distributed in $\mathbb{R}^2$ according to a homogeneous PPP, Φ_U with density λ_u. The density of the MTs is assumed to be much higher than that of the tiers of the BSs, such that saturated traffic conditions hold, i.e., all the BSs are active and serve one MT in the channel use of interest. The users in each cell of each tier transmit in orthogonal channel uses, similar to [199]. Furthermore, full-frequency reuse is assumed [33].

In any tier, each MT and each BS are assumed to be equipped with 1 and N antennas, respectively. Each MT is equipped with a rechargeable battery with large storage and is capable of converting the RF received power into a direct current (DC) voltage/current in order to recharge the available battery. An harvest-then-transmit communication protocol for wireless power transfer is considered [117]. More specifically, let T denote

the duration of a communication block, which comprises DL and UL transmissions (see Fig. 8.2). Without loss of generality, it is assumed that $T = 1$. Let $0 \leq \alpha \leq 1$. The first and second sub-blocks of duration αT and $(1-\alpha)\,T$ are allocated for DL and UL transmissions, respectively. In the DL, the typical MT harvests energy from all the active BSs of the K-tier heterogeneous cellular network. In the UL, the typical MT transmits information towards its serving BS. The fading channels in DL and UL transmissions are assumed to be quasi-static, i.e., they are fixed in the sub-blocks and independently change from one block to another.

8.2.1 Cell Association

Without loss of generality, using the Slivnyak-Mecke's theorem [200], it is assumed that the typical MT is located at the origin. The biased-received-power (BRP), $P_{r,k}$, from a BS at the location $\mathbf{x} \in \mathbb{R}^2$ can be formulated as follows:

$$P_{r,k} = P_{t,k} \left\|\mathbf{x}\right\|^{-\eta_k} B_k \tag{8.1}$$

where $\|\mathbf{x}\|$ denotes the BS-to-MT distance and B_k is the bias factor.

A cell association criterion based on DL maximum BRP is considered [197]. Accordingly, the selected serving BS x^* can be formulated as follows:

$$\begin{aligned} x^* &= \underset{x \in \left\{x_k^*\right\}}{\arg\max}\, P_{t,k} \left\|\mathbf{x}\right\|^{-\eta_k} B_k, \\ \text{with} \quad x_k^* &= \underset{x \in \Phi_k}{\arg\max}\, P_{t,k} \left\|\mathbf{x}\right\|^{-\eta_k}, \end{aligned} \tag{8.2}$$

where x_k^* for $k \in \{1, \ldots, K\}$ denotes the BS in kth tier that is closest to the MT, and Φ_k denotes the sets of BSs with various locations in kth tier.

It is worth mentioning that: i) if $B_k = 1$ for $k \in \{1, \ldots, K\}$, the MT is served by the BS providing the best received power and ii) if $B_k = 1/P_{t,k}$, the MT is served by the BS

providing the smallest path-loss [197].

To facilitate the analysis, the per-tier association probability of K-tier HCNs with BRP is derived in [197] as the following lemma.

Lemma 9. *The probability that the typical MT is associated with the BS in the kth tier is given by [197]*

$$W_k = 2\pi\lambda_k \int_0^\infty r \exp\Big\{-\sum_{j_0=1}^{K} \zeta_{k,j_0} r^{2\eta_k/\eta_{j_0}}\Big\} dr, \tag{8.3}$$

where

$$\zeta_{k,j} = \pi\lambda_j \rho_{j,k}{}^{2/\eta_j}, \quad \rho_{j,k} = P_{\mathrm{t},j} B_j / P_{\mathrm{t},k} B_k. \tag{8.4}$$

From [197, Eq.(4)], it is proved that the MT tends to associate with the BS in the tier with higher density of BSs, transmit power of BSs, and bias. More importantly, the BS density in kth tier dominates the probability that the typical MT is associated with the BS in the kth tier.

According to [197], the PDF of the distance $\left\|\mathbf{x}_{B_{k_{x^*}}}\right\|$ between the typical MT and its associated BS in the kth tier is presented in the following lemma.

Lemma 10. *The PDF of the distance between the typical MT and its associated BS in the kth tier is [197]*

$$f_{\left\|\boldsymbol{x}_{B_{k_{x^*}}}\right\|}(x) = \frac{x}{\Pi_k} \exp\Big\{-\sum_{j=1}^{K} \zeta_{k,j} x^{2\eta_k/\eta_j}\Big\}, \tag{8.5}$$

where

$$\Pi_k = \int_0^\infty r \exp\Big\{-\sum_{j_0=1}^{K} \zeta_{k,j_0} r^{2\eta_k/\eta_{j_0}}\Big\} dr, \tag{8.6}$$

where ζ_{k,j_0} is given in (8.4).

8.2.2 DL Power Transfer

In the DL power transfer phase, each N-antenna BS uses MRT BF for transmitting towards the intended MT located at the origin. This MT is denoted by u_0. Let the typical MT be served by a BS belongs to tier k.

For mathematical tractability, a short range propagation model is considered for the calculation of the received power at the intended MT to avoid the singularity caused by proximity between BSs and mobiles as [57, 201].

For a typical MT u_0 located at the origin that associated with its serving BS $S_{k_{x^*}}$ in the kth tier, its received power is presented as

$$P_{\mathrm{r}_{\mathrm{u}_0,\mathrm{k}}} = \underbrace{P_{\mathrm{t},S_{k_{x^*}}} \left\| \mathbf{h}_{S_{k_{x^*}}} \right\|^2 L_0 \Big(\max \Big\{ \left\| \mathbf{x}_{S_{k_{x^*}}} \right\|, d \Big\} \Big)^{-\eta_k}}_{I_{S_{k_{x^*}}}} + \underbrace{\sum_{j=1}^{K} \sum_{S_x \in \Phi_j \setminus S_{k_{x^*}}} P_{\mathrm{t},S_j} \left| \mathbf{h}_{S_x u_0} \frac{\mathbf{g}_{S_x u_j}^H}{\left\| \mathbf{g}_{S_x u_j} \right\|} \right|^2 L_0 (\max \{ \| \mathbf{x}_{S_x u_0} \|, d \})^{-\eta_j}}_{I_{S_x}}, \tag{8.7}$$

where $d \geq 1$ is a constant value, L_0 is the path loss for a reference distance $r_0 = 1$, which is typically $(4\pi/v)^{-2}$, and v is the wavelength. In (8.7), $\mathbf{h}_{S_{k_{x^*}}} \in \mathcal{C}^{1\times N}$ is the small-scale fading channel vector from the serving BS in the kth tier to the the typical MT , $\mathbf{h}_{S_x u_0} \in \mathcal{C}^{1\times N}$ is the small-scale fading interfering channel vector from the interfering BS at a location $\mathbf{x}$ to the typical MT, and $\frac{\mathbf{g}_{S_x u_j}^H}{\left\| \mathbf{g}_{S_x u_j} \right\|}$ is the MRT BF vector of interfering BS at a location $\mathbf{x}$, where $\mathbf{g}_{S_x u_j} \in \mathcal{C}^{1\times N}$ is the small-scale fading channel vector from the interfering BS at a location $\mathbf{x}$ to its associated MT. All the channels are assumed to experience Rayleigh fading such that $\left\| \mathbf{h}_{S_{k_{x^*}}} \right\|^2 \sim \mathrm{Gamma}\,(N, 1)$. According to [156], $\mathbf{h}_{S_x u_0} \frac{\mathbf{g}_{S_x u_j}^H}{\left\| \mathbf{g}_{S_x u_j} \right\|}$ is a zero-mean complex Gaussian variable, which is independent of $\mathbf{g}_{S_x u_j}^H$, such that $\left| \mathbf{h}_{S_x u_0} \frac{\mathbf{g}_{S_x u_j}^H}{\left\| \mathbf{g}_{S_x u_j} \right\|} \right|^2 \sim \exp(1)$.

8.2.3 UL Information Transmission

In the UL information transmission phase, the MTs keep associated with their serving BSs that powered them in the DL power transfer phase [1], and consume the stored energy to transmit the information signals to their corresponding BSs. Remind that it is assumed that the saturated traffic conditions holds, and each BS only serves one user per channel in each snap of time [199]. As such, the density of interfering users on each channel is $\lambda_u = \sum_{k=1}^{K} \lambda_k$.

The MTs are assumed to have large energy storage that enables reliable transmission power. As suggested by Lemma 2 in [57], for the MTs with large storage battery, the randomness of instantaneous received power is lost and the active MTs in the kth tier can transmit with fixed power up to $P_{\mathrm{t_u},k} = \phi \mathbb{E}\left\{P_{\mathrm{r_{u_0,k}}}\right\}$, where $\phi = \eta \frac{\alpha}{1-\alpha}$ [2]. Here, η is the the RF-to-DC conversion efficiency [203].

In the UL information transmission phase, each N-antenna BS employs MRC to combine the received signals. The SINR at the typical BS with MRC in the kth tier is given by

$$SINR_k = \frac{\phi \mathbb{E}\left\{P_{r_{\mathrm{u}_0},k}\right\} \left\| \mathbf{h}_{\mathrm{u}_0,S_{k_{x^*}}} \right\|^2 L_0 \left\| \mathbf{x}_{\mathrm{u}_0,S_{k_{x^*}}} \right\|^{-\eta_k}}{I_U + \delta^2}, \tag{8.8}$$

where $I_U = \sum_{j=1}^{K} I_{U,j}$, $I_{U,j} = \sum_{\mathrm{u}_{x,j} \in \tilde{\Phi}_j \setminus \mathrm{u}_0} \phi \mathbb{E}\{P_{r_{\mathrm{u}_j},j}\} \left| \frac{\mathbf{h}^H_{\mathrm{u}_0,S_{k_{x^*}}}}{\left\| \mathbf{h}^H_{\mathrm{u}_0,S_{k_{x^*}}} \right\|} \mathbf{h}_{\mathrm{u}_{x,j},S_{k_{x^*}}} \right|^2 L_0 \left\| \mathbf{x}_{\mathrm{u}_{x,j},S_{k_{x^*}}} \right\|^{-\eta_j}$, $\mathbf{h}_{\mathrm{u}_0,S_{k_{x^*}}} \in \mathcal{C}^{N\times 1}$ is the small-scale fading channel vector from the typical MT u_0 to its serving typical BS in the kth tier, $\mathbf{h}_{\mathrm{u}_{x,j},S_{k_{x^*}}} \in \mathcal{C}^{N\times 1}$ is the small-scale fading interfering channel vector from the interfering MT $\mathrm{u}_{x,j}$ in the jth tier to the typical BS in the kth tier, $\frac{\mathbf{h}^H_{\mathrm{u}_0,S_{k_{x^*}}}}{\left\| \mathbf{h}^H_{\mathrm{u}_0,S_{k_{x^*}}} \right\|}$ is the MRC vector of the typical BS in the kth tier, $\tilde{\Phi}_j$ is the point process representing the interfering MTs in the jth tier, and δ^2 is the noise power.

[1] In the current conventional cellular networks, the UL cell association is based on DL cell association criterion [202].

[2] The processing power for UL is ignored as [117].

8.3 System-Level Performance Evaluation of DL Power Transfer

In this section, it is assumed that the typical MT located at the origin, and associated with the kth tier BS. To determine the transmit power of the typical MT, the average received power at the typical MT in the kth tier is derived based on (8.7) in the following theorem.

8.3.1 Average Received Power

8.3.1.1 General Case

Theorem 20. *The average received power at the typical MT associated with kth tier BS using BRP cell association rule is given by*

$$\mathbb{E}\left\{P_{\mathrm{r_u},k}\right\} = \frac{P_{\mathrm{t},B_{k_{x^*}}} N_k L_0}{\Pi_k}\left(d^{-\eta_k}\Psi_1 + \Psi_2\right) + \frac{L_0}{\Pi_k}\sum_{j=1}^{K} 2\pi P_{\mathrm{t},j}\lambda_j\left(\Psi_3 + (\eta_j - 2)^{-1}\Psi_4\right), \tag{8.9}$$

where

$$\begin{aligned}
\Psi_1 &= \int_0^d x \exp\{-\sum_{j_1=1}^{K} \zeta_{k,j_1} x^{2\eta_k/\eta_{j_1}}\} dx \\
\Psi_2 &= \int_d^\infty x^{-(\eta_k-1)} \exp\{-\sum_{j_2=1}^{K} \zeta_{k,j_2} x^{2\eta_k/\eta_{j_2}}\} dx \\
\Psi_3 &= \int_0^\chi \frac{x}{2d^{\eta_j}}\left(\frac{\eta_j d^2}{(\eta_j-2)} - {\rho_{j,k}}^{2/\eta_j} x^{2\eta_j/\eta_k}\right) \exp\{-\sum_{j_3=1}^{K} \zeta_{k,j_3} x^{2\eta_k/\eta_{j_3}}\} dx \\
\Psi_4 &= \int_\chi^\infty \frac{x \exp\{-\sum_{j_4=1}^{K} \zeta_{k,j_4} x^{2\eta_k/\eta_{j_4}}\}}{\left({\rho_{j,k}}^{1/\eta_j} x^{\eta_j/\eta_k}\right)^{\eta_j-2}} dx, \\
\chi &= d^{\eta_k/\eta_j} {\rho_{j,k}}^{-\eta_k/{\eta_j}^2}.
\end{aligned} \tag{8.10}$$

Proof. See Appendix F.1. □

The results in Theorem 20 is in single integral, which can be easily computed using Matlab. In the following, the average received power of typical MT in HCNs with equal path loss exponent for each tier is presented in simple closed-form.

8.3.1.2 Special Case 1: Equal path loss exponent for all tiers

Corollary 7. With $\{\eta_k\} = \eta$, the average received power of typical MT associated with the kth tier is given by

$$\begin{aligned}
&\mathbb{E}\left\{P_{\mathrm{r_u},k}\right\} = \\
&P_{\mathrm{t},k}N_kL_0\Big[\Big(1-\exp\Big\{-d^2\varpi_k\Big\}\Big)d^{-\eta} + \left(\varpi_k\right)^{\frac{\eta}{4}}d^{-\frac{\eta}{2}}\exp\left\{-\frac{1}{2}d^2\varpi_k\right\}W_{-\frac{\eta}{4},\frac{1}{2}\left(1-\frac{\eta}{2}\right)}\left(d^2\varpi_k\right)\Big] \\
&\quad + \sum_{j=1}^{K}\pi P_{\mathrm{t},j}\lambda_jL_0\Big[\frac{\eta}{\eta-2}d^{(2-\eta)}\Big(1-\exp\Big\{-\varpi_kd^2{\rho_{j,k}}^{-2}\Big\}\Big) - \frac{{\rho_{j,k}}^{2/\eta}}{d^\eta\varpi_k}\Upsilon\left(2,\varpi_kd^2{\rho_{j,k}}^{-2/\eta}\right) \\
&\quad + 2(\eta-2)^{-1}{\rho_{j,k}}^{\frac{1}{\eta}-\frac{1}{2}}{\varpi_k}^{\frac{7}{2}-\frac{3\eta}{4}}d^{-\frac{\eta}{2}+1}\exp\{-\frac{d^2}{2}{\rho_{j,k}}^{-\frac{2}{\eta}}\varpi_k\}W_{-(\eta/2-1)/2,-\eta/4}\left(d^2{\rho_{j,k}}^{-2/\eta}\varpi_k\right)\Big],
\end{aligned} \tag{8.11}$$

where

$$\varpi_k = \sum_{j_1=1}^{K}\zeta_{k,j_1} = \sum_{j_1=1}^{K}\pi\lambda_{j_1}(P_{\mathrm{t},j_1}B_{j_1}/P_{\mathrm{t},k}B_k)^{2/\eta}, \tag{8.12}$$

and $W_{\lambda,\mu}\left(z\right)$ is Whittaker function.

Proof. See Appendix F.2. □

8.4 System-Level Performance Evaluation of UL Information Transmission

To focus on the impact of DL wireless power transfer, the power control is not considered in the UL transmission [199]. Two important performance metrics of UL transmission in HCNs are characterized: the outage probability and the average ergodic rate.

8.4.1 Outage Probability

With RF wireless power transfer in HCNs, the outage probability becomes a crucial metric, which reflects the energy efficiency of DL power transfer and transmission reliability of UL information delivering. Here, the outage occurs when the instantaneous UL SINR is less than the target SINR. Considering that the typical MT may associated with any tier but only one tier in HCNs, the outage probability is given by [34]

$$P_{out} = \sum_{k=1}^{K} W_k P_{out,k}, \tag{8.13}$$

where W_k is the association probability that the typical MT is associated with the kth tier given in (8.3), $P_{out,k}$ is the outage probability of a typical MT associated with kth tier.

For a target SINR γ_{th} and a typical MT at a distance $\left\|\mathbf{x}_{\mathrm{u}_0,B_{k_{x^*}}}\right\|$ from its associated BS, the kth tier outage probability is defined as

$$P_{out,k}(\gamma_{th}) = \mathbb{E}_{\left\|\mathbf{x}_{\mathrm{u}_0,S_{k_{x^*}}}\right\|}\left\{\Pr\left(SINR_k(\left\|\mathbf{x}_{\mathrm{u}_0,S_{k_{x^*}}}\right\|) \leq \gamma_{th}\right)\right\}. \tag{8.14}$$

8.4.1.1 General Case

Theorem 21. *The UL outage probability of a typical MT in the kth tier is derived as*

$$\begin{aligned}P_{out,k}\left(\gamma_{th}\right) =& 1-\frac{1}{\Pi_k}\int_0^{\infty} x\exp\Big\{-\sigma^2\tau_k\gamma_{th}x^{\eta_k}-\sum_{j=1}^{K}x^{\frac{2\eta_k}{\eta_j}}\left(\vartheta_{k,j}(\gamma_{th})^{\frac{2}{\eta_j}}+\zeta_{k,j}\right)\Big\}dx\\ &-\frac{1}{\Pi_k}\sum_{m=1}^{N-1}\frac{\phi^{-m}}{(-1)^m}\sum\frac{1}{\prod_{i=1}^{m}m_i!i!^{m_i}}\int_0^{\infty}x\exp\Big\{-\sigma^2\tau_k\gamma_{th}x^{\eta_k}-\sum_{j=1}^{K}x^{\frac{2\eta_k}{\eta_j}}\left(\vartheta_{k,j}(\gamma_{th})^{\frac{2}{\eta_j}}+\zeta_{k,j}\right)\Big\}\\ &\Big(-\sigma^2\tau_k\phi\gamma_{th}x^{\eta_k}-\sum_{j=1}^{K}\vartheta_{k,j}(\gamma_{th})^{\frac{2}{\eta_j}}\frac{2}{\eta_j}\phi x^{\frac{2\eta_k}{\eta_j}}\Big)^{m_1}\prod_{l=2}^{m}\Big(-\sum_{j=1}^{K}\vartheta_{k,j}(\gamma_{th})^{\frac{2}{\eta_j}}\prod_{i=0}^{l-1}(\frac{2}{\eta_j}-i)\phi^l x^{\frac{2\eta_k}{\eta_j}}\Big)^{m_l}dx,\end{aligned} \tag{8.15}$$

where

$$\vartheta_{k,j}=\pi\lambda_j\Big(\mathbb{E}\left\{P_{r_{\mathrm{u}_j},j}\right\}\Big/\mathbb{E}\left\{P_{r_{\mathrm{u}_0},k}\right\}\Big)^{\frac{2}{\eta_j}}\Gamma\big(1+\frac{2}{\eta_j}\big)\Gamma\big(1-\frac{2}{\eta_j}\big), \tag{8.16}$$

$$\tau_k=\Big(\phi\mathbb{E}\left\{P_{r_{\mathrm{u}_0},k}\right\}L_0\Big)^{-1}, \tag{8.17}$$

$\zeta_{k,j}$ *and* $\mathbb{E}\left\{P_{\mathrm{r_{u_0}},k}\right\}$ *are given in* (8.4) *and* (8.9).

Proof. See Appendix F.3. □

The expression for the outage probability in general case is single integral, which is easy to be evaluated.

In the UL transmission of HCNs, when the density of MTs is dense, the interference power from those interfering MTs in each tier may dominate the performance, and the thermal noise can be ignored. To gain more insights, the UL outage probability with no noise in a simple closed-form is presented in the following corollaries.

8.4.1.2 Special Case 1: No noise, equal path loss exponent for each tier

Corollary 8. When $\sigma^2 = 0$ and $\{\eta_k\} = \eta$, the outage probability of a typical MT associated with the kth tier is derived as

$$P_{out,k}(\gamma_{th}) = 1 - (1 + \varpi_k)^{-1} \sum_{j=1}^{K} \vartheta_{k,j}(\gamma_{th})^{\frac{2}{\eta}})^{-1} - \sum_{m=1}^{N-1} \frac{\phi^{-m}}{(-1)^m} \sum \frac{\varpi_k}{\prod_{i=1}^{m} m_i! i!^{m_i}} \prod_{l=1}^{m} \Big(- \sum_{j=1}^{K} \vartheta_{k,j}(\gamma_{th})^{\frac{2}{\eta}} \prod_{i=0}^{l-1} (\frac{2}{\eta_j} - i)\phi^l \Big)^{m_l} \Gamma(\sum_{l=1}^{m} m_l + 1) \Big(\varpi_k + \sum_{j=1}^{K} \vartheta_{k,j}(\gamma_{th})^{\frac{2}{\eta}} \Big)^{-\left(1+\sum_{l=1}^{m} m_l\right)}, \tag{8.18}$$

where ϖ_k and $\vartheta_{k,j}$ are given in (8.12) and (8.16).

Note that substituting $\{\eta_k\} = 4$ into (8.18), the outage probability of a typical MT associated with the kth tier in HCNs with the same path loss exponent $\{\eta_k\} = 4$ is obtained.

The outage probability of a typical MT associated with the kth tier in HCNs with no noise, equal path loss exponent, and single antenna BSs is presented in the following corollary.

8.4.1.3 Special Case 2: No noise, equal path loss exponent, single antenna

Corollary 9. When $\sigma^2 = 0$, $\{\eta_k\} = \eta$ and $N_k = 1$, the outage probability of a typical MT associated with the kth tier is derived as

$$P_{out,k}(\gamma_{th}) = \frac{1}{\frac{\varpi_k}{\sum_{j=1}^{K} \vartheta_{k,j}(\gamma_{th})^{\frac{2}{\eta}}} + 1}, \tag{8.19}$$

where

$$\frac{\varpi_k}{\sum_{j=1}^{K}\vartheta_{k,j}} = \sum_{j=1}^{K}\Big[\frac{(P_{\mathrm{t},j_1}B_{j_1}/P_{\mathrm{t},k}B_k)}{\left(\mathbb{E}\left\{P_{r_{\mathrm{u}_j},j}\right\}\Big/\mathbb{E}\left\{P_{r_{\mathrm{u}_0},k}\right\}\right)}\Big]^{2/\eta}(\Gamma(1+2/\eta)\Gamma(1-2/\eta))^{-1} \tag{8.20}$$

Remark 3. Here are some observations from (8.19):

- Intrinsically, the UL outage probability is determined by the density of BSs in each tier;
- It is revealed that the outage probability is independent of the RF-to-DC conversion efficiency, and the ratio between the time allocated to the DL power transfer and the UL informations transmission. This is because for no noise case ($\delta^2 = 0$), the term $\phi = \eta\frac{\alpha}{1-\alpha}$ in (8.8) is counteracted, and the UL SINR is independent of ϕ.
- More importantly, the path loss exponent and the ratio of BS transmit power between different tiers determine the DL outage probability.

Note that substituting $\{\eta_k\} = 4$ into (8.19), the outage probability of a typical MT associated with the kth tier in HCNs with the same path loss exponent $\{\eta_k\} = 4$ for each tier and single antenna BS is obtained.

8.4.2 Average Ergodic Rate

In K-tier HCNs, the average ergodic rate is an important performance indicator for spectral efficiency. Similar as the definition of the overall outage probability of HCNs in (8.13), the overall average ergodic rate of HCNs is given by [34]

$$R = \sum_{k=1}^{K} W_k R_k, \tag{8.21}$$

where W_k is given in (8.3), and R_k is the average ergodic rate of a typical MT associated with kth tier, which represents the average data rate of a random MT associated with

kth tier including single active user per cell.

For a typical randomly located MT at a distance $\left\|\mathbf{x}_{\mathrm{u}_0,B_{k_{x^*}}}\right\|$ from its associated BS, the average ergodic rate of a typical MT associated with kth tier is defined as

$$R_k = \mathbb{E}_{\left\|\mathbf{x}_{\mathrm{u}_0,S_{k_{x^*}}}\right\|}\left[\mathbb{E}_{SINR_k}\left[\ln\left(1+SINR_k\left(\left\|\mathbf{x}_{\mathrm{u}_0,S_{k_{x^*}}}\right\|\right)\right)\right]\right]. \tag{8.22}$$

8.4.2.1 General Case

The average ergodic rate of a typical MT associated with the kth tier is derived in the following theorem.

Theorem 22. *The average ergodic rate of a typical MT associated with the kth tier is derived as*

$$\begin{aligned}R_k = {} & \frac{1}{\Pi_k}\int_0^\infty\int_0^\infty \frac{r}{1+x}\exp\Big\{-\sigma^2\tau_k x r^{\eta_k} - \sum_{j=1}^{K}\left(\vartheta_{k,j}x^{\frac{2}{\eta_j}}+\zeta_{k,j}\right)r^{\frac{2\eta_k}{\eta_j}}\Big\}dxdr \\ & - \frac{1}{\Pi_k}\sum_{m=1}^{N-1}\frac{\phi^{-m}}{(-1)^m}\sum\frac{1}{\prod_{i=1}^{m} m_i!i!^{m_i}}\int_0^\infty\frac{r}{1+x}\exp\left\{-\sigma^2\tau_k x r^{\eta_k} - \sum_{j=1}^{K}\left(\vartheta_{k,j}x^{\frac{2}{\eta_j}}+\zeta_{k,j}\right)r^{\frac{2\eta_k}{\eta_j}}\right\} \\ & \left(-\sigma^2\tau_k\phi x r^{\eta_k} - \sum_{j=1}^{K}\vartheta_{k,j}\frac{2}{\eta_j}\phi x^{\frac{2}{\eta_j}}r^{\frac{2\eta_k}{\eta_j}}\right)^{m_1}\prod_{l=2}^{m}\left(-\sum_{j=1}^{K}\vartheta_{k,j}\prod_{i=0}^{l-1}\left(\frac{2}{\eta_j}-i\right)\phi^l x^{\frac{2}{\eta_j}}r^{\frac{2\eta_k}{\eta_j}}\right)^{m_l}dxdr\end{aligned} \tag{8.23}$$

where $\vartheta_{k,j}$, τ_k, $\zeta_{k,j}$ and $\mathbb{E}\{P_{\mathrm{u},k}\}$ are given in (8.16), (8.17), (8.4) *and* (8.9), *respectively.*

8.4.2.2 Special Case 1: No noise, equal path loss exponent

The average ergodic rate of a typical MT associated with the kth tier in HCNs with no noise and equal path loss exponent is presented in the following.

Corollary 10. When $\sigma^2 = 0$ and $\{\eta_k\} = \eta$, the average ergodic rate of a typical MT

associated with the kth tier is derived as

$$R_k = \int_0^\infty \varpi_k \Big[(1+x)\left(\varpi_k + \sum_{j=1}^{K} \vartheta_{k,j} x^{\frac{2}{\eta}}\right)\Big]^{-1} dx - \frac{1}{\Pi_k} \sum_{m=1}^{N-1} \frac{\phi^{-m}}{(-1)^m} \sum \frac{1}{\prod_{i=1}^{m} m_i! i!^{m_i}} \prod_{l=1}^{m} \Gamma\Big(\sum_{l=1}^{m} m_l + 1\Big)$$
$$\Big(-\sum_{j=1}^{K} \vartheta_{k,j} \prod_{i=0}^{l-1} \Big(\frac{2}{\eta} - i\Big) \phi^l x^{\frac{2}{\eta}}\Big)^{m_l} \int_0^\infty \varpi_k \Big[(1+x)\left(\varpi_k + \sum_{j=1}^{K} \vartheta_{k,j} x^{\frac{2}{\eta}}\right)^{\left(\sum_{l=1}^{m} m_l + 1\right)}\Big]^{-1} dx. \tag{8.24}$$

The result in the corollary is composed of single integration, and can be easily computed.

8.4.2.3 Special Case 2: No noise, equal path loss exponent, single antenna

The average ergodic rate of a typical MT associated with the kth tier in HCNs with no noise, equal path loss exponent, and single antenna at each BS is presented.

Corollary 11. When $\sigma^2 = 0$, $\{\eta_k\} = \eta$, and $N = 1$, the average ergodic rate of a typical MT associated with the kth tier is derived as

$$R_k = \int_0^\infty \Big[(1+x)\Big(1 + x^{\frac{2}{\eta}} \frac{\sum_{j=1}^{K} \vartheta_{k,j}}{\varpi_k}\Big)\Big]^{-1} dx. \tag{8.25}$$

8.4.2.4 Special Case 3: No noise, equal path loss exponent $\eta = 4$, single antenna

Corollary 12. When $\sigma^2 = 0$, $\{\eta_k\} = 4$, and $N = 1$, the average ergodic rate of a typical MT associated with the kth tier reduces to

$$R_k = \Big[\pi\Big(\frac{\sum_{j=1}^{K}\vartheta_{k,j}}{\varpi_k}\Big) - 2\log\Big(\frac{\sum_{j=1}^{K}\vartheta_{k,j}}{\varpi_k}\Big)\Big]\Big[1 + \Big(\frac{\sum_{j=1}^{K}\vartheta_{k,j}}{\varpi_k}\Big)^2\Big], \tag{8.26}$$

where

$$\frac{\sum_{j=1}^{K}\vartheta_{k,j}}{\varpi_k} = \sum_{j=1}^{K}\Big[\frac{(P_{\mathrm{t},j_1}B_{j_1}/P_{\mathrm{t},k}B_k)}{\big(\mathbb{E}\left\{P_{r_{\mathrm{u}_j},j}\right\}/\mathbb{E}\left\{P_{r_{\mathrm{u}_0},k}\right\}\big)}\Big]^{-2/\eta}\Gamma(1+2/\eta)\Gamma(1-2/\eta). \tag{8.27}$$

It is observed that (8.26) is in simple closed form. The average ergodic rate in (8.26) is independent of the RF-to-DC conversion efficiency, and the ratio between the time allocated to the DL power transfer and the UL information transmission.

8.5 Performance Evaluations: Asymptotic analysis

In this section, the asymptotic performance of K-tier HCNs in which each BS is equipped with large antenna array, is analyzed. The asymptotic DL average received power, UL outage probability and UL average ergodic rate of HCNs, when the number of antennas at each BS goes to infinity, is then examined. To perform the asymptotic analysis, it is assumed that all BSs in this network are equipped with same number of antennas $N_k = N$.

According to the law of large numbers, it is known that

$$\lim_{N\to\infty}\left\|\mathbf{h}_{\mathrm{u}_0,S_{k_{x^*}}}\right\|^2 = N. \tag{8.28}$$

8.5.1 Microwave Power Transfer

In the DL HCNs with sufficiently large number of antennas N at the BS, the received power at the typical MT associated with kth tier is rewrote using (8.28) as

$$P^{\infty}_{\mathrm{r_{u_0,k}}} = \underbrace{P_{\mathrm{t},S_{k_{x^*}}} N L_0 \Big(\max\Big\{\Big\|\mathbf{x}_{S_{k_{x^*}}}\Big\|, d\Big\}\Big)^{-\eta_k}}_{I^{\infty}_{S_{k_{x^*}}}}. \tag{8.29}$$

Theorem 23. *When N is sufficiently large, the average received power at the typical MT in the kth tier with BRP cell association rule is derived as*

$$\begin{aligned}\mathbb{E}\left\{P^{\infty}_{\mathrm{r_u},k}\right\} =& \frac{P_{\mathrm{t},S_{k_{x^*}}} N L_0}{\Pi_k}\Big[d^{-\eta_k}\int_0^d x \exp\Big\{-\sum_{j_1=1}^{K}\zeta_{k,j_1}x^{2\eta_k/\eta_{j_1}}\Big\}dx \\ &+ \int_d^{\infty} x^{-(\eta_k-1)}\exp\Big\{-\sum_{j_2=1}^{K}\zeta_{k,j_2}x^{2\eta_k/\eta_{j_2}}\Big\}dx\Big].\end{aligned} \tag{8.30}$$

It is seen that the average received power proportionally increases with N, i.e. $\mathbb{E}\left\{P^{\infty}_{\mathrm{r_u},k}\right\} \propto N$.

8.5.2 UL Information Transmission

When the number of antennas at each BS is sufficiently large, by using (8.28), the SINR of the UL transmission with MRC at the typical BS is given by

$$SINR^{\infty}_{k} = \frac{\phi\mathbb{E}\left\{P^{\infty}_{r_{\mathrm{u}_0},k}\right\} N L_0 \Big\|\mathbf{x}_{\mathrm{u}_0,S_{k_{x^*}}}\Big\|^{-\eta_k}}{I^{\infty}_{U}+\delta^2}, \tag{8.31}$$

where $I^{\infty}_{U} = \sum_{j=1}^{K} I^{\infty}_{U,j}$, and $I^{\infty}_{U,j} = \sum_{\mathrm{u}_{x,j}\in\tilde{\Phi}_j\setminus\mathrm{u}_0} \phi\mathbb{E}\{P^{\infty}_{r_{\mathrm{u}_j},j}\}\Big|\frac{\mathbf{h}^H_{\mathrm{u}_0,S_{k_{x^*}}}}{\Big\|\mathbf{h}^H_{\mathrm{u}_0,S_{k_{x^*}}}\Big\|}\mathbf{h}_{\mathrm{u}_{x,j},S_{k_{x^*}}}\Big|^2 L_0\Big\|\mathbf{x}_{\mathrm{u}_{x,j},S_{k_{x^*}}}\Big\|^{-\eta_j}$.
In (8.31), it is obtained that $SINR^{\infty}_{k} \propto \mathbb{E}\left\{P^{\infty}_{\mathrm{r_u},k}\right\} \propto N$.

8.5.2.1 Asymptotic Outage Probability

The asymptotic outage probability of a typical MT associated with the kth tier is presented in the following theorem.

Theorem 24. *As $N \to \infty$, the outage probability of a typical MT associated with the kth tier is derived as*

$$P_{out,k}^{\infty}(\gamma_{th}) = \frac{1}{2} + \frac{1}{\pi \Pi_k} \int_0^{\infty} \int_0^{\infty} \mathrm{Im}\Big[\exp\Big\{-jw\big(N_k r^{-\eta_k}(\tau_k \gamma_{th})^{-1} - \sigma^2\big)\Big\} \psi^*(w)\Big] \frac{1}{w} dw r \exp\Big\{-\sum_{j_0=1}^{K} \zeta_{k,j_0} r^{2\eta_k/\eta_{j_0}}\Big\} dr, \tag{8.32}$$

where $\psi^*(w)$ is the conjugate of the characteristic function, and

$$\psi(w) = \exp\Big\{-\sum_{j=1}^{K} \lambda_j \pi \big(\phi \mathbb{E}\left\{P_{r_{\mathrm{u}_j},j}\right\} L_0\big)^{\frac{2}{\eta_j}} \Gamma\big(1+\frac{2}{\eta_j}\big)\Gamma\big(1-\frac{2}{\eta_j}\big)(jw)^{\frac{2}{\eta_j}}\Big\}. \tag{8.33}$$

Proof. See Appendix F.4. □

Due to the conjugate of the characteristic function and double integrations in (8.32), the impact of system parameters on the UL performance can not be observed. However, it is a much simplified expression compared with (8.15) having different sets of summation that changes according to N.

8.5.2.2 Asymptotic Average Ergodic Rate

The asymptotic average ergodic rate of a typical MT associated with the kth tier when N is sufficiently large is then presented in the following theorem.

Theorem 25. *As $N \to \infty$, the average ergodic rate of a typical MT associated with the*

kth tier is derived as

$$R_k^{\infty} = \frac{1}{2} - \frac{1}{\pi \Pi_k} \int_0^{\infty} \int_0^{\infty} \int_0^{\infty} \mathrm{Im}\left[\exp\left\{-jw\left(N_k r^{-\eta_k} (\tau_k t)^{-1} - \sigma^2\right)\right\} \psi^*(w)\right] \exp\left\{-\sum_{j_0=1}^{K} \zeta_{k,j_0} r^{2\eta_k/\eta_{j_0}}\right\} \frac{r}{w(t+1)} dw dt dr, \tag{8.34}$$

where $\psi(w)$ *is given in* (8.33).

Even though the asymptotic average ergodic rate is composed of triple integrations, the results is in more simple form with faster computation time compared with exact average ergodic rate in (8.23).

8.6 Numerical results

In this section, the exact average received power, outage probability and average ergodic rate are plotted using (8.9), (8.15) and (8.23), respectively, and the asymptotic outage probability and the asymptotic average ergodic rate are plotted using (8.32) and (8.34), respectively. The correctness of those analytical results are validated by Monte Carlo methods as shown in each figure, where BSs and MTs are deployed as the given model. In all figures, it is assumed that the path loss at 1 meters of $L_0 = -38.5$ dB, and the thermal noise $\sigma^2 = -104$ dB for 10 MHz bandwidth. Even though the numerical results are given for two-tier HCNs model, it can be easily expanded to K-tier HCNs without loss of generality.

8.6.1 Impact of Number of BS Antennas and Picocell BS Density

In this subsection, the effect of the number of antennas at each BS and the density of BSs in picocell on the DL average received power, the UL outage probability, and the UL average ergodic rate of the proposed model is discussed. In Fig. 8.3(a), 8.3(b), and 8.3(c), it is assumed that $\alpha_1 = 2.8$, $\alpha_2 = 2.5$, $\lambda_1 = 10^{-3}$, $B_1 = B_2 = 1$, $P_{t,S_1} = 46$ dBm,

$P_{t,S_2} = 30$ dBm, $d = 1$, $\gamma_{th} = 10$ dB, $\eta = 0.5$, and $\alpha = 0.45$.

Fig. 8.3(a) plots the average received power at the typical MT versus the density of picocell BS λ_2 for various number of antennas at each BS. Following insights can be observed: 1) As expected, the average received power of the MT in macrocell and picocell increase with increasing λ_2, due to the more energy harvested from the DL power transfer with the number of BSs at the picocell increases. 2) For $N_1 = N_2 = 6$, the average received powers with and without interference from macrocell and picocell interfering BSs are compared. It is interesting to know that the energy harvested from the ambient interference is small compared with the energy harvested from the associated BS using MRT BF when λ_2 is not high enough. This reflects that the energy harvested from the direct BF source dominates the average received power. 3) It is seen that the average received power of the MT in macrocell is higher and increases faster than the counterpart of the MT in picocell. This can be explained by the fact that based on (8.5), the increasing of λ_2 decreases the distance $\left\|\mathbf{x}_{S_{k_{x^*}}}\right\|$ between the typical MT and the associated BS, and the transmit power of macrocell BS is much higher than the counterpart in picocell BS. 4) Furthermore, it is noticed that for $N_1 = 6$, increasing the number of antennas at the picocell BS N_2 has no influence on the average received power of the MT in macrocell; similarly, for $N_2 = 6$, increasing the number of antennas at macrocell BS N_1 has no influence on the average received power of MT in picocell. This is because changing the number of antennas at the interfering BS does not change the distribution of $\left|\mathbf{h}_{S_x u_0} \frac{\mathbf{g}_{S_x u_j}^H}{\left\|\mathbf{g}_{S_x u_j}\right\|}\right|^2$ in (8.7).

Fig. 8.3(b) and Fig. 8.3(c) plot the UL outage probability and the UL average ergodic rate versus the density of picocell BSs λ_2 for various number of antennas at each BS. Following are the observations: Firstly, it is observed that the UL outage probability and the UL average ergodic rate of the UL transmission with the typical BS in macrocell and picocell degrades with increasing λ_2, which is due to the increased interference from the other MTs in picocell. Second, It is shown that the overall outage probability and overall average ergodic rate can hardly be improved by increasing the number of BS in

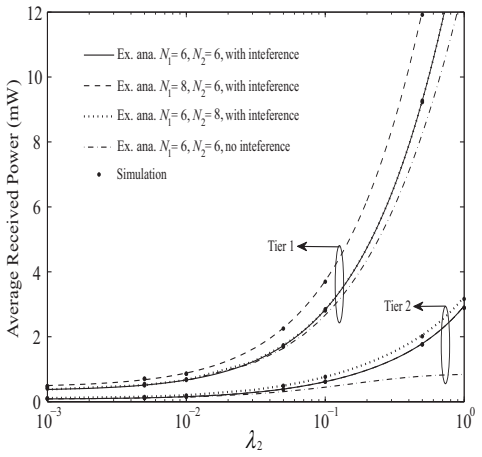

(a) Average Received Power.

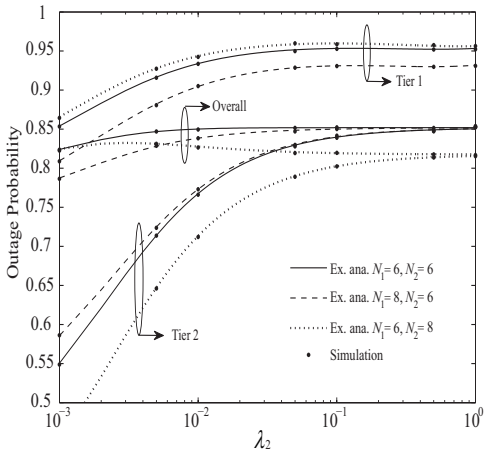

(b) Outage Probability.

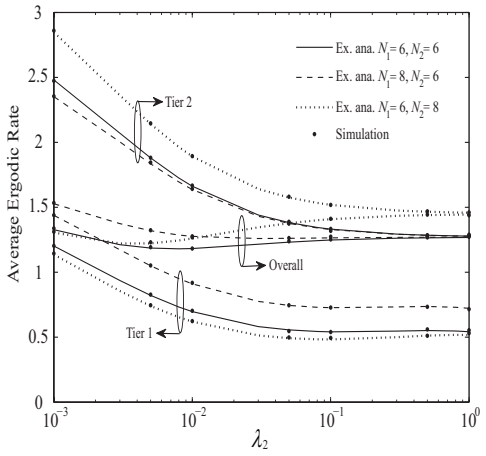

(c) Average Ergodic Rate.

Figure 8.3: Impact of Number of BS Antennas and Picocell BS Density

picocell.

Interestingly, it is further seen that the UL performance of the typical MT in a specific cell with $N_1 = 6, N_2 = 6$ outperforms the counterpart with $N_1 = 6, N_2 = 8$, and the UL performance of the typical MT in a specific cell with $N_1 = 8, N_2 = 6$ outperforms the counterpart with $N_1 = 6, N_2 = 6$, This can be explained by the following reason: In conventional HCNs without DL power transfer, increase the number of antennas at the BS will not influence the aggregate interference with fixed transmit power on the macrocell BS. In the HCNs with DL power transfer, increasing N_2

will only increase the average received power at the typical MT in picocell $\mathbb{E}\left\{P_{r_{\mathrm{u}_2},2}\right\}$. By rewriting the SINR at the typical macrocell MT in two-tier HCNs as $SINR_1 = \frac{\left\|\mathbf{h}_{\mathrm{u}_0,S_{k_{x^*}}}\right\|^2 L_0 \left\|\mathbf{x}_{\mathrm{u}_0,S_{k_{x^*}}}\right\|^{-\eta_k} B_k}{\sum_{\mathrm{u}_{x,1}\in\tilde{\Phi}_1\setminus\mathrm{u}_0} G_1 + \sum_{\mathrm{u}_{x,2}\in\tilde{\Phi}_2} \mathbb{E}\left\{P_{r_{\mathrm{u}_2},2}\right\}/\mathbb{E}\left\{P_{r_{\mathrm{u}_0},1}\right\} G_2}$, where $G_j = \left|\frac{\mathbf{h}^H_{\mathrm{u}_0,S_{k_{x^*}}}}{\left\|\mathbf{h}^H_{\mathrm{u}_0,S_{k_{x^*}}}\right\|}\mathbf{h}_{\mathrm{u}_{x,j},S_{k_{x^*}}}\right|^2 L_0$ $\left\|\mathbf{x}_{\mathrm{u}_{x,j},S_{k_{x^*}}}\right\|^{-\eta_j} B_j, \quad j \in [1,2]$. In this equation, increasing N_2 does not change the numerator, G_1, G_2, and $\mathbb{E}\left\{P_{r_{\mathrm{u}_0},1}\right\}$, but increases $\mathbb{E}\left\{P_{r_{\mathrm{u}_2},2}\right\}$, thus, the $SINR_1$ decreases and the outage probability and the average ergodic rate degrade. Similarly, increasing N_1 for the same N_2 does not change G_1, G_2, and $\mathbb{E}\left\{P_{r_{\mathrm{u}_2},2}\right\}$, but $\mathbb{E}\left\{P_{r_{\mathrm{u}_0},1}\right\}$ in numerator increases, thus the UL $SINR$ in macrocell increases, and the UL performance improves. This is an important observation as it means that increasing the number of antennas at BS in a specific tier does not always improve the performance.

8.6.2 Impact of BS Transmit Power

In this subsection, the effect of the transmit power at the BS on the DL average received power, the UL outage probability, and the UL average ergodic rate are examined. In Fig. 8.4(a), 8.4(b), and 8.4(c), it is assumed that $\alpha_1 = 2.8$, $\alpha_2 = 2.5$, $\lambda_1 = 10^{-3}$, $N_1 = N_2 = 6$, $B_1 = B_2 = 1$, $d = 1$, $\gamma_{th} = 10$ dB, $\eta = 0.5$, and $\alpha = 0.45$.

Fig. 8.4(a) plots the average received power at the typical MT versus the density of picocell BS λ_2 for various transmit power at the BS. Following insights can be observed: 1) The average received power can be improved by increasing the transmit power of BS in either tier, which can be shown in (8.7). 2) The average received power of typical MT in macrocell is higher and increases more sharply than the counterpart of typical MT in picocell, which is due to the dominant effect of energy harvested from the associated BS using energy BF.

Fig. 8.4(b) and Fig. 8.4(c) plot the UL outage probability and the UL average ergodic rate versus the density of picocell BSs λ_2 for various transmit power at the BS. Following are the observations: 1) Interestingly, for $P_{t,B_1} = 46$ dBm, it is shown that the UL performance in picocell with $P_{t,B_2} = 30$ dBm outperforms that with $P_{t,B_2} = 37$ dBm.

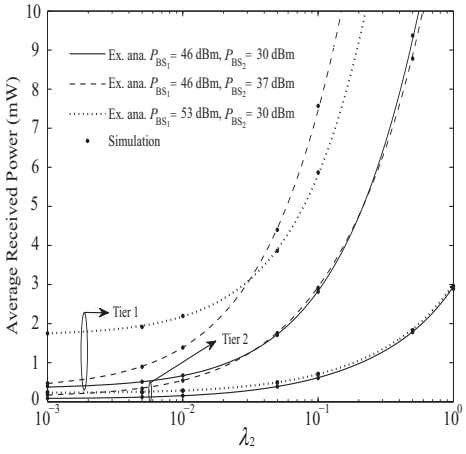

(a) Average Received Power.

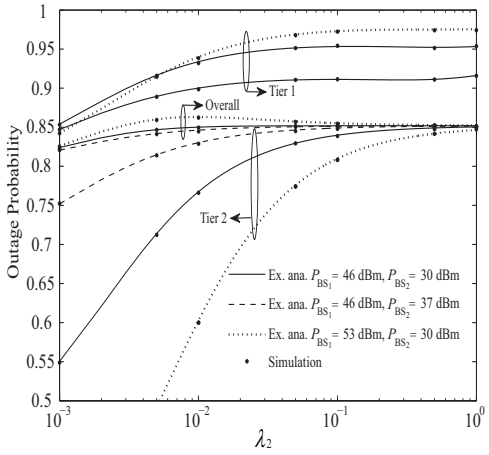

(b) Outage Probability.

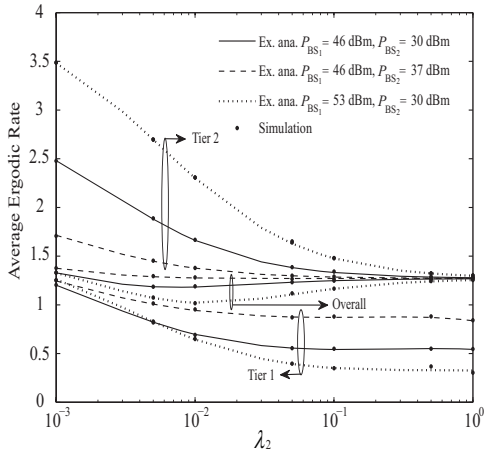

(c) Average Ergodic Rate.

Figure 8.4: Impact of BS Transmit Power

Based on (8.5), it is noticed that the distance between the typical MT and the associated typical BS in the picocell increases with increasing P_{t,B_2}, thus the SINR of picocell BS decreases, and the UL performance in picocell degrades. For $P_{t,B_2} = 30$ dBm, it is observed that the UL performance in picocell with $P_{t,B_1} = 53$ dBm outperforms that with $P_{t,B_1} = 46$ dBm. This can be explained by (8.5) that the distance between the typical MT and the associated typical BS in the picocell decreases with increasing P_{t,B_1}, thus the SINR of picocell BS increases, and the UL performance in picocell improves. Therefore, it is concluded that increasing the transmit power of picocell BS or macrocell

BS will not always improves the UL performance. 2) It is further concluded that the overall outage probability and overall average ergodic rate may not be improved by increasing the transmit power of marcocell BS and picocell BS.

8.6.3 Impact of Biasing and Path Loss Exponent

In this subsection, the effect of the bias factor and the path loss exponent on the DL average received power, the UL outage probability, and the UL average ergodic rate are examined. In Fig. 8.5(a), 8.5(b), and 8.5(c), it is assumed that $\lambda_1 = 10^{-1}$, $\lambda_2 = 2\times10^{-1}$, $P_{t,B_1} = 46$ dBm, $P_{t,B_2} = 30$ dBm, $N_1 = N_2 = 5$, $B_1 = 1$, $d = 1$, $\gamma_{th} = 10$ dB, $\eta = 0.3$, and $\alpha = 0.45$.

Fig. 8.5(a) plots the average received power at the typical MT versus the density of picocell BS B_2 for various path loss exponent. It is observed that the average received power of the typical MT in macrocell increases with increasing B_2. This is because with the biased association, more macrocell MTs with low SINR become associated with the picocell. In order to connect with macrocell BS, the distance between the typical MT and its associated macrocell BS becomes smaller, thus more power from nearby marcocell BSs are received at the typical marcocell MT. It is also seen that the average received power of picocell BS and macrocell BS increases with decreasing α_1 and α_2, which is due to the reduced path loss in both useful signal and interference.

Fig. 8.5(b) and Fig. 8.5(c) plot the UL outage probability and UL average ergodic rate at the typical MT versus the density of picocell BSs B_2 for various path loss exponent. On one hand, with the increase of the bias factor B_2, more macrocell MTs become associated with the picocell BSs, which results in higher aggregate interference on the picocell BS and degrades the UL performance in picocell. On the other hand, the typical MT associated with macrocell is able to transmit with higher power as increasing the bias factor, which improves the UL performance in macrocell. It is also seen that the overall UL performance can not be greatly improved by using biased association.

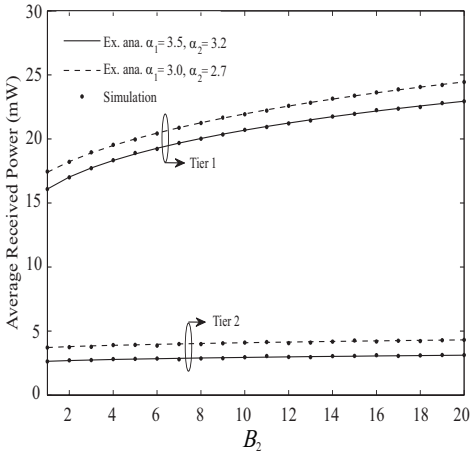

(a) Average Received Power.

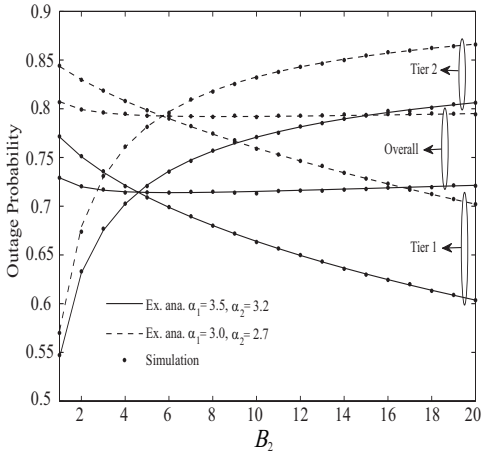

(b) Outage Probability.

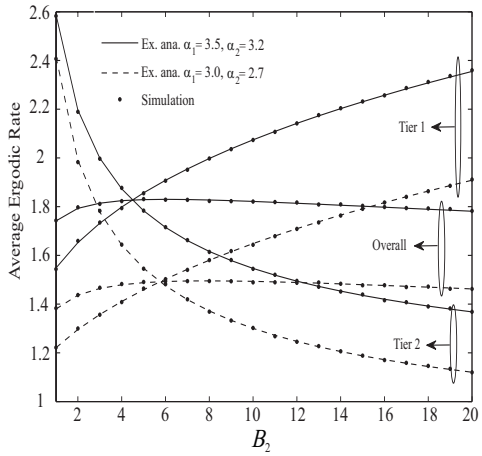

(c) Average Ergodic Rate.

Figure 8.5: Impact of Biasing and Path Loss Exponent

Furthermore, it is shown that the UL performance improves with increasing α_1 and α_2. This is because the aggregate interference, which has dominant negative effect on the SINR, decreases with increasing those path loss exponent.

8.6.4 Impact of Energy Conversion Efficiency and Time Allocation Factor

In this subsection, the effect of the energy conversion efficiency and the time allocation factor on the UL outage probability, and the UL average ergodic rate are examined. In Fig. 8.6(a) and 8.6(b), it is assumed that $\alpha_1 = 3.8$, $\alpha_2 = 3.5$, $\lambda_1 = 10^{-3}$, $\lambda_2 = 2 \times 10^{-3}$, $P_{t,S_1} = 46$ dBm, $P_{t,S_2} = 30$ dBm, $N_1 = N_2 = 5$, $B_1 = B_2 = 1$, $d = 1$, and $\gamma_{th} = 10$ dB.

Fig. 8.6(a) plots the outage probability versus the energy conversion efficiency η for various time allocation factor α. One phenomenon out of expectation is that the outage probability decreases with increasing η, and exists error floor in the high η region. This is because, when η is small, the noise in (8.8) is not negligible, and SINR in (8.8) increases with increasing η. However, when η is large, the aggregate interference overtakes the effect of noise, the SIR can be used instead of SINR to quantify the performance. In this case, SIR is not changed by increasing η. Remind that $\phi = \eta\frac{\alpha}{1-\alpha}$. Similarly, it is instinct to know that the outage probability decreases with increasing $\frac{\alpha}{1-\alpha}$, and exists error floor. As we know $0.8/0.2 > 0.45/0.55 > 0.2/0.8$, the outage probability with $\alpha = 0.8$ outperforms that with $\alpha = 0.45$, and it also outperforms that with $\alpha = 0.2$. Therefore, it is now concluded that the outage probability exists error floor when increasing the energy conversion efficiency.

Fig. 8.6(b) plots the average ergodic rate versus the time allocation factor α for various the energy conversion efficiency η. It is observed that the average ergodic rate first increases with increasing α, then saturates to the rate ceiling. It is also seen that the average ergodic rate increases with increasing η. These observations can be similarly explained as Fig. 8.6(a).

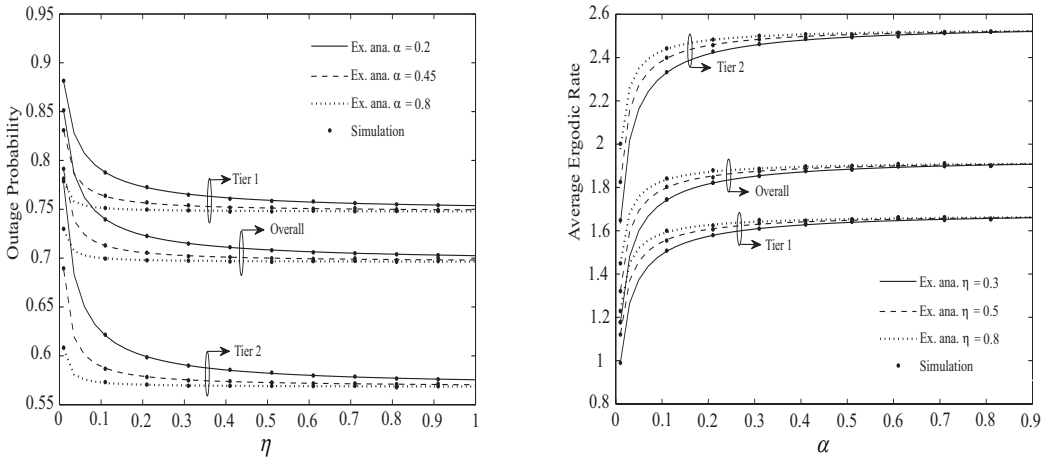

(a) Outage Probability.

(b) Average Ergodic Rate.

Figure 8.6: Impact of Energy Conversion Efficiency and Time Allocation Factor

8.6.5 Impact of BS Large Antenna Array

In this subsection, the effect of the BS large antenna array on the UL outage probability and the UL average ergodic rate is examined. In Fig. 8.7(a) and 8.7(b), it is assumed that $N_1 = N_2$, $\alpha_1 = 3.8$, $\alpha_2 = 3.5$, $\lambda_1 = 10^{-3}$, $\lambda_2 = 2 \times 10^{-3}$, $P_{t,S_1} = 46$ dBm, $P_{t,S_2} = 30$ dBm, $B_1 = B_2 = 1$, $d = 1$, $\gamma_{th} = 10$ dB, $\eta = 0.3$, and $\alpha = 0.45$.

Fig. 8.7(a) and 8.7(b) plot the outage probability and the average ergodic rate versus the number of BS antennas N. It is seen that the asymptotic outage probability and asymptotic ergodic rate converge to the exact outage probability and the exact ergodic rate in high N regime. It is also seen that for sufficient large N, the UL performance improves with increasing the number of antennas at each BS, which can be seen from (8.31) that $SINR_k^{\infty} \propto N$. This also suggests that the UL performance can be greatly improved by using massive arrays at each BS.

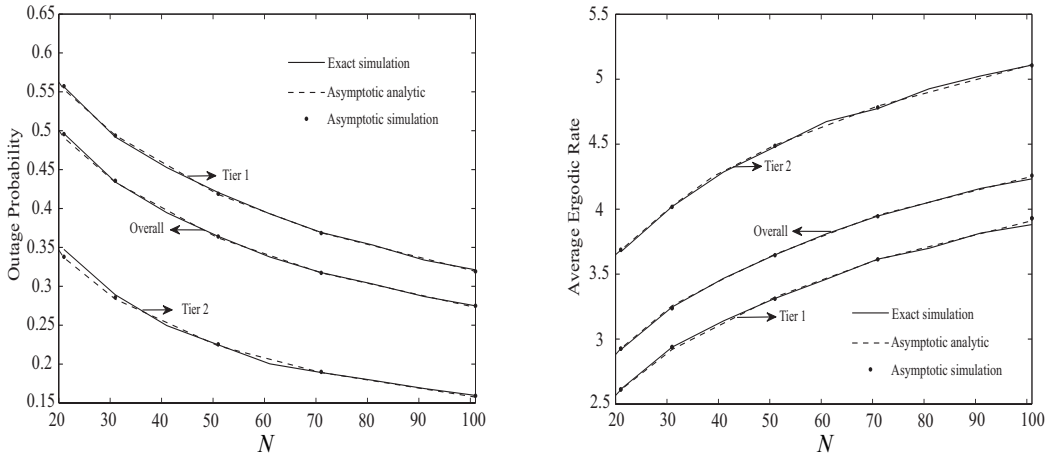

(a) Outage Probability.

(b) Average Ergidic Rate.

Figure 8.7: Impact of BS Large Antenna Array

8.7 Summary

A tractable model for the DL wireless power transfer along with UL information transmission in HCNs is provided. The mathematical expressions for the exact average received power, UL outage probability and UL average ergodic rate, as well as the asymptotic expressions for those important metrics when the number of antennas at BS goes to infinity, are presented. The intrinsic relationship between the energy harvested from BSs in the DL and the MT performance in the UL is well demonstrated in the derived results and the simulation results. It is shown that although the average received power at the MT can be improved by adding more picocell BS, the overall outage probability and overall average ergodic rate is not significantly improved. More importantly, the UL performance can not be significantly improved by increasing the time allocation factor and improving the energy conversion efficiency.

Chapter 9

Conclusions and Future Works

In this chapter, the main contributions of this thesis are summarized, some future research directions are also presented.

9.1 Summary of Contributions and Insights

To cope with the skyrocketing growth of band-hungry devices and meet with the 5G data challenge, this thesis focuses on the system design and performance improvement of spectral-efficient wireless networks, the so called spectrum sharing networks and HCNs. Different aspects of system enhancement design are considered in each chapter. Chapters 3, 4 and 5 aim at improving the link reliability of spectrum sharing networks using the performance indicator: outage probability, SER, and ergodic capacity; Chapter 6 focuses on the security enhancement of large-scale spectrum sharing networks by examining the average secrecy rate and secrecy outage probability; Chapters 7 and 8 concentrate on the energy efficiency improvement of spectrum sharing networks and HCNs, respectively.

First, GSC was proposed as a low power design at the SU-Rx for the performance enhancement of spectrum sharing networks with outdated CSI between the SU-Tx and PU-Rxs. Suffered from the interference from multiple PU-Txs, the secondary network subjects to the maximum transmit power constraint and the peak interference power constraint. The derived exact and asymptotic outage probability showcased the interfer-

ence reduction, reliability enhancement and diversity gain brought by GSC. The results demonstrated that the number of PU-TXs imposes a negative impact on the outage probability, while the number of selected number of antennas at SU-Rx has a positive impact on the outage probability. It is also confirmed that the outage probability can be improved by obtaining more accurate CSI of the interference channel.

Second, TAS/GSC was introduced in cognitive relay networks for the performance enhancement and achieving diversity gain. To concentrate on the impact of TAS/GSC on the cognitive relay networks under proportional and fixed interference power constraint, the interference from the PU-Tx was ignored. The exact and asymptotic outage probability and SER were derived for the proposed networks over Rayleigh fading channel and Nakagami-m fading channel. The closed-form expression for the ergodic capacity over Nakagami-m fading was derived for the first time. The important conclusion is that the diversity order is determined by the fading parameters and the antenna configuration of the secondary network, and the high SNR slope is 1/2 for the proportional interference power constraint scenario.

Third, BF&AN was proposed to enhance the secure secondary transmission in large-scale spectrum sharing networks under the potential malicious eavesdropping. The locations of PU-Txs, SU-Txs, and Eves follow homogeneous PPPs with different densities. The exact and asymptotic maximum permissive transmit power, average secrecy rate wall, and secrecy outage probability of secondary network, when the number of antennas at the SU-Txs goes to infinity, were studied. The optimal power allocation strategy that achieves the maximum average secrecy rate was also investigated. It is proved that the equal power allocation may not guarantee near optimal average secrecy rate. One interesting conclusion is that the advantage of BF&AN over BF demonstrated by the average secrecy rate may lost in some parameter settings.

Fourth, a new wireless energy harvesting protocol was proposed to power the energy-constrained SU-Txs in cognitive relay networks with multiple PU transceivers. The energy harvested from the PU interference signals determines the maximum transmit

power of SU-Txs. The exact and asymptotic outage probability, delay-sensitive throughput, and delay-tolerant throughput, when the number of PU transceivers goes to infinity, were studied to showcase the interplay between the energy harvested from the PU-Tx and the interference imposed by the PU-Txs. One interesting conclusion is that there exists an optimal number of PU transceivers that achieves the lowest outage probability and highest throughput. As the number of PU transceivers further increases, the harmful impact of the interference imposed on the secondary network from PU-Txs counterbalances the benefits gained from the energy harvested from PU-Txs.

Fifth, a harvest-then-transmit protocol was proposed in K-tier HCNs, where all the multiple-antennas BSs with constant power supply provide RF energy for the single-antenna MTs with no internal energy sources, then the MTs utilize the harvested energy to deliver the information to the BSs. A tractable model using stochastic geometry was built to analyze the DL wireless power transfer and UL information transmission of HCNs. The average received power of MTs, the UL outage probability and the UL average ergodic rate were derived to demonstrate the intrinsic relationship between the energy harvested from BS in the DL and the MT performance in the UL. It is concluded that the overall UL outage probability and UL average ergodic rate are not significantly improved by adding more picocell BSs, increasing the time allocation factor or improving the energy conversion efficiency.

9.2 Future Research

In this section, the potential extensions of this thesis are investigated in the following.

9.2.1 Imperfect CSI of Secondary Channel

Most of literature assume the perfect CSI of all channels in spectrum sharing networks, which might not be practical in reality. The work in Chapter 3 only considers the

outdated CSI of the interference channel between the SU-Tx and the PU-Rx. It would be interesting to look into the outdated CSI of secondary channel, and examine the impact of GSC on the secondary performance with imperfect CSI channel in the secondary channel. It would be even more interesting to look at some other transmit and receive diversity techniques, which improve the performance of spectrum sharing networks.

9.2.2 Cognitive Device to Device communication in Cellular Network

Recently, the underlay spectrum sharing has become popular for the D2D enhanced cellular networks. It is recognized that with D2D communications, new opportunities have been brought for proximity-based commercial services, especially social networking applications. One type of spectrum sharing between D2D and cellular users is the underlay mode where the D2D transmitters opportunistically access the time/frequency resources occupied by cellular users. An exciting area is to model and analyze the D2D-enabled cellular network using stochastic geometry. The works done in Chapter 6 and Chapter 8 laid some background on the stochastic geometry modeling of spectrum sharing networks and HCNs. Potential interference cancelation and wireless power transfer techniques for D2D and cellular users is also very interesting research topic.

9.2.3 Downlink and Uplink Transmission in HCNs with SWIPT

In the work done in Chapter 8 of this thesis, the DL information transmission of K-tier HCNs is not considered. A more realistic model might be to consider simultaneous power transfer and information transmission in the DL of HCNs, and the harvested energy at MT is utilized to power the uplink transmission. Power control of the UL information transmission determined by the BS sensitivity along with the harvested energy in the DL is even more realistic. Different from the work in Chapter 8, a battery-free communication where the user uses all the harvested energy in the first time slot of each frame to transmit the information signal to the serving BS and cannot store energy

for the future use, can be another direction to consider.

9.2.4 Massive MIMO in Cellular Networks

Another interesting topic is to extend the research topic to massive MIMO in multi-cell cellular network and HCNs. With massive MIMO at the BS, high spectral and energy efficiency can be achieved using relatively simple (linear) processing. Multiuser MIMO is even more interesting, in which multiple antenna BS simultaneously serves a set of single antenna MTs, as such, the multiplexing gain is shared by these MTs. The system design surrounding the transmit and receive scheme for multi-cell cellular network and HCNs, which can improve the link performance, reduce the interference from other cells and the negative effect brought by the pilot contamination problem, is my main focus in future research.

Appendix A

Proof of in Chapter 3

A.1 Proof of Theorem 1

According to (3.5), the CDF of $\tilde{\gamma}$ conditioned on V is written as

$$F_{\tilde{\gamma}|V}(\gamma) = \underbrace{\Pr\left\{\|\boldsymbol{G}\|^2 \leq \frac{\gamma V}{P_T}, \left|\hat{h}_{1m^*}\right|^2 < k_I \frac{Q}{P_T}\right\}}_{I_1(V)} + \underbrace{\Pr\left\{\frac{\|\boldsymbol{G}\|^2}{\left|\hat{h}_{1m^*}\right|^2} \leq \frac{\gamma V}{k_I Q}, \left|\hat{h}_{1m^*}\right|^2 \geq k_I \frac{Q}{P_T}\right\}}_{I_2(V)}. \tag{A.1.1}$$

By substituting (3.7) and (3.12) into (A.1.1), the first term $I_1(Z)$ is obtained as

$$I_1(V) = \sum_{S_k \in S_K} \alpha_k \left(\frac{\gamma V}{P_T}\right)^{\beta_k} e^{-\frac{\delta_k \gamma V}{\alpha_3 P_T}} \left(1 - e^{-\frac{k_I Q}{\alpha_1 P_T}}\right)^M. \tag{A.1.2}$$

Integrating (A.1.2) with respect to the PDF of V given by (3.13) results in

$$E_V\{I_1(V)\} = \left(1 - e^{-\frac{k_I Q}{\alpha_1 P_T}}\right)^M \left(\frac{1}{P_I \alpha_2}\right)^M \frac{1}{\Gamma(M)} \sum_{S_k \in S_K} \alpha_k \left(\frac{\gamma}{P_T}\right)^{\beta_k} \frac{\Gamma(\beta_k + M)}{\left(\frac{\delta_k \gamma}{P_T \alpha_3} + \frac{1}{P_I \alpha_2}\right)^{\beta_k + M}}. \tag{A.1.3}$$

Applying the same approach, $E_V\left\{I_2\left(V\right)\right\}$ can be derived with the help of [157, Eq. (8.352.2)], [157, Eq. (9.211.4.8)], and the polynomial expansion, which yields

$$\begin{aligned} E_V\left\{I_2\left(V\right)\right\} = & \sum_{m=1}^{M}\binom{M}{m}(-1)^{m+1}\sum_{S_k\in S_K}\alpha_k\left(\frac{\gamma}{k_I Q}\right)^{\beta_k}\beta_k! \\ & \left(\frac{1}{P_I\alpha_2}\right)^{M}\frac{\Gamma\left(\beta_k+M\right)}{\Gamma\left(M\right)}e^{-\frac{mk_IQ}{\hat{\alpha}_1 P_T}}\sum_{i=0}^{\beta_k}\frac{\left(\frac{k_IQ}{P_T}\right)^{i}}{i!}\left(\frac{\alpha_3 k_I Q}{\hat{\alpha}_1\delta_k\gamma}\right)^{\beta_k+M} \\ & \left(\frac{m}{\hat{\alpha}_1}\right)^{i+M}\Phi\left(\beta_k+M, M+i; \left(\frac{1}{P_I\alpha_2}+\frac{\delta_k\gamma}{\alpha_3 P_T}\right)\frac{\alpha_3 m k_I Q}{\hat{\alpha}_1\delta_k\gamma}\right). \end{aligned} \tag{A.1.4}$$

Substituting (A.1.3) and (A.1.4) into (A.1.1), the CDF of the SIR is finally derived as (3.14).

Appendix B

Proof in Chapter 4

B.1 Proof of Theorem 3

According to (4.4), the CDF of γ_1 is written as

$$\begin{aligned} F_{\gamma_1}(x) =& \Pr\left\{\frac{P_S\left\|\mathbf{g}_{1i^*\theta_{i^*}}\right\|^2}{N_0} \leq x\right\} \\ =& \Pr\left\{\left\|\mathbf{g}_{1i^*\theta_{i^*}}\right\|^2 \leq \frac{x}{\overline{\gamma}_P}, \left|h_{1i^*}\right|^2 \leq \frac{Q}{P}\right\} + \Pr\left\{\frac{\left\|\mathbf{g}_{1i^*\theta_{i^*}}\right\|^2}{\left|h_{1i^*}\right|^2} \leq \frac{x}{\overline{\gamma}_Q}, \left|h_{1i^*}\right|^2 \geq \frac{Q}{P}\right\} \\ =& I_1 + I_2. \end{aligned} \tag{A.2.1}$$

By substituting (4.6) and (4.11) into (A.2.1), the first term I_1 is obtained as

$$I_1 = F_{\left\|\mathbf{g}_{1i^*\theta_{i^*}}\right\|^2}\left(\frac{x}{\overline{\gamma}_P}\right) F_{\left|h_{1i^*}\right|^2}\left(\frac{Q}{P}\right) = \sum_{S_k \in S_K} \alpha_k \left(\frac{x}{\overline{\gamma}_P}\right)^{\beta_k} e^{-\frac{\delta_k}{\overline{\gamma}_P}x}\left(1 - e^{-\frac{Q}{P}}\right)^M. \tag{A.2.2}$$

The second term I_2 is written in terms of the CDF of $\left\|\mathbf{g}_{1i^*\theta_{i^*}}\right\|^2$ and the PDF of

$\left|h_{1i^*}\right|^2$ as

$$I_2 = \int_{\frac{Q}{P}}^{\infty} f_{\left|h_{1i^*}\right|^2}(y)\, F_{\left\|\mathbf{g}_{1i^*\theta_{i^*}}\right\|^2}\left(\frac{xy}{\overline{\gamma}_Q}\right) dy. \tag{A.2.3}$$

Based on (4.11), the PDF of $\left|h_{1i^*}\right|^2$ is derived as

$$f_{\left|h_{1i^*}\right|^2}(x) = \sum_{m=1}^{M} \binom{M}{m} (-1)^{m+1} m e^{-mx}. \tag{A.2.4}$$

By substituting (4.6) and (A.2.4) into (A.2.3), the integral in I_2 is solved using [161, eq. (3.351.2)]

$$\int_u^{\infty} x^n e^{-\mu x} dx = e^{-u\mu} \sum_{k=0}^{n} \frac{n!}{k!} \frac{u^k}{\mu^{n-k+1}} = \mu^{-n-1}\Gamma(n+1, \mu u) \tag{A.2.5}$$

and the second term I_2 is represented as

$$I_2 = \sum_{m=1}^{M} \binom{M}{m} (-1)^{m+1} m \sum_{S_k \in S_K} \alpha_k \left(\frac{x}{\bar{\gamma}_Q}\right)^{\beta_k} \left(m + \frac{\delta_k x}{\bar{\gamma}_Q}\right)^{-(\beta_k+1)} \Gamma\left(\beta_k + 1, \left(m + \frac{\delta_k x}{\bar{\gamma}_Q}\right)\frac{Q}{P}\right). \tag{A.2.6}$$

Substituting (A.2.2) and (A.2.6) into (A.2.1), the CDF of the SNR in the first hop is finally derived as (4.12).

Appendix C

Proofs in Chapter 5

C.1 Proof of Lemma 2

The PDF and CDF for the channel power gain of a single branch of the secondary network channel with the Nakagami-m fading is presented as [204]

$$f\left(x\right)=\frac{x^{m_{g1}-1}}{\left(m_{g1}-1\right)!}\left(\frac{m_{g1}}{\Omega_{g1}}\right)^{m_{g1}}e^{-\frac{m_{g1}}{\Omega_{g1}}x} \tag{C.1}$$

and

$$F\left(x\right)=1-\frac{\Gamma\left(m_{g1},x\frac{m_{g1}}{\Omega_{g1}}\right)}{\Gamma\left(m_{g1}\right)}, \tag{C.2}$$

respectively. The marginal moment generating function (MGF) of (C.1) is given by [45]

$$\Phi\left(s,x\right)=\left(\frac{m_{g1}}{\Omega_{g1}}\right)^{m_{g1}}\sum_{i=0}^{m_{g1}-1}\frac{x^{i}e^{-\left(s+\frac{m_{g1}}{\Omega_{g1}}\right)x}}{i!\left(s+\frac{m_{g1}}{\Omega_{g1}}\right)^{m_{g1}-i}}. \tag{C.3}$$

As shown in [45, 166], the MGF expression for the channel power gain with GSC is expressed as

$$\Phi_{GSC}(s) = L_R \binom{N_R}{L_R} \int_0^\infty e^{-sx} f(x) \left(\Phi(s,x)\right)^{L_R-1} \left(F(x)\right)^{N_R-L_R} dx. \tag{C.4}$$

Here the MGF is defined as $\Phi_\gamma(s) = E[e^{-\gamma s}]$.

Based on (C.3), and using the multinomial theorem [155], $\left(\Phi(s,x)\right)^{L_R-1}$ is rewrote as

$$\left(\Phi(s,x)\right)^{L_R-1} = \left(\frac{m_g}{\Omega_g}\right)^{m_g\left(L_R-1\right)} \sum_{\mathcal{S}_K^\Phi} a_k^\Phi x^{b_k^\Phi} e^{-c_k^\Phi x} \left(s + \frac{m_{g1}}{\Omega_{g1}}\right)^{b_k^\Phi - m_{g1}\left(L_R-1\right)}, \tag{C.5}$$

where $\mathcal{S}_K^\Phi = \left\{ \left(n_{k,0}^\Phi, \ldots, n_{k,m_{g1}-1}^\Phi\right) \middle| \sum_{i=0}^{m_{g1}-1} n_{k,i}^\Phi = L_R - 1 \right\}$ with $\left\{n_{k,i}^\Phi\right\} \in \mathbb{Z}^+$, a_k^Φ, b_k^Φ, and c_k^Φ are, respectively, given by

$$a_k^\Phi = \frac{(L_R-1)!}{\prod_{i=0}^{m_{g1}-1} n_{k,i}^\Phi!} \prod_{i=0}^{m_{g1}-1} \left(\frac{1}{i!}\right)^{n_{k,i}^\Phi}, b_k^\Phi = \sum_{i=0}^{m_{g1}-1} n_{k,i}^\Phi i, \tag{C.6}$$

$$\text{and} \quad c_k^\Phi = (L_R-1)\left(s + \frac{m_{g1}}{\Omega_{g1}}\right). \tag{C.7}$$

Based on (C.2), the multinomial theorem is employed to express $\left(F(x)\right)^{N_R-L_R}$ as

$$\left(F(x)\right)^{N_R-L_R} = \sum_{\mathcal{S}_K^F} a_k^F x^{b_k^F} e^{-c_k^F x}, \tag{C.8}$$

where $\mathcal{S}_K^F = \left\{ \left(n_{k,0}^F, \ldots, n_{k,m_{g1}}^F\right) \middle| \sum_{j=0}^{m_g} n_{k,j}^F = N_R - L_R \right\}$ with $\left\{n_{k,j}^F\right\} \in \mathbb{Z}^+$, a_k^F, b_k^F, and

c_k^F are, respectively, given by

$$a_k^F = \frac{\big(N_R - L_R\big)!}{\prod\limits_{j=0}^{m_{g1}} n_{k,j}^F!} \prod_{j=0}^{m_{g1}-1} \big(\frac{-1}{j!}\big)^{n_{k,j+1}^F} \big(\frac{m_{g1}}{\Omega_{g1}}\big)^{b_k^F}, \tag{C.9}$$

$$b_k^F = \sum_{j=0}^{m_{g1}-1} j n_{k,j+1}^F, \text{and} \quad c_k^F = \frac{m_{g1}}{\Omega_{g1}} \sum_{j=1}^{m_{g1}} n_{k,j}^F. \tag{C.10}$$

Substituting (C.1), (C.5) and (C.8) into (C.4), and applying [172, eq. (3.351.3)], $\Phi_{GSC}(s)$ is derived as

$$\begin{aligned}\Phi_{GSC}(s) =& \frac{L_R}{\big(m_{g1}-1\big)!}\binom{N_R}{L_R}\big(\frac{m_{g1}}{\Omega_{g1}}\big)^{m_{g1}L_R} \sum_{S_k^\Phi \in \mathcal{S}_K^\Phi} \sum_{S_k^F \in \mathcal{S}_K^F} a_k^\Phi a_k^F \\ & \frac{\big(b_k^\Phi + b_k^F + m_{g1} - 1\big)!\big(s + \frac{m_{g1}}{\Omega_{g1}}\big)^{b_k^\Phi - m_{g1}\left(L_R - 1\right)}}{\big(s + c_k^\Phi + c_k^F + \frac{m_{g1}}{\Omega_{g1}}\big)^{b_k^\Phi + b_k^F + m_{g1}}}.\end{aligned} \tag{C.11}$$

Let $F_{GSC}(x)$ denote the CDF of the channel power gain of the secondary network with GSC. The Laplace transform of $F_{GSC}(x)$ is given by $\mathcal{L}\left[F_{GSC}(x)\right] = \Phi_{GSC}(s)/s$ [46]. Therefore, the Laplace transform for $F_{GSC}(x)$ is

$$\begin{aligned}\mathcal{L}\left[F_{GSC}(x)\right] =& \frac{L_R}{\big(m_{g1}-1\big)!}\binom{N_R}{L_R}\big(\frac{m_{g1}}{\Omega_{g1}}\big)^{m_{g1}L_R} \sum_{\mathcal{S}_K^\Phi} \sum_{\mathcal{S}_K^F} a_k^\Phi a_k^F \frac{\big(b_k^\Phi + b_k^F + m_{g1} - 1\big)!}{\big(L_R\big)^{b_k^\Phi + b_k^F + m_{g1}}} \\ & \frac{\big(s + \frac{m_{g1}}{\Omega_{g1}}\big)^{b_k^\Phi - m_{g1}\left(L_R - 1\right)}}{s\big(s + \frac{c_k^F}{L_R} + \frac{m_{g1}}{\Omega_{g1}}\big)^{b_k^\Phi + b_k^F + m_{g1}}}.\end{aligned} \tag{C.12}$$

Using the partial fraction expansion [172, eq. (2.102)], (C.12) is rewrote in an equivalent form. Then, taking the inverse Laplace transform of $\mathcal{L}\left[F_{GSC}(x)\right]$ to obtain

$$F_{GSC}(x) = \frac{L_R}{\big(m_{g1}-1\big)!}\binom{N_R}{L_R} \sum_{\mathcal{S}_K} \sum_{n=0}^{m_{g1}L_R + b_k^F} a_k^\Phi a_k^F \frac{\big(b_k^\Phi + b_k^F + m_{g1} - 1\big)!}{{L_R}^{b_k^\Phi + b_k^F + m_{g1}}} \ell_k(n) x^{\mu_k(n)} e^{-\nu_k(n)x}, \tag{C.13}$$

where the set $\mathcal{S}_K$ has been defined in *Lemma 2*, $\ell_k(n)$, $\mu_k(n)$ and $\nu_k(n)$ are, respectively, given by

$$\ell_k(n) = \begin{cases} \left(\frac{m_{g1}}{\Omega_{g1}}\right)^{\mu_k(n)-b_k^F} \left(\frac{1}{L_R}\sum_{j=1}^{m_{g1}} n_{k,j}^F + 1\right)^{-n_2} \\ \qquad\qquad\qquad\qquad n = 0 \\ \left(\frac{m_{g1}}{\Omega_{g1}}\right)^{\mu_k(n)-b_k^F} \left(\Upsilon_{k1} + \Upsilon_{k2} - \frac{1-\mathrm{sgn}\left(c_k^F\right)}{(n-1)!}\right) \\ \qquad\qquad 1 \le n \le m_{g1}\left(L_R - 1\right) - b_k^\Phi \\ \left(\frac{m_{g1}}{\Omega_{g1}}\right)^{\mu_k(n)-b_k^F} \left(\Upsilon_{k3} + \Upsilon_{k4} - \frac{1-\mathrm{sgn}\left(c_k^F\right)}{\left(n-1\right)!}\right) \\ \qquad m_{g1}\left(L_R - 1\right) - b_k^\Phi < n \le m_{g1}L_R + b_k^F\ , \end{cases} \tag{C.14}$$

$$\mu_k(n) = \begin{cases} 0, & n = 0 \\ n-1, & 1 \le n \le m_{g1}\left(L_R - 1\right) - b_k^\Phi \\ n - \mathrm{sgn}\left(c_k^F\right)\left(m_{g1}\left(L_R - 1\right) - b_k^\Phi\right) - 1, & \\ \qquad m_{g1}\left(L_R - 1\right) - b_k^\Phi < n \le m_{g1}L_R + b_k^F\ , & \end{cases} \tag{C.15}$$

and

$$\nu_k(n) = \begin{cases} 0, & n = 0 \\ \frac{m_{g1}}{\Omega_{g1}}, & 1 \le n \le m_{g1}\left(L_R - 1\right) - b_k^\Phi \\ \frac{c_k^F}{L_R} + \frac{m_{g1}}{\Omega_{g1}}, & m_{g1}\left(L_R - 1\right) - b_k^\Phi < n \le m_{g1}L_R + b_k^F, \end{cases} \tag{C.16}$$

with $n_2 = b_k^{\Phi} + b_k^F + m_{g1}$. In (C.14), Υ_{k1}, Υ_{k2}, Υ_{k3}, and Υ_{k4} are given by

$$\Upsilon_{k1} = -\frac{\operatorname{sgn}\left(c_k^F\right)}{\left(n-1\right)!}\left(\frac{1}{L_R}\sum_{j=1}^{m_{g1}} n_{k,j}^F + 1\right)^{-n_2}, \tag{C.17}$$

$$\Upsilon_{k2} = \left(-1\right)^{1-n_1}\frac{\operatorname{sgn}\left(c_k^F\right)}{\left(n-1\right)!}\sum_{l=1}^{n_2}\left(\frac{1}{L_R}\sum_{n=1}^{m_{g1}} n_{k,n}^F + 1\right)^{-(n_2-l+1)}\binom{l-n_1-1}{l-1}\left(\frac{1}{L_R}\sum_{n=1}^{m_{g1}} n_{k,n}^F\right)^{n_1-l}, \tag{C.18}$$

$$\Upsilon_{k3} = -\frac{\operatorname{sgn}\left(c_k^F\right)}{\left(n_1-1\right)!}\left(\frac{1}{L_R}\sum_{j=1}^{m_{g1}} n_{k,j}^F + 1\right)^{-(n_2-n_1+1)}, \tag{C.19}$$

and

$$\Upsilon_{k4} = \frac{\operatorname{sgn}\left(c_k^F\right)}{\left(n_1-1\right)!}\sum_{l=1}^{m_{g1}\left(L_R-1\right)-b_k^{\Phi}}\left(-1\right)^{l+1}\binom{n_2-n_1+l-1}{l-1}\left(\frac{1}{L_R}\sum_{j=1}^{m_{g1}} n_{k,j}^F\right)^{-(n_2-n_1+l)}, \tag{C.20}$$

where $n_1 = n - m_{g1}\left(L_R - 1\right) + b_k^{\Phi}$.

The CDF of $\left\|\mathbf{g}_{1i^*\theta_{i^*}}\right\|^2$ is given by $F_{\left\|\mathbf{g}_{1i^*\theta_{i^*}}\right\|^2}(x) = \left(F_{GSC}(x)\right)^{N_S}$. Based on (C.13), and employing the multinomial theorem, the CDF of $\left\|\mathbf{g}_{1i^*\theta_{i^*}}\right\|^2$ is derived as (5.6).

C.2 Proof of Lemma 3

According to (5.4), the CDF of γ_1 can be written as

$$F_{\gamma_1}(x) = \Pr\left\{\left\|\mathbf{g}_{1i^*\theta_{i^*}}\right\|^2 \le \frac{x}{\overline{\gamma}_P}, \left|h_{1i^*}\right|^2 \le \frac{Q}{P}\right\} + \Pr\left\{\frac{\left\|\mathbf{g}_{1i^*\theta_{i^*}}\right\|^2}{\left|h_{1i^*}\right|^2} \le \frac{x}{\overline{\gamma}_Q}, \left|h_{1i^*}\right|^2 \ge \frac{Q}{P}\right\}. \tag{C.2}$$

The CDF of $\left|h_{1i^*}\right|^2$ is expressed as

$$F_{\left|h_{1i^*}\right|}(x) = 1 - \frac{\Gamma\left(m_{h1}, x\frac{m_{h1}}{\Omega_{h1}}\right)}{\Gamma\left(m_{h1}\right)} \tag{C.3}$$

By substituting (C.3) and (5.6) into (C.2), the closed-form expression of $F_{\gamma_1}(x)$ is derived as (5.10).

C.3 Proof of Theorem 10

Based on (C.8), the high SNR regime with $\bar{\gamma}_P \to \infty$ is considered. Applying the Taylor series expansion truncated to the kth order given by $e^x = \sum_{j=0}^{k} \frac{x^j}{j!} + o\big(x^k\big)$ in (C.8), the asymptotic expression for (C.8) is written as

$$\big(F\big(x\big)\big)^{N_R-L_R} = \frac{\big(\frac{m_{g1}}{\Omega_{g1}}\big)^{m_{g1}\left(N_R-L_R\right)} x^{m_{g1}\left(N_R-L_R\right)}}{\big(m_{g1}!\big)^{N_R-L_R}}. \tag{C.3}$$

Substituting (C.1), (C.5) and (C.3) into (C.4) yields

$$\Phi_{GSC}\big(s\big)=\big(\frac{m_{g1}}{\Omega_{g1}}\big)^{m_{g1}N_R}\frac{\mathrm{K}\left(\mathcal{S}_K^{\Phi}, N_R, L_R, m_{g1}, a_k^{\Phi}, b_k^{\Phi}\right)}{\big(s+\frac{m_{g1}}{\Omega_{g1}}\big)^{m_{g1}N_R}}. \tag{C.4}$$

Note that $\mathcal{L}\left[F_{GSC}\left(x\right)\right] = \Phi_{GSC}\left(s\right)/s$ [46], which is derived as

$$L\big[F_{GSC}\big(x\big)\big] =\mathrm{K}\left(\mathcal{S}_K^{\Phi}, N_R, L_R, m_{g1}, a_k^{\Phi}, b_k^{\Phi}\right)\big(\frac{1}{s}-\sum_{r=1}^{m_{g1}N_R}\frac{\big(\frac{m_{g1}}{\Omega_{g1}}\big)^{r-1}}{\big(s+\frac{m_{g1}}{\Omega_{g1}}\big)^{r}}\big). \tag{C.5}$$

Taking the inverse Laplace transform of (C.5), $F_{GSC}\big(x\big)$ is obtained as

$$F_{GSC}\big(x\big) =\mathrm{K}\left(\mathcal{S}_K^{\Phi}, N_R, L_R, m_{g1}, a_k^{\Phi}, b_k^{\Phi}\right)\big(1-\sum_{r=1}^{m_{g1}N_R}\frac{\big(\frac{m_{g1}}{\Omega_{g1}}\big)^{r-1}}{\big(r-1\big)!}x^{r-1}e^{-\frac{m_{g1}}{\Omega_{g1}}x}\big). \tag{C.6}$$

Again, employing the Taylor series expansion truncated to the kth order given by $e^x = \sum_{j=0}^{k} \frac{x^j}{j!} + o\big(x^k\big)$ in (C.6), (C.6) can be rewritten as

$$F_{GSC}\big(x\big) =\big(\frac{m_{g1}x}{\Omega_{g1}}\big)^{m_{g1}N_R}\mathrm{K}\left(\mathcal{S}_K^{\Phi}, N_R, L_R, m_{g1}, a_k^{\Phi}, b_k^{\Phi}\right). \tag{C.7}$$

Based on (C.7), the asymptotic expression for the CDF of $\left\|\mathbf{g}_{1i^*\theta_{i^*}}\right\|^2$ is given by

$$F_{\left\|\mathbf{g}_{1i^*\theta_{i^*}}\right\|^2}(x) = \Big[\big(\frac{m_{g1}x}{\Omega_{g1}}\big)^{m_{g1}N_R} \mathrm{K}\left(\mathcal{S}_K^{\Phi}, N_R, L_R, m_{g1}, a_k^{\Phi}, b_k^{\Phi}\right)\Big]^{N_S}. \tag{C.8}$$

By substituting (C.8) into (C.2), the first non-zero order expansion of the CDF of γ_1 is attained and yields the asymptotic outage probability of cognitive relay network with the proportional interference power constraint as (5.14).

Appendix D

Proofs in Chapter 6

D.1 Proof of Lemma 4

Consider a homogeneous PPP Φ_s with density λ_s, the aggregate interference from the SU-Txs is given by $I_{s,z} = \sum_{i\in\Phi_s} W_{s_i,z}|X_{i,z}|^{-\alpha}$. The Laplace transform of $I_{s,z}$ is

$$\mathcal{L}_{I_{s,z}}(s) = \mathbb{E}\Big(\prod_{i\in\Phi_s} \mathbb{E}_{W_{s_i,z}}\left(\exp\left(-sW_{s_i,z}|X_{i,z}|^{-\alpha}\right)\right)\Big). \tag{D.1.1}$$

Applying the Generating functional of homogeneous PPP in [134] and the polar-coordinate system, $\mathcal{L}_{I_{s,z}}(s)$ is derived as

$$\begin{aligned}\mathcal{L}_{I_{s,z}}(s) &= \exp\left(-\int_0^\infty \left(1-\mathbb{E}_{W_{s_i,z}}\left[\exp\left(-sW_{s_i,z}r^{-\alpha}\right)\right]\right)\lambda_s 2\pi r dr\right)\\ &= \exp\left(-\lambda_s\pi\mathbb{E}\big[W_{s_i,z}^{\frac{2}{\alpha}}\big]\Gamma\big(1-\frac{2}{\alpha}\big)s^{\frac{2}{\alpha}}\right).\end{aligned} \tag{D.1.2}$$

Then the focus turns to derive the expectation of $W_{s_i,z}$. According to [156] and [101], $\left|\mathbf{h}_{0,z}\frac{\mathbf{h}_{i,s_i}^\dagger}{\left\|\mathbf{h}_{i,s_i}^\dagger\right\|}\right|^2 \sim Exp(1)$, and $\|\mathbf{h}_{i,z}\mathbf{G}_{i,s_i}\|^2 \sim Gamma(N_s-1,1)$. Thus, the PDF

distribution of $W_{s_i,z} = \sigma_s^2 \left| \mathbf{h}_{i,z} \frac{\mathbf{h}_{i,s_i}^{\dagger}}{\left\| \mathbf{h}_{i,s_i}^{\dagger} \right\|} \right|^2 + \sigma_n^2 \| \mathbf{h}_{i,z} \mathbf{G}_{i,s_i} \|^2$ is derived as

$$f_{W_{s_i,z}}(x) = \begin{cases} \left(1 - \frac{P_A}{(N_s-1)P_I}\right)^{1-N_s} \left(P_I e^{\frac{x}{P_I}}\right)^{-1} \left[1 - \sum_{k=0}^{N_s-2} \left(\frac{N_s-1}{P_A} - \frac{1}{P_I}\right)^k \frac{x^k}{k!} e^{-\left(\frac{N_s-1}{P_A} - \frac{1}{P_I}\right)x}\right] & \\ & \mu \neq \frac{1}{N_s} \\ \frac{x^{N_s-1} e^{-\frac{x}{P_I}}}{{P_I}^{N_s-1}(N_s-1)!} & \mu = \frac{1}{N_s}. \end{cases} \tag{D.1.3}$$

Taking the expectation of $W_{s_i,z}$ by using $\mathbb{E}\left[W_{s_i,z}^{\frac{2}{\alpha}}\right] = \int_0^\infty x^{\frac{2}{\alpha}} f_{W_{s_i,z}}(x)\, dx$, and substituting the derived expression of $\mathbb{E}\left[W_{s_i,z}^{\frac{2}{\alpha}}\right]$ into (D.1.2), the result is derived as (6.5).

D.2 Proof of Theorem 2

According to the SIR of the typical PU-Rx in (6.2), the sum interference at the typical PU-Rx is defined as $I_{Pri,AN} = I_{p,p_0} + P_p^{-1} I_{s,p_0}$, thus the CDF of $\gamma_{\mathtt{SIR}}^p$ is expressed as

$$\begin{aligned} F_{\gamma_{\mathtt{SIR}}^p}^{\{p\}}\left(\gamma_{th}^{\{p\}}\right) =& \mathbb{E}_{\Phi_p}\left\{\mathbb{E}_{\Phi_s}\left\{\Pr\left\{ |h_{p_0}|^2 \leq \gamma_{th}^{\{p\}} I_{Pri,AN} {r_p}^{\alpha} \middle|\ \Phi_s, \Phi_p \right\}\right\}\right\} \\ =& 1 - \mathbb{E}_{\Phi_p}\left\{\mathbb{E}_{\Phi_s}\left\{\int_0^\infty e^{-\tau \gamma_{th}^{\{p\}} {r_p}^{\alpha}} d \Pr\left(I_{Pri,AN} \leq \tau\right)\right\}\right\} = 1 - \mathcal{L}_{I_{Pri,AN}}\left(\gamma_{th}^{\{p\}} {r_p}^{\alpha}\right). \end{aligned} \tag{D.1.2}$$

By utilizing similar approach in the Appendix A of [205] and based on **Lemma 4**, the outage probability at the typical PU-Rx is derived as

$$P_{out}^{pri,AN}\left(\gamma_{th}^{\{p\}}\right) = \begin{cases} 1 - \exp\left(-\pi\left(\lambda_p \Gamma\left(1 + \frac{2}{\alpha}\right) + \lambda_s \left(\frac{P_s}{P_p}\right)^{\frac{2}{\alpha}} \Upsilon_1\right)\delta\right) & \mu \neq \frac{1}{N_s} \\ 1 - \exp\left(-\pi\left(\lambda_p \Gamma\left(1 + \frac{2}{\alpha}\right) + \lambda_s \left(\mu \frac{P_s}{P_p}\right)^{\frac{2}{\alpha}} \frac{\Gamma\left(N_s + \frac{2}{\alpha}\right)}{\Gamma(N_s)}\right)\delta\right) & \mu = \frac{1}{N_s}, \end{cases} \tag{D.1.3}$$

where $\delta = \Gamma\left(1 - \frac{2}{\alpha}\right)\left(\gamma_{th}^{\{p\}}\right)^{\frac{2}{\alpha}} {r_p}^2$. By inverting (D.1.3), the maximum permissive transmit power at the SU-Txs is derived as (6.8).

D.3 Proof of Lemma 5

The PDF and CDF of $\|\mathbf{h}_{0,s_0}\|^2$ are given by

$$f_{\|\mathbf{h}_{0,s_0}\|^2}(x) = \frac{x^{N_s-1}e^{-x}}{(\mathrm{N}_s-1)!}, \quad \text{and} \quad F_{\|\mathbf{h}_{0,s_0}\|^2}(x) = 1 - e^{-x}\Big(\sum_{m=0}^{N_s-1}\frac{x^m}{m!}\Big), \quad \text{respectively.} \tag{D.1.3}$$

Let us define $I_{Sec,AN} = P_p I_{p,s_0} + I_{s,s_0}$. Based on the SIR in (6.3), the CDF of $\gamma_{\mathtt{SIR}}^{s,AN}$ is represented as

$$\begin{aligned}
F_{\gamma_{\mathtt{SIR}}^{s,AN}}^{\{s\}}\big(\gamma_{th}^{\{s\}}\big) &= \mathbb{E}_{\Phi_p}\Big\{\mathbb{E}_{\Phi_s}\Big\{\Pr\Big\{\|\mathbf{h}_{0,s_0}\|^2 \le \gamma_{th}^{\{s\}} I_{Sec,AN} r_s^{\alpha}\sigma_s^{-2}|\Phi_s,\Phi_p\Big\}\Big\}\Big\} \\
&= 1 - \sum_{m=0}^{N_s-1}\mathbb{E}_{\Phi_p}\Big\{\mathbb{E}_{\Phi_s}\Big\{\int_0^{\infty} e^{-\tau\gamma_{th}^{\{s\}}r_s^{\alpha}\sigma_s^{-2}}\big(\tau\gamma_{th}^{\{s\}}r_s^{\alpha}\sigma_s^{-2}\big)^m d\Pr\big(I_{Sec,AN}\le\tau\big)\Big\}\Big\}\frac{1}{m!} \\
&\overset{(a)}{=} 1 - \mathbb{E}_{\Phi_p}\Big\{\mathbb{E}_{\Phi_s}\Big\{\int_0^{\infty} e^{-\tau\gamma_{th}^{\{s\}}r_s^{\alpha}\sigma_s^{-2}} d\Pr\big(I_{Sec,AN}\le\tau\big)\Big\}\Big\} \\
&\quad - \sum_{m=1}^{N_s-1}\frac{(r_s^{\alpha})^m}{m!(-1)^m}\mathbb{E}_{\Phi_p}\Big\{\mathbb{E}_{\Phi_s}\Big\{\int_0^{\infty}\frac{d^m\big(e^{-\tau\gamma_{th}^{\{s\}}x\sigma_s^{-2}}\big)}{dx^m}\Big|_{x=r_s^{\alpha}} d\Pr\big(I_{Sec,AN}\le\tau\big)\Big\}\Big\},
\end{aligned} \tag{D.1.4}$$

where (a) follows from the fact that $\frac{d^m(e^{-\tau\gamma_{th}^{\{s\}}x\sigma_s^{-2}})}{dx^m}\Big|_{x=r_s^{\alpha}} = (-\tau\gamma_{th}^{\{s\}}\sigma_s^{-2})^m e^{-\tau\gamma_{th}^{\{s\}}r_s^{\alpha}\sigma_s^{-2}}, m > 0$. After some manipulations, it is derived that

$$F_{\gamma_{\mathtt{SIR}}^{s,AN}}^{\{s\}}\big(\gamma_{th}^{\{s\}}\big) = 1 - \mathcal{L}_{I_{Sec,AN}}\big(\gamma_{th}^{\{s\}}r_s^{\alpha}\sigma_s^{-2}\big) - \sum_{m=1}^{N_s-1}\frac{\big(r_s^{\alpha}\big)^m}{m!\big(-1\big)^m}\frac{d^m\big\{\mathcal{L}_{I_{Sec,AN}}\big(\gamma_{th}^{\{s\}}x\sigma_s^{-2}\big)\big\}}{dx^m}\Big|_{x=r_s^{\alpha}}. \tag{D.1.5}$$

Utilizing [205, eq. (4)] and **Lemma 4**, it is derived that

$$\mathcal{L}_{I_{Sec,AN}}\big(\gamma_{th}^{\{s\}}r_s^{\alpha}\sigma_s^{-2}\big) = \exp\big(-\Lambda_l\big(\gamma_{th}^{\{s\}}\big)^{\frac{2}{\alpha}}r_s^2\big), \tag{D.1.6}$$

where Λ_l is given in (6.11). The the Faà di Bruno's formula is applied to solve the

derivative of mth order as follows:

$$\frac{d^m\left[\exp\left(-\Lambda_l\left(\gamma_{th}^{\{s\}}\right)^{\frac{2}{\alpha}}x^{\frac{2}{\alpha}}\right)\right]}{dx^m}\Big|_{x=r_s^\alpha}=\exp\left(-\Lambda_l\left(\gamma_{th}^{\{s\}}\right)^{\frac{2}{\alpha}}r_s^2\right)\sum m!\prod_{j=1}^{m}\frac{\left((-\Lambda_l(\gamma_{th}^{\{s\}})^{\frac{2}{\alpha}})\prod_{k=0}^{j-1}(\frac{2}{\alpha}-k)(r_s)^{2-j\alpha}\right)^{m_j}}{m_j!j!^{m_j}}. \quad \text{(D.1.7)}$$

By substituting (D.1.7) into (D.1.5), the closed-form expression for the CDF of SIR at the typical SU is derived as (6.10).

D.4 Proof of Lemma 6

Let us define $I_{Eve,AN}=P_pI_{p,e_k}+I_{s,e_k}+\sigma_n^2I_{s_0,e_k,an}$, the CDF of $\gamma_{\mathtt{SIR}}^e$ can be written as

$$F_{\gamma_{\mathtt{SIR}}^{e,AN}}^{\{e\}}\left(\gamma_{th}^{\{e\}}\right)=\mathbb{E}_{\Phi_e}\Big\{\mathbb{E}_{\Phi_p}\Big\{\mathbb{E}_{\Phi_s}\Big\{\prod_{e_k\in\Phi_e}\Pr\left\{\left|\mathbf{h}_{0,e}\frac{\mathbf{h}_{0,s_i}^\dagger}{\left\|\mathbf{h}_{0,s_i}^\dagger\right\|}\right|^2\leq\sigma_s^{-2}I_{Eve,AN}\gamma_{th}^{\{e\}}\left|X_{e_k}\right|^\alpha\Big|\Phi_s,\Phi_p,\Phi_e\right\}\Big\}\Big\}\Big\}. \quad \text{(D.1.4)}$$

According to [156], $\mathbf{h}_{0,e_k}\frac{\mathbf{h}_{0,s_i}^\dagger}{\left\|\mathbf{h}_{0,s_i}^\dagger\right\|}$ is a zero-mean complex Gaussian variable, which is independent of $\mathbf{h}_{0,s_i}^\dagger$, and $\left|\mathbf{h}_{0,e_k}\frac{\mathbf{h}_{0,s_i}^\dagger}{\left\|\mathbf{h}_{0,s_i}^\dagger\right\|}\right|^2$ follows the exponential distribution with unit mean. Thus, the CDF of $\gamma_{\mathtt{SIR}}^e$ can be represented as

$$F_{\gamma_{\mathtt{SIR}}^{e,AN}}^{\{e\}}\left(\gamma_{th}^{\{e\}}\right)=\mathbb{E}_{\Phi_e}\Big\{\prod_{e_k\in\Phi_e}\Big(1-\mathbb{E}_{\Phi_p}\Big\{\mathbb{E}_{\Phi_s}\Big\{\int_0^\infty e^{-\tau\sigma_s^{-2}\gamma_{th}^{\{e\}}}\left|X_{e_k}\right|^\alpha d\Pr\left(I_{Eve,AN}\leq\tau\right)\Big\}\Big\}\Big)\Big\}. \quad \text{(D.1.5)}$$

According to the proof of Lemma 3.1 in [206], (D.1.5) is expressed as

$$F^{\{e\}}_{\gamma^{e,AN}_{\mathtt{SIR}}}\big(\gamma_{th}\big) =\mathbb{E}_{\Phi_e}\Big\{\prod_{e_k\in\Phi_e}\Big(1-\mathcal{L}_{I_{Eve,AN}}\big(\sigma_s^{-2}\gamma^{\{e\}}_{th}|X_{e_k}|^{\alpha}\big)\Big)\Big\}. \tag{D.1.6}$$

By using the Generating functional of homogeneous PPP Φ_e [134], (D.1.6) is solved as

$$F^{\{e\}}_{\gamma^{e,AN}_{\mathtt{SIR}}}\left(\gamma_{th}\right) = \exp\Big[-2\pi\lambda_e\int_0^{\infty}\mathcal{L}_{I_{Eve,AN}}\big(\sigma_s^{-2}\gamma^{\{e\}}_{th}|X_{e_k}|^{\alpha}\big)\,|X_{e_k}|\,d\,|X_{e_k}|\Big]. \tag{D.1.7}$$

Now utilizing [205, eq. (4)] and **Lemma 4**, the Laplace transform of $I_{Eve,AN}$ is derived as

$$\mathcal{L}_{I_{Eve,AN}}\left(s\right) = \begin{cases} \exp\Big(-\pi\big(\lambda_p\Gamma\big(1+\frac{2}{\alpha}\big)\eta^{-\frac{2}{\alpha}}\mu^{-\frac{2}{\alpha}}+\lambda_s\frac{\Gamma\left(N_s+\frac{2}{\alpha}\right)}{\Gamma\left(N_s\right)}\big) \\ \quad\Gamma\big(1-\frac{2}{\alpha}\big)\big(\gamma^{\{e\}}_{th}\big)^{\frac{2}{\alpha}}\big|X_{e_k}\big|^2\Big)\big(\frac{1-\mu}{\left(N_s-1\right)\mu}\gamma^{\{e\}}_{th}+1\big)^{-(N_s-1)} & \mu=\frac{1}{N_s}, \\ \exp\Big(-\pi\big(\lambda_p\Gamma\left(1+\frac{2}{\alpha}\right)\eta^{-\frac{2}{\alpha}}+\lambda_s\Upsilon_1\big)\Gamma\left(1-\frac{2}{\alpha}\right) \\ \quad\big(\gamma^{\{e\}}_{th}\big)^{\frac{2}{\alpha}}\mu^{-\frac{2}{\alpha}}|X_{e_k}|^2\Big)\big(\frac{1-\mu}{(N_s-1)\mu}\gamma^{\{e\}}_{th}+1\big)^{-(N_s-1)} & \mu\neq\frac{1}{N_s}. \end{cases} \tag{D.1.8}$$

By substituting (D.1.8) into (D.1.7), it is obtained that

$$F^{\{e\}}_{\gamma^{e}_{\mathtt{SIR}}}\big(\gamma^{\{e\}}_{th}\big) = \exp\Big[-2\pi\lambda_e\Big(\frac{1-\mu}{\left(N_s-1\right)\mu}\gamma^{\{e\}}_{th}+1\Big)^{-(N_s-1)}\int_0^{\infty}\exp\left(-\Lambda_l\big(\gamma^{\{e\}}_{th}\big)^{\frac{2}{\alpha}}|X_{e_k}|^2\right)|X_{e_k}|\,d\,|X_{e_k}|\Big], \tag{D.1.9}$$

where Λ_l is given in (6.11). By applying [161, Eq. 3.326.2.10], the CDF of $\gamma^{e,AN}_{\mathtt{SIR}}$ is derived as (6.14).

Appendix E

Proofs in Chapter 7

E.1 Proof of Theorem 18

Recall that Γ_R and Γ_D are two random variables, which are dependent on Z_2. In order to express (7.7) in terms of the product of two independent random variables, the term $\Pr\{\Gamma_R \geq \gamma_{th}, \Gamma_D \geq \gamma_{th}\}$ is conditioned on Z_2. Thus,

$$\Pr\{\Gamma_R \geq \gamma_{th}, \Gamma_D \geq \gamma_{th}\} \quad = \quad \Pr\{\Gamma_R \geq \gamma_{th}|Z_2\} \Pr\{\Gamma_D \geq \gamma_{th}|Z_2\}, \tag{E.1}$$

where $\Pr\{\Gamma_R \geq \gamma_{th}|Z_2 = z_2\}$ and $\Pr\{\Gamma_D \geq \gamma_{th}|Z_2 = z_2\}$ are two independent probabilities for a given z_2. The expressions for $\Pr\{\Gamma_R \geq \gamma_{th}|Z_2 = z_2\}$ and $\Pr\{\Gamma_D \geq \gamma_{th}|Z_2 = z_2\}$ are then derived and simplified in the following. The term $\Pr\{\Gamma_R \geq \gamma_{th}|Z_2 = z_2\}$ can be

obtained as

$$\begin{aligned}\Pr\{\Gamma_R \geq \gamma_{th}|Z_2\} &= \Pr\left\{\min\left(\rho Z_1, \frac{P_{\mathcal{I}}}{Y_1}\right)\frac{X_1}{Z_2} \geq \gamma_{th}\right\} \\ &= \underbrace{\Pr\left\{X_1 \geq \frac{Z_2\gamma_{th}}{Z_1\rho}, Y_1 \leq \frac{P_{\mathcal{I}}}{Z_1\rho}\right\}}_{\mathcal{J}_{R,I}} \\ &\quad + \underbrace{\Pr\left\{X_1 \geq \frac{Y_1 Z_2\gamma_{th}}{P_{\mathcal{I}}}, \frac{P_{\mathcal{I}}}{Y_1\rho} \leq Z_1\right\}}_{\mathcal{J}_{R,II}}, \end{aligned} \tag{E.2}$$

where (E.2) presents the probability that SIR is greater than γ_{th} based on the three important power constraints. Note that (E.2) is presented in terms of the addition of $\mathcal{J}_{R,I}$ and $\mathcal{J}_{R,II}$ based on two possibilities: $\rho Z_1 < \frac{P_{\mathcal{I}}}{Y_1}$ and $\rho Z_1 > \frac{P_{\mathcal{I}}}{Y_1}$. Conditioning $\mathcal{J}_{R,I}$ in (E.2) on Z_1 and taking the expected value of the results over the distribution of Z_1, it is derived as

$$\begin{aligned}\mathcal{J}_{R,I} &= \int_0^\infty e^{-\frac{Z_2\gamma_{th}}{z_1\rho\lambda_1}}(1 - e^{-\frac{P_{\mathcal{I}}}{z_1\rho\omega_1}})^M f_{Z_1}(z_1)dz_1 \\ &= \int_0^\infty e^{-\frac{Z_2\gamma_{th}}{z_1\rho\lambda_1}}(1 - e^{-\frac{P_{\mathcal{I}}}{z_1\rho\omega_1}})^M \frac{z_1^{N-1}e^{-\frac{z_1}{P_{PU_{tx}}\nu_1}}}{\Gamma(N)(P_{PU_{tx}}\nu_1)^N}dz_1. \end{aligned} \tag{E.3}$$

Note that by conditioning $\mathcal{J}_{R,I}$ on Z_1, the two terms in $\mathcal{J}_{R,I}$ become independent with respect to one another and therefore, $\mathcal{J}_{R,I}$ can be presented as the product of the two terms. Similarly, by conditioning $\mathcal{J}_{R,II}$ in (E.2) on Y_1 and by taking the expected value of the result over the distribution of Y_1, it is derived as

$$\begin{aligned}\mathcal{J}_{R,II} &= \int_0^\infty e^{-\frac{y_1 Z_2\gamma_{th}}{P_{\mathcal{I}}\lambda_1}}\left(1 - F_{Z_1}(\frac{P_{\mathcal{I}}}{y_1\rho})\right)f_{Y_1}(y_1)dy_1 \\ &= \int_0^\infty e^{-\frac{y_1 Z_2\gamma_{th}}{P_{\mathcal{I}}\lambda_1}}\left(1 - \frac{\Gamma(N, \frac{P_{\mathcal{I}}}{P_{PU_{tx}}\nu_1 y_1\rho})}{\gamma(N)}\right)\frac{M}{\omega_1}\sum_k^{M-1}\binom{M-1}{k}(-1)^k e^{-(\frac{k+1}{\omega_1})y_1}dy_1. \end{aligned} \tag{E.4}$$

In the same manner, the term $\Pr\{\Gamma_D \geq \gamma_{th}|Z_2\}$ in (7.12) can be obtained as

$$\begin{aligned}\Pr\{\Gamma_D \geq \gamma_{th}|Z_2\} &= \Pr\left\{\min\left(\rho Z_2, \frac{P_{\mathcal{I}}}{Y_2}\right)\frac{X_2}{Z_3} \geq \gamma_{th}\right\} \\ &= \underbrace{\Pr\left\{X_2 \geq \frac{\gamma_{th}Z_3}{Z_2\rho}, Y_2 \leq \frac{P_{\mathcal{I}}}{Z_2\rho}\right\}}_{\mathcal{J}_{D,I}} \\ &\quad + \underbrace{\Pr\left\{X_2 \geq \frac{\gamma_{th}Y_2Z_3}{P_{\mathcal{I}}}, Y_2 \geq \frac{P_{\mathcal{I}}}{Z_2\rho}\right\}}_{\mathcal{J}_{D,II}}.\end{aligned} \tag{E.5}$$

Since $\mathcal{J}_{D,I}$ is conditioned on Z_2, the joint probability can be presented as the product of two independent probabilities, which is written as

$$\begin{aligned}\mathcal{J}_{D,I} &= \underbrace{\Pr\{X_2 \geq \frac{\gamma_{th}Z_3}{\rho Z_2}\}}_{\mathcal{I}_1}\underbrace{\Pr\{Y_2 \leq \frac{P_{\mathcal{I}}}{\rho Z_2}\}}_{\mathcal{I}_2}, \\ &= \frac{(P_{PU_{tx}}\nu_3)^{-N}(1 - e^{\frac{P_{\mathcal{I}}}{Z_2\rho\omega_2}})^M}{N(\frac{\gamma_{th}}{\rho Z_2\lambda_2} + \frac{1}{P_{PU_{tx}}\nu_3})},\end{aligned} \tag{E.6}$$

where $\mathcal{I}_1$ is obtained by applying [207, Eq 3.326.2]

$$\mathcal{I}_1 = \int_0^\infty e^{-\frac{\gamma_{th}z_3}{\rho Z_2\lambda_2}} f_{Z_3}(z_3)dz_3 = \frac{(P_{PU_{tx}}\nu_3)^{-N}}{N(\frac{\gamma_{th}}{\rho Z_2\lambda_2} + \frac{1}{P_{PU_{tx}}\nu_3})}, \tag{E.7}$$

and

$$\mathcal{I}_2 = (1 - e^{-\frac{P_{\mathcal{I}}}{Z_2\rho\omega_2}})^M. \tag{E.8}$$

Let us condition $\mathcal{J}_{D,II}$ on Z_3

$$\begin{aligned}\mathcal{J}_{D,II}|Z_3 &= \Pr\{X_2 \geq \frac{Y_2Z_3\gamma_{th}}{P_{\mathcal{I}}}, Y_2 \geq \frac{P_{\mathcal{I}}}{\rho Z_2}\} \\ &= \int_{\frac{P_{\mathcal{I}}}{\rho Z_2}}^\infty e^{-\frac{y_2Z_3\gamma_{th}}{P_{\mathcal{I}}\lambda_2}} f_{Y_2}(y_2)dy_2 \\ &= \int_{\frac{P_{\mathcal{I}}}{\rho Z_2}}^\infty e^{-\frac{y_2Z_3\gamma_{th}}{P_{\mathcal{I}}\lambda_2}} \frac{M}{\omega_2}\sum_k^{M-1}\binom{M-1}{k}(-1)^k e^{-(\frac{k+1}{\omega_2})y_2}dy_2.\end{aligned} \tag{E.9}$$

$$\begin{aligned}\Theta_R =& \Pr\{\Gamma_R^{\infty} \geq \gamma_{th}\} \\ =& \Pr\left\{X_1 \geq \frac{P_{PU_{tx}} N \nu_2 \gamma_{th}\left(\omega_1 + \omega_1 \ln M + \overline{Y}_1\right)}{P_I}, \overline{Y}_1 \geq \frac{P_I}{\rho N P_{PU_{tx}} \nu_1} - \omega_1 - \omega_1 \ln M\right\} \\ &+ \Pr\left\{X_1 \geq \frac{P_{PU_{tx}} \nu_2 \gamma_{th}}{\rho P_{PU_{tx}} \nu_1}\right\} \Pr\left\{-\omega_1 - \omega_1 \ln M \leq \overline{Y}_1 \leq \frac{P_I}{\rho P_{PU_{tx}} N \nu_1} - \omega_1 - \omega_1 \ln M\right\} \quad \text{(E.2)} \\ =& \int_{u_R}^{\infty} \left(1 - F_{X_1}\left(\frac{\left(\omega_1 + \omega_1 \ln M + \overline{Y}_1\right) P_{PU_{tx}} N \nu_2 \gamma_{th}}{P_I}\right)\right) f\left(\overline{y}_1\right) d\overline{y}_1 \\ &+ e^{-\frac{\nu_2 \gamma_{th}}{\lambda_1 \rho \nu_1}} \left(\frac{1}{2}\left[\Phi\left(\frac{u_R}{2\omega_1}\right) - \Phi\left(\frac{u_{R^*}}{2\omega_1}\right)\right]\right) \quad \text{(E.3)} \\ =& \frac{e^{-\frac{P_{PU_{tx}} N \nu_2 \gamma_{th} \omega_1 (1 + \ln M)}{\lambda_1 P_I}}}{2\omega_1 \pi} \int_{u_R}^{\infty} e^{-\frac{\overline{y}_1{}^2}{4{\omega_1}^2} - \frac{P_{PU_{tx}} N \nu_2 \gamma_{th} \overline{y}_1}{\lambda_1 P_I}} d\overline{y}_1 \\ &+ \frac{1}{2} e^{-\frac{\nu_2 \gamma_{th}}{\lambda_1 \rho \nu_1}} \left[\Phi\left(\frac{u_R}{2\omega_1}\right) - \Phi\left(\frac{u_{R^*}}{2\omega_1}\right)\right]. \quad \text{(E.4)}\end{aligned}$$

Averaging $\mathcal{J}_{D,II}$ over the PDF of Z_3 , it is derived as

$$\begin{aligned}\mathcal{J}_{D,II} &= \int_0^{\infty} \mathcal{J}_{D,II} | Z_3 f_{Z_3}(z_3) dz_3 \\ &= \int_{\frac{P_{\mathcal{I}}}{\rho Z_2}}^{\infty} \frac{M}{\omega_2} \sum_k^{M-1} \binom{M-1}{k} (-1)^k e^{-(\frac{k+1}{\omega_2}) y_2} \frac{(P_{PU_{tx}} \nu_3)^{-N}}{N(\frac{y_2 \gamma_{th}}{P_{\mathcal{I}} \lambda_2} + \frac{1}{P_{PU_{tx}} \nu_3})} dy_2 \quad \text{(E.10)}\end{aligned}$$

The outage probability can be evaluated using the results obtained from (E.3), (E.4), (E.6), and (E.10) in (7.12).

E.2 Proof of Theorem 19

The term Θ_R is obtained in (E.4) at the top of next page. The terms in (E.3) can be obtained using the CDF and PDF expressions for X_1 and $\overline{Y}_1$. Applying [207, Eq

3.322.1], Θ_R in (E.4) is simplified as

$$\begin{aligned}\Theta_R =& \frac{e^{\omega_1 {\gamma_R}^2 - \omega_1 \gamma_R (1+\ln M)}}{2} \left(1 - \Phi\left(\gamma_R \sqrt{\omega_1} + \frac{u_R}{2\omega_1}\right)\right) \\ &+ \frac{1}{2} e^{-\frac{\nu_2 \gamma_{th}}{\lambda_1 \rho \nu_1}} \left[\Phi\left(\frac{u_R}{2\omega_1}\right) - \Phi\left(\frac{u_{R^*}}{2\omega_1}\right)\right], \end{aligned} \tag{E.5}$$

where $\gamma_R = \frac{P_{PU_{tx}} N \nu_2 \gamma_{th}}{\lambda_1 P_I}$, $\Phi(x) = \frac{2}{\sqrt{\pi}} \int_0^x e^{-t^2} dt$, $u_R = \frac{P_I}{\rho N P_{PU_{tx}} \nu_1} - \omega_1 - \omega_1 \ln M$, and $u_{R^*} = -\omega_1 - \omega_1 \ln M$. Similarly, by substituting the parameters of (E.5) using $\nu_1 \to \nu_2$, $\omega_1 \to \omega_2$, $\lambda_1 \to \lambda_2$, and $\nu_2 \to \nu_3$, Θ_D is obtained as

$$\begin{aligned}\Theta_D =& \frac{e^{\omega_2 {\gamma_D}^2 - \omega_2 \gamma_D (1+\ln M)}}{2} \left(1 - \Phi\left(\gamma_D \sqrt{\omega_2} + \frac{u_D}{2\omega_2}\right)\right) \\ &+ \frac{1}{2} e^{-\frac{\nu_3 \gamma_{th}}{\lambda_2 \rho \nu_2}} \left[\Phi\left(\frac{u_D}{2\omega_2}\right) - \Phi\left(\frac{u_{D^*}}{2\omega_2}\right)\right], \end{aligned} \tag{E.6}$$

where $u_D = \frac{P_I}{\rho N P_{PU_{tx}} \nu_2} - \omega_2 - \omega_2 \ln M, u_{D^*} = -\omega_2 - \omega_2 \ln M$, and $\gamma_D = \frac{P_{PU_{tx}} N \nu_3 \gamma_{th}}{\lambda_2 P_I}$. Substituting (E.5) and (E.6) into (7.23), a closed-form expression for the asymptotic outage probability can be obtained.

Appendix F

Proofs in Chapter 8

F.1 Proof of Theorem 20

According to (8.7) and $\mathbb{E}\left\{\left\|\mathbf{h}_{S_{k_{x^*}}}\right\|^2\right\} = N_k$, $\mathbb{E}\{I_{S_{k_{x^*}}}\}$ is rewrote as

$$\begin{aligned}\mathbb{E}\{I_{S_{k_{x^*}}}\} &= \mathbb{E}\Big\{P_{\mathrm{t},S_{k_{x^*}}}\left\|\mathbf{h}_{S_{k_{x^*}}}\right\|^2 L_0\Big(\max\Big\{\left\|\mathbf{x}_{S_{k_{x^*}}}\right\|, d\Big\}\Big)^{-\eta_k}\Big\} \\ &= P_{\mathrm{t},S_{k_{x^*}}} N_k L_0 \mathbb{E}\Big\{\Big(\max\Big\{\left\|\mathbf{x}_{S_{k_{x^*}}}\right\|, d\Big\}\Big)^{-\eta_k}\Big\} \\ &= P_{\mathrm{t},S_{k_{x^*}}} N_k L_0 \Big[\int_0^d f_{\left\|\mathbf{x}_{S_{k_{x^*}}}\right\|}(x)\, d^{-\eta_k} dx \qquad + \int_d^\infty f_{\left\|\mathbf{x}_{S_{k_{x^*}}}\right\|}(x)\, x^{-\eta_k} dx\Big]\end{aligned} \tag{F.1.1}$$

By using the PDF of $\left\|\mathbf{x}_{S_{k_{x^*}}}\right\|$ in (8.5) of Lemma 10, it is derived that

$$\begin{aligned}\mathbb{E}\left\{I_{S_{k_{x^*}}}\right\} =& \frac{P_{\mathrm{t},S_{k_{x^*}}} N_k L_0}{\Pi_k}\Big[d^{-\eta_k}\int_0^d x \exp\Big\{-\sum_{j_1=1}^{K}\zeta_{k,j_1} x^{2\eta_k/\eta_{j_1}}\Big\}dx \\ &+ \int_d^\infty x^{-(\eta_k-1)}\exp\Big\{-\sum_{j_2=1}^{K}\zeta_{k,j_2} x^{2\eta_k/\eta_{j_2}}\Big\}dx\Big].\end{aligned} \tag{F.1.2}$$

Then $\mathbb{E}\{I_{B_x}\}$ is derived as

$$\begin{aligned}\mathbb{E}\{I_{S_x}\} = & \sum_{j=1}^{K}\Big\{\mathbb{E}\Big\{\sum_{S_x\in\Phi_j\setminus S_{x^*}} P_{\mathrm{t},j}\Big|\mathbf{h}_{S_xu_0}\frac{\mathbf{g}_{S_xu_j}^H}{\|\mathbf{g}_{S_xu_j}\|}\Big|^2 L_0(\max\{\|\mathbf{x}_{S_xu_0}\|,d\})^{-\eta_j}\Big\}\Big\} \\ = & \sum_{j=1}^{K}\mathbb{E}_h\Big\{P_{\mathrm{t},j}L_0\Big|\mathbf{h}_{S_xu_0}\frac{\mathbf{g}_{S_xu_j}^H}{\|\mathbf{g}_{S_xu_j}\|}\Big|^2\Big\}\mathbb{E}_{S_{x^*}}\Big\{\mathbb{E}_{\Phi_j}\Big\{\sum_{S_x\in\Phi_j\setminus\mathcal{S}_{x^*}}(\max\{\|\mathbf{x}_{S_xu_0}\|,d\})^{-\eta_j}\Big\}\Big\}\end{aligned} \tag{F.1.3}$$

Given the distance between the typical MT and the associated BS as $\left\|\mathbf{x}_{S_{k_{x^*}}}\right\| = x$, the interfering BSs need to be located outside a disc of radius ${\rho_{j,k}}^{1/\eta_j}x^{\eta_j/\eta_k}$ to satisfy the BRP cell association, in which the biased received power at the typical MT resulting from the associated BS is higher than the biased received power at the typical MT resulting from any other BSs [197]. Therefore, the radius between the the interfering BSs and the typical MT should be larger than $r_{I,\min}$, where $r_{I,\min} = {\rho_{j,k}}^{1/\eta_j}x^{\eta_j/\eta_k}$. The Campbell's Theorem [31] is applied to (F.1.3) to give

$$\begin{aligned}\mathbb{E}\{I_{S_x}\} = & \sum_{j=1}^{K}\mathbb{E}\Big\{P_{\mathrm{t},j}L_0\Big|\mathbf{h}_{S_xu_0}\frac{\mathbf{g}_{S_xu_j}^H}{\|\mathbf{g}_{S_xu_j}\|}\Big|^2\Big\}\mathbb{E}_{S_{x^*}}\Big\{\lambda_j\int\limits_{R^2/r_{I,\min}^2}(\max\{x,d\})^{-\eta_j}dx\Big\} \\ = & \sum_{j=1}^{K}2\pi P_{\mathrm{t},j}L_0\lambda_j\mathbb{E}_{S_{x^*}}\Big\{\int_{r_{I,\min}}^{\infty}(\max\{r,d\})^{-\eta_j}rdr\Big\} \\ = & \sum_{j=1}^{K}2\pi P_{\mathrm{t},j}L_0\lambda_j\int_0^{\infty}\int_{r_{I,\min}}^{\infty}(\max\{r,d\})^{-\eta_j}rdrf_{\left\|\mathbf{x}_{S_{k_{x^*}}}\right\|}(x)\,dx\end{aligned} \tag{F.1.4}$$

As such, $\mathbb{E}\{I_{S_x}\}$ is derived as

$$\begin{aligned}\mathbb{E}\{I_{S_x}\} = & \sum_{j=1}^{K}2\pi P_{\mathrm{t},j}L_0\lambda_j\Big[\int_0^{x_d}\Big(d^{-\eta_j}\int_{{\rho_{j,k}}^{1/\eta_j}x^{\eta_j/\eta_k}}^{d}rdr+\int_d^{\infty}r^{-(\eta_j-1)}dr\Big)f_{\left\|\mathbf{x}_{S_{k_{x^*}}}\right\|}(x)\,dx+ \\ & \int_{x_d}^{\infty}\int_{{\rho_{j,k}}^{1/\eta_j}x^{\eta_j/\eta_k}}^{\infty}r^{-(\eta_j-1)}rdrf_{\left\|\mathbf{x}_{S_{k_{x^*}}}\right\|}(x)\,dx\Big]\end{aligned} \tag{F.1.5}$$

where $x_d = {d^{\eta_k/\eta_j}\rho_{j,k}}^{-\eta_k/\eta_j}$.

Substituting the PDF of $\left\|\mathbf{x}_{S_{k_{x^*}}}\right\|$ in (8.5) into (F.1.5), $\mathbb{E}\left\{I_{S_x}\right\}$ is derived as

$$\mathbb{E}\left\{I_{S_x}\right\} = \frac{L_0}{\Pi_k}\sum_{j=1}^{K} 2\pi P_{\mathrm{t},j}\lambda_j \Big[\int_0^{{d^{\eta_k}}/{\eta_j}\,{\rho_{j,k}}^{-{\eta_k}/{\eta_j}^2}} \frac{x}{2d^{\eta_j}} \exp\Big\{-\sum_{j_3=1}^{K}\zeta_{k,j_3}x^{2\eta_k/\eta_{j_3}}\Big\}$$
$$\Big(\frac{\eta_j d^2}{(\eta_j-2)} - {\rho_{j,k}}^{2/\eta_j}x^{2\eta_j/\eta_k}\Big)dx + (\eta_j-2)^{-1}\int_{{d^{\eta_k}}/{\eta_j}\,{\rho_{j,k}}^{-{\eta_k}/{\eta_j}^2}}^{\infty} x\Big({\rho_{j,k}}^{1/\eta_j}x^{\eta_j/\eta_k}\Big)^{-(\eta_j-2)}$$
$$\exp\Big\{-\sum_{j_4=1}^{K}\zeta_{k,j_4}x^{2\eta_k/\eta_{j_4}}\Big\}dx\Big]. \tag{F.1.6}$$

Combining (F.1.2) and (F.1.6), the average received power at the typical MT associated with the kth tier is derived as Theorem 20.

F.2 Proof of Corollary 7

By substituting $\eta_k = \eta_j = \eta$ into (8.9), $\mathbb{E}\left\{P_{\mathrm{r_u},k}\right\}$ is derived as

$$\mathbb{E}\left\{P_{\mathrm{r_u},k}\right\} = \frac{P_{\mathrm{t},S_{k_{x^*}}}N_k L_0}{\Pi_k}\Big[d^{-\eta}\underbrace{\int_0^d t\exp\left\{-\varpi_k t^2\right\}dt}_{\mathrm{A}_1} + \underbrace{\int_d^{\infty} t^{-(\eta-1)}\exp\left\{-\varpi_k t^2\right\}dt}_{A_2}\Big]$$
$$+\frac{L_0}{\Pi_k}\sum_{j=1}^{K}2\pi P_{\mathrm{t},j}\lambda_j\underbrace{\Big[\frac{\eta d^2}{2d^{\eta}(\eta-2)}\int_0^{d{\rho_{j,k}}^{-1/\eta}} x\exp\left\{-\varpi_k x^2\right\}dx}_{A_3} - \frac{{\rho_{j,k}}^{2/\eta}}{2d^{\eta}}$$
$$\underbrace{\int_0^{d{\rho_{j,k}}^{-1/\eta}} x^3\exp\left\{-\varpi_k x^2\right\}dx}_{A_4} + (\eta-2)^{-1}{\rho_{j,k}}^{-(\eta-2)/\eta}\underbrace{\int_{d{\rho_{j,k}}^{-1/\eta}}^{\infty} x^{-(\eta-3)}\exp\left\{-\varpi_k x^2\right\}dx}_{A_5}\Big], \tag{F.2.1}$$

where $\Pi_k = \int_0^{\infty} r\exp\left(-\varpi_k r^2\right)dr$.

To derive (8.11), A_1, A_2, and Π_k can be solved by changing the variable $t = x^2$, solve A_2 and A_5 by using $\int_u^{\infty}\frac{e^{-x}}{x^v}dx = u^{-\frac{v}{2}}e^{-\frac{u}{2}}W_{-\frac{v}{2},\frac{(1-v)}{2}}(u)$ in [172, eq. (3.381.6)], and A_3 can be solved by using $\int_0^x e^{-t}t^{\alpha-1}dt = \Upsilon(\alpha,x)$ in [172, eq. (8.350.1)].

F.3 Proof of Theorem 21

According to (8.8) and (8.14), the outage probability of the typical MT in the kth tier is written as

$$P_{out,k}\left(\gamma_{th}\right) = 1 - \int_0^\infty \Pr\Big[\frac{\left\|\mathbf{h}_{\mathrm{u}_0,S_{k_{x^*}}}\right\|^2 \left\|\mathbf{x}_{\mathrm{u}_0,S_{k_{x^*}}}\right\|^{-\eta_k}}{\left(I_U+\sigma^2\right)\tau_k} > \gamma_{th}\Big] f_{\left\|\mathbf{x}_{\mathrm{u}_0,S_{k_{x^*}}}\right\|}(x)\,dx, \quad \text{(F.3.1)}$$

where $f_{\left\|\mathbf{x}_{\mathrm{u}_0,S_{k_{x^*}}}\right\|}(x)$ is given in Lemma 2. The complementary cumulative distribution function (CCDF) of the typical MT at distance $\mathbf{x}$ from its associated BS in kth tier is given by

$$\begin{aligned}
&\Pr\Big[\frac{\left\|\mathbf{h}_{\mathrm{u}_0,S_{k_{x^*}}}\right\|^2 \left\|\mathbf{x}_{\mathrm{u}_0,S_{k_{x^*}}}\right\|^{-\eta_k}}{\left(I_U+\sigma^2\right)\tau_k} > \gamma_{th}\Big] \\
&\quad = \mathbb{E}_{I_U}\Big\{\Pr\Big[\Big\|\mathbf{h}_{\mathrm{u}_0,B_{k_{x^*}}}\Big\|^2 > \left(I_U+\sigma^2\right)\gamma_{th}\tau_k\Big\|\mathbf{x}_{\mathrm{u}_0,B_{k_{x^*}}}\Big\|^{\eta_k}\Big]\Big|I_U\Big\} \\
&\quad = \sum_{m=0}^{N-1}\frac{1}{m!}\int_0^\infty \exp\Big\{-\left(\tau+\sigma^2\right)\gamma_{th}\tau_k\Big\|\mathbf{x}_{\mathrm{u}_0,B_{k_{x^*}}}\Big\|^{\eta_k}\Big\} \\
&\quad \Big(\left(\tau+\sigma^2\right)\gamma_{th}\tau_k\Big\|\mathbf{x}_{\mathrm{u}_0,B_{k_{x^*}}}\Big\|^{\eta_k}\Big)^m d\Pr\left(I_U\le\tau\right).
\end{aligned} \quad \text{(F.3.2)}$$

By using $\left.\frac{d^m(e^{-\left(\tau+\sigma^2\right)\gamma_{th}\tau_k\phi\left\|\mathbf{x}_{\mathrm{u}_0,B_{k_{x^*}}}\right\|^{\eta_k}x})}{dx^m}\right|_{x=\phi^{-1}} = (-\left(\tau+\sigma^2\right)\gamma_{th}\tau_k\phi\Big\|\mathbf{x}_{\mathrm{u}_0,B_{k_{x^*}}}\Big\|^{\eta_k})^m$ $e^{-\left(\tau+\sigma^2\right)\gamma_{th}\tau_k\left\|\mathbf{x}_{\mathrm{u}_0,B_{k_{x^*}}}\right\|^{\eta_k}}$ for $m>0$, (F.3.2) can be rewrote as

$$\begin{aligned}
\Pr\left[SINR_k > \gamma_{th}\right] = &\exp\left\{-\sigma^2\gamma_{th}\tau_k\left\|\mathbf{x}_{\mathrm{u}_0,S_{k_{x^*}}}\right\|^{\eta_k}\right\}\mathcal{L}_{I_U}\left(\gamma_{th}\tau_k\left\|\mathbf{x}_{\mathrm{u}_0,S_{k_{x^*}}}\right\|^{\eta_k}\right) + \sum_{m=1}^{N-1}\frac{\phi^{-m}}{(-1)^m m!} \\
&\left.\frac{d^m\Big(\frac{\mathcal{L}_{I_U}\left(\gamma_{th}\tau_k\phi\left\|\mathbf{x}_{\mathrm{u}_0,S_{k_{x^*}}}\right\|^{\eta_k}x\right)}{e^{\sigma^2\gamma_{th}\tau_k\phi\left\|\mathbf{x}_{\mathrm{u}_0,S_{k_{x^*}}}\right\|^{\eta_k}x}}\Big)}{dx^m}\right|_{x=\phi^{-1}},
\end{aligned} \quad \text{(F.3.3)}$$

The Laplace transform of I_U is $\mathcal{L}_{I_U}(s) = \prod_{j=1}^{K}\mathcal{L}_{I_{U,j}}(s)$. Here, it is assumed that $H_j = \left|\frac{\mathbf{h}_{\mathrm{u}_{x,j},B_{x,j}}^H}{\left\|\mathbf{h}_{\mathrm{u}_{x,j},B_{x,j}}^H\right\|}\mathbf{h}_{\mathrm{u}_0,\mathrm{u}_{x,j}}\right|^2$. According to the Generating functional of homogeneous

PPP in [134], $\mathcal{L}_{I_{U,j}}(s)$ is derived as

$$\begin{aligned}\mathcal{L}_{I_{U,j}}(s) &= \exp\Big\{-\int\left[1-\mathbb{E}_{H_j}\left(\exp\left(-s\tau_j H_j r^{-\alpha}\right)\right)\right]\lambda_j 2\pi r dr\Big\}\\ &= \exp\Big\{-\lambda_j\pi\tau_j{}^{\frac{2}{\eta_j}}\mathbb{E}_h\{H_j{}^{\frac{2}{\eta_j}}\}\Gamma\big(1-\frac{2}{\eta_j}\big)s^{\frac{2}{\eta_j}}\Big\}\\ &= \exp\Big\{-\sum_{j=1}^{K}\lambda_j\pi\tau_j{}^{\frac{2}{\eta_j}}\Gamma\big(1+\frac{2}{\eta_j}\big)\Gamma\big(1-\frac{2}{\eta_j}\big)s^{\frac{2}{\eta_j}}\Big\}. \end{aligned} \tag{F.3.4}$$

Substituting the expression for $\mathcal{L}_{I_U}(s)$ into (F.3.3), $\Pr[SINR_k>\gamma_{th}]$ is derived as

$$\begin{aligned}\Pr[SINR_k>\gamma_{th}] =& \exp\Big\{-\sigma^2\gamma_{th}\tau_k\big\|\mathbf{x}_{\mathrm{u}0,S_{k_{x^*}}}\big\|^{\eta_k}-\sum_{j=1}^{K}\vartheta_j\big\|\mathbf{x}_{\mathrm{u}0,S_{k_{x^*}}}\big\|^{\frac{2\eta_k}{\eta_j}}(\gamma_{th})^{\frac{2}{\eta_j}}\Big\}\\ &+\sum_{m=1}^{N-1}\frac{\phi^{-m}}{(-1)^m m!}\frac{d^m}{dx^m}\Big[\exp\Big\{-\sigma^2\gamma_{th}\tau_k\phi\big\|\mathbf{x}_{\mathrm{u}0,S_{k_{x^*}}}\big\|^{\eta_k}x\\ &-\sum_{j=1}^{K}\vartheta_{k,j}\big\|\mathbf{x}_{\mathrm{u}0,S_{k_{x^*}}}\big\|^{\frac{2\eta_k}{\eta_j}}(\phi\gamma_{th})^{\frac{2}{\eta_j}}x^{\frac{2}{\eta_j}}\Big\}\Big|_{x=\phi^{-1}}. \end{aligned} \tag{F.3.5}$$

It is assumed that $A(x)=-\sigma^2\gamma_{th}\tau_k\phi\big\|\mathbf{x}_{\mathrm{u}0,S_{k_{x^*}}}\big\|^{\eta_k}x-\sum_{j=1}^{K}\vartheta_{k,j}\big\|\mathbf{x}_{\mathrm{u}0,S_{k_{x^*}}}\big\|^{\frac{2\eta_k}{\eta_j}}\left(\phi\gamma_{th}\right)^{\frac{2}{\eta_j}}x^{\frac{2}{\eta_j}}$, then the derivative of mth order is solved by applying the Faà di Bruno's formula as follows:

$$\begin{aligned}&\frac{d^m\left[\exp\left(A(x)\right)\right]}{dx^m}\Big|_{x=\phi^{-1}} =\\ &\sum\frac{m!}{\prod_{i=1}^{m}m_i!i!^{m_i}}\exp\Big\{-\sigma^2\gamma_{th}\tau_k\big\|\mathbf{x}_{\mathrm{u}0,S_{k_{x^*}}}\big\|^{\eta_k}-\sum_{j=1}^{K}\vartheta_{k,j}\big\|\mathbf{x}_{\mathrm{u}0,S_{k_{x^*}}}\big\|^{\frac{2\eta_k}{\eta_j}}\gamma_{th}{}^{\frac{2}{\eta_j}}\Big\}\\ &\Big(-\sigma^2\gamma_{th}\tau_k\phi\big\|\mathbf{x}_{\mathrm{u}0,B_{k_{x^*}}}\big\|^{\eta_k}-\sum_{j=1}^{K}\vartheta_{k,j}(\gamma_{th})^{\frac{2}{\eta_j}}\big\|\mathbf{x}_{\mathrm{u}0,B_{k_{x^*}}}\big\|^{\frac{2\eta_k}{\eta_j}}\frac{2}{\eta_j}\phi\Big)^{m_1}\\ &\prod_{l=2}^{m}\Big(-\sum_{j=1}^{K}\vartheta_{k,j}(\gamma_{th})^{\frac{2}{\eta_j}}\big\|\mathbf{x}_{\mathrm{u}0,B_{k_{x^*}}}\big\|^{\frac{2\eta_k}{\eta_j}}\prod_{i=0}^{l-1}\big(\frac{2}{\eta_j}-i\big)\phi^l\Big)^{m_l}. \end{aligned} \tag{F.3.6}$$

Substituting (F.3.6) into (F.3.5), $\Pr\left[SINR_k > \gamma_{th}\right]$ is derived as

$$\begin{aligned}\Pr\left[SINR_k > \gamma_{th}\right] = &\exp\left\{-\sigma^2\gamma_{th}\tau_k\left\|\mathbf{x}_{\mathrm{u}_0,B_{k_{x^*}}}\right\|^{\eta_k} - \sum_{j=1}^{K}\vartheta_{k,j}\gamma_{th}^{\frac{2}{\eta_j}}\left\|\mathbf{x}_{\mathrm{u}_0,B_{k_{x^*}}}\right\|^{2\eta_k/\eta_j}\right\}\\
&+\sum_{m=1}^{N-1}\frac{\phi^{-m}}{(-1)^m}\sum\frac{1}{\prod_{i=1}^{m}m_i!i!^{m_i}}\left(-\sigma^2\gamma_{th}\tau_k\phi\left\|\mathbf{x}_{\mathrm{u}_0,B_{k_{x^*}}}\right\|^{\eta_k} - \sum_{j=1}^{K}\vartheta_{k,j}(\gamma_{th})^{\frac{2}{\eta_j}}\frac{2}{\eta_j}\phi\left\|\mathbf{x}_{\mathrm{u}_0,B_{k_{x^*}}}\right\|^{\frac{2\eta_k}{\eta_j}}\right)^{m_1}\\
&\prod_{l=2}^{m}\left(-\sum_{j=1}^{K}\vartheta_{k,j}(\gamma_{th})^{\frac{2}{\eta_j}}\left\|\mathbf{x}_{\mathrm{u}_0,B_{k_{x^*}}}\right\|^{\frac{2\eta_k}{\eta_j}}\prod_{i=0}^{l-1}\left(\frac{2}{\eta_j}-i\right)\phi^l\right)^{m_l}\Big]. \qquad \text{(F.3.7)}\end{aligned}$$

Now, theorem 21 can be proved by substituting (F.3.7) and (8.5) into (F.3.1).

F.4 Proof of Theorem 24

Based on (8.31), the outage probability of a typical MT associated with the kth tier as $N \to \infty$ can be given as

$$\begin{aligned}P_{out,k}^{\infty}\left(\gamma_{th}\right) =&1 - \int_0^{\infty}\Pr\Big[\frac{\phi\mathbb{E}\left\{P_{r_{\mathrm{u}_0},k}\right\}N_kL_0\left\|\mathbf{x}_{\mathrm{u}_0,S_{k_{x^*}}}\right\|^{-\eta_k}}{I_U+\sigma^2} > \gamma_{th}\Big]f_{\left\|\mathbf{x}_{\mathrm{u}_0,S_{k_{x^*}}}\right\|}(x)\,dx\\
=&1 - \int_0^{\infty}F_{I_U}\Big(\phi\mathbb{E}\left\{P_{r_{\mathrm{u}_0},k}\right\}N_kL_0\left\|\mathbf{x}_{\mathrm{u}_0,S_{k_{x^*}}}\right\|^{-\eta_k}(\gamma_{th})^{-1} - \sigma^2\Big)f_{\left\|\mathbf{x}_{\mathrm{u}_0,S_{k_{x^*}}}\right\|}(x)\,dx. \qquad \text{(F.4.1)}\end{aligned}$$

The Gil-Pelaez theorem is utilized to derive the CDF of I_U as

$$F_{I_U}\left(x\right) = \frac{1}{2} - \frac{1}{\pi}\int_0^{\infty}\frac{\mathrm{Im}\left[e^{-jwx}\phi^*\left(w\right)\right]}{w}dw. \qquad \text{(F.4.2)}$$

Substituting (F.4.2) into (F.4.1), the outage probability of a typical MT associated with the kth tier as $N \to \infty$ is derived as (8.32).

References

[1] Ahmed, W.: Spectrum sharing in cognitive radio networks. Master's thesis, Victoria University (2012)

[2] Wyglinski, A.M., Nekovee, M., Hou, T.: Cognitive radio communications and networks: principles and practice. Academic Press (2009)

[3] Wang, Z.: Resource management in wireless cellular networks with heterogeneous capacity supply and heterogeneous traffic demand. Master's thesis, Carleton University (2014)

[4] Dhillon, H.S.: Fundamentals of heterogeneous cellular networks. PhD thesis (2013)

[5] Ing, E.: Multipath propagation. `Available:http://www.cs.nccu.edu.tw/~lien/NIIslide/WirelessTech/hardcopy.htm` (2009)

[6] El-Mahdy, A.: Multiple antenna selection of multi-antenna-multi-relay cooperative networks. **1**(2) (2013) 62

[7] Surobhi, N.A.: Outage performance of cooperative cognitive relay networks. PhD thesis, Victoria University (2009)

[8] Bassily, R., Ekrem, E., He, X., Tekin, E., Xie, J., Bloch, M., Ulukus, S., Yener, A.: Cooperative security at the physical layer: A summary of recent advances. IEEE Signal Process. Mag. **30**(5) (2013) 16–28

[9] Zhou, X., Zhang, R., Ho, C.K.: Wireless information and power transfer: Architecture design and rate-energy tradeoff. In: Proc. IEEE Global Commun. Conf. (GLOBECOM). (Dec. 2012) 3982–3987

[10] Cisco: Cisco visual networking index: Global mobile data traffic forecast update, 2010-2015. white paper, Feb. (2012)

[11] Nokia Siemens Networks: LTE release 12 and beyond. white paper, Oct. (2012)

[12] Wang, C.X., Haider, F., Gao, X., You, X.H., Yang, Y., Yuan, D., Aggoune, H., Haas, H., Fletcher, S., Hepsaydir, E.: Cellular architecture and key technologies for 5G wireless communication networks. IEEE Commun. Mag. **52**(2) (Feb. 2014) 122–130

[13] Corson, M.S., Laroia, R., Li, J., Park, V., Richardson, T., Tsirtsis, G.: Toward proximity-aware internetworking. IEEE Wireless Commun. Mag. **17**(6) (Dec. 2010) 26–33

[14] Hilton, S.: Machine-to-machine device connections: worldwide forecast 2010–2020. Analysys Mason Report (2010)

[15] Rappaport, T.S., Sun, S., Mayzus, R., Zhao, H., Azar, Y., Wang, K., Wong, G.N., Schulz, J.K., Samimi, M., Gutierrez, F.: Millimeter wave mobile communications for 5G cellular: It will work! IEEE Access **1** (May. 2013) 335–349

[16] Kolodzy, P., Avoidance, I.: Spectrum policy task force. Federal Commun. Comm., Washington, DC, Rep. ET Docket (02-135) (2002)

[17] : Cognitive radio technology. `http://www.ofcom.org.uk/research/technology/overview/emer_tech/cograd/cograd_main.pdf`

[18] : United states frequency allocations. `Available:http://www.ntia.doc.gov/osmhome/allochrt.pdf`

[19] Andrews, J.G., Buzzi, S., Choi, W., Hanly, S.V., Lozano, A., Soong, A.C.K., Zhang, J.C.: What will 5G be? IEEE J. Sel. Areas Commun. **32**(6) (Jun. 2014) 1065–1082

[20] : Secondary markets initiative. `http://wireless.fcc.gov/licensing/index.htm?job=secondary_markets`

[21] Mitola, J.: Cognitive Radio: An Integrated Agent Architecture for Software Defined Radio. PhD thesis, KTH Royal Inst. Technology, Stockholm, Sweden (2000)

[22] Akyildiz, I.F., Lee, W.Y., Vuran, M.C., Mohanty, S.: Next generation/dynamic spectrum access/cognitive radio wireless networks: A survey. Computer Networks **50**(13) (September 2006) 2127–2159

[23] Haykin, S.: Cognitive radio: brain-empowered wireless communications. IEEE J. Sel. Areas Commun. **23**(2) (2005) 201–220

[24] Srinivasa, S., Jafar, S.A.: Cognitive radios for dynamic spectrum access - the throughput potential of cognitive radio: A theoretical perspective. IEEE Commun. Mag. **45**(5) (May 2007) 73–79

[25] Haykin, S.: Cognitive radio: Brain-empowered wireless communications. IEEE J. Sel. Areas Commun. **23**(2) (February 2005) 201–220

[26] Goldsmith, A., Jafar, S., Maric, I., Srinivasa, S.: Breaking spectrum gridlock with cognitive radios: An information theoretic perspective. Proc. IEEE **97**(5) (May 2009) 894–914

[27] Gastpar, M.: On capacity under receive and spatial spectrum-sharing constraints. IEEE Trans. Inf. Theory **53**(2) (Feb. 2007) 471–487

[28] Cramton, P.: Spectrum auction design. Review of Industrial Organization **42**(2) (2013) 161–190

[29] Quek, T.Q., de la Roche, G., Güvenç, I., Kountouris, M.: Small cell networks: Deployment, PHY techniques, and resource management. Cambridge University Press (2013)

[30] ElSawy, H., Hossain, E., Haenggi, M.: Stochastic geometry for modeling, analysis, and design of multi-tier and cognitive cellular wireless networks: A survey. IEEE Commun. Surveys and Tutorials **15**(3) (2013) 996–1019

[31] Haenggi, M.: Stochastic geometry for wireless networks. Cambridge University Press (2012)

[32] Dhillon, H.S., Ganti, R.K., Baccelli, F., Andrews, J.G.: Modeling and analysis of K-tier downlink heterogeneous cellular networks. IEEE J. Sel. Areas Commun. **30**(3) (Apr. 2012) 550–560

[33] Andrews, J.G., Baccelli, F., Ganti, R.K.: A tractable approach to coverage and rate in cellular networks. IEEE Trans. Wireless Commun. **59**(11) (Nov. 2011) 3122–3134

[34] Jo, H.S., Sang, Y.J., Xia, P., Andrews, J.G.: Heterogeneous cellular networks with flexible cell association: A comprehensive downlink SINR analysis. IEEE Trans. Wireless Commun. **11**(10) (2012) 3484–3495

[35] Zhang, R.: On peak versus average interference power constraints for protecting primary users in cognitive radio networks. IEEE Trans. Wireless Commun. **8**(4) (April 2009) 2112–2120

[36] Foschini, G.J., Gans, M.J.: On limits of wireless communications in a fading

environment when using multiple antennas. Wireless personal communications **6**(3) (1998) 311–335

[37] Telatar, E.: Capacity of multi-antenna gaussian channels. European transactions on telecommunications **10**(6) (1999) 585–595

[38] Laneman, J., Wornell, G.: Energy-efficient antenna sharing and relaying for wireless networks. In: Proc. IEEE Wireless Commun. Netw. Conf. (WCNC). (October 2000)

[39] Sendonaris, A., Erkip, E., Aazhang, B.: Increasing uplink capacity via user cooperation diversity. In: Proc. IEEE Int. Symp. Inf. Theory (ISIT). (Aug. 1998)

[40] Letaief, K., Zhang, W.: Cooperative communications for cognitive radio networks. Proc. IEEE **97**(5) (May 2009) 878–893

[41] Zhang, R., Liang, Y.C.: Exploiting multi-antennas for opportunistic spectrum sharing in cognitive radio networks. IEEE J. Select. Topics Signal Processing **2**(1) (Aug. 2008) 88–102

[42] Zhang, H., Molisch, A.F., Zhang, J.: Applying antenna selection in WLANs for achieving broadband multimedia communications. IEEE Trans. Broadcast. **52**(4) (Dec. 2006) 475–482

[43] Li, Q., Lin, X., Zhang, J., Roh, W.: Advancement of MIMO technology in WiMAX: from IEEE 802.16 d/e/j to 802.16 m. IEEE Commun. Mag. **47**(6) (Jun. 2009) 100–107

[44] Mehta, N.B., Kashyap, S., Molisch, A.F.: Antenna selection in LTE: from motivation to specification. IEEE Commun. Mag. **50**(10) (Oct. 2012) 144–150

[45] Annamalai, A., Tellambura, C.: A new approach to performance evaluation of generalized selection diversity receivers in wireless channels. In: Proc. IEEE Veh. Technol. Conf. (VTC). (Fall 2001) 2309–2313

[46] Cai, X., Giannakis, G.B.: Performance analysis of combined transmit selection diversity and receive generalized selection combining in Rayleigh fading channels. IEEE Trans. Wireless Commun. **3**(6) (November 2004) 1980–1983

[47] Win, M., Winters, J.: Virtual branch analysis of symbol error probability for hybrid selection/maximal-ratio combining in Rayleigh fading. IEEE Trans. Commun.

49(11) (Nov. 2001) 1926–1934

[48] El-Hajj, W., Safa, H., Guizani, M.: Survey of security issues in cognitive radio networks. J. Internet Tech. **12**(2) (2011) 181–198

[49] Parvin, S., Hussain, F.K., Hussain, O.K., Han, S., Tian, B., Chang, E.: Cognitive radio network security: A survey. Journal of Network and Computer Applications **35**(6) (2012) 1691–1708

[50] Shu, Z., Qian, Y., Ci, S.: On physical layer security for cognitive radio networks. IEEE Netw. **27**(3) (Jun. 2013) 28–33

[51] Wang, L., Yang, N., Elkashlan, M., Yeoh, P.L., Yuan, J.: Physical layer security of maximal ratio combining in two-wave with diffuse power fading channels. IEEE Trans. Inf. Forensics Security **9**(2) (Feb. 2014) 247–258

[52] Wang, B., Wu, Y., Liu, K.J.R., Clancy, T.C.: An anti-jamming stochastic game for cognitive radio networks. IEEE J. Sel. Areas Commun. **29**(4) (Apr. 2011) 877–889

[53] Wyner, A.D.: The wire-tap channel. Bell System Technical Journal **54**(8) (Oct. 1975) 1355–1387

[54] Grobe, K., Roppelt, M., Autenrieth, A., Elbers, J.P., Eiselt, M.: Cost and energy consumption analysis of advanced WDM-PONs. IEEE Commun. Mag. **49**(2) (Feb. 2011) s25–s32

[55] Lu, X., Wang, P., Niyato, D., Kim, D.I., Han, Z.: Wireless networks with RF energy harvesting: A contemporary survey. arXiv preprint arXiv:1406.6470 (2014)

[56] Balouchi, F., Gohn, B.: Wireless power. Pike Res. Rep., 2Q (2012)

[57] Huang, K., Lau, V.K.N.: Enabling wireless power transfer in cellular networks: Architecture, modeling and deployment. IEEE Trans. Wireless Commun. **13**(2) (Feb. 2014) 902–912

[58] Andrews, J.G.: Seven ways that hetnets are a cellular paradigm shift. IEEE Commun. Mag. **51**(3) (Mar. 2013) 136–144

[59] Kim, K.J., Duong, T.Q., Tran, X.N.: Performance analysis of cognitive spectrum-sharing single-carrier systems with relay selection. IEEE Trans. Signal Process. **60**(12) (Dec. 2012) 6435–6449

[60] Xu, T., Ge, J., Ding, H.: An efficient distributed link selection scheme for AF-based cognitive selection relaying networks. IEEE Commun. Lett. **18**(2) (Feb. 2014) 253–256

[61] Y. Han, S.H.T., Pandharipande, A.: Cooperative decode-and-forward relaying for secondary spectrum access. IEEE Trans. Wireless Commun. **8**(10) (2009) 4945–4950

[62] Y. Han, A.P., Ting, S.H.: Cooperative spectrum sharing protocol with secondary user selection. IEEE Trans. Wireless Commun. **9**(9) (2010) 2914–2923

[63] Asghari, V., Aissa, S.: Cooperative relay communication performance under spectrum-sharing resource requirements. Proc. IEEE International Conference on Communications (2010)

[64] Y. Guo, G. Kang, S.Q.M.Z., Zhang, P.: Outage performance of cognitive-radio relay system based on the spectrum-sharing environment

[65] C. Zhong, T.R., Wong, K.K.: Outage analysis of decode-and-forward cognitive dual-hop systems with the interference constraint in nakagami-m fading channels. IEEE Trans. Veh. Technol. **60**(6) (2011) 2875–2879

[66] H. Tran, T.Q.D., Zepernick, H.J.: Performance analysis of cognitive relay networks under power constraints of multiple primary users

[67] Kim, K.J., Duong, T., Poor, H.: Performance analysis of cyclic prefixed single-carrier cognitive amplify-and-forward relay systems. IEEE Trans. Wireless Commun. **12**(1) (January 2013) 195–205

[68] Bao, V., Duong, T., D. B. da Costa, Alexandropoulos, G., Nallanathan, A.: Cognitive amplify-and-forward relaying with best relay selection in non-identical Rayleigh fading. IEEE Commun. Lett. (99) (March 2013) 475 – 478

[69] Fredj, K., Aissa, S.: Performance of amplify-and-forward systems with partial relay selection under spectrum-sharing constraints. IEEE Trans. Wireless Commun. **11**(2) (February 2012) 500–504

[70] Xia, M., Aissa, S.: Cooperative af relaying in spectrum-sharing systems: Outage probability analysis under co-channel interferences and relay selection. IEEE Trans. Commun. **60**(11) (November 2012) 3252–3262

[71] Lee, J., Wang, H., Andrews, J.G., Hong, D.: Outage probability of cognitive relay networks with interference constraints. IEEE Trans. Wireless Commun. **10**(2) (February 2011) 390–395

[72] Zhang, Y., Xie, Y., Liu, Y., Feng, Z., Zhang, P., Wei, Z.: Outage probability analysis of cognitive relay networks in Nakagami-m fading channels. In: Proc. IEEE Veh. Technol. Conf. (VTC). (Sep. 2012)

[73] El-Moutaouakkil, Z., Tourki, K., Qaraqe, K., Saoudi, S.: Exact outage probability analysis for relay-aided underlay cognitive communications. In: Proc. IEEE Veh. Technol. Conf. (VTC). (Sep. 2012)

[74] Alkheir, A., Ibnkahla, M.: Performance analysis of cognitive radio relay networks using decode and forward selection relaying over Rayleigh fading channels. In: Proc. IEEE Global Commun. Conf. (GLOBECOM). (Dec. 2011)

[75] Chamkhia, H., Hasna, M., Hamila, R., Hussain, S.: Performance analysis of relay selection schemes in underlay cognitive networks with decode and forward relaying. In: Proc. IEEE Int. Symp.(PIMRC). (September 2012) 1552–1558

[76] D. B. da Costa, Elkashlan, M., Yeoh, P.L., Yang, N., Yacoub, M.: Dual-hop cooperative spectrum sharing systems with multi-primary users and multi-secondary destinations over Nakagami-m fading. In: Proc. IEEE Int. Symp.(PIMRC). (September 2012) 1577–1581

[77] Duong, T.Q., Yeoh, P.L., Bao, V.N.Q., Elkashlan, M., Yang, N.: Cognitive relay networks with multiple primary transceivers under spectrum-sharing. IEEE Signal Process. Lett. **19**(11) (November 2012) 741–744

[78] Tarokh, V., Jafarkhani, H., Calderbank, A.R.: Space-time block codes from orthogonal designs. IEEE Trans. Inf. Theory **45**(5) (Jul. 1999) 1456–1467

[79] Ding, H., Ge, J., da Costa, D.B., Jiang, Z.: Link selection schemes for selection relaying systems with transmit beamforming: New and efficient proposals from a distributed concept. IEEE Trans. Veh. Technol. **61**(2) (Feb. 2012) 533–552

[80] Rashid-Farrokhi, F., Tassiulas, L., Liu, K.J.R.: Joint optimal power control and beamforming in wireless networks using antenna arrays. IEEE Trans. Commun. **46**(10) (Oct. 1998) 1313–1324

[81] Zhang, R., Liang, Y.C.: Exploiting multi-antennas for opportunistic spectrum sharing in cognitive radio networks. IEEE J. Sel. Topics Signal. Process. (2008)

[82] Duan, R., Jäntti, R., Elmusrati, M., Virrankoski, R.: Capacity for spectrum sharing cognitive radios with MRC diversity and imperfect channel information from primary user. In: Proc. IEEE Global Telecommunications Conference (GLOBECOM), Miami, USA (2010)

[83] Li, D.: Performance analysis of MRC diversity for cognitive radio systems. IEEE Trans. Veh. Technol. **61**(2) (February 2012) 849–853

[84] Wu, Q., Huang, Y., Wang, J., Cheng, Y.: Effective capacity of cognitive radio systems with GSC diversity under imperfect channel knowledge. IEEE Commun. Lett. **16**(11) (November 2012) 1792–1795

[85] Asaduzzaman, Kong, H.: Ergodic and outage capacity of interference temperature-limited cognitive radio multi-input multi-output channel. IET Commun. **5**(5) (May 2011) 652–659

[86] Blagojevic, V., Ivanis, P.: Ergodic capacity of spectrum sharing cognitive radio with MRC diversity and Nakagami fading. In: Proc. IEEE Wireless Commun. Netw. Conf. (WCNC), Sydney, Australia (2012)

[87] Duong, T., D. B. da Costa, Elkashlan, M., Bao, V.N.Q.: Cognitive amplify-and-forward relay networks over nakagami- fading. IEEE Trans. Veh. Technol. **61**(5) (2012) 2368–2374

[88] Kim, J.B., Kim, D.: Outage probability and achievable diversity order of opportunistic relaying in cognitive secondary radio networks. IEEE Trans. Commun. **60**(9) (September 2012) 2456–2466

[89] Sarkar, M.Z.I., Ratnarajah, T., Sellathurai, M.: On the outage behavior of cognitive relay assisted mimo multiple access channel. In: Proc. IEEE Intern. Symp. Pers. Indoor Mobile Commun. (PIMRC). (Sep. 2009) 1–6

[90] Blagojevic, V., Ivanis, P.: Ergodic capacity for TAS/MRC spectrum sharing cognitive radio. IEEE Commun. Lett. **16**(3) (Mar. 2012) 321–323

[91] Yeoh, P.L., Elkashlan, M., Duong, T.Q., Yang, N., da Costa, D.B.: Transmit antenna selection for interference management in cognitive relay networks. IEEE

Trans. Veh. Technol. (2014)

[92] Zou, Y., Wang, X., Shen, W.: Physical-layer security with multiuser scheduling in cognitive radio networks. IEEE Trans. Commun. **61**(12) (Dec. 2013) 5103–5113

[93] Pei, Y., Liang, Y.C., Zhang, L., Teh, K.C., Li, K.H.: Secure communication over MISO cognitive radio channels. IEEE Trans. Wireless Commun. **9**(4) (Apr. 2010) 1494–1502

[94] Pei, Y., Liang, Y.C., Teh, K.C., Li, K.H.: Secure communication in multiantenna cognitive radio networks with imperfect channel state information. IEEE Trans. Signal Process. **59**(4) (Apr. 2011) 1683–1693

[95] Pinto, P.C., Barros, J., Win, M.Z.: Secure communication in stochastic wireless networks—part I: connectivity. IEEE Trans. Inf. Forensics Security **7**(1) (Feb. 2012) 125–138

[96] Geraci, G., Dhillon, H.S., Andrews, J.G., Yuan, J., Collings, I.B.: Physical layer security in downlink multi-antenna cellular networks. IEEE Trans. Commun. **62**(6) (Jun. 2014) 2006–2021

[97] Shafiee, S., Ulukus, S.: Achievable rates in Gaussian MISO channels with secrecy constraints. In: Proc. IEEE ISIT. (Nice, France, Jun. 2007) 2466–2470

[98] Swindlehurst, A.L.: Fixed SINR solutions for the MIMO wiretap channel. In: Proc. IEEE Int. Conf. Acoust. Speech Signal Process. (Taipei, China, Apr. 2009) 2437–2440

[99] Goel, S., Negi, R.: Guaranteeing secrecy using artificial noise. IEEE Trans. Wireless Commun. **7**(6) (Jun. 2008) 2180–2189

[100] Zhou, X., McKay, M.R.: Secure transmission with artificial noise over fading channels: Achievable rate and optimal power allocation. IEEE Trans. Veh. Technol. **59**(8) (Oct. 2010) 3831–3842

[101] Zhang, X., Zhou, X., McKay, M.R.: Enhancing secrecy with multi-antenna transmission in wireless ad hoc networks. **8**(11) (Nov. 2013) 1802–1814

[102] Varshney, L.R.: Transporting information and energy simultaneously. In: Pro. IEEE Int. Symp. Inf. Theory (ISIT). (Jul. 2008) 1612–1616

[103] Grover, P., Sahai, A.: Shannon meets tesla: Wireless information and power

transfer. In: Pro. IEEE Int. Symp. Inf. Theory (ISIT). (Jun. 2010) 2363–2367

[104] Zhang, R., Ho, C.K.: Mimo broadcasting for simultaneous wireless information and power transfer. IEEE Trans. Wireless Commun. **12**(5) (May. 2013) 1989–2001

[105] Zhou, X., Zhang, R., Ho, C.: Wireless information and power transfer in multiuser OFDM systems. to appear on IEEE Trans. Wireless Commun. (Available on-line at arxiv.org/abs/1308.2462.)

[106] Park, J., Clerckx, B.: Joint wireless information and energy transfer in a two-user MIMO interference channel. IEEE Trans. Wireless Commun. **12**(8) (Aug. 2013) 4210–4221

[107] Popovski, P., Fouladgar, A.M., Simeone, O.: Interactive joint transfer of energy and information. IEEE Trans. Commun. **61**(5) (May. 2013) 2086–2097

[108] Nasir, A.A., Zhou, X., Durrani, S., Kennedy, R.A.: Relaying protocols for wireless energy harvesting and information processing. IEEE Trans. Wireless Commun. **12**(7) (Jul. 2013) 3622–3636

[109] Usman, M., Koo, I.: Access strategy for hybrid underlay-overlay cognitive radios with energy harvesting. IEEE Sensors J. **PP**(99) (2014) 1–10

[110] Park, S., Heo, J., Kim, B., Chung, W., Wang, H., Hong, D.: Optimal mode selection for cognitive radio sensor networks with RF energy harvesting. In: Proc. IEEE PIMRC. (2012) 2155–2159

[111] Park, S., Kim, H., Hong, D.: Cognitive radio networks with energy harvesting. IEEE Trans. Wireless Commun. **12**(3) (Mar. 2013) 1386–1397

[112] Lu, X., Xu, W., Li, S., Lin, J., He, Z.: Simultaneous information and power transfer for relay-assisted cognitive radio networks. In: Proc IEEE ICC. (2014) 331–336

[113] Xu, C., Zhang, Q., Li, Q., Tan, Y., Qin, J.: Robust transceiver design for wireless information and power transmission in underlay mimo cognitive radio networks. IEEE Commun. Lett. **18**(9) (Sep. 2014) 1665–1668

[114] Wang, Z., Chen, Z., Luo, L., Hu, Z., Xia, B., Liu, H.: Outage analysis of cognitive relay networks with energy harvesting and information transfer. In: Proc IEEE ICC. (2014) 4348–4353

[115] Sibomana, L., Zepernick, H.J., Hung, T.: Wireless information and power transfer in an underlay cognitive radio network. In: Proc. IEEE ICC. (2014) 1–6

[116] Lee, S., Zhang, R., Huang, K.: Opportunistic wireless energy harvesting in cognitive radio networks. IEEE Trans. Wireless Commun. **12**(9) (Sep. 2013) 4788–4799

[117] Ju, H., Zhang, R.: Throughput maximization in wireless powered communication networks. IEEE Trans. Commun. **13**(1) (Jan. 2014) 418–428

[118] Liu, L., Zhang, R., Chua, K.C.: Multi-antenna wireless powered communication with energy beamforming. submitted for publication (available online at arXiv:1312.1450)

[119] Ju, H., Zhang, R.: User cooperation in wireless powered communication networks. submitted for publication (available online at arXiv:1403.7123)

[120] Kang, X., Ho, C.K., Sun, S.: Full-duplex wireless-powered communication network with energy causality. submitted for publication (available online at arXiv:1404.0471)

[121] Yang, G., Ho, C.K., Zhang, R., Guan, Y.L.: Throughput optimization for massive mimo systems powered by wireless energy transfer. submitted for publication (available online at arXiv:1403.3991)

[122] Sakr, A.H., Hossain, E.: Cognitive and energy harvesting-based D2D ommunication in cellular networks: Stochastic geometry modeling and analysis. submitted for publication (available online at arXiv:1405.2013)

[123] Simon, M.K., Alouini, M.S.: Digital communication over fading channels. Volume 95. John Wiley & Sons (2005)

[124] Tse, D., Viswanath, P.: Fundamentals of Wireless Communication. Cambridge University Press, Cambridge, U.K. (2005)

[125] Lodhi, A., Said, F., Dohler, M., Aghvami, A.H.: Closed-form symbol error probabilities of STBC and CDD MC-CDMA with frequency-correlated subcarriers over Nakagami-m fading channels. IEEE Trans. Veh. Technol. **57**(2) (Mar. 2008) 962–973

[126] Brennan, D.G.: Linear diversity combining techniques. Proceedings of the IEEE **91**(2) (Feb. 2003) 331–356

[127] Zheng, L., Tse, D.N.C.: Diversity and multiplexing: a fundamental tradeoff in

multiple-antenna channels. IEEE Trans. Inf. Theory **49**(5) (May. 2003) 1073–1096

[128] Mehta, N.B., Kashyap, S., Molisch, A.F.: Antenna selection in LTE: from motivation to specification. IEEE Commun. Mag. **50**(10) (Oct. 2012) 144–150

[129] Alouini, M.S., Simon, M.K.: An MGF-based performance analysis of generalized selection combining over rayleigh fading channels. IEEE Trans. Commun. **48**(3) (Mar. 2000) 401–415

[130] Van Veen, B.D., Buckley, K.M.: Beamforming: A versatile approach to spatial filtering. IEEE ASSP Magazine **5**(2) (1988) 4–24

[131] Kelly, V.: New ieee 802.11 ac specification driven by evolving market need for higher, multi-user throughput in wireless lans. IEEE Standards Association (2014)

[132] Goldsmith, A.: Wireless communications. Cambridge university press (2005)

[133] Tao, X., Xu, X., Cui, Q.: An overview of cooperative communications. IEEE Commun. Mag. **50**(6) (Jun. 2012) 65–71

[134] Stoyan, D., Kendall, W., Mecke, J.: Stochastic geometry and its applications. Wiley New York **2** (1987)

[135] Haenggi, M., Andrews, J.G., Baccelli, F., Dousse, O., Franceschetti, M.: Stochastic geometry and random graphs for the analysis and design of wireless networks. IEEE J. Sel. Areas Commun. **27**(7) (Sep. 2009) 1029–1046

[136] Venkataraman, J., Haenggi, M., Collins, O.: Shot noise models for outage and throughput analyses in wireless ad hoc networks. In: Proc. 44th Annu. Allerton Conf. Communication, Control, and Computing, Monticello, IL. (Sep. 2006) 1–7

[137] Rice, S.O.: Mathematical analysis of random noise. Bell System Technical Journal, The **24**(1) (Jan. 1945) 46–156

[138] Delfs, H., Knebl, H.: Introduction to cryptography: principles and applications. Springer (2007)

[139] Goldreich, O.: Foundations of Cryptography: Volume 2, Basic Applications. Volume 2. Cambridge university press (2009)

[140] Vernam, G.S.: Cipher printing telegraph systems: For secret wire and radio telegraphic communications. Trans. of the AIEE **45**(2) (Jan. 1926) 109–115

[141] Bloch, M., Barros, J.: Physical-Layer Security: From Information Theory to Security Engineering. Cambridge University Press, Cambridge (2011)

[142] Wyner, A.D.: The wire-tap channel. Bell System Technical Journal **54**(8) (1975) 1355–1387

[143] Visser, H.J., Vullers, R.J.M.: RF energy harvesting and transport for wireless sensor network applications: Principles and requirements. Proceedings of the IEEE **101**(6) (Jun. 2013) 1410–1423

[144] Nishimoto, H., Kawahara, Y., Asami, T.: Prototype implementation of ambient rf energy harvesting wireless sensor networks. In: 2010 IEEE Sensors. (Nov. 2010) 1282–1287

[145] Zhang, X., Jiang, H., Zhang, L., Zhang, C., Wang, Z., Chen, X.: An energy-efficient asic for wireless body sensor networks in medical applications. IEEE Trans. Biomed. Circuits Syst. **4**(1) (Feb. 2010) 11–18

[146] Michalopoulos, D.S., Suraweera, H.A., Karagiannidis, G.K., Schober, R.: Amplify-and-Forward relay selection with outdated channel estimates. IEEE Trans. Commun. **60**(5) (May. 2012) 1278–1290

[147] Wu, Q., Zhang, Z., Wang, J.: Outage analysis of cognitive relay networks with relay selection under imperfect CSI environment. IEEE Commun. Lett. **17**(7) (Jul. 2013) 1297–1300

[148] Kim, H., Wang, H., Lim, S., Hong, D.: On the impact of outdated channel information on the capacity of secondary user in spectrum sharing environments. IEEE Trans. Wireless Commun. **11**(1) (Dec. 2012) 284–295

[149] Ghasemi, A., Sousa, E.S.: Fundamental limits of spectrum-sharing in fading environments. IEEE Trans. Wireless Commun. **6**(2) (Feb. 2007) 649–658

[150] Cai, X., Giannakis, G.B.: Performance analysis of combined transmit selection diversity and receive generalized selection combining in Rayleigh fading channels. IEEE Trans. Wireless Commun. **3**(6) (November 2004) 1980–1983

[151] Singal, T.L.: Wireless communications. Tata McGraw-Hill Education, New Delhi (2010)

[152] Yeoh, P.L., Elkashlan, M., Kim, K.J., Duong, T.Q., Karagiannidis, G.K.: Cog-

nitive MIMO relaying with multiple primary transceivers. Proc. IEEE Global Commun. Conf. (Atlanta, GA, Dec. 2013)

[153] A. R. Zaidi, S., Ghogho, M., McLernon, D., Swami, A.: Achievable spatial throughput in multi-antenna cognitive underlay networks with multi-hop relaying. IEEE J. Sel. Areas Commun. **31**(8) (Aug. 2013) 1278–1290

[154] Kim, K.J., Duong, T.Q., Poor, H.V., Shu, L.: Performance analysis of cyclic prefixed single-carrier spectrum sharing relay systems in primary user interference. IEEE Trans. Signal Process. **60**(12) (Dec. 2012) 6729–6734

[155] Graham, R.L., Knuth, D.E., Patashnik, O.: Concrete Mathematics. Addison-Wesley, New York (1989)

[156] Ngo, H.Q., Matthaiou, M., Duong, T.Q., Larsson, E.G.: Uplink performance analysis of multicell MU-MIMO systems with ZF receivers. IEEE Trans. Veh. Technol. **62**(9) (Nov. 2013) 4471–4482

[157] Gradshteyn, I.S., Ryzhik, I.M.: Table of Integrals, Series and Products. sixth edn. Academic Press, New York, NY, USA (2000)

[158] Suraweera, H.A., Smith, P.J., Shafi, M.: Capacity limits and performance analysis of cognitive radio with imperfect channel knowledge. IEEE Trans. Veh. Technol. **59**(4) (May 2010) 1811–1822

[159] Xu, W., Zhang, J., Zhang, P., Tellambura, C.: Outage probability of decode-and-forward cognitive relay in presence of primary user's interference. IEEE Commun. Lett. **16**(8) (August 2012) 1252–1255

[160] Liu, K.J.R., Sadek, A.K., Su, W.: et al., Cooperative Communications and Networking. Cambridge University Press (2009)

[161] Gradshteyn, I.S., Ryzhik, I.M.: Table of Integrals, Series and Products. sixth edn. Academic Press, New York, NY, USA (2000)

[162] Hong, J.P., Hong, B., Ban, T.W., Choi, W.: On the cooperative diversity gain in underlay cognitive radio systems. IEEE Trans. Commun. **60**(1) (January 2012) 209–219

[163] Zhong, C., Ratnarajah, T., Wong, K.K.: Outage analysis of decode-and-forward cognitive dual-hop systems with the interference constraint in Nakagami-m fading

channels. IEEE Trans. Veh. Technol. **60**(6) (July 2011) 2875–2879

[164] Clancy, T.C.: Formalizing the interference temperature model. Wireless Commun. Mobile Comput. **7**(9) (May 2007) 1077–1086

[165] McKay, M.R., Grant, A.J., Collings, I.B.: Performance analysis of mimo-mrc in double-correlated rayleigh environments. IEEE Trans. Commun. **55**(3) (2007) 497–507

[166] Ma, Y., Pasupathy, S.: Efficient performance evaluation for generalized selection combining on generalized fading channels. IEEE Trans. Wireless Commun. **3**(1) (January 2004) 29–34

[167] Lee, J., Wang, H., Andrews, J.G., Hong, D.: Outage probability of cognitive relay networks with interference constraints. IEEE Trans. Wireless Commun. **10**(2) (Feb. 2011) 390–395

[168] Ding, H., Ge, J., da Costa, D.B., Jiang, Z.: Asymptotic analysis of cooperative diversity systems with relay selection in a spectrum-sharing scenario. IEEE Trans. Veh. Technol. **60**(2) (Feb. 2011) 457–472

[169] Krikidis, I., Suraweera, H., Smith, P., Yuen, C.: Full-duplex relay selection for amplify-and-forward cooperative networks. IEEE Trans. Wireless Commun. **11**(12) (Dec. 2012) 4381–4393

[170] Peha, J.M.: Approaches to spectrum sharing. IEEE Commun. Mag. **43**(2) (Feb. 2005) 10–12

[171] Simon, M.K., Alouini, M.S.: Digital communication over fading channels. New York: Wiley (2005)

[172] Gradshteyn, I.S., Ryzhik, I.M.: Table of Integrals, Series and Products. 7th edn. Academic Press, San Diego, C.A. (2007)

[173] Shin, H., Lee, J.H.: Capacity of multiple-antenna fading channels: spatial fading correlation, double scattering, and keyhole. IEEE Trans. Inf. Theory **49**(10) (Oct. 2003) 2636–2647

[174] Ikki, S.S., Aissa, S.: Multihop wireless relaying systems in the presence of cochannel interferences: Performance analysis and design optimization. IEEE Trans. Veh. Technol. **61**(2) (Feb. 2012) 566–573

[175] Gopal, V., Matthaiou, M., Zhong, C.: Performance analysis of distributed MIMO systems in Rayleigh/Inverse-Gaussian fading channels. In: Proc. IEEE Global Commun. Conf. (GLOBECOM). (Dec. 2012) 2468–2474

[176] Matthaiou, M., Chatzidiamantis, N.D., Karagiannidis, G.K., Nossek, J.A.: On the capacity of generalized-K fading MIMO channels. IEEE Trans. Signal Process. **58**(11) (Nov. 2010) 5939–5944

[177] Jin, S., McKay, M.R., Zhong, C., Wong, K.K.: Ergodic capacity analysis of amplify-and-forward MIMO dual-hop systems. IEEE Trans. Inf. Theory **56**(5) (May 2010) 2204–2224

[178] Bjornson, E., Zetterberg, P., Bengtsson, M., Ottersten, B.: Capacity limits and multiplexing gains of MIMO channels with transceiver impairments. IEEE Commun. Lett. **17**(1) (Jan. 2013) 91–94

[179] Weber, S., Andrews, J.G., Jindal, N.: An overview of the transmission capacity of wireless networks. IEEE Trans. Commun. **58**(12) (Dec. 2010) 3593–3604

[180] han Lee, C., Haenggi, M.: Interference and outage in Poisson cognitive networks. IEEE Trans. Wireless Commun. **11**(4) (Apr. 2012) 1392–1401

[181] Dong, L., Han, Z., Petropulu, A.P., Poor, H.V.: Improving wireless physical layer security via cooperating relays. IEEE Trans. Signal Process. **58**(3) (March 2010) 1875–1888

[182] Zhou, X., Ganti, R.K., Andrews, J.G., Hjorungnes, A.: On the throughput cost of physical layer security in decentralized wireless networks. IEEE Trans. Wireless Commun. **10**(8) (Aug. 2011) 2764–2775

[183] Zhou, X., McKay, M.R.: Secure transmission with artificial noise over fading channels: Achievable rate and optimal power allocation. IEEE Trans. Veh. Technol. **59**(8) (October 2010) 3831–3842

[184] Hong, Y.W.P., Lan, P.C., Kuo, C.C.J.: Enhancing physical-layer secrecy in multiantenna wireless systems: An overview of signal processing approaches. IEEE Signal Processing Mag. **30**(5) (Sep. 2013) 29–40

[185] Hollenbeck, K.J.: Invlap.m: A matlab function for numerical inversion of Laplace transforms by the de hoog algorithm. `Available:http://www.mathworks.com/`

matlabcentral/fileexchange/%32824-numerical-inversion-of-Laplace-/transforms-in-content/INVLAP.m (1998)

[186] Wendel, J.G.: The non-absolute convergence of Gil-Pelaez' inversion integral. The Annals of Mathematical Statistics **32**(1) (Mar. 1961) 338–339

[187] Duong, T., Yeoh, P.L., Bao, V.N.Q., Elkashlan, M., Yang, N.: Cognitive relay networks with multiple primary transceivers under spectrum-sharing. IEEE Signal Process. Lett. **19** (Nov. 2012)

[188] Nasir, A., Zhou, X., Durrani, S., Kennedy, R.: Relaying protocols for wireless energy harvesting and information processing. IEEE Trans. Wireless Commun. **12**(7) (Jul. 2013) 3622–3636

[189] Krikidis, I., Sasaki, S., Timotheou, S., Ding, Z.: A low complexity antenna switching for joint wireless information and energy transfer in MIMO relay channels. IEEE Trans. Commun. **62**(5) (May 2014) 1577–1587

[190] Liu, C.F., Lee, C.H.: Information and power transfer under MISO channel with finite-rate feedback. In: Proc. IEEE GLOBECOM. (Dec. 2013) 2497–2501

[191] Yeoh, P.L., Elkashlan, M., Kim, K.J., Duong, T.Q., Karagiannidis, G.K.: Cognitive MIMO relaying with multiple primary transceivers. In: Proc. IEEE GLOBECOM. (2013) 1956 – 1961

[192] Verdu, S.: Multiuser detection. Cambridge University Press (1998)

[193] Cui, S., Goldsmith, A.J., Bahai, A.: Energy-constrained modulation optimizationmodulation optimization. IEEE Trans. Wireless Commun. **4**(6) (Sep. 2005) 2349–2360

[194] Zhou, X., Zhang, R., Ho, C.K.: Wireless information and power transfer: Architecture design and rate-energy tradeoff. In: Proc. IEEE GLOBECOM. (2012) 3982–3987

[195] Biglieri, E., Proakis, J., Shamai, S.: Fading channels: information-theoretic and communications aspects. IEEE Trans. Inf. Theory **44**(6) (Oct. 1998) 2619–2692

[196] Hesami, P., Laneman, J.N.: Limiting behavior of receive antennae selection. In: Proc. CISS. (Mar. 2011) 1–6

[197] Jo, H.S., Sang, Y.J., Xia, P., Andrews, J.G.: Heterogeneous cellular networks with

flexible cell association: A comprehensive downlink SINR analysis. IEEE Trans. Wireless Commun. **11**(10) (October 2012) 3484–3495

[198] Kim, Y., Lee, S., Hong, D.: Performance analysis of two-tier femtocell networks with outage constraints. IEEE Trans. Wireless Commun. **9**(9) (Sep. 2010) 2695–2700

[199] ElSawy, H., Hossain, E.: On stochastic geometry modeling of cellular uplink transmission with truncated channel inversion power control. IEEE Trans. Wireless Commun. (2014)

[200] Baccelli, F., Blaszczyszyn, B.: Stochastic geometry and wireless networks: Volume 1: Theory. Volume 1. Now Publishers Inc (2009)

[201] Baccelli, F., Blaszczyszyn, B., Muhlethaler, P.: An aloha protocol for multihop mobile wireless networks. IEEE Trans. Inf. Theory **52**(2) (Feb. 2006) 421–436

[202] Smiljkovikj, K., Popovski, P., Gavrilovska, L.: Analysis of the decoupled access for downlink and uplink in wireless heterogeneous networks. [Online]. Available: arxiv.org/abs/1407.0536 (2014)

[203] Zhou, X., Zhang, R., Ho, C.K.: Wireless information and power transfer: architecture design and rate-energy tradeoff. In: Proc. IEEE GLOBECOM, IEEE (2012) 3982–3987

[204] da Costa, D.B., Aissa, S.: Cooperative dual-hop relaying systems with beamforming over Nakagami-m fading channels. IEEE Trans. Wireless Commun. **8**(8) (August 2009) 3950–3954

[205] Zaidi, S., McLernon, D., Ghogho, M.: Breaking the area spectral efficiency wall in cognitive underlay networks. IEEE J. Sel. Areas Commun. **32**(11) (Feb. 2014) 1–17

[206] Baccelli, F., Blaszczyszyn, B., Muhlethaler, P.: An aloha protocol for multihop mobile wireless networks. IEEE Trans. Inf. Theory **52**(2) (Feb. 2006) 421–436

[207] Gradsheteyn, I.S., Ryzhik, I.M.: Table of Integrals, Series, and Products. Academic Press, 6th Edition, San Diego, CA (2000)